
Space-Time Discretization of Maxwell's Equations in the Setting of Geometric Algebra

Zur Erlangung des akademischen Grades Doktor-Ingenieur (Dr.-Ing.)
genehmigte Dissertation von M.Sc. Mariusz Klimek aus Lublin
Tag der Einreichung: 19.09.2017, Tag der Prüfung: 19.01.2018
Darmstadt 2018 – D 17

1. Gutachten: Prof.dr. Sebastian Schöps
2. Gutachten: Prof.dr. Stefan Kurz



TECHNISCHE
UNIVERSITÄT
DARMSTADT

Fachbereich Elektrotechnik und
Informationstechnik
Institut für Theorie
Elektromagnetischer Felder

Space-Time Discretization of Maxwell's Equations in the Setting of Geometric Algebra

Genehmigte Dissertation von M.Sc. Mariusz Klimek aus Lublin

1. Gutachten: Prof.dr. Sebastian Schöps

2. Gutachten: Prof.dr. Stefan Kurz

Tag der Einreichung: 19.09.2017

Tag der Prüfung: 19.01.2018

Darmstadt 2018 – D 17

Bitte zitieren Sie dieses Dokument als:

URN: [urn:nbn:de:tuda-tuprints-72325](https://nbn-resolving.org/urn:nbn:de:tuda-tuprints-72325)

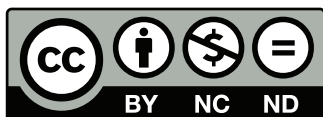
URL: <http://tuprints.ulb.tu-darmstadt.de/id/eprint/7232>

Dieses Dokument wird bereitgestellt von tuprints,

E-Publishing-Service der TU Darmstadt

<http://tuprints.ulb.tu-darmstadt.de>

tuprints@ulb.tu-darmstadt.de



Die Veröffentlichung steht unter folgender Creative Commons Lizenz:

Namensnennung – Keine kommerzielle Nutzung – Keine Bearbeitung 4.0 International

<http://creativecommons.org/licenses/by-nc-nd/4.0/>

Erklärung zur Dissertation

Hiermit versichere ich, die vorliegende Dissertation ohne Hilfe Dritter nur mit den angegebenen Quellen und Hilfsmitteln angefertigt zu haben. Alle Stellen, die aus Quellen entnommen wurden, sind als solche kenntlich gemacht. Diese Arbeit hat in gleicher oder ähnlicher Form noch keiner Prüfungsbehörde vorgelegen.

Darmstadt, den February 6, 2018

(M. Klimek)

Contents

1	Background and Motivation	5
2	Introduction	7
2.1	Mathematical Formalism: Geometric Algebra and Calculus	7
2.1.1	Geometric Algebra	7
2.1.2	Geometric Calculus	12
2.1.3	Calculus in Curved Spaces	17
2.1.4	Relation to the Exterior Algebra and Calculus of Differential Forms	21
2.2	Space-Time and Relativity	26
2.3	Maxwell's Equations	30
2.4	Material Equations	31
2.5	Summary: Electrodynamics in Four Dimensions	33
2.5.1	Magnetic Gauss Law in Rotating Reference Frame	33
3	Discretization	35
3.1	Discretization Concepts	35
3.1.1	4D Mesh Construction	37
3.2	Discretization of Maxwell's Equations	38
3.3	Discretization of Material Equations	41
3.3.1	Diagonal Material Matrices	41
3.3.2	Non-diagonal Material Matrices	45
3.3.3	Whitney Interpolation	45
3.3.4	Finite Integration Technique with Whitney Interpolation	51
3.3.5	Energetic Approach and Galerkin Hodge	52
3.4	Summary: the Discrete Equations	54
4	Mesh Pair Optimization	55
4.1	Numerical Example in 2D	56
4.2	3D Considerations	57
4.3	Conclusion	60
5	Sagnac Effect in a Rotating Ring Resonator	60
5.1	Description of the Numerical Experiment	61
5.2	Analytic Predictions	62
5.3	Comparison with Analytic Formula	63
5.4	Numerical Investigation of Stability of the Implicit Schemes	65
5.5	Numerical Investigation of Instabilities due to Extrapolation	66
5.6	Numerical Convergence Analysis (non-rotating case)	68
5.7	Symmetrised FIT Material Matrices (non-rotating case)	68
5.8	Geometric Optics Approximation	72
6	Rotating Photonic Crystal	73
7	Conclusion and Outlook	75
A	GA Elaborations	78
A.1	Basis of GA	78
A.2	Levi-Civita Connection is Natural to Geometric Calculus	78
A.3	Inverse of a Pseudoscalar	79
B	Technical Relativistic Derivations	79
B.1	Lorentz Boost as a Rotation	79
B.2	Velocity Field of a Rotating Observer	80
B.3	Technical Details of Derivation of the Gauss Law in Rotating Reference Frame	80

C	Elaborations Associated with Whitney Elements	83
C.1	Dual Exterior Derivative	83
C.2	Whitney Interpolation	84
C.3	Explicit Formulae for Whitney Elements	85
C.4	Derivation of Affine Mapping to Physical Space	86
C.5	Transformations in Tangent Space Induced due to a Change of Coordinates	87
C.6	The Transformation to the Physical Domain	89
C.7	Changing the Dual in Order to Prove Convergence	89
C.8	3D Whitney Interpolation at the Barycenter of a Hexahedron	91
D	Neumann Series as a Predictor-Corrector Scheme	92

Abstract

In this dissertation a FIT-like discretisation of Maxwell's equations is performed directly in four-dimensional space-time using the mathematical formalism of Clifford's Geometric Algebra.

The thesis extends the Finite Integration Technique (FIT) to 4D space-time without introducing any non-relativistic assumptions. The coordinate-free formulation in terms of geometric algebra enhances explicitly relativistic, i.e., without splitting space and time, treatment, which reveals in the fact that any non-relativistic assumptions are not made. The relation of geometric algebra to the existing concepts from differential geometry in the language of differential forms is established in the context of electromagnetic field description. An alternative to the existing approaches formula for the discretisation of material laws on non-orthogonal mesh pairs is derived, investigated and applied. The developed theory is applied to obtain the condition for 3D problems when material matrices are diagonal, and due to quantitative nature of this condition a mesh optimisation procedure is proposed, as well as its limitations in 3D case, which do not occur in 2D, are derived. The other application is simulation of electromagnetic wave propagation in a rotating reference frame. Due to coordinate-free formalism and encoding the movement of the observer in 4D mesh's geometry, derivation of the numerical scheme for rotating observer's resembles the one for inertial (stationary) observers. In other words, relativistic coordinate-free treatment includes inertial and non-inertial observers as special cases, which do not need to be diversified. The comparison of the obtained numerical results with the ones known from literature is performed in order to validate the theoretical results.

Kurzfassung

In dieser Dissertation wird mit Hilfe der formalen mathematischen Methoden von Cliffords geometrischer Algebra eine Diskretisierung der Maxwell Gleichungen in vier-dimensionalen Raumzeit vorgenommen, die der Finiten Integrationstechnik ähnelt.

Die Erweiterung kommt ohne Hinzunahme von nicht-relativistischen Annahmen aus. Die koordinatenfreie Formulierung im Formalismus der geometrischen Algebra ermöglicht explizite relativistische Rechnungen. Das Verhältnis zwischen geometrischer Algebra und differentialgeometrischen Konzepten wird im Rahmen von Differentialformen und mit Blick auf die Beschreibung elektromagnetischer Felder, erläutert. Eine alternative Formulierung zur Diskretisierung der Materialgesetze auf nicht-orthogonalen Gittern wird eingeführt, analysiert und getestet. Die dadurch entwickelte Theorie zeigt für den wichtigen drei-dimensionalen Sonderfall, unter welchen Bedingungen die Diskretisierung auf diagonale Materialmatrizen führt. Dies erlaubt eine Gitteroptimierungsstrategie und zeigt die Grenzen der Strategie für drei-dimensionale Probleme, die in zwei Dimensionen nicht auftreten. Mit der Simulation der Ausbreitung elektromagnetischer Wellen in einem rotierenden Referenzgebiet wird eine Anwendung diskutiert. Durch die koordinatenfreie Formulierung und die spezielle Behandlung der Bewegung des Beobachters in vier Dimensionen wird eine numerische Methode entwickelt, die analog zu Methoden mit stationären Beobachtern angewendet werden kann. Hierdurch wird deutlich, dass die relativistische, koordinatenfreie Beschreibung inertialer und nicht inertialer als Spezialfälle in der erarbeiteten Theorie enthalten sind. Die vorgestellten Methoden werden mit numerischen Methoden aus der Literatur verglichen und getestet.

1 Background and Motivation

Mankind has been investigating electromagnetism for centuries now. We also started to exploit it to serve our needs already two centuries ago by, e.g., building first electric machines. While there are still many unanswered questions concerning electromagnetic theory, we may soundly claim that the classical electromagnetism¹ is currently well understood and used to serve humanity. However, it is only recently, when we can say that we are mastering exploitation of its capabilities. For example, nowadays for a specified task it is not only possible to design an electromagnetic device performing this task, but also to guarantee its performance.

At some point of the design process, the prototype has to be built, which usually does not work as intended. Then one needs to redesign the device and built another prototype, which is hoped to perform better. However, usually there are no exact rules how to change the current prototype in order to reach the desired performance. Therefore, the next prototype has to be tested and again improved if necessary. Repetitive building and testing prototypes is costly², and one would like to have a cheaper substitute for that. The cure comes with developments in physics (or natural sciences in general), mathematics and computer science. Namely, if for a prototype of a certain device we can:

1. approximate physical reality, i.e., building and testing of the prototype, by a mathematical model,
2. extract (possibly approximately, up to the desired accuracy) quantities of interest from the model in an algorithmic way,
3. execute the algorithm in short enough time, i.e., we can afford its execution,

then we can build and test the prototype virtually in a computer reality, which process is called **simulation** of the device. We would like to mention that Modelling, Simulation and Optimisation are parts of Virtual Product Engineering which is a well-established practice in science, technology and industry. However, space-time simulations are less common and this thesis contributes to this particular aspect of this field of knowledge. While the cost issue has been mentioned in the last point above, it is important in all of them as they are related to each other. Moreover, the cost is the main limiting factor in simulation. Therefore, we require from the three aforementioned branches of science two (usually contradicting) solutions. Being more precise; physics should provide a model that captures enough of the physical phenomena and is simple enough to be tackled by efficient algorithms; mathematics should bring as simple as possible way to calculate quantities of interest with as high as possible precision. Computer science should deliver an implementation of the algorithm that is as general as possible, i.e., can be executed on wide range of computer architectures, while exploiting as much of the hardware's computational power as possible. For classical electromagnetism there have been many successful approaches to simulation, i.e., the ones whose cost could be afforded and the results obtained are helpful in the design process.

The electromagnetic field simulation, although never exactly representing reality due to modelling errors, has become an important and useful tool in developing devices to be built. We would naturally wish that our simulation tool can treat as broad variety of devices as possible. For a certain mathematical model it means that we would not like to restrict its generality by the steps carried out to obtain a simulation software. In other words, we would not like to abandon certain properties of the model. Having classical electromagnetism as the model in mind, we would not like to violate Special Relativity Theory³. Approaches consistent with Special Relativity are called in the literature relativistic or space-time approaches⁴. All considerations in this dissertation are relativistic.

¹ By “classical” we mean that quantum and gravitational effects are disregarded. However, if quantum theory is used to derive the model, e.g., material equations, to be used within classical framework, we still consider it as a part of classical electromagnetism.

² By saying “costly” we use the common rule, e.g., used in English idiomatic expressions, that time equals money. While money is human invention and restricted to human beings, time is a physical property, and “cost” in that sense is simply time, which is a physical quantity, which applies to the whole nature. For example if we would like to build a device that performs a certain task, and the cost is “too high” it might mean that we are not able to built it during our lifetime (or working day).

³ Which might be seen as a consequent theory of classical electromagnetism. However, classical electromagnetism, i.e., Maxwell's equations, can be derived from Coulomb force law (taught in school)

$$F = k \frac{q_1 q_2}{r^2},$$

where F is the force acting on two charges q_1 and q_2 separated by a distance r , k is Coulomb proportionality constant, and Special Relativity Theory, e.g., by accepting Lorentz transformations as proper physical transformations. Nevertheless, it is not important whether the framework is imposed by the model or vice versa; it is only important that they are compatible in the sense that they do not lead to contradictions.

⁴ We would like to point that in principle any computational framework that involves space and time might be called (and unfortunately often actually is) “space-time approach”. However, if such approach is not compatible with Special Relativity, it cannot be called relativistic. Thus such approaches might be called “space-time”, but not “relativistic”. Nevertheless, in this thesis we will not distinguish between “space-time” and “relativistic” approaches, and by “space-time” we always mean “relativistic”, which simply means “consistent with Special Relativity Theory”.

The mathematical formalism used to express the model should be as convenient as possible. While convenience is in general a matter of taste, it can be in many situations defined well to some extent. For example, Maxwell's equations, i.e., equations describing classical electromagnetism, can be written using basic algebraic operations and partial derivatives or using vector notation with “nabla” operator ∇ . In the first case a part of Maxwell's equations, written actually in a seemingly complicated form proposed originally by Maxwell, reads

$$\begin{aligned} -\frac{\partial B^x}{\partial t} &= \frac{\partial E^z}{\partial y} - \frac{\partial E^y}{\partial z} \\ -\frac{\partial B^y}{\partial t} &= \frac{\partial E^x}{\partial z} - \frac{\partial E^z}{\partial x} \\ -\frac{\partial B^z}{\partial t} &= \frac{\partial E^y}{\partial x} - \frac{\partial E^x}{\partial y} \end{aligned} \qquad 0 = \frac{\partial B^x}{\partial x} + \frac{\partial B^y}{\partial y} + \frac{\partial B^z}{\partial z},$$

while in the second notation it becomes

$$-\frac{\partial \vec{B}}{\partial t} = \vec{\nabla} \times \vec{E} \qquad 0 = \vec{\nabla} \cdot \vec{B}.$$

The second equations are more convenient not only in the sense that they require less ink to be printed, but also because the symbols $\vec{\nabla} \times$ and $\vec{\nabla} \cdot$ have clear geometric interpretation providing thus a better intuition of the physical content of the equations. In other words, one can focus more on the structure of equations rather than on their particular representation in terms of operators, i.e., partial derivatives, which are not directly related to the structure. Moreover, the latter equations are actually a generalisation of the former ones; namely, the latter can be expanded in any coordinate system, while the former is their representation in Cartesian coordinates, and is valid only in such coordinates. Therefore, the latter are more convenient as the conclusions valid in all coordinates systems can be drawn, without choosing any specific coordinates. Additionally, the coordinates may be specified later, e.g., adapted to geometric properties of the system considered, and we can be sure that all the coordinate-free results remain true.

The above equations written using the mathematical formalism of this thesis, i.e., Space-Time Algebra described in Section 2.1, read (2.209)

$$\nabla \wedge F = 0. \tag{1.1}$$

This is more convenient than vector algebra formulation in the similar sense as vector algebra formulation is more convenient than partial derivatives formulation as described above. Namely (besides keeping all the benefits of the previous approach), it is a generalisation of the previous equations as the previous ones hold only in 4D coordinates associated with an inertial observer, see Section 2.2, while (1.1) holds for arbitrary observers. In other words; while partial differential formulation is the expansion of vector algebra formulation in a specified 3D coordinates, the latter is the expansion of Space-Time Algebra formulation in an inertial observer's 4D coordinate system, and Space-Time Algebra formulation is valid in arbitrary 4D coordinates, i.e., for arbitrary observer. In Space-Time Algebra, we have incorporated Minkowski metric, which is specific to Special Relativity Theory; therefore, the conclusions about classical electromagnetism drawn using Space-Time Algebra are valid independently of the particular observer. This is due to the fact, that our mathematical formulation is compatible with the model, i.e., classical electromagnetism and thus Special Relativity as well, and is coordinate-free. In that sense, we may say that Space-Time Algebra is a convenient framework for (a discretisation of) classical electromagnetism.

We hope the thesis' subject has been motivated, i.e., it is worth to study (a discretised version of) classical electromagnetism (Maxwell's equations) and Geometric Algebra (of space-time) is a promising tool for relativistic treatment of the topic.

The outline of the dissertation is the following. Section 2 serves as an introduction to the framework. First the mathematical formalism, i.e., Clifford's Geometric Algebra, is established in Section 2.1, where we separate the purely algebraic treatment in Section 2.1.1 from concepts involving calculus in Section 2.1.2. Most of the concepts presented are commonly available in the literature, e.g., in [14, 26, 49, 50]. We deal separately with the calculus concepts specific to curved spaces in Section 2.1.3. Besides presenting our mathematical framework, we provide a practitioner's dictionary, Section 2.1.4, between ours and Differential Forms formalism used, e.g., in [6, 19, 23]. The relation between these both formalisms in a different setting has been spotted in [10, 14, 20, 26]. Section 3 is the theoretical heart of the thesis, where a new computational method is proposed. It is motivated by the approaches presented in [6, 60], which treat, as opposed to ours, space and time separately. The way to discretise Maxwell's equations in Section 3.2 bare close resemblance (independent whether carried out in 3D or in 4D space-time) to the Cell Method [58], Discrete Exterior Calculus [56], Mimetic Methods, Whitney Finite Elements [5] and to the Finite Integration Technique (FIT) [60]. Sections 4, 5 and 6 are applications of the general theory established in Section 3. In Section 4 the optimisation of the numerical scheme (obtaining diagonal material matrices) is performed and the limitations for this approach are

derived, see also [32]. Sections 5 and 6 are devoted to the simulation of electromagnetic fields in a rotating reference frame, studied also in [37, 38, 53, 54, 55]. In Section 5 we treat a simple problem focusing, however, on investigation of numerical properties of the method proposed in this thesis. Section 6 treats a more real-life application, namely a rotating photonic crystal structure is simulated. Such simulation might be helpful in a design of a miniature optical gyroscope as indicated in [53].

From time to time throughout the thesis we pose Open Research Questions, which are not crucial for the dissertation, but we find them interesting (and they also point possible future research directions).

2 Introduction

In this introductory chapter we introduce the framework that is used to present the results of this dissertation. The purpose here is twofold; besides defining the concepts necessary for the sequel, the notation and a certain point of view on certain topics is outlined. Examples of such topics include:

- Although introduction of metric is inevitable in Geometric Algebra, the definitions and results should be stated in a way that is valid for any metric, whenever possible.
- If in arbitrary coordinates some reasoning becomes simpler, they should be introduced. Naturally, without specifying them explicitly.
- How Geometric Calculus can be linked to differential geometry or the exterior calculus of differential forms.
- How calculus in curved spaces may be handled.
- How rotation with constant angular velocity should be generalised to the relativistic setting.
- How material equations associated with moving media should be incorporated to Maxwell's equations.

Section 2.1 is devoted to the mathematical formalism, which⁵ is not widespread, but enables us to express the concepts important for the dissertation in a compact way. In Section 2.2 we review fundamentals of special relativity theory using the formalism of Section 2.1. Section 2.3 is derivation of Maxwell's equations in the form that is useful in the considerations carried out in the sequel. We separately treat (constitutive to Maxwell's) material equations in Section 2.4. The conclusion of this introduction is an exemplary calculation in relativistic electrodynamics in Section 2.5. This serves as a verification whether our formalism captures the physical phenomena, whose simulation we are interested in. Moreover, it is an illustration of the use of the concepts introduced before in practice.

2.1 Mathematical Formalism: Geometric Algebra and Calculus

In this Section we outline the mathematical formalism used throughout the dissertation. In Section 2.1.1 we built the geometric algebra $\mathcal{G}(L, g)$ on any linear space L and metric tensor g . Although L can be in principle arbitrary, it will be later identified with the tangent space of a manifold. Therefore, Section 2.1.1 tells us how to do algebra at any single point of the manifold. The whole algebraic reasoning extends immediately to the whole manifold as GA can be built at every point independently. However, the answer how to perform analytic calculations (such as integration or differentiation) is missing in Section 2.1.1. The role of Section 2.1.2 is to fill this gap, i.e., to introduce the calculus of algebraic objects introduced in Section 2.1.1. We illustrate the concepts introduced so far by a few examples in Section 2.1.2. In other words Section 2.1.2 is an answer how to extend the ideas in Section 2.1.1 to the whole manifold and link the algebras built at different points. Throughout Section 2.1.2 we assume that the manifold is flat. However, in many applications it is necessary to perform calculus on curved manifolds. Therefore, in Section 2.1.3 we present a way to generalise some exemplary concepts from Section 2.1.2 to curved manifolds. The Section 2.1.3 is concluded with an illustrative example. Section 2.1.4 is a practitioner's dictionary between Geometric Calculus and the formalism of Differential Forms.

2.1.1 Geometric Algebra

Suppose we have defined an n -dimensional linear space L over the field of real numbers \mathbb{R} . Therefore, we know how to add vectors and multiply them by scalars. In this work the scalars are always assumed to be real. Let us now elaborate on different possibilities of defining the product of vectors.

⁵ Although not recent, as its foundations were published already in [11, e.g., paper XLIII, pp. 397–401]. However, after the authors death (at the age of 33) his ideas seemed to be not pursued by anyone. Please note that Clifford used the name "Geometric Algebra" for what is now often called "Clifford Algebra". Therefore, we find more appropriate to use the term "Clifford's Geometric Algebra" in order to tribute the inventor, without skipping the intention he devised the algebra for.

One possible choice is an inner (or dot, or scalar) product from linear algebra. It is defined by assuming that there is a symmetric bilinear form g , called later the *metric tensor*. If⁶ [19, Section 2.4]

$$g : L \times L \rightarrow \mathbb{R}, \quad (a, b) \mapsto g(a, b) = g(b, a) \quad (2.1)$$

$$[\forall b \in L, g(a, b) = 0] \Leftrightarrow a = 0, \quad (2.2)$$

then the inner product of vectors $a, b \in L$ is just

$$a \cdot b := g(a, b). \quad (2.3)$$

This product inherits the symmetry property from the symmetry of the bilinear form g .

Let us recall of any product that is antisymmetric. The cross product in 3D vector algebra is antisymmetric, i.e., $a \times b = -b \times a$. However, the cross product is defined only in $n = 3$ dimensions. Please also note that it is *not* associative, i.e., $(a \times b) \times c \neq a \times (b \times c)$.

Assume that the antisymmetric product of vectors has been defined, see [49, Chapter 4.3], [24, Chapter A.1.6] or [19, Chapter 5.2], in a mathematically precise way. Let us assume that it is associative and distributive over addition. We will call it the *exterior* (or wedge) product⁷ and denote by⁸

$$a \wedge b \equiv -b \wedge a \quad \Leftrightarrow \quad a \wedge a \equiv 0. \quad (2.4)$$

Of course, we have not yet specified what actually *is* the value of the exterior product $a \wedge b$; for the moment it is only important to accept that this product exists and is antisymmetric.

Now we have two products: one symmetric and the other one antisymmetric. Therefore, we can postulate the existence of yet another product, whose symmetric and antisymmetric parts are inner and exterior products, respectively. That means⁹

$$\begin{cases} a \cdot b \equiv \frac{1}{2}(ab + ba) \\ a \wedge b \equiv \frac{1}{2}(ab - ba) \end{cases} \quad \Leftrightarrow \quad ab \equiv a \cdot b + a \wedge b. \quad (2.5)$$

We have not used any special symbol to denote the new product ab , which we call the *geometric product*. That is due to two reasons; first, it will be the default product of our algebra; second, it is the extension of the product of real numbers in the sense that it is, for generic elements A, B, C of GA called multivectors,

$$\begin{aligned} (AB)C &= A(BC), && \text{(associative)} \\ A(B + C) &= AB + AC, && \text{(left-distributive)} \\ (A + B)C &= AC + BC, && \text{(right-distributive)} \end{aligned}$$

i.e., the only difference with respect to the product of real numbers is that it is in general

$$AB \neq BA. \quad \text{(noncommutative)}$$

However, there exist multivectors, e.g., scalars, for which $AB = BA$.

Parallel Vectors Commute. Assume that $a \in L$ and $b \in L$ are parallel¹⁰, i.e., $b = \lambda a$, $\lambda \in \mathbb{R}$, then the geometric product is commutative

$$ab = a \cdot b + a \wedge b = a \cdot b = b \cdot a = b \cdot a + b \wedge a = ba. \quad (2.6)$$

Orthogonal Vectors Anticommute. Now assume that a and b are orthogonal with respect to the metric tensor g , i.e., $a \cdot b = 0$. Then the geometric product is anticommutative

$$ab = a \cdot b + a \wedge b = a \wedge b = -b \wedge a = -b \cdot a - b \wedge a = -ba. \quad (2.7)$$

⁶ We require only non-degeneracy (2.2); the metric tensor can have mixed signature and thus there exist vectors $a \neq 0$ for which $g(a, a) = 0$. The “norm” associated with the metric tensor is actually a pseudo-norm, i.e., the property $g(a, a) = 0 \Leftrightarrow a = 0$ is skipped. We do not assume that the metric tensor is positive definite, which is a root of some complications, e.g., dealing with pseudo-norm rather than norm.

⁷ The reader familiar with the exterior algebra of differential forms, please be informed that that the exterior product is the same, i.e., isomorphic to, the product from that algebra. See also Section 2.1.4

⁸ By \equiv we mean $[a \wedge a \equiv 0] \Leftrightarrow [\forall a \in L, a \wedge a = 0]$.

⁹ We use the same symbol $+$ for addition of real numbers and elements of GA. This stems from the fact, as will be explained later, that GA is a factor algebra of general tensor algebra. Thus, we follow the common practice to use the same symbol for addition in factor and original algebra, although they, strictly speaking, are different mathematical operations. We would like to point the analogy to complex numbers; one also uses the same symbol for addition of complex and real numbers. Moreover, two complex numbers 1 and i cannot be added “explicitly” to produce “one” number; the result of addition is just $1 + i$, and cannot be further simplified. The same holds true in GA for, e.g., sum of a scalar and (bi)vector; it cannot be further simplified.

¹⁰ The consequence is that $a \wedge b = a \wedge (\lambda a) = \lambda a \wedge a = 0$

The fact that the geometric product of vectors ab is commutative or anticommutative depending on the colinearity or orthogonality of vectors is an example of a characteristic feature of geometric algebra: the algebraic properties and operations are directly related to geometric properties and operations.

Division by a Vector. Suppose $a \cdot a \neq 0$. Then there exists the inverse of the vector a given by¹¹

$$a^{-1} := \frac{a}{a^2}, \quad (2.8)$$

where¹²

$$a^2 = aa = a \cdot a + a \wedge a = a \cdot a + 0 = g(a, a) \neq 0. \quad (2.9)$$

One can easily verify that a^{-1} such defined is indeed an inverse of a

$$a^{-1}a = aa^{-1} = 1. \quad (2.10)$$

The Magnitude of a Bivector; Interpretation of the Exterior Product. Please note that in linear algebra the pseudo-norm, with respect to the metric tensor g , of a vector a is usually defined as

$$\|a\| = \sqrt{|g(a, a)|}. \quad (2.11)$$

This is equal to

$$\|a\| = \sqrt{|g(a, a)|} = \sqrt{|a \cdot a|} = \sqrt{|a^2|}. \quad (2.12)$$

Therefore, we can try to investigate the “norm” of a bivector¹³ $a \wedge b$, see [14, Equation (2.15)]. First, note that¹⁴

$$\begin{aligned} (a \wedge b)(a \wedge b) &= -(ab - a \cdot b)(ba - b \cdot a) = -(abba + (a \cdot b)^2 - (a \cdot b)ab - (a \cdot b)ba) = \\ &= -\left(a^2b^2 + (a \cdot b)^2 - 2(a \cdot b)\frac{1}{2}(ab + ba)\right) = -(a^2b^2 + (a \cdot b)^2 - 2(a \cdot b)^2) = \\ &= -(a^2b^2 - a^2b^2 \cos^2 \alpha) = -a^2b^2 \sin^2 \alpha, \end{aligned} \quad (2.13)$$

where α is the angle between the vectors a and b . Consequently, the “norm” of $a \wedge b$ is (cf. (2.12))

$$\|a \wedge b\| = \sqrt{|(a \wedge b)^2|} = \|a\| \|b\| |\sin \alpha|, \quad (2.14)$$

which is the area of the parallelogram spanned by the vectors a and b . As discussed in, e.g., [49, Section 4.3, especially Equation (4.41)], the exterior product of p vectors

$$V_p := a_1 \wedge a_2 \wedge \cdots \wedge a_p \quad (2.15)$$

describes an oriented p -dimensional volume of a p -parallelotope spanned by the vectors a_i , $i = 1, 2, \dots, p$.

The exterior product of p -vectors in (2.15) is called a p -blade. Any sum of p -blades

$$A_p := \sum_k V_p^k \quad (2.16)$$

is called a p -vector. A general element of Geometric Algebra can be written as a sum of blades¹⁵

$$A = \sum_{p=0}^n A_p, \quad (2.17)$$

¹¹ The notation $\frac{1}{a}$ is avoided as in non-commutative algebras $(ab)^{-1} \neq a^{-1}b^{-1}$, thus in general $\frac{1}{ab} \neq \frac{1}{a} \frac{1}{b}$, which might be confusing.

¹² Please note that we need to assume that the vector is not only non-zero, $a \neq 0$, but non-null, i.e., $a^2 \neq 0$, to be invertible. This does not follow from the non-degeneracy of the metric tensor g . We could omit this assumption if the metric tensor was positive definite; then it would be sufficient to assume that the vector is non-zero, $a \neq 0$, as in positive definite case the only null vector is the zero vector. However, this is not the case in this thesis. In other words, in our case there are vectors $a \neq 0$ that are not invertible.

¹³ We refrain ourselves from defining the norm of a general multivector; this is not trivial and not necessary for the sequel of this thesis.

¹⁴ Please note that, e.g., $abba = ab^2a = ag(b, b)a = a^2g(b, b) = a^2b^2 = aabb$, where we used the fact that $a^2 \in \mathbb{R} \ni b^2$ is a scalar and commutes with everything. Such manipulations are carried out in this thesis without explicit commenting on that.

¹⁵ This consequence is often exploited in computer implementations, see Appendix A.1

where n is the dimension of L . The p -vector A_p in this decomposition is called the p -grade¹⁶ component of A . We define the grade projector $\langle \rangle_p$ that extracts the p -grade component of A

$$\langle A \rangle_p := A_p. \quad (2.18)$$

Thus by definition for any multivector A it holds

$$A \equiv \sum_{p=0}^n \langle A \rangle_p. \quad (2.19)$$

The Exterior Product of Arbitrary Multivectors. For the sake of mathematical precision, we define the outer product of arbitrary blades

$$A_p \wedge B_q := \langle A_p B_q \rangle_{p+q}. \quad (2.20)$$

This definition is extended to arbitrary multivectors by exploiting the distributivity of the exterior product over addition.

The inner product of arbitrary multivectors. In opposition to the outer product, the generalisation of the inner one to arbitrary multivectors is not unique, see [15] for the explanation and a few alternative extensions. However, for the purpose of this work we adopt the definition for blades

$$A_p \cdot B_q := \begin{cases} \langle A_p B_q \rangle_{|p-q|} & p \neq 0 \neq q \\ 0 & p = 0 \vee q = 0 \end{cases} \quad (2.21)$$

and extend to generic multivectors by distributivity.

The Definition of the Geometric Product. So far we have investigated the properties of the geometric product and defined other concepts in terms of it. However, we have not yet *defined* what it actually is. The approach of defining the geometric products via axioms [14, 25, 49] has a drawback as it should be additionally shown that the geometric product is well defined. Fortunately, we can define Clifford's GA as a factor-algebra of tensor algebra built on our linear space L as explained in [19, Section 22.1].

Let us elaborate on this fact. The purpose of this elaboration is twofold. First, it should be indicated that the two approaches, namely axiomatic and factorisation one, are equivalent. Secondly, we would like to motivate the concept of factorisation of an algebra with respect to an ideal¹⁷.

In [19, Section 22.1, pp. 638] it is stated that the GA is obtained by factorisation of the tensor algebra with respect to the ideal generated by elements of the form¹⁸

$$a \otimes a - g(a, a), \quad (2.22)$$

which is equivalent to requiring that the product in factor-algebra (our desired GA) obeys

$$\forall a \in L, aa = g(a, a). \quad (2.23)$$

Please note that in [19, Exercise 22.1.1 (ii)] it is mentioned that the same ideal (thus the same factor-algebra is obtained) is generated by elements of the form

$$a \otimes b + b \otimes a - 2g(a, b), \quad (2.24)$$

which is equivalent to postulating the axiom

$$\forall a, b \in L, \frac{1}{2}(ab + ba) = g(a, b). \quad (2.25)$$

Since both ideals are the same, then both corresponding axioms should be equivalent as well. This is in agreement with what is usually exploited in GA literature. First, assume that the square of a vector is a real scalar, as done, e.g., in [14, Section 4.1], i.e.,

$$a^2 = g(a, a). \quad (2.26)$$

¹⁶ The term "grade" is a bit unfortunate as it does not coincide with the grade of the algebra from the context of abstract algebra. The grade of GA in that sense is 2. Or being more precise, GA has "plus modulo 2" grading.

¹⁷ The reader scared by the name "factorisation of an algebra with respect to an ideal", please be informed that this is just a very abstract way of requiring that some algebraic identity holds as an axiom in resultant algebra.

¹⁸ For the simplicity of presentation we have replaced the dual space L^* by L , as we have not introduced the dual space at all. See also Section 2.1.4.

Then by letting $a \rightarrow a + b$ we obtain by using bilinearity and symmetry of g that the following should be equal

$$a^2|_{a \rightarrow a+b} = (a + b)^2 = (a + b)(a + b) = a^2 + b^2 + ab + ba = g(a, a) + g(b, b) + ab + ba \quad (2.27)$$

$$g(a, a)|_{a \rightarrow a+b} = g(a + b, a + b) = g(a, a) + g(b, b) + 2g(a, b), \quad (2.28)$$

which means

$$\frac{1}{2}(ab + ba) = g(a, b). \quad (2.29)$$

Conversely, if this holds, then by letting $a = b$ above we see

$$g(a, a) = \frac{1}{2}(aa + aa) = a^2. \quad (2.30)$$

Thus we see that the **axiomatic statement**: both axioms are equivalent

$$a^2 = g(a, a) \iff \frac{1}{2}(ab + ba) = g(a, b), \quad (2.31)$$

is a translation of the **abstract algebraic statement**:

$$[\text{Ideal generated by } a \otimes a - g(a, a)] = [\text{Ideal generated by } a \otimes b + b \otimes a - 2g(a, b)]. \quad (2.32)$$

Pseudoscalar. Note that the summation in (2.17) extends only up to n . The reason is that one cannot construct a non-zero p -blade, with $p > n$. This comes from the fact that if vectors a_i in (2.15) are linearly dependent, then V_p is zero due to antisymmetry of the exterior product, and in n -dimensional space L one can find at most n linearly independent vectors. Geometrically it means that one cannot construct a p -dimensional, with $p > n$, volume in n -dimensional space.

Moreover, all n -vectors are similar in the sense that they are all multiplicity of each other, i.e., for arbitrary A'_n and A_n one can find a unique $\lambda \in \mathbb{R}$ such that

$$A'_n = \lambda A_n. \quad (2.33)$$

Therefore, all n -vectors can be expressed as a scalar multiple of some chosen n -vector. The natural choice is a unit n -vector; by unit we mean that¹⁹ $|A_n^2| = 1$. However, the choice of this n -vector is not yet unique; there are two unit n -vectors, I_1 and I_2 , related via $I_2 = -I_1$. They correspond to the two possible orientations of the space L , see [19, Section 5.5] or [24, Section A.1.8] for the definition of the orientation. Choosing one of them is thus equivalent to choosing the orientation of the underlying linear space L . The chosen one is denoted by I and called the *pseudoscalar*²⁰.

Once an ordered set of basis vectors $\gamma_k \in L$, $k = 1, \dots, n$ is given, the pseudoscalar is uniquely defined via

$$I := \frac{\gamma_1 \wedge \dots \wedge \gamma_n}{\sqrt{|(\gamma_1 \wedge \dots \wedge \gamma_n)^2|}}. \quad (2.34)$$

Reciprocal Basis. The basis vectors of L are denoted by γ_i , $i = 1, \dots, n$. The reciprocal basis γ^i is defined by requiring that

$$\gamma_j \cdot \gamma^i = \delta_j^i, \quad i, j = 1, \dots, n. \quad (2.35)$$

¹⁹ As A_n is a blade, thus $A_n^2 \in \mathbb{R}$ and it is sufficient to write $|A_n^2| = 1$ as the norm without introducing the norm of general multivectors. We want to stress that the norm $|A_n^2|$ of a blade A_n follows from the metric tensor and absolute value of real numbers. However, the norm of a general multivector requires additional definitions, thus it is skipped in this work. Let us investigate the square of an n -blade A_n^2 . First, note that an n -blade is (by definition) the exterior product of n vectors a'_i and can be expressed as the geometric product of (e.g. Gram-Schmidt) orthogonalised vectors a_i

$$A_n = a'_1 \wedge a'_2 \wedge \dots \wedge a'_n = a_1 a_2 \dots a_n.$$

Second, the square of a blade is a scalar and its value is determined by the metric tensor

$$A_n^2 = (a_1 a_2 \dots a_n)(a_1 a_2 \dots a_n) = (a_1 a_2 \dots a_n)(a_n \dots a_2 a_1)(-1)^{n(n-1)/2} = (-1)^{n(n-1)/2} \prod_{i=1}^n a_i^2 = (-1)^{n(n-1)/2} \prod_{i=1}^n g(a_i, a_i) \in \mathbb{R}.$$

²⁰ Sometimes in the literature the word “pseudoscalar” refers to any n -vector, and I is referred to as “unit pseudoscalar”. However, here we follow the nomenclature of [14, Equation (4.67)], namely the word “pseudoscalar” means the chosen unit n -vector and it is unique.

Let us solve (2.35) for γ^i using first geometric and successively algebraic reasoning. The equation (2.35) requires that the vector γ^i is orthogonal to all basis vectors $\gamma_j, j \neq i$ except γ_i . First, we construct the $(n-1)$ -blade corresponding to a parallelepiped contained in the hyperplane spanned by all basis vectors except γ_i

$$\gamma_1 \wedge \cdots \wedge \check{\gamma}_i \wedge \cdots \wedge \gamma_n. \quad (2.36)$$

Above, by a check mark above the symbol we mean that it is omitted in the product, e.g., $\gamma_1 \wedge \cdots \wedge \check{\gamma}_3 \wedge \cdots \wedge \gamma_5 = \gamma_1 \wedge \gamma_2 \wedge \gamma_4 \wedge \gamma_5$. Then we use the fact that multiplication by the pseudoscalar I gives a multivector associated with the subspace orthogonal to the original object. Thus the vector

$$\gamma^i := \lambda \gamma_1 \wedge \cdots \wedge \check{\gamma}_i \wedge \cdots \wedge \gamma_n I \quad (2.37)$$

is by construction orthogonal to all $\gamma_j, j \neq i$. We will determine the normalisation factor λ in an algebraic way, namely we substitute our postulated reciprocal basis vector γ^i in (2.35) and use the basic identity [14, Equation (4.69)] $a \cdot (A_r I) = (a \wedge A_r) I$

$$\gamma_j \cdot (\lambda \gamma_1 \wedge \cdots \wedge \check{\gamma}_i \wedge \cdots \wedge \gamma_n I) = \lambda (\gamma_j \wedge \gamma_1 \wedge \cdots \wedge \check{\gamma}_i \wedge \cdots \wedge \gamma_n) I. \quad (2.38)$$

We see that our geometric construction was correct, namely if $j \neq i$, then the product above is zero due to antisymmetry. Therefore, we only need to consider the case $j = i$, i.e., make sure that the result is equal to $\delta_i^i = 1$ for $j = i$. This reads

$$\lambda (\gamma_i \wedge \gamma_1 \wedge \cdots \wedge \check{\gamma}_i \wedge \cdots \wedge \gamma_n) I = \lambda (-1)^{i-1} (\gamma_1 \wedge \cdots \wedge \gamma_n) I = \lambda (-1)^{i-1} \sqrt{|\gamma_1 \wedge \cdots \wedge \gamma_n|^2} I^2 = 1. \quad (2.39)$$

This will hold for (please recall that $I^2 = \pm 1$)

$$\lambda := \frac{(-1)^{i-1} I^2}{\sqrt{|\gamma_1 \wedge \cdots \wedge \gamma_n|^2}}, \quad (2.40)$$

where the inverse of the square root happens to be

$$\frac{1}{\sqrt{|\gamma_1 \wedge \cdots \wedge \gamma_n|^2}} = \frac{1}{\sqrt{|\text{Det } g|}} = \sqrt{|\text{Det } g^{ij}|} = \frac{1}{\sqrt{|\text{Det } g_{ij}|}}, \quad (2.41)$$

with $\text{Det } g$ being the determinant of the metric tensor. For the reference we mention that it follows that

$$\sqrt{|\gamma^1 \wedge \cdots \wedge \gamma^n|^2} = \sqrt{|\text{Det } g^{ij}|} = \frac{1}{\sqrt{|\text{Det } g|}}. \quad (2.42)$$

By this considerations we have derived the analogous expression to [14, Equation (6.41)].

Definition 1. The geometric algebra build on linear space L and using metric tensor g is denoted by $\mathcal{G}(L, g)$

2.1.2 Geometric Calculus

Up to now, all the concepts we introduced are purely algebraic and could be performed point-wise, i.e., the GA at each point of the manifold was completely independent of the other points. However, physical processes are often modelled by integral or differential equations, thus we will introduce geometric calculus now.

The differential operators of traditional 3D vector calculus are usually introduced by defining the nabla vector in Cartesian coordinates

$$\nabla = [\partial_x, \partial_y, \partial_z] \quad (2.43)$$

and then transformed to other coordinates if necessary. Then as a consequence one can prove some well-known integral theorems. For example, let V be a compact 3D domain of volume $|V|$ with piecewise smooth and orientable boundary ∂V on a flat 3D manifold, e.g., $V \subset \mathbb{R}^3$, and $\phi : V \rightarrow \mathbb{R}$ be a piecewise continuously differentiable scalar field; then it can be shown that²¹

$$\int_V \nabla \phi dV = \int_{\partial V} \phi d\vec{S}. \quad (2.44)$$

²¹ By exploiting, e.g., generalised Stokes theorem presented in [24, Section A.3.4] or [19, Chapter 7.5].

One can, however, use this identity to **define** a gradient

$$\nabla\phi(x) := \lim_{V \rightarrow x} \frac{1}{|V|} \int_{\partial V} \phi d\vec{S}, \quad (2.45)$$

where $|V| \rightarrow 0$ as the volume V is contracted to the point x .

The benefit of defining the derivative as a limit of an integral is twofold. First, all integral theorems are straightforward consequences of the definition. Second, (2.45) is explicitly coordinate-free. This fits into the overall philosophy of GA; the definitions should be coordinate-free and geometrically meaningful, while at the same time expanding and using them in particular coordinates should be easy as well. Therefore, we first introduce integration in GA and define the geometric derivative in terms of that as proposed in [27, 50].

For the purpose of this thesis it is sufficient to study geometric calculus in flat, pseudo-Euclidean space²² as carried out in [50]. Thus we will start with that and discuss later the possibilities of extension of that framework to curved spaces. This attempt is motivated by an

Open research question 1. *There are some mathematical difficulties, e.g., with the precise definition of a multivector-valued integral, in curved space. However, if that was overcome, then it would be expected that all the steps carried out in this work can be repeated for a general non-flat metric which corresponds to solving the electromagnetic field equations in a background gravitational field. Under which conditions the computational method developed here can be applied to curved spaces?*

Let K_r be an r -dimensional hypersurface. The geometric differential on K_r is defined as

$$d^r x := e_1 \wedge \cdots \wedge e_r dx^1 \dots dx^r, \quad (2.46)$$

where dx^i are scalar differentials (known from real analysis) of the coordinate functions $x^i(x)$ and e_i are tangent vectors (2.87) associated with that coordinates. Please note that e_i span the tangent space of the hypersurface K_r at given point $x \in K_r$, and thus $e_1 \wedge \cdots \wedge e_r$ is a (non-unit) pseudoscalar of the hypersurface K_r , compare [50, Equation (3.4)].

We define the integral of a multivector field A , by first expanding the multivector integrand $d^r x A$ in some Cartesian basis,²³ i.e., all derivatives of basis vectors vanish,

$$(e_1 \wedge \cdots \wedge e_r)A =: \sum_{q=0}^n \chi^{i_1 \dots i_q} \gamma_{i_1} \dots \gamma_{i_q}. \quad (2.47)$$

We assume that χ 's are integrable functions on \mathbb{R}^n . Then the integral should be understood as

$$\int_{K_r} d^r x A := \sum_{q=0}^n \left[\int_{K_r} \chi^{i_1 \dots i_q} dx^1 \dots dx^r \right] \gamma_{i_1} \dots \gamma_{i_q}, \quad (2.48)$$

with the real-valued integrals defined, e.g., as the limit of a sum as is usually done in traditional multivariable calculus of real functions. In general, the integrand $(e_1 \wedge \cdots \wedge e_r)A$ is not a scalar, thus one needs to define how to transport non-scalar quantities (in order to sum them up). This issue is, however, irrelevant at the moment as we restricted ourselves to flat pseudo-Euclidean space (the connection is flat, i.e., the curvature is zero) and defined the integral in terms of Cartesian basis, which is covariantly constant and thus trivial to transport.

As promised before, we start with the definition of the derivative as a limit of an integral and then move towards building some intuition. The definition, although mathematically more precise, is difficult to apply directly to calculate derivatives²⁴.

For the purpose of the thesis it is sufficient to employ the definition

$$\nabla A := \lim_{K_r \rightarrow x} (W_r)^{-1} \int_{\partial K_r} (d^{r-1} x) A, \quad (2.49)$$

where W_r is the multivector²⁵ representing K_r

$$W_r := \int_{K_r} (d^r x). \quad (2.50)$$

²² The 4D Minkowski space-time is an exemplary member of this class.

²³ As in flat space there always exist Cartesian bases.

²⁴ The same holds true for Riemann integrals. They are defined as a limit of a sum, but in analytic computations one uses antiderivatives rather than apply the definition directly to evaluate an integral.

²⁵ The “directed content of K_r ” in the language of [50].

See [50, Especially Equation (5.5)] for the more precise explanations and definitions.

Taking a practitioners perspective it is convenient that one does not need to recall the definition (2.49) in order to perform calculations involving the geometric derivative. This is due to the fact that the geometric derivative can be represented by [50, Equation (5.10)]

$$\nabla = \sum_{i=1}^n \gamma^i \partial_i. \quad (2.51)$$

Let us elaborate on what is γ^i above. Previously, we have introduced the geometric algebra build on some linear space L and γ^i were reciprocal basis vectors. Here, however, we deal with the whole manifold, i.e., infinitely many points, and it should be perceived that the GA is built at each point, thus basis vectors as well depend on the position on the manifold. In other words, as explained in [19, First paragraph of Section 2.5], to build the tensor algebra (thus GA, as it is a quotient algebra) on the manifold, one needs to use as the linear space L the tangent space at each point of a manifold²⁶. Since for the moment we have restricted our attention to flat manifolds, i.e., pseudo-Euclidean spaces, there is an affine structure available, thus there exists a position vector x , which can be identified with points on the manifold. Therefore, we can follow what is usually done in GA literature, e.g., [49, Equations (4.8), (4.10) and Section 5.2], [14, Section 6.2, especially Equation (6.30)] and [27]. We introduce coordinates x^i , $i = 1 \dots n$, by paramtrising the position vector

$$x = x(x^1, \dots, x^n) = x(x^i) \quad (2.52)$$

and the inverse functions give the scalar value of a coordinate as a function of position vector

$$x^i = x^i(x) \in \mathbb{R}. \quad (2.53)$$

Then the basis associated with these coordinates is given by

$$\gamma_i := \frac{\partial x}{\partial x^i} \quad (2.54)$$

and the reciprocal basis γ^i can be calculated using (2.37) and (2.40). Thus γ^i in (2.51) should be understood as constructed in that way.

1D Example: Length of a Line Segment. Let us investigate the geometric meaning of the integral. Let l be a line segment of length b parametrised by t

$$l : x = t\gamma_1, t \in [0, b], \quad (2.55)$$

where γ_1 is a unit vector. The multivector representing the line segment

$$\int_l d^1x = \int_0^b e_1 dx^1 = \int_0^b \frac{\partial x}{\partial t} dt = \gamma_1 \int_0^b dt = b\gamma_1 \quad (2.56)$$

has the magnitude equal to the length of the segment. Negative length represents the segment oriented oppositely to the basis vector γ_1 . Let us change the paramtrisation of the segment to $t' = t/a$

$$l : x = at'\gamma_1, t' \in [0, b/a] \quad (2.57)$$

and calculate again the multivector associated with it

$$\int_l d^1x = \int_0^{b/a} e_1 dx^1 = \int_0^{b/a} \frac{\partial x}{\partial t'} dt' = a\gamma_1 \int_0^{b/a} dt' = b\gamma_1. \quad (2.58)$$

Therefore, we see that the change of paramtrisation (which is equivalent to changing the coordinates) of the line segment does not change the multivector associated with it. This is an instance of the more general statement that all GA quantities are coordinate-free, i.e., they give the same value in every coordinate system.

1D Example: the Derivative. Let us explore (2.49) in 1D and $A = f$ being a scalar function. The boundary of the line segment

$$l : x = x_0 + t\gamma_1, t \in [0, h] \quad (2.59)$$

²⁶ This procedure will, however, not answer the question how to do calculus on the manifold. For that, additional structure is required, namely the connection.

is

$$\partial l = \{-x_0, x_0 + h\gamma_1\}, \quad (2.60)$$

where the minus sign comes from the fact that the point x_0 has a different orientation than the edge l . This comes into play, when evaluating integrals over points, which are defined to taking the value of the integrand at that point, but taking the orientation of a point into account. As a consequence

$$\int_{\partial l} d^0 x A(x) = \int_{-x_0} A(x) + \int_{x_0+h\gamma_1} A(x) = -A(x_0) + A(x_0 + h\gamma_1). \quad (2.61)$$

Thus the geometric derivative of a function $f(x)$ is according to (2.49)

$$\nabla f = \lim_{l \rightarrow x_0} \frac{1}{h\gamma_1} \int_{\partial l} d^0 x f = \lim_{h \rightarrow 0} \frac{f(x_0 + h\gamma_1) - f(x_0)}{h} \gamma_1^{-1} = f'(x_0) \gamma_1^{-1}. \quad (2.62)$$

Thus if we recall that γ_1 is unit, i.e., $\gamma_1^2 = 1 \Leftrightarrow \gamma_1^{-1} = \gamma_1$, then the length of ∇f is

$$|\nabla f| = f'(x). \quad (2.63)$$

Letting $A = A^1 \gamma_1$, we obtain analogously²⁷

$$\nabla A = \lim_{h \rightarrow 0} \frac{A^1(x_0 + h\gamma_1) - A^1(x_0)}{h} = \left. \frac{dA^1(x)}{dx} \right|_{x=x_0} \quad (2.64)$$

that the geometric derivative reduces to the one known from the real analysis.

2D Example: Complex Analysis. Here we will show how complex numbers and analysis emerge from a subalgebra of GA in 2D Euclidean plane. This example is inspired by [14, Sections 2.6.1 and 6.3.1] and [50, Equations (7.10)–(7.12)].

Suppose we are given a vector r in the 2D plane. We **define** the real axis as x -coordinate line. The induced unit basis vectors are e_x and e_y . Due to the fact that the basis is orthonormal, the basis vectors γ_i coincide with reciprocal basis γ^i , i.e.,

$$\gamma^1 = \gamma_1 = e_x \quad \gamma^2 = \gamma_2 = e_y. \quad (2.65)$$

Please note that we can define the real axis as any line in the plane, i.e., we can choose arbitrary unit vector instead of e_x . Then we identify the complex number z associated with r with

$$z = e_x r = e_x(xe_x + ye_y) = x + ye_x e_y = x + Iy. \quad (2.66)$$

First, we note that the 2D pseudoscalar $I := e_x e_y$ commutes with every complex number. Therefore, the algebra of complex numbers is commutative²⁸. Secondly, we see that its square is

$$I^2 = II = e_x e_y e_x e_y = -e_x e_x e_y e_y = -1. \quad (2.67)$$

Therefore, it is natural to identify I with the imaginary unit. The complex conjugate of z is $z^\dagger = r e_x$. Suppose we are given a complex function $f = u(x, y) + I v(x, y)$. Then we can state the Cauchy-Riemann equations as $\nabla f = 0$. We show it by expanding

$$\nabla f = (e_x \partial_x + e_y \partial_y)(u + I v) = e_x(\partial_x u - \partial_y v) + e_y(\partial_y u + \partial_x v) = 0 \quad (2.68)$$

and noting that the equations in brackets are exactly the Cauchy-Riemann equations. Therefore, $\nabla f = 0$ holds for all analytic functions f . The result is less surprising if we multiply this condition by e_x from the left and note that

$$e_x \nabla = e_x(e_x \partial_x + e_y \partial_y) = \partial_x + I \partial_y = \frac{\partial}{\partial x} - \frac{1}{I} \frac{\partial}{\partial y} = \frac{\partial}{\partial(x - Iy)} = \frac{\partial}{\partial z^\dagger} \quad (2.69)$$

²⁷ Without the assumption that the basis vector is unit $\gamma_1^2 = 1$

²⁸ This can be easily proven by taking two complex numbers $z_k = x_k + I y_k$, $k = 1, 2$ and showing $z_1 z_2 = (x_1 x_2 - y_1 y_2) + I(x_1 y_2 + x_2 y_1)$. In other words the basis of 2D GA is $\{1, e_x, e_y, I\}$, and the basis of a subalgebra isomorphic to complex numbers is $\{1, I\}$ in which all two elements commute, thus all the complex numbers commute.

Therefore, (2.68) is equivalent to more familiar property of analytic functions

$$\frac{\partial f}{\partial z^\dagger} = 0, \quad (2.70)$$

where in f we changed the coordinates from (x, y) to $z = x + Iy$ and $z^\dagger = x - Iy$.

Moreover, the residue theorem (see also 3D examples below) stated in [50, Equation (7.9)] reduces to Cauchy's integral formula

$$f(z_0) = \frac{1}{2\pi I} \int_{\partial K_2} \frac{f(z)}{z - z_0} dz, \quad (2.71)$$

provided f is analytic in a 2D region K_2 in complex plane.

Thus we see that complex analysis is a special case of geometric calculus, namely it is obtained by restricting the multivectors to be of the form $a + Ib$, with $a, b \in \mathbb{R}$, in 2D GA build on Euclidean metric.

The point we want to make is that operations on complex numbers have a clear geometric interpretation in the 2D plane and this remains a characteristic feature of GA in arbitrary dimensions.

2D Example: Geometric Derivative in Cartesian and Polar Coordinates. It is a common practice to **define** the geometric derivative via (2.51). By doing so, one may be anxious whether ∇ is a coordinate-free object, i.e., it is the same in every coordinate system. Let us compare ∇ in Cartesian and polar coordinate systems as an illustration.

In 2D Cartesian coordinates (x, y) we have $\gamma^i = \gamma_i$, $i = x, y$, and thus the geometric derivative of a vector field A is

$$\nabla A = (\gamma_x \partial_x + \gamma_y \partial_y)(A^x \gamma_x + A^y \gamma_y) = \partial_x A^x + \partial_y A^y + \gamma_x \gamma_y (\partial_x A^y - \partial_y A^x), \quad (2.72)$$

that is the scalar part of ∇A is a divergence of A and pseudoscalar (grade two) component is the z -th component of the curl of A .

Now we will obtain the analogous expression in polar coordinates. The position vector in polar coordinates r and φ is

$$x = r \cos \varphi \gamma_x + r \sin \varphi \gamma_y \quad (2.73)$$

and coordinate basis vectors are

$$\gamma_r = \frac{\partial x}{\partial r} = \cos \varphi \gamma_x + \sin \varphi \gamma_y, \quad \gamma_\varphi = \frac{\partial x}{\partial \varphi} = -r \sin \varphi \gamma_x + r \cos \varphi \gamma_y. \quad (2.74)$$

For convenience we introduce a unit azimuthal vector

$$\hat{\gamma}_\varphi := -\sin \varphi \gamma_x + \cos \varphi \gamma_y, \quad (2.75)$$

which enables us to write

$$\gamma_\varphi = r \hat{\gamma}_\varphi. \quad (2.76)$$

Using (2.37) we find

$$\gamma^r = \gamma_r, \quad \gamma^\varphi = \frac{1}{r} \hat{\gamma}_\varphi. \quad (2.77)$$

First, we calculate

$$\partial_r \gamma_r = 0, \quad \partial_r \hat{\gamma}_\varphi = 0, \quad \partial_\varphi \gamma_r = \hat{\gamma}_\varphi, \quad \partial_\varphi \hat{\gamma}_\varphi = -\gamma_r \quad (2.78)$$

and use it in expanding the geometric derivative in polar coordinates

$$\nabla A = (\gamma^r \partial_r + \gamma^\varphi \partial_\varphi)(A^r \gamma_r + A^\varphi \hat{\gamma}_\varphi) = (\gamma_r \partial_r + \frac{1}{r} \hat{\gamma}_\varphi \partial_\varphi)(A^r \gamma_r + A^\varphi \hat{\gamma}_\varphi) = \quad (2.79)$$

$$= \gamma_r \partial_r (A^r \gamma_r) + \gamma_r \partial_r (A^\varphi \hat{\gamma}_\varphi) + \frac{1}{r} \hat{\gamma}_\varphi \partial_\varphi (A^r \gamma_r) + \frac{1}{r} \hat{\gamma}_\varphi \partial_\varphi (A^\varphi \hat{\gamma}_\varphi) = [\text{use of (2.78)}] = \quad (2.80)$$

$$= \partial_r A^r + \frac{1}{r} A^r + \frac{1}{r} \partial_\varphi A^\varphi + \gamma_r \hat{\gamma}_\varphi \left(\partial_r A^\varphi - \frac{1}{r} \partial_\varphi A^r + \frac{1}{r} A^\varphi \right). \quad (2.81)$$

Again we see that the scalar and pseudoscalar components are divergence and z -th component of curl, respectively, but now expressed in polar coordinates.

To conclude this example; we have shown that the formula (2.51) is valid in both Cartesian and polar coordinates. That is in contrast in what is often done in textbooks, where the differential operators are defined in Cartesian coordinates and expressions in different coordinates are obtained by means of transforming these operators. In other words the basic textbook reasoning may be sketched as

$$\nabla \Rightarrow \text{Cartesian coordinates} \Rightarrow \text{Arbitrary coordinates}, \quad (2.82)$$

while GA reasoning looks rather like

$$\text{Cartesian coordinates} \Leftarrow \nabla \Rightarrow \text{Arbitrary coordinates}, \quad (2.83)$$

i.e., the expressions in Cartesian and polar coordinate system stem as special cases from a coordinate-free²⁹ expression (2.51).

3D Example: Helmholtz Theorem as a Special Case of the Residue Theorem. The geometric derivative of a vector field A in Cartesian coordinates reads³⁰

$$\nabla A = \nabla \cdot A + \nabla \wedge A = \partial_x A^x + \partial_y A^y + \partial_z A^z + \gamma_x \gamma_y (\partial_x A^y - \partial_y A^x) + \gamma_y \gamma_z (\partial_y A^z - \partial_z A^y) + \gamma_z \gamma_x (\partial_z A^x - \partial_x A^z) \quad (2.84)$$

from which we see that it is a combination of divergence and curl of A . Helmholtz theorem [22, Appendix B] says that if we prescribe the divergence and curl (accompanied by proper boundary conditions) of a vector field on a bounded 3D domain, then the field A is uniquely determined. But prescribing divergence and curl is equivalent to prescribing the geometric derivative of the field. Therefore, according to Helmholtz theorem, the operator ∇ should be invertible³¹ in the resemblance to non-null vectors in GA. This is in accordance with the residue theorem in n -dimensional Euclidean space [50, Equation (7.9)], namely it expresses the value of $A(x)$ in terms of ∇A and the values of A at the boundary of some region.

2.1.3 Calculus in Curved Spaces

So far we have restricted our considerations to flat pseudo-Euclidean spaces. The study of calculus in curved spaces is important as it arises in many applications. For example, in the general relativity theory all physics laws are described as intrinsic equations in curved space-time treated as a pseudo-Riemannian manifold, whose metric tensor models the influence of gravitation. As yet another example let us mention that Boundary Element Method [45, 52] is a computational method, which starts from equations intrinsic to the boundary of a computational domain, which in general is a curved manifold. While switching to curved manifolds, the whole algebraic part remains the same: we build the geometric algebra $\mathcal{G}(L, g)$ taking the tangent space as L and the metric tensor g at each point separately. Nevertheless, the calculus part changes as the connection may have non-vanishing curvature, see [24, Equation (C.1.44)], [49, Section 5.5] or [27, Section 19.6].

One possible solution would be to repeat the work done in [50] starting from space-dependent metric and non-flat connection. This is, however, non-trivial as in curved spaces there is no position vector [24, Section C.1.6] available and the definition of the integral [50, Equation (4.1)] implicitly assumes that the connection is flat. Due to these mathematical complications we will follow a different reasoning.

Another possibility presented in [49, Section 5.2], [27] and [14, Section 6.5] is to treat the curved manifold as an n -dimensional surface embedded in a higher dimensional flat pseudo-Euclidean space. As shown in [36, Theorem 2], this is always possible in such a way that the metric on the manifold is induced by the pseudo-Euclidean metric of the $2n + 1$ dimensional ambient space. Then, heuristically speaking, the traditional calculus of differential geometry is obtained by restricting all considerations to the objects lying completely in the surface (the vector manifold).

Since in the following we deal with the vector manifold itself as well as the embedding space, we will denote all quantities associated with the ambient space by a bar over a symbol. Moreover, Greek indices run from 1 to n and Latin

²⁹ By “coordinate-free”, we mean that it is the same object in every coordinate system and coordinates might be used in the definition. By “explicitly coordinate-free” we mean that it is not only coordinate-free, but also the definition does not involve any coordinates.

³⁰ In the first equality we formally used the property (2.5) of vectors applied to the case when one vector is replaced by the operator ∇ . This property is inherited by ∇ from the basis vectors γ_i . As explained in [50] the operator ∇ is invariant with respect to change of coordinates. Thus we can expand it in Cartesian coordinates for which $\partial_i \gamma_j = 0$ holds. Then it can be proven that

$$\nabla A = (\gamma^i \partial_i) (A^j \gamma_j) = \gamma^i \gamma_j \partial_i A^j = (\gamma^i \cdot \gamma_j + \gamma^i \wedge \gamma_j) \partial_i A^j = (\gamma^i \partial_i) \cdot (A^j \gamma_j) + (\gamma^i \partial_i) \wedge (A^j \gamma_j) = \nabla \cdot A + \nabla \wedge A.$$

³¹ The inverse of ∇ turns out to be an integral operator, which cannot be constructed neither algebraically nor locally. Therefore, this is an example that not all properties of vectors are inherited by ∇ .

ones from 1 to m ; with m being the dimension of the ambient space. As the embedding space is flat, there exists a unique position vector associated with each point, e.g., in m -dimensional Cartesian or spherical coordinates,

$$\bar{x} = \sum_{k=1}^m \bar{x}^k \bar{\gamma}_k = \bar{r} \bar{\gamma}_r, \quad (2.85)$$

with $\bar{r} = \sqrt{\sum_{k=1}^m (\bar{x}^k)^2}$ and $\bar{\gamma}_r$ a unit radial vector.

Suppose the points on the n -dimensional manifold are parametrised by n coordinates x^α

$$\bar{x} = \bar{x}(x^1, x^2, \dots, x^n) = \bar{x}(x^\alpha). \quad (2.86)$$

Then, due to existence of the position vector \bar{x} , the definition (2.54) can be directly applied to calculate the (covariant) coordinate basis γ_α

$$\gamma_\alpha = \frac{\partial \bar{x}}{\partial x^\alpha}. \quad (2.87)$$

Having the coordinate basis, the reciprocal basis and the pseudoscalar can be computed using (2.37) and (2.34)³². Once the position dependent pseudoscalar of the vector manifold is in place, we define the projector onto the manifold, [14, Equation (6.194)]³³ (also briefly mentioned in [27, second paragraph of 19.6]),

$$A_r := P(\bar{A}_r(x), x) = \begin{cases} \bar{A}_r(x) \cdot I(x) I^{-1}(x), & r \leq n \\ 0, & r > n \end{cases}, \quad (2.88)$$

where by x we emphasise that this is the position vector $\bar{x}(x^\alpha)$ of points belonging to the manifold. Therefore, studying intrinsic geometry involves only the projected quantities, namely the ones for which

$$A = P(A), \quad (2.89)$$

which comes from the idempotence of the projector, i.e., $P^2 = P$. The geometric derivative ∇ intrinsic to the manifold is just the projection of the ambient derivative $\bar{\nabla}$, see [14, Equation (6.198)]

$$\nabla := P(\bar{\nabla}) = \sum_{\alpha=1}^n \gamma^\alpha \gamma_\alpha \cdot \bar{\nabla} = \sum_{\alpha=1}^n \gamma^\alpha \partial_\alpha. \quad (2.90)$$

Now we are at the point to define the *intrinsic covariant geometric derivative*

$$\partial A := P[P(\bar{\nabla})P(A)], \quad (2.91)$$

whose name we shall motivate in the following. We would like to stress the presence of the additional projection despite both quantities in (2.91) are already projected. Let us elaborate on this issue in the case $A = a = P(a)$ is a vector projected onto the manifold. Then we see that the intrinsic derivative of a

$$P(\bar{\nabla})P(a) = \nabla a = \gamma^\alpha \partial_\alpha (a^\beta \gamma_\beta) = \partial_\alpha a^\beta \gamma^\alpha \gamma_\beta + a^\beta \gamma^\alpha \partial_\alpha \gamma_\beta \quad (2.92)$$

splits into two terms; the first one is explicitly intrinsic to the manifold as it involves only the geometric product of intrinsic basis vectors; the other one, however, contains derivatives of basis vectors $\partial_\alpha \gamma_\beta$, whose values are not necessarily intrinsic as explained below. Extending [49, Equation (5.14)] to n -dimensional manifold yields

$$\partial_\alpha \gamma_\beta = \Gamma_{\alpha\beta}^\gamma \gamma_\gamma + h_{\alpha\beta} p, \quad (2.93)$$

where Christoffel symbols

$$\Gamma_{\alpha\beta}^\gamma := \gamma^\gamma \cdot (\partial_\alpha \gamma_\beta) \quad (2.94)$$

and vector p is orthogonal to the manifold, i.e.,

$$I(x) \cdot p = 0 \implies P(p) = 0. \quad (2.95)$$

³² For a coordinate-free definition of the pseudoscalar see [50, Equation (3.4)].

³³ The split into two cases if r is greater or less than n can be avoided by using the left contraction [15, Equation (2.6)] instead of our scalar product. However, we prefer to avoid introducing multiple inner products.

As a consequence

$$P[\partial_\alpha \gamma_\beta] = P[\Gamma_{\alpha\beta}^\gamma \gamma_\gamma] + P[h_{\alpha\beta} P] = \Gamma_{\alpha\beta}^\gamma \gamma_\gamma + 0. \quad (2.96)$$

Therefore, the covariant geometric derivative reads

$$P[\nabla P(a)] = P[\partial_\alpha a^\beta \gamma^\alpha \gamma_\beta] + P[a^\beta \gamma^\alpha \partial_\alpha \gamma_\beta] = \partial_\alpha a^\beta \gamma^\alpha \gamma_\beta + a^\beta \gamma^\alpha P[\partial_\alpha \gamma_\beta] = (\partial_\alpha a^\beta + \Gamma_{\alpha\gamma}^\beta a^\gamma) \gamma^\alpha \gamma_\beta \quad (2.97)$$

from which we see that its components are equal to components of what is defined as covariant derivative in standard textbooks. Clearly, the scalar part of ∂a is a covariant divergence, while the bivector part can be perceived as the generalisation of curl to n -dimensions and can be related to the exterior derivative³⁴ [24, Section A.2.7].

Intrinsic and Extrinsic Calculus on a 1D Circle Embedded in 2D Euclidean Plane. To illustrate the concepts concerning calculus on curved manifolds, we will study the parallel transport on the circle. The circle of radius r embedded in flat 2D Euclidean space with coordinates (x, y) is given by the position vector (2.86)

$$\bar{x}(\varphi) = r \cos \varphi \gamma_x + r \sin \varphi \gamma_y, \quad \varphi \in [0, 2\pi). \quad (2.98)$$

Since the circle is a 1D manifold, the basis (2.87) consists of just one vector

$$\gamma_\varphi = \frac{\partial \bar{x}}{\partial \varphi} = -r \sin \varphi \gamma_x + r \cos \varphi \gamma_y = r \hat{\gamma}_\varphi, \quad (2.99)$$

where for convenience we have defined the unit basis vector

$$\hat{\gamma}_\varphi := \frac{\gamma_\varphi}{|\gamma_\varphi|} = \frac{\gamma_\varphi}{r} = -\sin \varphi \gamma_x + \cos \varphi \gamma_y. \quad (2.100)$$

The reciprocal basis vector (2.37) is

$$\gamma^\varphi = \frac{1}{r} \hat{\gamma}_\varphi, \quad (2.101)$$

which clearly satisfies (2.35)

$$\gamma^\varphi \cdot \gamma_\varphi = \left(\frac{1}{r} \hat{\gamma}_\varphi \right) \cdot (r \hat{\gamma}_\varphi) = (-\sin \varphi \gamma_x + \cos \varphi \gamma_y)^2 = \sin^2 \varphi + \cos^2 \varphi = 1 = \delta_\varphi^\varphi. \quad (2.102)$$

The unit pseudoscalar (2.34) of a 1D manifold is a 1-vector

$$I(x) = \hat{\gamma}_\varphi \quad (2.103)$$

and thus the projection (2.88) of a vector a onto the circle is

$$P(a) = \hat{\gamma}_\varphi (\hat{\gamma}_\varphi \cdot a). \quad (2.104)$$

We say that the multivector field A is parallel transported along a curve with tangent vector u [24, Equation (C.1.34)] if

$$\partial_u A := P[(u \cdot \nabla) A] = 0. \quad (2.105)$$

In particular, a curve is called a geodesic (or an autoparallel) if its tangent vector u is parallel transported along the curve [24, Equation (C.1.36)]

$$\partial_u u = P[(u \cdot \nabla) u] = 0. \quad (2.106)$$

To make this concept more visual, suppose we would like to parallel transport the tangent vector from the north pole of the circle in Fig. 1. The field γ_x is plotted as green arrows and $-\hat{\gamma}_\varphi$ as red ones. They are chosen such that at the north pole they are equal, i.e., $-\hat{\gamma}_\varphi = \gamma_x$. Taking a look at Fig. 1 we would probably agree that the green field γ_x is parallel to the vector at the north pole. However, if the circle is a part of the Earth and the red arrow $-\hat{\gamma}_\varphi$ is a rod carried by a person walking from the north to the south pole, then for that person the rod is always transported parallel to itself. Therefore, intuitively there are at least two ways to parallel transport a rod from the north pole. Let us investigate this issue using the mathematical description introduced so far.

³⁴ Provided torsion-free connection such as Levi-Civita one, which is natural to GA as explained in the Appendix A.2, is employed.

The unit tangent vector (associated with the chosen parametrisation) to the part of the circle from the north to south pole is $u = -\hat{\gamma}_\varphi$. Let us first calculate the derivative of γ_x along u

$$\bar{\nabla}_{-\hat{\gamma}_\varphi} \gamma_x = (-\hat{\gamma}_\varphi \cdot \bar{\nabla}) \gamma_x = -\hat{\gamma}_\varphi \cdot 0 = 0, \quad (2.107)$$

which is indeed zero, but this is the “extrinsic” derivative $\bar{\nabla}$ associated with the 2D Euclidean metric of the plane. This justifies our first intuition of parallelism of arrows as we thought of Euclidean metric³⁵. However, the field γ_x is not intrinsic to the manifold, i.e., it does not satisfy (2.89)

$$P(\gamma_x) \neq \gamma_x. \quad (2.108)$$

One can easily check that the projection of γ_x onto the circle is not parallel transported

$$\bar{\nabla}_{-\hat{\gamma}_\varphi} P(\gamma_x) \neq 0. \quad (2.109)$$

Thus we see that the field γ_x albeit parallel transported in embedding space is not (nor its projection) parallel transported in the intrinsic sense.

Now let us check whether the other candidate for a parallel transported field, namely $-\hat{\gamma}_\varphi$, satisfies (2.106)

$$\partial_{-\hat{\gamma}_\varphi} (-\hat{\gamma}_\varphi) = P[\hat{\gamma}_\varphi \cdot \nabla \hat{\gamma}_\varphi] = 0. \quad (2.110)$$

For illustration we will calculate the derivative first via

$$\nabla_{\hat{\gamma}_\varphi} = \hat{\gamma}_\varphi \cdot \bar{\nabla}, \quad (2.111)$$

and next via

$$\nabla_{\hat{\gamma}_\varphi} = \frac{1}{r} \nabla_{\gamma_\varphi} = \frac{1}{r} \partial_\varphi \quad (2.112)$$

in order to illustrate that they are indeed equivalent as stated in (2.90).

We expand

$$\nabla_{\hat{\gamma}_\varphi} \hat{\gamma}_\varphi = (\hat{\gamma}_\varphi \cdot \bar{\nabla}) \hat{\gamma}_\varphi = (\hat{\gamma}_\varphi \cdot \gamma_x) \partial_x \hat{\gamma}_\varphi + (\hat{\gamma}_\varphi \cdot \gamma_y) \partial_y \hat{\gamma}_\varphi \quad (2.113)$$

and noting that

$$\hat{\gamma}_\varphi = -\sin \varphi \gamma_x + \cos \varphi \gamma_y = \frac{-y}{\sqrt{x^2 + y^2}} \gamma_x + \frac{x}{\sqrt{x^2 + y^2}} \gamma_y \quad (2.114)$$

calculate

$$\hat{\gamma}_\varphi \cdot \gamma_x = -\sin \varphi \quad \partial_x \hat{\gamma}_\varphi = \frac{xy}{\sqrt{x^2 + y^2}^3} \gamma_x + \frac{y^2}{\sqrt{x^2 + y^2}^3} \gamma_y = \frac{1}{r} \sin \varphi \cos \varphi \gamma_x + \frac{1}{r} \sin^2 \varphi \gamma_y \quad (2.115)$$

$$\hat{\gamma}_\varphi \cdot \gamma_y = \cos \varphi \quad \partial_y \hat{\gamma}_\varphi = \frac{-x^2}{\sqrt{x^2 + y^2}^3} \gamma_x + \frac{-xy}{\sqrt{x^2 + y^2}^3} \gamma_y = -\frac{1}{r} \cos^2 \varphi \gamma_x - \frac{1}{r} \sin \varphi \cos \varphi \gamma_y \quad (2.116)$$

to obtain

$$\nabla_{\hat{\gamma}_\varphi} \hat{\gamma}_\varphi = -\frac{1}{r} \sin^2 \varphi \cos \varphi \gamma_x - \frac{1}{r} \sin^3 \varphi \gamma_y - \frac{1}{r} \cos^3 \varphi \gamma_x - \frac{1}{r} \sin \varphi \cos^2 \varphi \gamma_y = -\frac{1}{r} (\cos \varphi \gamma_x + \sin \varphi \gamma_y). \quad (2.117)$$

The same result is obtained with less calculations via (2.112)

$$\nabla_{\hat{\gamma}_\varphi} \hat{\gamma}_\varphi = \frac{1}{r} \partial_\varphi (-\sin \varphi \gamma_x + \cos \varphi \gamma_y) = -\frac{1}{r} (\cos \varphi \gamma_x + \sin \varphi \gamma_y) =: p, \quad (2.118)$$

where p , depicted in Fig. 1 by blue arrows, turns out to be orthogonal to the manifold, cf. (2.93) and (2.95),

$$\hat{\gamma}_\varphi \cdot p = 0 \implies P(p) = 0 \quad (2.119)$$

and thus we see that the field $u = \hat{\gamma}_\varphi$ is indeed parallel transported (in the intrinsic sense) along the circle

$$\partial_u u = P[\nabla_{\hat{\gamma}_\varphi} \hat{\gamma}_\varphi] = P(p) = 0. \quad (2.120)$$

This manifests that one can handle intrinsic calculus of a pseudo-Riemannian manifold by simply projecting all the quantities onto the manifold using (2.88).

³⁵ Which is somehow natural to piece of paper.

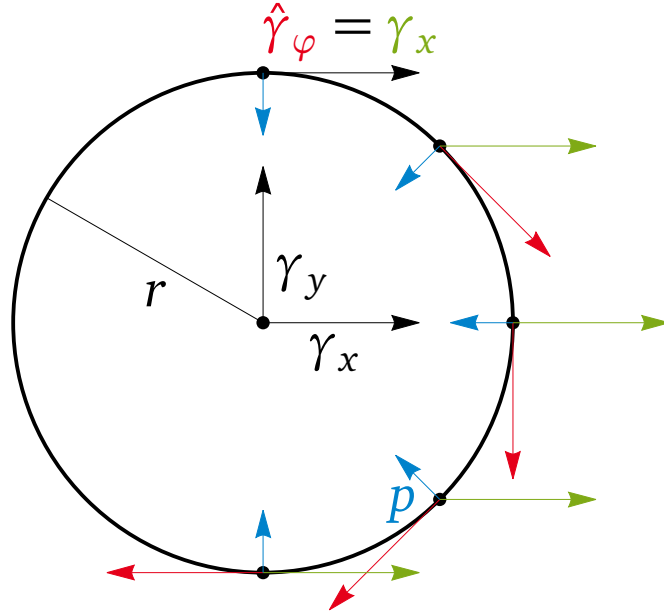


Figure 1: Intrinsic calculus on the circle. The green arrows represent the field γ_x , which is the black arrow at the north pole parallel transported along the circle in the extrinsic sense. The red arrows correspond to the field $-\hat{\gamma}_\varphi$, which is parallel transported but in the intrinsic sense. The blue arrows represent the intrinsic (but not covariant) derivative p of $-\hat{\gamma}_\varphi$. As p is orthogonal to the manifold at each point, the covariant derivative, i.e., the projection of the intrinsic derivative onto the manifold, is zero.

2.1.4 Relation to the Exterior Algebra and Calculus of Differential Forms

Due to the abundance of literature on differential geometry in the formalism of the exterior algebra and calculus of differential forms (DF), we would like to relate concepts specific to GA and DF with each other. This is by no means excessive and complete treatment of this issue³⁶; the goal is to ease reading and relating the works written in one formalism by people familiar with the other one. An attempt to relate both formalisms was carried out, e.g., in [10] and less formally in [26]. As in this thesis we will deal with flat Minkowski space-time, we assume here that the manifold is flat. Moreover, we introduce explicitly some arbitrary coordinates and associated with them a vector basis in tangent space. We will now browse through objects arising in DF and GA and try to relate them.

Vectors. As both exterior algebra of DF and GA are built on the same vector space L (tangent bundle) it seems natural to identify vectors (vector fields) present in both algebras with each other. Let us advocate this idea by considering coordinate basis vectors. In DF they are usually denoted by ∂_i and transform according to

$$\partial_k = \frac{\partial}{\partial x^k} = \frac{\partial \bar{x}^j}{\partial x^k} \frac{\partial}{\partial \bar{x}^j} = \frac{\partial \bar{x}^j}{\partial x^k} \bar{\partial}_j, \quad (2.121)$$

where x^j and \bar{x}^j are two coordinate systems. On the other hand, in GA we have analogously according to (2.54)

$$\gamma_k = \frac{\partial x}{\partial \bar{x}^k} = \frac{\partial \bar{x}^j}{\partial \bar{x}^k} \frac{\partial x}{\partial \bar{x}^j} = \frac{\partial \bar{x}^j}{\partial \bar{x}^k} \bar{\gamma}_j. \quad (2.122)$$

Thus it seems natural to identify coordinate basis vectors

$$\partial_i \doteq \gamma_i \quad (2.123)$$

and thus arbitrary vectors are simply identified in both algebras

$$a = a^i \partial_i \doteq a^i \gamma_i = a. \quad (2.124)$$

One-forms. One-forms are linear operators acting on vectors in L and they form a linear space called the dual space L^* ³⁷. As in GA we have not introduced the dual space at all,³⁸ we expect that there are no equivalents of one-forms in

³⁶ See open research questions at the end of this section.

³⁷ See for example [19, Section 2.4] or [24, Section A.1.1].

³⁸ As this is not necessary.

GA. However, the lack of equivalents of one-forms does not mean that we cannot mimic their functionality. Let us follow this way and look for candidate members of GA that provide us with the functionality of one-forms. In other words, we exploit Riesz representation theorem [1, Paragraph 1.11], which states that the action of any operator in L^* is uniquely represented by composing the inner product with certain vector in L .

First, with any basis ∂_i of L is associated the dual basis dx^i of L^* defined by

$$(dx^k)(\partial_i) = \delta_i^k. \quad (2.125)$$

Next, we recall that there is a canonical musical sharp isomorphism associated with the metric, which is used to canonically identify one-forms with vectors. For (co-)basis it reads³⁹

$$(dx^k)^\sharp = g^{kj} \partial_j. \quad (2.126)$$

Finally, taking (2.123) and $\gamma^k = g^{kj} \gamma_j$ ⁴⁰ into account, we obtain

$$(dx^k)^\sharp = g^{kj} \partial_j \doteq g^{kj} \gamma_j = \gamma^k. \quad (2.127)$$

Equation (2.126) is defined such that the action of the one form on a vector can be replaced by taking the inner product with its sharpened version. For example (2.125) now reads

$$(dx^k)(\partial_i) = (dx^k)^\sharp \cdot \partial_i = g^{kj} \partial_j \cdot \partial_i = g^{kj} g_{ji} = \delta_i^k. \quad (2.128)$$

Comparing

$$(dx^k)^\sharp \cdot \partial_i = \delta_i^k \quad \text{and} \quad \partial_i \doteq \gamma_i \quad (2.129)$$

with the equation defining reciprocal vectors γ^k in GA (2.35) it is reasonable to identify reciprocal basis with the sharpened co-basis as proposed in (2.127)

$$(dx^k)^\sharp \doteq \gamma^k. \quad (2.130)$$

Let us check the transformation properties. In DF we have

$$(dx^k)^\sharp = \left(\frac{\partial x^k}{\partial \bar{x}^j} d\bar{x}^j \right)^\sharp = \frac{\partial x^k}{\partial \bar{x}^j} (d\bar{x}^j)^\sharp. \quad (2.131)$$

Using the representation (2.51) in \bar{x}^i coordinate system, i.e., $\nabla = \bar{\gamma}^i \bar{\partial}_i$, of the geometric derivative, we have⁴¹

$$\gamma^k = \nabla x^k = \frac{\partial x^k}{\partial \bar{x}^j} \bar{\gamma}^j. \quad (2.133)$$

Therefore, we see that γ^i and $(dx^i)^\sharp$ transform in the same manner due to change of coordinates, which backs our proposition that $\gamma^i \doteq (dx^i)^\sharp$.

Exterior Product and p -forms. Both in DF and GA the exterior product is completely antisymmetric in its one-form (vector) components. Namely, in DF it holds by definition

$$dx^{i_1} \wedge dx^{i_2} \wedge \dots \wedge dx^{i_r} = \frac{1}{r!} \sum_{j_1, j_2, \dots, j_r} \text{sign}_{j_1, j_2, \dots, j_r}^{i_1, i_2, \dots, i_r} dx^{j_1} \wedge dx^{j_2} \wedge \dots \wedge dx^{j_r}, \quad (2.134)$$

where the signature of permutation $\text{sign}_{j_1, j_2, \dots, j_r}^{i_1, i_2, \dots, i_r} = +1$ if (i_1, i_2, \dots, i_r) and (j_1, j_2, \dots, j_r) are even permutations of each other, and is equal to -1 if they are odd. On the other hand in GA it holds⁴²

$$\gamma^{i_1} \wedge \gamma^{i_2} \wedge \dots \wedge \gamma^{i_r} = \frac{1}{r!} \sum_{j_1, j_2, \dots, j_r} \text{sign}_{j_1, j_2, \dots, j_r}^{i_1, i_2, \dots, i_r} \gamma^{j_1} \gamma^{j_2} \dots \gamma^{j_r} = \frac{1}{r!} \sum_{j_1, j_2, \dots, j_r} \text{sign}_{j_1, j_2, \dots, j_r}^{i_1, i_2, \dots, i_r} \gamma^{j_1} \wedge \gamma^{j_2} \wedge \dots \wedge \gamma^{j_r}. \quad (2.135)$$

³⁹ As explained, e.g., in [19, Exercise 2.4.13] or [24, Equation (C.2.7)].

⁴⁰ As can be easily verified by substituting $\gamma^k = g^{kj} \gamma_j$ in (2.35); $\gamma^k \cdot \gamma_i = g^{kj} \gamma_j \cdot \gamma_i = g^{kj} g_{ji} = \delta_i^k$.

⁴¹ Please note the identity

$$\nabla x^k = \gamma^i \partial_i x^k = \gamma^i \frac{\partial x^k}{\partial x^i} = \gamma^i \delta_i^k = \gamma^k. \quad (2.132)$$

⁴² Interestingly, all the dot products emerging from the geometric products cancel out, and the completely antisymmetrized product involve only the wedge products, i.e., metric is not necessary to calculate it.

Thus we postulate that the exterior products of DF and GA are the same in the sense that they are completely antisymmetric in their factors. Therefore, we can establish

$$(dx^{i_1} \wedge dx^{i_2} \wedge \dots \wedge dx^{i_r})^\sharp = (dx^{i_1})^\sharp \wedge (dx^{i_2})^\sharp \wedge \dots \wedge (dx^{i_r})^\sharp \doteq \gamma^{i_1} \wedge \gamma^{i_2} \wedge \dots \wedge \gamma^{i_r}. \quad (2.136)$$

Keeping in mind that every multivector (differential form) can be written as a sum of p -blades (simple p -forms) we can translate any multivector (differential form) using distributivity over addition. Namely, an r -form α is translated to the r -vector A_r via

$$\alpha^\sharp = \alpha_{i_1 i_2 \dots i_r} (dx^{i_1} \wedge dx^{i_2} \wedge \dots \wedge dx^{i_r})^\sharp \doteq \alpha_{i_1 i_2 \dots i_r} \gamma^{i_1} \wedge \gamma^{i_2} \wedge \dots \wedge \gamma^{i_r} = A_r. \quad (2.137)$$

Exterior Derivative. The exterior derivative of an r -form α is, see [19, Exercise 6.2.6] or [24, Equation (A.2.16)],

$$d\alpha = d\alpha_{i_1 i_2 \dots i_r} \wedge dx^{i_1} \wedge dx^{i_2} \wedge \dots \wedge dx^{i_r} = \partial_k \alpha_{i_1 i_2 \dots i_r} dx^k \wedge dx^{i_1} \wedge dx^{i_2} \wedge \dots \wedge dx^{i_r}. \quad (2.138)$$

While in GA the exterior product of geometric derivative and the multivector A_r equivalent to α is

$$\nabla \wedge A_r = (\gamma^k \partial_k) \wedge (\alpha_{i_1 i_2 \dots i_r} \gamma^{i_1} \wedge \gamma^{i_2} \wedge \dots \wedge \gamma^{i_r}) = \partial_k \alpha_{i_1 i_2 \dots i_r} \gamma^k \wedge \gamma^{i_1} \wedge \gamma^{i_2} \wedge \dots \wedge \gamma^{i_r}, \quad (2.139)$$

where we used that for the coordinate reciprocal basis it holds

$$\nabla \wedge \gamma^i = \nabla \wedge \nabla x^i = 0. \quad (2.140)$$

Thus it follows that the exterior derivative can be mimicked by

$$(d\alpha)^\sharp \doteq \nabla \wedge A_r. \quad (2.141)$$

Hodge Star. Without elaborating on this fact, we cite the result that the Hodge star \star^{43} applied to the form α is equivalent to [14, Equation (6.306)]

$$(\star\alpha)^\sharp \doteq (I^{-1}A_r)^\dagger =: \star A_r. \quad (2.142)$$

Above, by A^\dagger we denote the *reversion operation*

$$A^\dagger = (a_1 a_2 \dots a_r)^\dagger := a_r \dots a_2 a_1, \quad (2.143)$$

which consists of reversing the order of all vectors in all geometric products, see [14, Section 4.1.3].

Integral of a Differential Form. The integral of a simple form α is defined in terms of integral of a scalar multivariable function, see [19, Section 7.4] or [24, Equation (A.3.3)],

$$\int \alpha := \int \alpha_{12\dots r} dx^1 dx^2 \dots dx^r, \quad (2.144)$$

where dx^i on the RHS are understood as **scalar** differentials from multivariable calculus.

Let us investigate the following GA integral of $A_r \doteq \alpha$

$$\int (d^r x) \cdot A_r^\dagger = \int (\gamma_1 \wedge \gamma_2 \wedge \dots \wedge \gamma_r) \cdot (\gamma^r \wedge \gamma^{r-1} \wedge \dots \wedge \gamma^1) \alpha_{12\dots r} dx^1 dx^2 \dots dx^r = \int \alpha_{12\dots r} dx^1 dx^2 \dots dx^r. \quad (2.145)$$

Thus we see that both quantities reduce to the same multivariable integral and it is natural to identify

$$\int \alpha \doteq \int (d^r x) \cdot A_r^\dagger. \quad (2.146)$$

Covariant Derivative. The components of the covariant derivative of a tensor T of rank $\binom{r}{s}$ in a coordinate basis are⁴⁴

$$\nabla_a T^{u_1 \dots u_r}_{d_1 \dots d_s} = \partial_a T^{u_1 \dots u_r}_{d_1 \dots d_s} + \Gamma_{sa}^{u_1} T^{su_2 \dots u_r}_{d_1 \dots d_s} + \dots + \Gamma_{sa}^{u_r} T^{u_1 \dots u_{r-1} s}_{d_1 \dots d_s} - \Gamma_{d_1 a}^s T^{u_1 \dots u_r}_{sd_2 \dots d_s} - \dots - \Gamma_{d_s a}^s T^{u_1 \dots u_r}_{d_1 \dots d_{s-1} s}. \quad (2.147)$$

⁴³ See, e.g., [19, Section 5.8] or [24, Section C.2.8].

⁴⁴ This magic rule well-known as “covariant derivative is a partial derivative plus (respectively minus) proper contraction with Christoffel symbol for each covariant (respectively contravariant) index” can be derived directly from [24, Equations (C.1.12–14)] or [19, Exercise 15.2.1].

Thus the covariant derivative of T is a tensor of rank $\binom{r}{s+1}$

$$\nabla T = \left(\nabla_a T^{u_1 \dots u_r}_{d_1 \dots d_s} \right) dx^a \otimes \partial_{u_1} \otimes \dots \otimes \partial_{u_r} \otimes dx^{d_1} \otimes \dots \otimes dx^{d_s}, \quad (2.148)$$

and the directional covariant derivative in the direction u , i.e., contraction with the vector field u , is a scalar operator

$$\nabla_u T = \left(u^a \nabla_a T^{u_1 \dots u_r}_{d_1 \dots d_s} \right) \partial_{u_1} \otimes \dots \otimes \partial_{u_r} \otimes dx^{d_1} \otimes \dots \otimes dx^{d_s}. \quad (2.149)$$

Let us postulate that the tensor T is translated via

$$T^\sharp = T^{u_1 \dots u_r}_{d_1 \dots d_s} \partial_{u_1} \otimes \dots \otimes \partial_{u_r} \otimes (dx^{d_1})^\sharp \otimes \dots \otimes (dx^{d_s})^\sharp \doteq T^{u_1 \dots u_r}_{d_1 \dots d_s} \gamma_{u_1} \dots \gamma_{u_r} \gamma^{d_1} \dots \gamma^{d_s} =: A \quad (2.150)$$

and calculate the geometric derivative in the direction u

$$\begin{aligned} \nabla_u A &= (u \cdot \nabla) A = (u \cdot \gamma^a) \partial_a \left[T^{u_1 \dots u_r}_{d_1 \dots d_s} \gamma_{u_1} \dots \gamma_{u_r} \gamma^{d_1} \dots \gamma^{d_s} \right] = \\ &= u^a \left[\left(\partial_a T^{u_1 \dots u_r}_{d_1 \dots d_s} \right) \gamma_{u_1} \dots \gamma_{u_r} \gamma^{d_1} \dots \gamma^{d_s} + \right. \\ &+ T^{u_1 \dots u_r}_{d_1 \dots d_s} \left(\partial_a \gamma_{u_1} \right) \gamma_{u_2} \dots \gamma_{u_r} \gamma^{d_1} \dots \gamma^{d_s} + \dots + T^{u_1 \dots u_r}_{d_1 \dots d_s} \gamma_{u_1} \dots \gamma_{u_{r-1}} \left(\partial_a \gamma_{u_r} \right) \gamma^{d_1} \dots \gamma^{d_s} + \\ &\left. + T^{u_1 \dots u_r}_{d_1 \dots d_s} \gamma_{u_1} \dots \gamma_{u_r} \left(\partial_a \gamma^{d_1} \right) \gamma^{d_2} \dots \gamma^{d_s} + \dots + T^{u_1 \dots u_r}_{d_1 \dots d_s} \gamma_{u_1} \dots \gamma_{u_r} \gamma^{d_1} \dots \gamma^{d_{s-1}} \left(\partial_a \gamma^{d_s} \right) \right]. \quad (2.151) \end{aligned}$$

The second term inside the square brackets reads

$$\begin{aligned} T^{u_1 \dots u_r}_{d_1 \dots d_s} \left(\partial_a \gamma_{u_1} \right) \gamma_{u_2} \dots \gamma_{u_r} \gamma^{d_1} \dots \gamma^{d_s} &= T^{u_1 \dots u_r}_{d_1 \dots d_s} \Gamma_{a u_1}^s \gamma_s \gamma_{u_2} \dots \gamma_{u_r} \gamma^{d_1} \dots \gamma^{d_s} = \\ &= \text{Exchange summation indices } u_1 \leftrightarrow s = T^{s u_2 \dots u_r}_{d_1 \dots d_s} \Gamma_{a s}^{u_1} \gamma_{u_1} \dots \gamma_{u_r} \gamma^{d_1} \dots \gamma^{d_s}. \quad (2.152) \end{aligned}$$

Taking into account that

$$0 = \nabla_a \delta_c^b = \nabla_a (\gamma^b \cdot \gamma_c) = (\partial_a \gamma^b) \cdot \gamma_c + \gamma^b \cdot (\partial_a \gamma_c) = (\partial_a \gamma^b) \cdot \gamma_c + \Gamma_{ac}^b \Rightarrow \partial_a \gamma^b = -\Gamma_{ac}^b \gamma^c \quad (2.153)$$

and performing analogous manipulations for all the terms, we arrive at

$$\nabla_u A = \left(u^a \nabla_a T^{u_1 \dots u_r}_{d_1 \dots d_s} \right) \gamma_{u_1} \dots \gamma_{u_r} \gamma^{d_1} \dots \gamma^{d_s}. \quad (2.154)$$

Therefore, it seems natural to identify sharpened (2.149) with (2.154)

$$(\nabla_u T)^\sharp \doteq \nabla_u A, \quad (2.155)$$

which justifies that we have used the same notation ∇_u for a directional derivative in DF and GA settings.

Inner Product of Multivectors. The inner product of GA has an interesting geometric interpretation thus it is interesting whether we can mimic it in DF formalism. First, we note that the inner product of a vector a and an r -vector A_r can be rewritten using $a \cdot (A_r I) = a \wedge A_r I$ [14, Equation (4.69)]

$$a \cdot A_r = (a \wedge (A_r I^{-1})) I. \quad (2.156)$$

By noting that, cf. (2.142),

$$\star A_r = (I^{-1} A_r)^\dagger = A_r^\dagger (I^{-1})^\dagger = (-1)^{r(r-1)/2} (-1)^{n(n-1)/2} A_r I^{-1} \quad (2.157)$$

we can rewrite the inner product as

$$a \cdot A_r = (-1)^{r(r-1)/2 + n(n-1)/2} (a \wedge (\star A_r)) I. \quad (2.158)$$

We continue by noting that, see Appendix A.3,

$$I^{-1} = (-1)^{s+n(n-1)/2} I, \quad (2.159)$$

where s is the number of basis vectors squaring to negative values, i.e., the number of negative eigenvalues of the metric tensor. Therefore, it holds

$$a \cdot A_r = (-1)^{s+r(r-1)/2} (a \wedge (\star A_r)) I^{-1}. \quad (2.160)$$

By noting that the Hodge star of $n-r+1$ -vector $B_{n-r+1} := a \wedge (\star A_r)$ is

$$\star B_{n-r+1} = (-1)^{(n-r+1)(n-r)/2} (-1)^{n(n-1)/2} B_{n-r+1} I^{-1} = (-1)^{(n-r+1)(n-r)/2+n(n-1)/2} (a \wedge (\star A_r)) I^{-1} \quad (2.161)$$

we finally arrive at

$$a \cdot A_r = (-1)^w \star (a \wedge (\star A_r)), \quad (2.162)$$

with $w = s + n(n-r)$. Taking into account (2.142) and that the exterior products of DF and GA are equivalent we see that the dot product of GA has an equivalent

$$a \cdot A_r \doteq [(-1)^w \star (\tilde{a} \wedge (\star \alpha))]^\sharp, \quad (2.163)$$

where $\alpha \doteq A_r$ and $\tilde{a} \doteq a$ are equivalent differential forms.

The inner product of a vector and a multivector has been translated to DF formalism. Since the inner product of arbitrary multivectors can always be expressed in terms of products with vectors⁴⁵ the translation we have just proposed can be applied iteratively to translate generic inner products.

Geometric Product. As we have already translated the inner and outer products, we immediately get the translation of the geometric product of a vector a and an r -vector A_r

$$aA_r = a \cdot A_r + a \wedge A_r \doteq [(-1)^w \star (\tilde{a} \wedge (\star \alpha)) + \tilde{a} \wedge \alpha]^\sharp, \quad (2.164)$$

which is sufficient to translate the geometric product of generic multivectors by a recursive procedure.

Geometric Derivative. Setting formally⁴⁶ $a = \nabla$ in (2.164), taking into account (2.141) and assuming that the manifold is flat, we obtain

$$\nabla A_r = \nabla \cdot A_r + \nabla \wedge A_r \doteq [(-1)^w \star d \star \alpha + d \alpha]^\sharp. \quad (2.165)$$

Alternatively, we can use the representation (2.51) and translation (2.155) to arrive at

$$\nabla A_r = \gamma^a (\nabla_a A_r) \doteq [(-1)^w \star dx^a \star (\nabla_a \alpha) + dx^a \wedge (\nabla_a \alpha)]^\sharp. \quad (2.166)$$

Open research question 2. *We have related quantities and operations specific to both algebras with each other under the assumption that the manifold is flat. Do these relations hold in or can be extended to the case of curved manifold?*

Open research question 3. *All the derivations of translations have been done in some arbitrary coordinate system and basis of vector space L ⁴⁷. However, both DF and GA are well defined without introducing coordinates and basis in L . Can the quantities and operations specific to both algebras be related to each other in abstract algebraic setting, i.e., basing on the fact that they stem from the same tensor algebra but factorised with respect to different ideals, without introducing bases and coordinates?*

Open research question 4. *In most applications we are interested in formulae that give real numbers as they are easily handled by computers. Can the translation rules provided here be combined into computer algebra system algorithm that formulate arbitrary real-valued expression in one formalism in terms of the other?*

⁴⁵ See [25, Section 3] and [14, Chapter 4] for various formulae.

⁴⁶ This derivation is somewhat heuristic, as ∇ is not a vector, but an operator, and thus the identities that hold for vectors cannot be assumed to hold for ∇ . However, it is often the case, like here, that it can be proven (by direct calculation) that certain vector theorems hold for the geometric derivative ∇ as well. Therefore, formally one just replaces a vector by the operator ∇ .

⁴⁷ We have used coordinate (holonomic) basis, but all the derivations extend naturally to general non-holonomic bases as they are just linear combinations of holonomic ones. Therefore, we do not pose such extension as an open question.

2.2 Space-Time and Relativity

The overview: In this section we introduce the basic concepts from relativity theory. One of the key concepts here is the construct of an observer. However, we first use the term “observer” in a rather intuitive sense in order to outline some basics of special relativity theory, and only later we give a strict definition. These concepts are crucial for the proper physical interpretation of the quantities involved in the sequel. To properly define the concept of an observer we need some basic notions, which are presented next. The reader interested in more extensive introduction to the special relativity theory is referred to [34, Part II] and/or citations therein.

Space-Time Interval. According to the current understanding of nature, the speed of light is a universal constant for all inertial (non-accelerated) observers. Let us consider two observers moving with relative velocity \vec{v} along x -axis and coinciding at time $t = t' = 0$. Suppose at $t = 0$ a light bulb is switched on and off for a short moment. According to the absolute character of the speed of light, the wave front satisfies

$$x^2 + y^2 + z^2 = (ct)^2 \qquad x'^2 + y'^2 + z'^2 = (ct')^2. \quad (2.167)$$

As the spatial coordinates of points at the wave front are different⁴⁸, the time in both reference frames cannot be the same, i.e., $t \neq t'$. However, one can postulate that all observers measure the same *space-time interval squared*

$$s^2 = (ct)^2 - x^2 - y^2 - z^2 = (ct')^2 - x'^2 - y'^2 - z'^2 = \text{const}. \quad (2.168)$$

not only at the wave front, i.e., at the points satisfying $s = 0$, but for all space-time points also called events. Therefore, introducing the coordinates

$$x^0 = ct \qquad x^1 = x \qquad x^2 = y \qquad x^3 = z, \quad (2.169)$$

we require that

$$s^2 = (x^0)^2 - (x^1)^2 - (x^2)^2 - (x^3)^2 \quad (2.170)$$

is an invariant under the change of observer. The change of observer is modelled mathematically by the change of coordinates. Now, we need to find the change of coordinates that preserves the space-time interval. Before doing so, we will give physical meaning to some more mathematical concepts. In the sequel of this Section, we assume that the *natural units* are chosen such that the speed of light is equal to unity, $c = 1$, in that units. This effectively allows us to skip c in formulae, which is a common practice in literature concerning relativity.

Minkowski Metric. With every event in space-time we associate the position four-vector

$$p := x^i \gamma_i, \quad (2.171)$$

where the basis vectors satisfy

$$\gamma_i \cdot \gamma_j = \begin{cases} +1 & i = j = 0 \\ -1 & i = j = 1, 2, 3 \\ 0 & i \neq j. \end{cases} \quad (2.172)$$

Then the square of the position vector p is exactly the desired invariant s^2

$$p^2 = (x^i \gamma_i)(x^j \gamma_j) = s^2. \quad (2.173)$$

The square of the vector is usually referred to its length, which should be an invariant. However, our previous discussion showed that the notion of spatial or temporal distance depends of the observer, i.e., coordinates. The only notion of distance independent of observer is space-time interval, which coincides with the pseudo-norm of the vector following from the Minkowski metric introduced in (2.172).

Embedding 3D Vectors in Space-Time. The 3D basis

$$\sigma_\alpha := \frac{\gamma_\alpha \wedge \gamma_0}{\sqrt{(\gamma_\alpha \wedge \gamma_0)^2}}, \quad (2.174)$$

is used to embed 3D vectors in the space-time setting. This is also called space-time split (first introduced in [25, Chapter 7], but the name appeared later in publications by the same author) with respect to the observer with the four-velocity $\hat{\gamma}_0$.

⁴⁸ If $v \neq 0$.

By an arrow over a symbol we denote 3D vectors. For example, the electric field

$$\vec{E} := \sum_{\alpha=1}^3 E^\alpha \sigma_\alpha. \quad (2.175)$$

Please note, that this decomposition or space-time split is performed only in the tangent space at each point of the 4D manifold. Especially, we do not split the manifold into “relative space” and “time”; we split only the multivectors into their spatial and temporal components. For the complete split of 4D space-time into relative space and time of a particular observer, see [2]. We would like to justify the name “3D vectors”. From the point of view of 4D algebra (2.174) are bivectors. However, one can build a 3D (not necessarily geometric) algebra⁴⁹ treating σ_α as basis vectors. As a consequence, one can identify σ_α with 3D basis vectors from traditional vector analysis. Therefore, traditional 3D vector calculus can be used in a relative space of any observer, provided one uses (2.174) and (2.175) to embed 3D vectors in 4D algebra.

Given the four-velocity field u of an observer, any four-vector p can be decomposed into spatial 3D relative vector \vec{p} and temporal component p_0 according to the space-time split [25, Equation (7.12)]

$$pu = p_0 + \vec{p}, \quad p_0 := p \cdot u, \quad \vec{p} := p \wedge u. \quad (2.176)$$

Lorentz Boosts. To find a transformation that preserves space-time interval s , we first note that if⁵⁰

$$p' = \exp(\vec{\beta}/2)p \exp(-\vec{\beta}/2), \quad (2.177)$$

then the length of the vector is invariant, i.e.,

$$p'^2 = \exp(\vec{\beta}/2)p \overbrace{\exp(-\vec{\beta}/2)\exp(\vec{\beta}/2)}{=1} p \exp(-\vec{\beta}/2) = \exp(\vec{\beta}/2) \overbrace{p^2}^{\text{scalar}} \exp(-\vec{\beta}/2) = p^2. \quad (2.178)$$

Letting $\vec{\beta} = \beta \gamma_x \gamma_y \gamma_z$, after some calculations presented in Appendix B.1 one finds

$$p' = e^{-\vec{\beta}/2} p e^{\vec{\beta}/2} = [\gamma_t, \gamma_x, \gamma_y, \gamma_z] \begin{bmatrix} \cosh(\beta) & -\sinh(\beta) & 0 & 0 \\ -\sinh(\beta) & \cosh(\beta) & 0 & 0 \\ 0 & 0 & 1 & 0 \\ 0 & 0 & 0 & 1 \end{bmatrix} \begin{bmatrix} t \\ x \\ y \\ z \end{bmatrix}. \quad (2.179)$$

To establish the physical meaning of β suppose that the particle is at rest in one reference frame, e.g., $x' = 0$, and moves with constant velocity $v = x/t$ in the other reference frame. Then we arrive at the relation between physical velocity v and rapidity parameter β

$$x' = \cosh(\beta)x - \sinh(\beta)t = 0 \quad \Rightarrow \quad v = \tanh(\beta). \quad (2.180)$$

Thus we see that (2.179) represents Lorentz boost in x -direction. In general a transformation of p to the frame moving with a constant 3D velocity \vec{v} is obtained by calculating

$$p' = e^{-\vec{\beta}/2} p e^{\vec{\beta}/2}, \quad (2.181)$$

with

$$\vec{\beta} = \frac{\vec{v}}{|\vec{v}|} \operatorname{artanh} |\vec{v}|. \quad (2.182)$$

In general, any multivector A is transformed using the same formula, i.e.,

$$A' = e^{-\vec{\beta}/2} A e^{\vec{\beta}/2}. \quad (2.183)$$

⁴⁹ If we chose to build a 3D geometric algebra taking as a linear space L a span of σ_i , this will be equivalent to a sub-algebra of STA. This is due to the fact that the 3D GA basis $(1, \sigma_i, \sigma_i \sigma_j, I = \sigma_1 \sigma_2 \sigma_3)$ is a subset of STA basis and is closed under the geometric product, which is sufficient to show that the obtained algebra is actually a sub-algebra of STA.

⁵⁰ The exponential of a (multi-)vector should be understood as (convergent for any $a \in L$) Taylor series

$$\exp(a) := \sum_{j=0}^{\infty} \frac{a^j}{j!}.$$

Physical Interpretation of the Pseudonorm. Suppose the interval

$$s^2 = -l^2 < 0. \quad (2.184)$$

Then there exists an inertial frame in which p' associated with $s^2 = p'^2 = p^2 = -l^2$ is a purely spatial distance l ,

$$s^2 = t^2 - x^2 - y^2 - z^2 = -(x'^2 + y'^2 + z'^2) = -l^2 \Rightarrow l = \sqrt{x'^2 + y'^2 + z'^2}. \quad (2.185)$$

Thus vectors for which $s^2 = p^2 < 0$ are called spacelike.

We have already discussed that if $s^2 = p^2 = 0$, then p describes possible direction of propagation of light. Such vectors are referred in the literature as null or lightlike.

Finally, suppose that

$$s^2 = \tau^2 > 0. \quad (2.186)$$

Then in some reference frame p' associated with s^2 is a purely temporal distance τ ,

$$s^2 = t^2 - x^2 - y^2 - z^2 = t'^2 = \tau^2 \Rightarrow \tau = t'. \quad (2.187)$$

Thus vectors for which $s^2 = p^2 > 0$ are called timelike. τ is the proper time.

The timelike vector describes a possible direction of motion of a massive particle.

The proper time interval $\Delta\tau$ is related to the time increment Δt of any inertial system by

$$(\Delta\tau)^2 = (\Delta t)^2 - (\Delta\vec{r})^2 \Rightarrow \Delta\tau = \sqrt{1 - \left(\frac{\Delta\vec{r}}{\Delta t}\right)^2} \Delta t, \quad (2.188)$$

where $\Delta\vec{r}$ is the 3D position increment of a particle in time Δt . Thus the time measured in the (not necessarily inertial!) rest frame of the particle moving with 3D velocity

$$\vec{v}(t) := \lim_{\Delta t \rightarrow 0} \frac{\Delta\vec{r}}{\Delta t} \quad (2.189)$$

is

$$\tau = \int_{t_1}^{t_2} \sqrt{1 - [\vec{v}(t)]^2} dt. \quad (2.190)$$

To summarise, we adopt the following nomenclature.

$$\text{The vector } w \text{ is called } \begin{cases} \text{timelike if} & w^2 > 0 \\ \text{lightlike if} & w^2 = 0 \\ \text{spacelike if} & w^2 < 0 \end{cases} \quad (2.191)$$

This notion naturally extends to multi-vectors. We will refer only to 2D facets in this context.

The 2D facet Δ is called timelike or lightlike if it contains two orthogonal directions one of which⁵¹ is timelike or lightlike, respectively; otherwise it is called spacelike. Mathematically, one can test the type of Δ by squaring the bivector W associated with it; namely

$$\text{The facet } \Delta \text{ is called } \begin{cases} \text{timelike if} & W^2 > 0 \\ \text{lightlike if} & W^2 = 0 \\ \text{spacelike if} & W^2 < 0 \end{cases} \quad (2.192)$$

⁵¹ Please note that in 4D Minkowski space-time there are no two **orthogonal** timelike nor lightlike directions. Therefore one of the vectors in orthogonal decomposition of a 2D facet is always spacelike. Let us prove it. Timelike case: suppose u is a timelike vector. It is always possible to choose inertial coordinates such that $u = [\gamma_t, \gamma_x, \gamma_y, \gamma_z][1, 0, 0, 0]^T$. We seek for other vector $v = [\gamma_t, \gamma_x, \gamma_y, \gamma_z][t, x, y, z]^T$, which is orthogonal to u . If $u \cdot v = 0$, then $t = 0$, and the vector v is spacelike, i.e., $v^2 = -x^2 - y^2 - z^2 < 0$. Thus there are no two orthogonal timelike directions. Lightlike case: Assume u to be lightlike. Then in some inertial coordinates it takes the form $u = [\gamma_t, \gamma_x, \gamma_y, \gamma_z][1, 1, 0, 0]^T$. Now from $u \cdot v = 0$ follows that $v = [\gamma_t, \gamma_x, \gamma_y, \gamma_z][t, t, y, z]^T$. Requiring v to be lightlike, i.e., $v^2 = t^2 - t^2 - y^2 - z^2 = -y^2 - z^2 = 0$, leads us to $y = 0 = z$, i.e., $v = [\gamma_t, \gamma_x, \gamma_y, \gamma_z][t, t, 0, 0]^T$, which is proportional to u , i.e., the only orthogonal vectors to a given lightlike vector are proportional to it, i.e., they point in the same direction. This shows that the geometric intuition behind our classification of 2D facets is equivalent to the mathematical formulation.

Let us illustrate this concept by some examples. Let s_1 and s_2 be spacelike vectors, n lightlike and p timelike, i.e.,

$$s_1^2 = s_2^2 = -1 \qquad n^2 = 0 \qquad p^2 = +1. \quad (2.193)$$

Thus the bivectors

$$W_s := s_1 s_2 \qquad W_l := s_1 n \qquad W_t := s_1 p \quad (2.194)$$

represent, respectively, a spacelike, lightlike and timelike facet. For simplicity we assume that all the vectors are orthogonal; they can always be orthogonalised by, e.g., Gram-Schmidt process. Thus we confirm the type of facets by calculating W^2

$$W_s^2 = s_1 s_2 s_1 s_2 = -s_1 s_1 s_2 s_2 = -s_1^2 s_2^2 = -1 \quad (2.195)$$

$$W_l^2 = s_1 n s_1 n = -s_1^2 n^2 = 0 \quad (2.196)$$

$$W_t^2 = s_1 p s_1 p = -s_1^2 p^2 = +1. \quad (2.197)$$

Definition of an Observer. The family of 1D curves filling densely, continuously and without intersections the space-time region is called a congruence. If the tangent vector u to a curve (belonging to the congruence) passing through any point is timelike, then the congruence is called timelike. Time-like congruence may be interpreted as follows. Each member of a family represents a world-line of a particle. Particles can be imagined to form a body made of elastic rubber, which can deform freely but cannot tear apart. As a consequence particles whose distance is small have similar velocity.

The congruence is a purely geometrical concept; there was no notion of time so far. Since each particle of the congruence can move with different velocity, the time passes at different rates for each of them. The time measured by a particle is called the proper time τ of that particle; we will also refer to it as the physical time. In simple words, if a particle looks at its watch carried on its hand it sees τ .

The proper time τ is a natural parametrisation⁵² of any member of the time-like congruence. Of course, in the definition of the natural parameter there is a norm (associated with the metric) involved.

In our case, we deal with a pseudo-Riemannian metric, i.e., one which is not positive definite, thus resulting in the pseudonorm (allowing non-zero vectors to have zero length). However, since we have restricted ourselves to time-like curves, the pseudonorm of any tangent vector u fulfils norm axioms, and thus the proper time τ being a natural parameter is well defined (up to a constant as in the case of the positive definite metric and the norm associated with it).

The reference or coordinate time t_{ref} is a parameter (not necessarily a natural one) running along each member of the congruence. It is required that if we join the points of different curves associated with the same value of t_{ref} the obtained hypersurface, called hypersurface of simultaneity or constant time, is smooth enough.

With a time-like congruence there is associated the four-velocity field $u(x)$, with x the position in space-time, of tangent vectors. The congruence can be reconstructed from the four-velocity field by means of integration. The integration constants are fixed by the particular choice of time synchronisation.

The whole structure: time synchronisation and the four-velocity field $u(x)$ (thus also the time-like congruence) is referred to as the observer or the frame of reference. For examples of the use of congruences in General Relativity see [40].

The **inertial observer** is the one, whose congruence is set of straight lines parallel to each other, and whose hypersurfaces of simultaneity are flat hyperplanes orthogonal to the congruence.

Placement Map. We extend the Lagrangian description of motion to our space-time setting by defining the placement map

$$p : T_{\text{ref}} \times K_{\text{ref},3} \rightarrow K_4, (t_{\text{ref}}, \vec{r}_{\text{ref}}) \mapsto r, \quad (2.198)$$

where T_{ref} is a temporal reference domain, $K_{\text{ref},3}$ a spatial reference domain, K_4 a physical space-time domain of interest, t_{ref} is the reference time, \vec{r}_{ref} is the reference position, and r is the position vector in physical space-time⁵³.

Our description may be thought of as a map $r_{\text{ref}} \mapsto r$ between reference and physical 4D positions. Nonetheless, We explicitly include the reference time t_{ref} in the list of arguments

$$p_{t_{\text{ref}}}(\vec{r}_{\text{ref}}) := p(t_{\text{ref}}, \vec{r}_{\text{ref}}), \quad (2.199)$$

because this facilitates later explanations.

When comparing our placement map with the traditional Lagrangian description, we observe that

⁵² I.e., the one whose parameter is an arc length of a curve measured with respect to the underlying metric. In our case this is Minkowski metric. Thus τ is just an arc length in such a setting.

⁵³ The reference domain in Section 3.1.1 is meshed using any 3D mesh generator; we obtain coordinates of the nodes in the form $[r^x, r^y, r^z]$, then $\vec{r}_{\text{ref}} := r^x \sigma_x + r^y \sigma_y + r^z \sigma_z$.

1. We do not restrict the reference position \vec{r}_{ref} to be the position at time zero. One reason for this is that there is no unique notion of time (as discussed above when defining an observer).
2. We do not restrict the time component t of the position vector r to be the same as the reference time t_{ref} . This allows to impose various synchronization of the clocks, i.e., change hypersurfaces of simultaneity.

Rotation with Constant Angular Velocity Ω . In order to deal with rotation we must define what we mean by constant angular velocity Ω . (This discussion can be performed analogously to the discussion of constant acceleration in the relativistic setting, see [34, Chapter 6.2].) If one applies the constantly accelerated motion as $v = at$, then after a long enough time, one gets $v > c$, which is obviously not consistent with relativity. Therefore, one rather takes as definition that the velocity $v(t + dt)$ at a time instant $t + dt$ is adt greater, with a relativistic formula for the addition of velocities employed, i.e.,

$$v = \frac{v_1 + v_2}{1 + v_1 v_2 / c^2} \Rightarrow v(t) + \frac{dv}{dt} dt + \mathcal{O}(dt^2) = v(t + dt) = \frac{v(t) + adt}{1 + v(t)adt/c^2}. \quad (2.200)$$

This corresponds to stating that the acceleration is constant as observed by the accelerated observer. We do the same for constant rotation, that is, we define that the velocity v at the radius $r + dr$ is Ωdr higher than at r . (The reader familiar with the derivation for accelerated observer will see that from mathematical point of view we just replace t with r and a with Ω .)

Then at the radius $r + \Delta r$, we have that

$$v(r + \Delta r) = v(r) + \frac{dv}{dr} \Delta r + \mathcal{O}(\Delta r)^2 \quad (2.201)$$

$$v(r + \Delta r) = \frac{v(r) + \Omega \Delta r}{1 + v(r)\Omega \Delta r / c^2} = v(r) + \Omega \Delta r - \frac{v^2(r)}{c^2} \Omega \Delta r + \mathcal{O}(\Delta r)^2, \quad (2.202)$$

that is, in the limit $\Delta r \rightarrow 0$, the velocity v satisfies the following ordinary differential equation

$$\frac{dv}{dr} = \Omega \left(1 - \frac{v^2}{c^2} \right). \quad (2.203)$$

By imposing the condition that the velocity at the center of rotation is zero $v(0) = 0$, we arrive at the solution

$$v(r) = c \tanh \left(\frac{r\Omega}{c} \right). \quad (2.204)$$

For small radii, (2.204) gives $v(r) \approx r\Omega$, which corresponds to the Galilean setting. We would like to mention that the just constructed rotating observer is not Born-rigid, see [57, Equation (107)].

The cylindrical coordinates of \vec{r}_{ref} are denoted by $[r, \varphi, z]$. For a system rotating with constant angular velocity Ω around z -axis we have

$$p = p_t(\vec{r}_{\text{ref}}) = [t, r \cos(\theta), r \sin(\theta), z][\gamma_t, \gamma_x, \gamma_y, \gamma_z]^T, \text{ with } \theta = \varphi + \tanh \left(\frac{r\Omega}{c} \right) \frac{ct}{r}. \quad (2.205)$$

Above, p_t is such that it satisfies $t_{\text{ref}} = t$ and $\vec{r}_{\text{ref}} = p_0(\vec{r}_{\text{ref}}) \wedge \gamma_t$ coinciding thus with 3D Lagrangian description of motion. Moreover, one can verify that the four velocity u of a particle with reference coordinates $[r, \varphi, z]$ is consistent with (2.204), see Appendix B.2. We would like to note that (2.205) is equivalent to setting

$$\Omega(r) := \frac{c}{r} \tanh \left(\frac{r\Omega}{c} \right) \quad (2.206)$$

in [35, Equation (6.1)]. Our choice also complies with constraints proposed there, i.e., [35, Equation (6.2)].

2.3 Maxwell's Equations

The overview: Here we start from traditional 3D form of Maxwell's equations and constitutive laws and derive their space-time equivalents expressed using GA. This is our starting point for performing space-time discretization.

The traditional form of Maxwell's equations separating space and time reads

$$\begin{cases} \vec{\nabla} \times \vec{E} = -\partial_t \vec{B} \\ \vec{\nabla} \cdot \vec{B} = 0 \end{cases} \quad \begin{cases} \vec{\nabla} \times \vec{H} = \partial_t \vec{D} + \vec{J} \\ \vec{\nabla} \cdot \vec{D} = \rho, \end{cases} \quad (2.207)$$

Name	Symbol	Basis representation
Electric field strength	\vec{E}	$= E^x \gamma_x \gamma_t + E^y \gamma_y \gamma_t + E^z \gamma_z \gamma_t$
Magnetic flux density	\vec{B}	$= B^x \gamma_x \gamma_t + B^y \gamma_y \gamma_t + B^z \gamma_z \gamma_t$
Faraday bivector	$F = \vec{E} + Ic\vec{B}$	$= E^x \gamma_x \gamma_t + E^y \gamma_y \gamma_t + E^z \gamma_z \gamma_t + cB^x \gamma_z \gamma_y + cB^y \gamma_x \gamma_z + cB^z \gamma_y \gamma_x$
Electric flux density	\vec{D}	$= D^x \gamma_x \gamma_t + D^y \gamma_y \gamma_t + D^z \gamma_z \gamma_t$
Magnetic field strength	\vec{H}	$= H^x \gamma_x \gamma_t + H^y \gamma_y \gamma_t + H^z \gamma_z \gamma_t$
Dual Faraday bivector	$G = \vec{D} + c^{-1}I\vec{H}$	$= D^x \gamma_x \gamma_t + D^y \gamma_y \gamma_t + D^z \gamma_z \gamma_t + c^{-1}H^x \gamma_z \gamma_y + c^{-1}H^y \gamma_x \gamma_z + c^{-1}H^z \gamma_y \gamma_x$
Charge density	ϱ	$= \varrho$
Current density	\vec{J}	$= J^x \gamma_x \gamma_t + J^y \gamma_y \gamma_t + J^z \gamma_z \gamma_t$
Space-time current density	$J = (\varrho + \frac{1}{c}\vec{J})\gamma_0$	$= \varrho \gamma_t + c^{-1}J^x \gamma_x + c^{-1}J^y \gamma_y + c^{-1}J^z \gamma_z$

Table 1: Overview of the introduced fields. The four-velocity of the observer γ_0 should not be confused with a temporal basis vector γ_t of an inertial observer.

where ϱ , \vec{J} , \vec{E} , \vec{H} , \vec{D} and \vec{B} are the electric charge density, the electric current density, the electric and magnetic field strengths, and the electric and magnetic flux densities, respectively, see also Table 1. It should be stressed that Maxwell's equations take the form (2.207) only in an inertial reference frame.

Since we aim at performing space-time discretization, we must express (2.207) and (2.211) in the space-time setting. To this end, we combine all 3D scalar and vector fields into space-time counterparts in the following way (SI units in square brackets)

$$F := \vec{E} + cI\vec{B} \quad \left[\frac{V}{m} \right] \quad G := \vec{D} + \frac{1}{c}I\vec{H} \quad \left[\frac{C}{m^2} \right] \quad J := (\varrho + \frac{1}{c}\vec{J})\gamma_0 \quad \left[\frac{C}{m^3} \right], \quad (2.208)$$

where γ_0 is the four-velocity of the observer, I the pseudoscalar and c is the speed of light in vacuum; see also Table 1.

Thus, Maxwell's equations in the space-time form [14] ensue, viz.

$$\nabla \wedge F = 0 \quad \left[\frac{V}{m^2} \right], \quad \nabla \cdot G = J \quad \left[\frac{C}{m^3} \right]. \quad (2.209)$$

The space-time integral form of Maxwell's equations is obtained in a manner described in [26]. Namely, we integrate (2.209) over an arbitrary bounded 3D star-shaped domain $K_3 \subset K_4$, with K_4 the 4D space-time, and apply the fundamental theorem of geometric calculus [26, 50]. This results in

$$\oint_{\partial K_3} (d^2x) \cdot F = 0 \quad [V \cdot m], \quad \oint_{\partial K_3} (d^2x) \wedge G = \int_{K_3} (d^3x) \wedge J \quad [C]. \quad (2.210)$$

2.4 Material Equations

The overview: We use the formalism developed in Section 2.2 to state material equations in space-time form. Namely, we start with the well-established material equations in the reference frame in which material is at rest. Then we proceed by exploiting the four-velocity field γ_0 of the congruence (denoted by u in Section 2.2 and now assumed to be the four-velocity of the material, i.e., $u = \gamma_0$.) to state this equation in a form valid for arbitrary observer.

Maxwell's equations (2.207) need to be supplemented with constitutive material laws. Both equations (2.207) are linked by material equations in the rest frame of materials given by

$$\vec{D} = \mathcal{D}(\vec{E}, \vec{B}) \quad \text{and} \quad \vec{H} = \mathcal{H}(\vec{E}, \vec{B}). \quad (2.211)$$

Equations (2.207) and (2.211) (with given boundary conditions and initial values) form a complete set of equations, which we want to solve. Ohm's law is disregarded in this thesis. This is mainly due to the lack of proper space-time formulation of this law; see the criticism and proposition in [21] and more recent solution in [51], which would be more suitable for our application.

The space-time equivalent of (2.211) is called the *material mapping* ξ and implicitly defined by

$$G = \mathcal{D}(\vec{E}, \vec{B}) + \frac{I}{c}\mathcal{H}(\vec{E}, \vec{B}) = \xi(F), \quad (2.212)$$

where $\vec{E} = \frac{1}{2}(F - \gamma_0 F \gamma_0)$ and $\vec{B} = \frac{1}{2ic}(F + \gamma_0 F \gamma_0)$. The four-velocity field of the material is γ_0 . We want to stress that the introduction of ξ is not a complication of the material equations but a translation to the space-time algebra in a consistent manner. We will now discuss three special cases.

Local, Linear and Anisotropic Medium. Since we focus on lossless wave propagation without permanent polarisation nor magnetisation, the material laws (2.211) in the reference frame, in which the materials are at rest, read

$$\mathcal{D}(\vec{E}, \vec{B}) = \varepsilon \vec{E} \quad \text{and} \quad \mathcal{H}(\vec{E}, \vec{B}) = \nu \vec{B}, \quad (2.213)$$

with ε the electric permittivity and ν the magnetic reluctivity. We assume that the medium is local and linear, possibly inhomogeneous and anisotropic. From mathematical point of view this is equivalent to assuming that ε and ν are positive-definite, second rank tensor fields.

Therefore, the most complex case that should be considered is a symmetric anisotropic medium, i.e.,

$$\mathcal{D}(\vec{E}, \vec{B}) = (\sigma_x, \sigma_y, \sigma_z) \begin{pmatrix} \varepsilon_{xx} & \varepsilon_{xy} & \varepsilon_{xz} \\ \varepsilon_{xy} & \varepsilon_{yy} & \varepsilon_{yz} \\ \varepsilon_{xz} & \varepsilon_{yz} & \varepsilon_{zz} \end{pmatrix} \begin{pmatrix} E^x \\ E^y \\ E^z \end{pmatrix} \quad (2.214)$$

and

$$\mathcal{H}(\vec{E}, \vec{B}) = (\sigma_x, \sigma_y, \sigma_z) \begin{pmatrix} \nu_{xx} & \nu_{xy} & \nu_{xz} \\ \nu_{xy} & \nu_{yy} & \nu_{yz} \\ \nu_{xz} & \nu_{yz} & \nu_{zz} \end{pmatrix} \begin{pmatrix} B^x \\ B^y \\ B^z \end{pmatrix}. \quad (2.215)$$

In this case using the explicit definition of ξ obtained by inserting (2.214) and (2.215) into (2.212) one can verify that

$$\xi(B_1) \cdot B_2 = B_1 \cdot \xi(B_2) \quad (2.216)$$

holds for all bivectors B_1 and B_2 . Therefore, the material mapping is self-conjugate. Instead of presenting a general expression for ξ we rather present a few important special cases. Since ξ is linear, to evaluate for arbitrary F

$$\xi(F) = \xi(\vec{E}) + \xi(cI\vec{B}) = E^i \xi(\sigma_i) + cB^i \xi(I\sigma_i) \quad (2.217)$$

it is sufficient to know

$$\xi(\sigma_i) = \varepsilon_{ij} \sigma_j \quad \text{and} \quad \xi(I\sigma_i) = \nu_{ij} I\sigma_j. \quad (2.218)$$

For the inverse ξ^{-1} the interesting equations are

$$\xi^{-1}(\sigma_i) = [\varepsilon^{-1}]_{ij} \sigma_j \quad \text{and} \quad \xi^{-1}(I\sigma_i) = \mu_{ij} I\sigma_j, \quad (2.219)$$

with the permeability $\mu = \nu^{-1}$.

Isotropic Medium. If the medium is isotropic, i.e., permittivity ε and reluctivity ν are scalars in

$$\mathcal{D}(\vec{E}, \vec{B}) = \varepsilon \vec{E} \quad \text{and} \quad \mathcal{H}(\vec{E}, \vec{B}) = \nu \vec{B} \quad (2.220)$$

we can directly calculate G in terms of F in the coordinate frame of the medium

$$G = \vec{D} + \frac{1}{c} I\vec{H} = \varepsilon \vec{E} + \frac{\nu}{c} I\vec{B} = \varepsilon \frac{1}{2}(F - \gamma_0 F \gamma_0) + \frac{\nu}{c^2} \frac{1}{2}(F + \gamma_0 F \gamma_0) = \frac{1}{2} \left[\left(\varepsilon + \frac{\nu}{c^2} \right) F - \left(\varepsilon - \frac{\nu}{c^2} \right) \gamma_0 F \gamma_0 \right], \quad (2.221)$$

therefore we obtain a simple coordinate-free form of ξ for isotropic media

$$\xi_{\text{isotropic}}(X) = \frac{1}{2} \left[\left(\varepsilon + \frac{\nu}{c^2} \right) X - \left(\varepsilon - \frac{\nu}{c^2} \right) \gamma_0 X \gamma_0 \right]. \quad (2.222)$$

Vacuum. In vacuum, we have that $\varepsilon = \varepsilon_0$, $\nu = \nu_0$ and $c = \sqrt{\frac{\nu_0}{\varepsilon_0}}$, from which the following simple mapping ensues

$$G = \xi_{\text{vacuum}}(F) = \varepsilon_0 F. \quad (2.223)$$

2.5 Summary: Electrodynamics in Four Dimensions

The electromagnetic field in space-time is described by the Faraday bivector (2.208)

$$F := \vec{E} + Ic\vec{B}.$$

Knowing F one can split it into the electric and magnetic field observed in the reference frame with four-velocity u , see [25, Equation (8.3)] or [14, Equation (7.26)]⁵⁴

$$\vec{E} = \frac{1}{2}(F - uFu) \quad (2.227)$$

$$\vec{B} = \frac{1}{2Ic}(F + uFu). \quad (2.228)$$

This split is determined solely by the four-velocity field of the observer.

In Section 3.2 we will deal with two particular observers: a stationary and a rotating one. Therefore, we denote the fields observed by a stationary observer with the four-velocity $u = \gamma_t$ in (2.227) and (2.228) by \vec{E}_s and \vec{B}_s . Analogously the fields \vec{E}_r and \vec{B}_r correspond to the rotating observer with u following from (2.205).

2.5.1 Magnetic Gauss Law in Rotating Reference Frame

The overview: Our goal is to simulate electromagnetic fields in non-inertial frames. Before discretizing Maxwell's equations, we would like to make sure that the just outlined formulation is capable of handling such observers in a physically correct manner. To this end, we derive the explicit expression corresponding to the magnetic Gauss law in a uniformly rotating frame and relate it to other approaches existing in literature.

The source free part of Maxwell's equations (2.209) reads

$$\nabla \wedge F = 0, \quad (2.229)$$

where F in some orthonormal frame $\hat{\gamma}$ is given by

$$F = \vec{E} + cI\vec{B} = \hat{E}^i \sigma_i + c\hat{B}^i I\sigma_i = \hat{E}^i \hat{\gamma}_i \hat{\gamma}_0 + c\hat{B}^i I\hat{\gamma}_i \hat{\gamma}_0. \quad (2.230)$$

In flat Minkowski space-time with orthonormal Cartesian basis vectors γ the "time" component of (2.229) reads

$$\nabla \wedge F \wedge \gamma_0 = -cI \operatorname{div} \vec{B} = 0, \quad (2.231)$$

which is equivalent to the traditional magnetic Gauss law (no magnetic monopoles). We want to obtain the equivalent of this law in rotating reference frame.

In order to achieve that, we expand (2.229) in the orthonormal frame $\hat{\gamma}$ with four-velocity $\hat{\gamma}_0$ of the congruence describing motion of the system and some orthonormal space-like basis vectors $\hat{\gamma}_i$

$$\begin{aligned} \nabla \wedge F &= (\hat{\gamma}^\alpha \nabla_{\hat{\gamma}_\alpha}) \wedge (\hat{E}^i \hat{\gamma}_i \hat{\gamma}_0 + \hat{B}^i I\hat{\gamma}_i \hat{\gamma}_0) = \\ &= \hat{\gamma}^\alpha \wedge \left[\nabla_{\hat{\gamma}_\alpha} \hat{E}^i \hat{\gamma}_i \hat{\gamma}_0 + \hat{E}^i (\nabla_{\hat{\gamma}_\alpha} \hat{\gamma}_i) \hat{\gamma}_0 + \hat{E}^i \hat{\gamma}_i (\nabla_{\hat{\gamma}_\alpha} \hat{\gamma}_0) + \nabla_{\hat{\gamma}_\alpha} \hat{B}^i I\hat{\gamma}_i \hat{\gamma}_0 + I\hat{B}^i (\nabla_{\hat{\gamma}_\alpha} \hat{\gamma}_i) \hat{\gamma}_0 + I\hat{B}^i \hat{\gamma}_i (\nabla_{\hat{\gamma}_\alpha} \hat{\gamma}_0) \right] \end{aligned} \quad (2.232)$$

⁵⁴ Derivation: suppose (u, e_x, e_y, e_z) form an orthonormal basis. Then the electric and magnetic fields are given by

$$\vec{E} = E^i e_i u, \quad \vec{B} = B^i e_i u, \quad (2.224)$$

respectively. In order to calculate $uFu = u\vec{E}u + uIc\vec{B}u$ we note that

$$u\vec{E}u = u(E^i e_i u)u = -u^2(E^i e_i u) = -\vec{E}. \quad (2.225)$$

Analogously we derive $uIc\vec{B}u = Ic\vec{B}$. Thus we see that

$$uFu = -\vec{E} + Ic\vec{B}, \quad (2.226)$$

from which (2.227) and (2.228) follow.

We focus our attention on “time” component of this equation by wedging it with $\hat{\gamma}_0$. Then the first two terms vanish (as they contain $\hat{\gamma}_0$ and $a \wedge a = 0$) and index $\alpha = 0, 1, 2, 3$ can be replaced by $k = 1, 2, 3$ (due to $\hat{\gamma}^0 = \hat{\gamma}_0$) resulting in⁵⁵

$$\begin{aligned} \nabla \wedge F \wedge \hat{\gamma}_0 &= \hat{\gamma}^k \left[\hat{E}^i \hat{\gamma}_i (\nabla_{\hat{\gamma}_k} \hat{\gamma}_0) + \nabla_{\hat{\gamma}_k} \hat{B}^i I \hat{\gamma}_i \hat{\gamma}_0 + I \hat{B}^i (\nabla_{\hat{\gamma}_k} \hat{\gamma}_i) \hat{\gamma}_0 + I \hat{B}^i \hat{\gamma}_i (\nabla_{\hat{\gamma}_k} \hat{\gamma}_0) \right] \wedge \hat{\gamma}_0 = \\ &= \hat{E}^i \hat{\gamma}^k \wedge \hat{\gamma}_i \wedge (\nabla_{\hat{\gamma}_k} \hat{\gamma}_0) \wedge \hat{\gamma}_0 + \nabla_{\hat{\gamma}_k} \hat{B}^i \hat{\gamma}^k \wedge (I \hat{\gamma}_i \hat{\gamma}_0) \wedge \hat{\gamma}_0 + \hat{B}^i \hat{\gamma}^k \wedge (I (\nabla_{\hat{\gamma}_k} \hat{\gamma}_i) \hat{\gamma}_0) \wedge \hat{\gamma}_0 + \hat{B}^i \hat{\gamma}^k \wedge (I \hat{\gamma}_i (\nabla_{\hat{\gamma}_k} \hat{\gamma}_0)) \wedge \hat{\gamma}_0. \end{aligned} \quad (2.233)$$

Therefore, we see that the covariant derivatives of the basis vectors have to be calculated. This is equivalent to specifying the connection on the manifold. However, we assume that the connection is already defined by stating that in Cartesian coordinate frame γ_α , $\alpha = t, x, y, z$ all the derivatives $\nabla_{\gamma_\alpha} \gamma_\beta$ (thus connection coefficients too) vanish. Therefore, our calculations should be perceived as change in connection coefficients due to change of basis and coordinates.

Now we specify our attention to the observer rotating with constant angular velocity Ω . The axis of rotation is chosen to be the z axis. Cylindrical coordinates r and θ are natural choice due to the symmetry of the problem. They are introduced as

$$p = t\gamma_t + x\gamma_x + y\gamma_y + z\gamma_z = t\gamma_t + r \cos \theta \gamma_x + r \sin \theta \gamma_y + z\gamma_z, \quad (2.234)$$

where p is a position vector in space-time.

We define the motion of the system by stating that the position vector of each particle is parametrized by time t

$$p_t(\vec{r}_{\text{ref}}) = t\gamma_t + r \cos(\varphi + \Omega t) \gamma_x + r \sin(\varphi + \Omega t) \gamma_y + z\gamma_z, \quad (2.235)$$

where we assumed that the non-rotating polar angle θ is related to the polar angle in the rotating system via⁵⁶ $\theta = \varphi + \Omega t$. The tangent vector to this congruence is

$$\frac{dp}{dt} = \gamma_t - \Omega r \sin(\varphi + \Omega t) \gamma_x + \Omega r \cos(\varphi + \Omega t) \gamma_y \quad (2.237)$$

and

$$\left| \frac{dp}{dt} \right|^2 = 1 - \Omega^2 r^2. \quad (2.238)$$

So the normalized four velocity of the congruence is

$$\hat{\gamma}_0 = \frac{dp}{dt} / \left| \frac{dp}{dt} \right| = \frac{\gamma_t + \Omega r \hat{e}_\varphi}{\sqrt{1 - \Omega^2 r^2}}, \quad (2.239)$$

where we introduced the normalized vector of cylindrical coordinates

$$\hat{e}_\varphi = \hat{e}_\theta = -\sin \theta \gamma_x + \cos \theta \gamma_y \quad \hat{e}_\theta^2 = -1. \quad (2.240)$$

We use Gram-Schmidt orthogonalization to obtain the frame of a rotating observer

$$\hat{\gamma}_0 = \frac{\gamma_t + \Omega r \hat{e}_\varphi}{\sqrt{1 - \Omega^2 r^2}} \quad (2.241)$$

$$\hat{\gamma}_r = \gamma_r \quad (2.242)$$

$$\hat{\gamma}_\varphi = \frac{\hat{e}_\varphi + \Omega r \gamma_t}{\sqrt{1 - \Omega^2 r^2}} \quad (2.243)$$

$$\hat{\gamma}_z = \gamma_z, \quad (2.244)$$

where we denote by hat our orthonormal basis vectors as opposed to coordinate basis vectors γ . While calculations become easier in coordinate frames, the actual physical field components are described w.r.t. the orthonormal frame of the congruence.

⁵⁵ We use the properties of an orthonormal basis $\hat{\gamma}$, such as $\hat{\gamma}_a \hat{\gamma}_b = \hat{\gamma}_a \wedge \hat{\gamma}_b$, $a \neq b$ or $\hat{\gamma}_a \cdot \hat{\gamma}_b = 0$, $a \neq b$, to simplify the expression. For further details see Appendix B.3.

⁵⁶ Since in the end we are interested in the first order in $\delta = r\Omega/c$ approximation, we have replaced the angle dependency in (2.205) by

$$\theta = \varphi + \tanh\left(\frac{r\Omega}{c}\right) \frac{ct}{r} = \varphi + \frac{\tanh \delta}{\delta} \Omega t = \varphi + [1 + \mathcal{O}(\delta^2)] \Omega t = \varphi + \Omega t + \mathcal{O}\left(\left(\frac{r\Omega}{c}\right)^2\right). \quad (2.236)$$

Performing technical manipulations collected in Appendix B.3, (2.233) is expanded to

$$\nabla \wedge F \wedge \hat{\gamma}_0 = -I \left(\frac{2\Omega \hat{E}^z}{1 - \Omega^2 r^2} + \nabla_{\hat{\gamma}_k} \hat{B}^k + \frac{1}{r(1 - \Omega^2 r^2)} \hat{B}^r \right) = 0, \quad (2.245)$$

which could have been obtained alternatively by applying the theory outlined in [18, Section VI], [24, Chapter B.4.4] or [4, Section 2]. In [43, Equation (23)] or [40, Equation (2.14)] the 3D transverse metric of a rotating observer is introduced. In cylindrical coordinates its matrix representation is diagonal with entries $(1, \gamma^2 r^2, 1)$, where γ is the Lorentz factor $\gamma := 1/\sqrt{1 - v^2/c^2}$. If this metric is employed in the definition of divergence, then (2.245) is equivalent to (we introduce the speed of light $c = 1$ explicitly)

$$\operatorname{div} \vec{B} + \frac{2\vec{\Omega} \cdot \vec{E}}{c^2} = 0. \quad (2.246)$$

Please note that in our treatment Ω is the rotation rate of a rotating observer as seen by a stationary observer. Sometimes in the literature the other convention (passive versus active transformation) is chosen, which leads to the sign difference in Ω . We would like to mention that up to the first order in $r\Omega/c$ (2.245) reads

$$\operatorname{div} \vec{B} + \frac{2\vec{\Omega} \cdot \vec{E}}{c^2} = \mathcal{O}(\Omega^2), \quad (2.247)$$

where div is taken with respect to the 3D Euclidean metric, i.e.,

$$\operatorname{div} \vec{B} = \frac{1}{r} \hat{B}^r + \partial_r \hat{B}^r + \frac{1}{r} \partial_\varphi \hat{B}^\varphi + \partial_z \hat{B}^z. \quad (2.248)$$

3 Discretization

In this chapter we discretise the equations of classical electromagnetism, namely (2.209) supplemented by (2.212). We review some generic concepts associated with discretisation in Section 3.1. The discretisation of a computational domain is treated in more details in Section 3.1.1. It is convenient to construct the 4D mesh complex from 3D primal mesh due to the fact that there is a wide variety of available 3D mesh generators and the material distribution is constant in time with respect to the 3D mesh. In Section 3.2 we discretise Maxwell's equations directly in space-time by applying the integral form of Maxwell's equations (2.210) to this 4D complex. Later we reduce them to a form similar to 3D FIT with Leapfrog time integration. The material equations are discretised separately (and elaborately) in Section 3.3. In both methods described there, we use n -vector valued Whitney interpolating functions N_i^n associated with i -th n -dimensional element of the mesh to derive explicit expressions for the material matrix M_ξ , which is the discrete equivalent of the material mapping ξ . We summarise in Section 3.4 by deriving the set of linear equations that is solved in applications of Sections 4, 5 and 6.

In this chapter we use GA as well as linear algebra. Therefore, we introduce the following notation. The elements of linear algebra (vectors and matrices) are denoted with a bar under the symbol

$$\underline{f} := [f_1, f_2, \dots, f_n]^T, \quad (3.1)$$

where n follows from the context (for example, in the case of \underline{f} it is the number of 2D facets). Analogously \underline{M} is the matrix with entries M_{ij} . If the quantities from linear algebra are multiplied, the product from that algebra is employed. We skip bars under 3D material matrices and DoF (Degrees of Freedom) vectors in Section 3.4, through which only linear algebra is employed.

3.1 Discretization Concepts

Differential Equation in Continuous Setting. Let us consider

$$\mathcal{L}y(x) = 0 \quad x \in K, \quad (3.2)$$

where \mathcal{L} is a differential operator and K is the domain of interest. We do not restrict y nor x to be a scalar, e.g., to recast Maxwell's equations (2.207) in this form one would naturally choose $y(x) \in \mathbb{R}^{12}$ with components of $\vec{E}, \vec{B}, \vec{D}$ and \vec{H} , while $x \in \mathbb{R}^4$ would be the position vector in space-time.

Approximations. Suppose we want to solve (3.2) numerically. First, all arithmetic operations in \mathbb{R} need to be approximated by operations in floating point numbers due to finite precision of the machine. The error associated with that approximation is called the round-off error, and is assumed to be much smaller than other approximation errors. Moreover, to represent $y(x)$ in the entire domain of interest K one would need infinite memory as there are infinitely many points $x \in K$. Therefore, it is necessary to approximate the continuous function $y(x)$ by $\tilde{y}(x; y_k)$ which is parametrised by a finite number of DoFs y_k . By doing so, we introduce yet another error, which is called the discretisation error. We assume that this error is dominant in the resulting numerical scheme to be run on a computer.

Convergence. Suppose the discretisation $\tilde{y}(x; y_k)$ depends on the mesh size⁵⁷ h . Let $\tilde{y}(x, h)$ be a numerical solution (obtained using some computational scheme) to (3.2) associated with mesh size h . Then we say that the computational method converges iff

$$\lim_{h \rightarrow 0} \|\tilde{y}(x, h) - y(x)\| = 0. \quad (3.3)$$

In other words, the method is convergent iff as h tends to zero, the numerical solution tends to the continuous solution $y(x)$ being the solution to (3.2). i.e.,

$$\lim_{h \rightarrow 0} \mathcal{L} \tilde{y}(x, h) = 0. \quad (3.4)$$

Moreover, assume that there exists a convergent Taylor (or any asymptotic) expansion of $\tilde{y}(x, h)$ with respect to h

$$\tilde{y}(x, h) = y(x) + \sum_{r=0}^{\infty} \frac{\partial^r \tilde{y}}{\partial h^r} \Big|_{h=0} \frac{h^r}{r!}, \quad (3.5)$$

and

$$\frac{\partial^r \tilde{y}}{\partial h^r} \Big|_{h=0} = 0, \quad r = 1, \dots, (m-1). \quad (3.6)$$

Then the method is said to be m -th order convergent. In other words, the method exhibits m -th order convergence if the asymptotic expansion of $\tilde{y}(x, h) - y(x)$ with respect to h has the leading behaviour of h^m , i.e.,

$$\tilde{y}(x, h) - y(x) = \mathcal{O}(h)^m. \quad (3.7)$$

Stability. Suppose \mathcal{L} in (3.2) depends on a parameter $\eta \in [a, b]$, $a, b \in \mathbb{R}$, i.e., we want to solve

$$\mathcal{L}(\eta)y(x; \eta) = 0, \quad (3.8)$$

where the solution $y(x; \eta)$ depends parametrically on η . Then we say that the solution is stable with respect to η iff

$$[|\eta - \eta_0| < \infty] \implies [\|y(x; \eta) - y(x; \eta_0)\| < \infty]. \quad (3.9)$$

Consistency. The discretisation of the differential operator \mathcal{L} leads to its discrete counterpart $\tilde{\mathcal{L}}_h$ depending on the mesh size h . We say that the discretisation $\tilde{\mathcal{L}}_h$ is consistent, see [42, page 37, Section 2.2, Equation (2.13)] or [3, page 218, Section 8.3, Equation (8.3)], with continuous equation (3.2) if it tends to \mathcal{L} as the mesh is refined to the size $h \rightarrow 0$, i.e.,

$$\lim_{h \rightarrow 0} \tilde{\mathcal{L}}_h y(x) = \mathcal{L} y(x), \quad (3.10)$$

for all functions $y(x)$ belonging to a space considered.

⁵⁷ By mesh size, we mean a maximal characteristic length, e.g., a radius of a circumscribed circle, among all cells of the mesh.

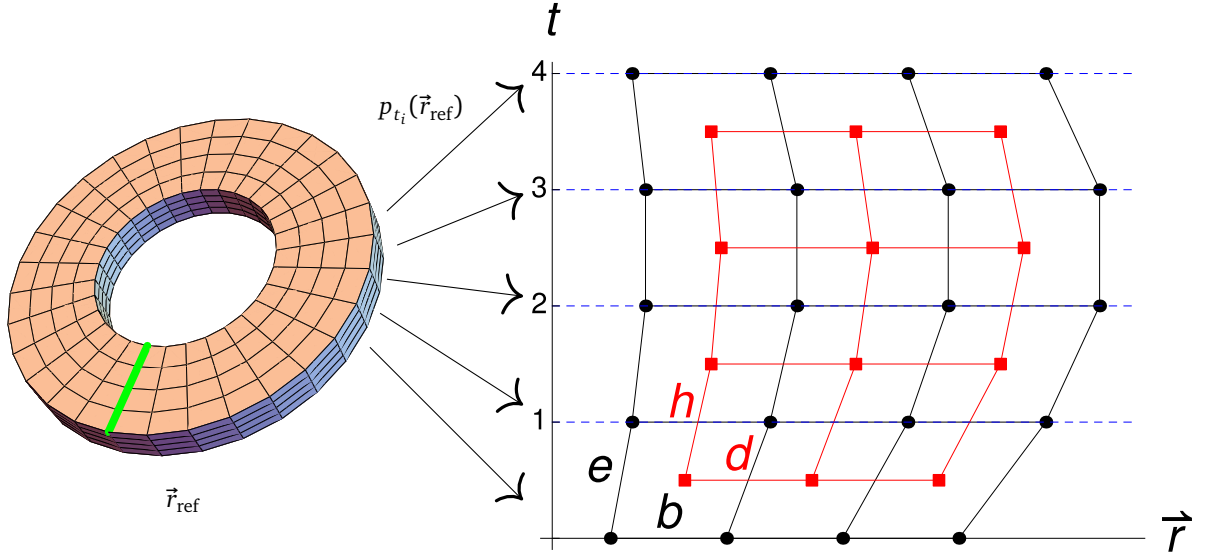


Figure 2: Sketch of a space-time mesh used in simulation. The thick green line in the left image is mapped to horizontal lines in the right figure. Alternatively, the horizontal lines may be perceived as images of the whole 3D reference mesh under the placement mapping.

3.1.1 4D Mesh Construction

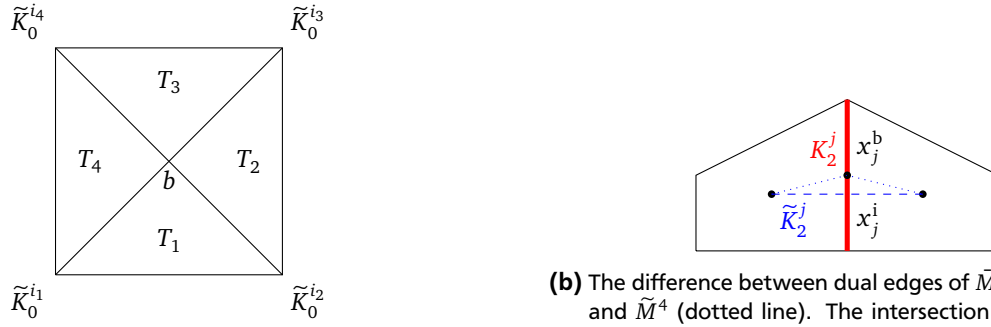
Here we use the placement map (2.205) to specify the observer. This map is used to create the 4D primal mesh from a 3D one⁵⁸. Thus, for the class of meshes discussed in this thesis, 4D elements are tensor products of 3D elements and 1D temporal intervals. Therefore, the extension of any particular 3D Whitney elements to 4D ones is straightforward. Since in our implementation we work with hexahedral 3D mesh, our 4D elements are “4D hexahedrons”. For the discretisation of Maxwell’s equations we need to consider a dual mesh derived from the primal one. Thus subsequently, the dual mesh is constructed from dual nodes, being barycenters of primal cells. In the end we introduce two possible choices for the barycentric dual. We want to stress that, one can use the barycentric dual mesh (with broken edges) in both FEM (Finite Element Method) and FIT (Finite Integration Technique) as well. We present, however, the FIT derivations for a dual with straight edges, as that is implemented in the code used to simulate numerical examples.

Extrusion of the 3D Mesh. We depict the mesh construction in Fig. 2. Let M^3 be a 3D reference mesh depicted as a toroid in the leftmost of Fig. 2. We proceed to create images of M^3 under the placement map (2.205) $p_t(M^3)$ at times $t = t_1, t_2, \dots, t_i$. This is readily carried out by applying p_t to the position vector \vec{r}_{ref} of the nodes in M^3 while preserving the connectivity, i.e., the incidence relations between elements. The resulting space-time nodes are depicted as black points in Fig. 2 and the elements inherited from M^3 as black horizontal lines joining these points. We then connect, along the “vertical” time line (see Fig. 2), the nodes corresponding to the same reference point in M^3 . The resulting 4D mesh is referred to as M^4 , and we refer to the i -th n -dimensional element of M^4 as K_n^i . Analogously elements of the dual mesh are denoted by \tilde{K}_n^i .

Two Choices for Barycentric Dual. We define two kinds of dual meshes; namely, one is \bar{M}^4 that will be used in a 4D FIT context, and the other is \tilde{M}^4 in a 4D FEM context. In both cases the connectivity and dual nodes are the same. As depicted in Fig. 2 with red squares, the dual nodes are the barycenters of the 4D cells of M^4 . Therefore, it appears natural to label a dual node within a 4D cell K_4^i with the same index i . Nodes are used to form higher dimensional elements in the following way. If $K_4^i \cap K_4^j = K_3^k$ then the dual nodes i and j are connected, and the resulting connecting edge is labelled with index k . In the same frame of ideas, the dual edge k belongs to the dual facet l if $K_2^l \subset K_3^k$, and so on for dual 3D and 4D elements. This enumeration of the dual cells \tilde{K}_n^i induced by enumeration of the primal cells K_4^i is a standard procedure in FIT.

Although we have defined the connectivity of all elements and positions of the dual nodes, the exact geometry of the dual elements is not settled by these definitions. In fact, there are two cases in which we are interested and describe them next.

⁵⁸ We follow the idea of extrusion of a 3D mesh, rather than meshing 4D domain at once, due to two reasons. First, the convergence analysis in 4D is not yet well understood. Second, as it will be shown later, the symmetries of motion (four-velocity field u) are manifested in resulting 3D material matrices being constant for each time step, which is a considerable benefit in terms of computational time.



(a) A dual facet of \bar{M}^4 with $n = 4$ edges. The barycenter of the dual nodes \tilde{K}_0^i is denoted by b . The facet consists of $n = 4$ flat triangles T_i .

(b) The difference between dual edges of \bar{M}^4 (dashed line) and \tilde{M}^4 (dotted line). The intersection point x_j^i of K_2^j and \tilde{K}_2^j in \bar{M}^4 is not the barycenter x_j^b of K_2^j as in \tilde{M}^4 . Nevertheless, we later use the interpolated fields at x_j^b in our extension of FIT material matrices.

Figure 3

The barycentric dual with straight edges \bar{M}^4 is obtained by joining the dual nodes with a straight line segment. The dual facet with n edges (see Fig. 3a) is composed of n flat triangles with the nodes at dual edge's nodes plus the barycenter of all dual nodes belonging to the dual facet. If the dual nodes are coplanar our definition reduces to the flat dual facet. The dual 3D element is defined as bounded by the dual facets.

The barycentric dual \tilde{M}^4 is defined as the 4D extension of the 3D construction described in [6, page 99]. Briefly speaking, the dual edge is defined as a broken line segment consisting of the dual nodes and the barycenter of a corresponding 3D element (see Fig. 3b). This construction is extended to higher dimensional dual elements in such a way that the intersection of the corresponding dual and primal objects is always the barycenter of the primal one. Moreover, each dual object is a sum of flat simplices. This construction in 2D and 3D case is depicted in [6, Fig. 4.3 and Fig. 4.4], respectively.

Now, let us assume that the reference mesh M^3 bears some orientation of facets and edges. To uniquely define the orientation of the 4D mesh M^4 we adopt the convention “first time then space”. Therefore, if the edge is represented by a vector p , then the timelike facet associated with that edge has the orientation given by the product $u \wedge p$.

Remark: We apply several heuristics in our space-time extension of the FIT material matrices, such as using barycenters of K_2^j as collocation points, see Fig. 3b. In brief, one may perceive 4D FIT as potentially more efficient, but there is no underlying theory, e.g., error analysis or convergence proof. On the other hand 4D FEM is built on the sound mathematical framework being, however, computationally more expensive. Therefore, we find it interesting to present both approaches to the discretization of material mapping.

3.2 Discretization of Maxwell's Equations

In this section we discretize Maxwell's equations. After general discretization in space-time, we introduce some further simplifications coming from our particular construction of the 4D mesh. The physical interpretation of DoFs coming from these simplifications is given, and relation to the discrete boundary conditions is briefly discussed. Our goal was to stick to the 3D FIT approach with leapfrog time integration, as close as possible.

We discretize Maxwell's equations by applying their integral form (2.210) to the primal-dual mesh pair. The (2.210)-left is applied to the primal grid and (2.210)-right to the dual one. This yields

$$\oint_{\partial K_3^i} (d^2x) \cdot F = 0, \quad \oint_{\partial \tilde{K}_3^i} (d^2x) \wedge G = \int_{\tilde{K}_3^i} (d^3x) \wedge J. \quad (3.11)$$

Please note that integrals over the boundary of primal and dual 3-cells ∂K_3^i and $\partial \tilde{K}_3^i$ are sums of integrals over 2D facets, i.e.,

$$\oint_{\partial K_3^i} (d^2x) \cdot F = \sum_j \int_{K_2^j} (d^2x) \cdot F, \quad \oint_{\partial \tilde{K}_3^i} (d^2x) \wedge G = \sum_j \int_{\tilde{K}_2^j} (d^2x) \wedge G. \quad (3.12)$$

Therefore, in the case of a general mesh, like a simplicial 4D one as used in [44], we would introduce scalar (thus dual ones are pre-multiplied by I^{-1}) DoFs

$$f_j := \int_{K_2^j} (d^2x) \cdot F, \quad g_j := I^{-1} \int_{\tilde{K}_2^j} (d^2x) \wedge G, \quad j_i := I^{-1} \int_{\tilde{K}_3^i} (d^3x) \wedge J, \quad (3.13)$$

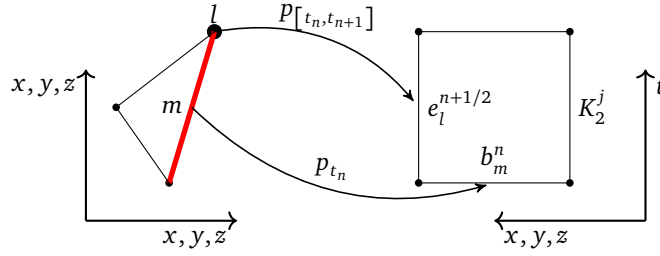


Figure 4: Illustration of the relation between indices in (3.17). The leftmost is the reference mesh. The l -th edge is depicted as a fat dot, and m -th 2D facet as a thick red line. The rightmost is the space-time mesh. 2D facets are depicted as lines.

obtaining thus the discrete Maxwell's equations

$$\underline{D}^2 \underline{f} = 0, \quad \underline{\tilde{D}}^2 \underline{g} = \underline{j}, \quad (3.14)$$

where \underline{D}^2 and $\underline{\tilde{D}}^2$ are incidence matrices describing adjacency of 2D to 3D elements of the primal and dual mesh, respectively. Matrices \underline{D}^n have entries

$$D_{ij}^n := \begin{cases} +1 & \text{if } K_n^j \subset K_{n+1}^i \text{ with matching orientation} \\ -1 & \text{if } K_n^j \subset K_{n+1}^i \text{ with opposite orientation} \\ 0 & \text{if } K_n^j \not\subset K_{n+1}^i \end{cases}, \quad (3.15)$$

and analogously for $\underline{\tilde{D}}^n$. According to Appendix C.1 primal and dual discrete exterior derivatives are related by

$$\underline{\tilde{D}}^n = (-1)^{d-n} [\underline{D}^{d-n}]^T, \quad (3.16)$$

with d being the dimension of the ambient space.

Nevertheless, we have chosen a structured 4D mesh, and we shall exploit this fact in order to simplify the discrete form of Maxwell's equations. Since in this work we are interested in wave propagation phenomena, we assume $J = 0$ in (2.208) to simplify our derivations. This assumption does not introduce any limitation of the method.

Next, we rename and renumber the DoFs on the primal mesh as follows

$$f_j = \int_{K_2^j} (d^2x) \cdot F =: \begin{cases} e_l^{n+1/2} & \text{if } K_2^j \text{ is timelike,} \\ b_m^n & \text{if } K_2^j \text{ is spacelike,} \end{cases} \quad (3.17)$$

where the relation between the indices j, l, m and n is as follows (see also Fig. 4). If the facet K_2^j is timelike, it is the edge l in the reference mesh M^3 extruded in time via the placement map p_t such that $t \in [t_n, t_{n+1}]$. Similarly, if the facet K_2^j is spacelike, then it is the image of a facet with index m in M^3 under the map p_t with $t = t_n$.

We perform a similar decomposition of the dual DoFs

$$g_j = I^{-1} \int_{\tilde{K}_2^j} (d^2x) \wedge G =: \begin{cases} d_l^{n+1/2} & \text{if } \tilde{K}_2^j \text{ is spacelike} \\ h_m^n & \text{if } \tilde{K}_2^j \text{ is timelike} \end{cases}. \quad (3.18)$$

In simple words, instead of an arbitrary enumeration of the 2D facets in M^4 , we rather label them by using the facet/edge numbering in M^3 and the time step to which they correspond. This numbering scheme is always possible and unique due to our particular construction of the 4D mesh. Such a decomposition aids the physical interpretation of the DoFs, as well as enables a simple time marching procedure, which is in general not possible on unstructured 4D meshes as considered in [44].

We now move towards the physical interpretation of the previously introduced DoFs. By \vec{E}_s and \vec{B}_s we denote the 3D fields obtained by performing the space-time split by a stationary observer, i.e., the one with the four-velocity $u = \gamma_t$ in (2.227) and (2.228). Analogously, the fields \vec{E}_r and \vec{B}_r are associated with (the four-velocity u given by (B.15) of) the rotating observer.

Spacelike case:

Let us consider a spacelike facet K_2^j , and let us suppose that it is spanned by orthonormal vectors γ_1 and γ_2 and parametrized with local coordinates x^1 and x^2 . The “normal” vector γ_3 is uniquely defined by requiring that γ_i , with $i = t, 1, 2, 3$ form an orthonormal set with the orientation $\gamma_t \gamma_1 \gamma_2 \gamma_3 = +I$. Then

$$b_m^n = \int_{K_2^j} (d^2x) \cdot F = \int_{K_2^j} ((\gamma_1 dx^1) \wedge (\gamma_2 dx^2)) \cdot (\vec{E}_s + I\vec{B}_s) = \int_{K_2^j} dx^1 dx^2 (\gamma_1 \gamma_2) \cdot (E_s^i \gamma_i \gamma_t + I B_s^i \gamma_i \gamma_t) = \int_{K_2^j} dx^1 dx^2 B_s^3. \quad (3.19)$$

Now we bring the expression above to the form from traditional 3D vector analysis. First, we note that vector surface element $d\vec{S} := \vec{n} dS$, where the normal vector \vec{n} is defined as a cross product of vectors spanning the surface; that is

$$\vec{n} := \sigma_1 \times \sigma_2 = -I \sigma_1 \wedge \sigma_2 = \sigma_3. \quad (3.20)$$

Next, the magnetic field component may be written as

$$B_s^3 = \sigma_3 \cdot \vec{B}_s = \vec{n} \cdot \vec{B}_s. \quad (3.21)$$

Therefore, in general it holds

$$b_m^n = \int_{K_2^j} dx^1 dx^2 B_s^3 = \int_{K_2^j} dS (\vec{n} \cdot \vec{B}_s) = \int_{K_2^j} d\vec{S} \cdot \vec{B}_s. \quad (3.22)$$

Therefore, \underline{b}^n coincides with \widehat{b}^n from FIT [60].

Timelike case:

Now, let us consider a timelike facet K_2^j , and let us suppose that it is spanned by orthonormal vectors u and p . The local coordinates of the facet are: the proper time τ and the distance along the edge l . Then we get analogously

$$e_l^{n+1/2} = \int_{K_2^j} (d^2x) \cdot F = \int_{K_2^j} ((u d\tau) \wedge (p dl)) \cdot (\vec{E}_r + I\vec{B}_r) = - \int_{K_2^j} d\tau dl \vec{p} \cdot \vec{E}_r, \quad (3.23)$$

where $\vec{p} := p \wedge u$ is a 3D vector representing an edge. Please note that $\underline{e}^{n+1/2}$ is (minus) time-integrated FIT $\widehat{e}^{n+1/2}$, i.e.,

$$\underline{e}^{n+1/2} = - \int d\tau \widehat{e}^{n+1/2}. \quad (3.24)$$

The same reasoning leads to the physical interpretation of the dual DoFs d and h . The DoFs denoted by e and h are related to the electric and magnetic fields \vec{E}_r and \vec{H}_r , respectively, in the moving reference frame, While the DoFs denoted by d and b are related to the electric and magnetic flux densities \vec{D}_s and \vec{B}_s , respectively, in the stationary reference frame.

The physical interpretation of the DoFs enhances the imposition of boundary conditions. For example, if we consider stationary Perfect Electric Conductor (PEC) boundary conditions, then in 3D formulation one sets $e = 0$ on the boundary, which corresponds to setting the tangential component of \vec{E}_s to zero, i.e.,

$$\vec{n}_s \times \vec{E}_s = 0, \quad (3.25)$$

where \vec{n}_s is the vector normal to PEC in a stationary reference frame.

If the PEC is rotating, then one needs to set the tangential component of \vec{E}_r to zero at the boundary, i.e.,

$$\vec{n}_r \times \vec{E}_r = 0, \quad (3.26)$$

where \vec{n}_r is the vector normal to PEC in a rotating reference frame. Nevertheless, due to the particular construction of the mesh and the resulting physical interpretation of the DoFs, it is clear that (3.26) is equivalent to setting $e = 0$ on the boundary. Therefore, from the implementation point of view nothing has changed due to movement.

Using (3.17) gives another advantage, namely, allows for a straightforward time marching procedure. The Maxwell's grid equations (3.14) (with omitted discrete equivalents of $\text{div} \vec{B}_s = 0$ and $\text{div} \vec{D}_s = \rho_s$) now read

$$\underline{b}^{n+1} = \underline{b}^n + \underline{C} \underline{e}^{n+1/2}, \quad \underline{d}^{n+1/2} = \underline{d}^{n-1/2} + \underline{\tilde{C}} \underline{h}^n, \quad (3.27)$$

which are first solved for $n = 1$, then for $n = 2$, and so on. \underline{C} and $\widetilde{\underline{C}}$ [60] are, respectively, primal and dual facets to edges incidence matrices of the reference 3D mesh, that is discrete curl operators.

The signs in (3.27) depend on our convention “first time then space” for orientations of elements. The convention affects the decomposition of, e.g., \underline{D}^2 , in (3.14) to the temporal difference and 3D curl-matrix \underline{C} . For relation of our DoFs to the FIT ones, see (3.123).

We want to point out the similarity with 3D FIT + leapfrog [60]. It was shown, e.g., in [31, 33], that leapfrog is implied by the topology of the primal/dual mesh pair. However, this is only true if the material matrices are local in time, that is they relate only the fields at the same time step, i.e.,

$$\underline{d}^{n+1/2} = \underline{M}_{ee} e^{n+1/2}, \quad \underline{h}^n = \underline{M}_{vb} b^n. \quad (3.28)$$

Nevertheless, Maxwell’s grid equations, i.e., topological laws [23, Equation (4)], have not changed, because the movement is encoded only in the geometry of the mesh, not in the topology. However, our scheme does not always reduce to leapfrog as we consider space-time setting. Material matrices may relate DoFs at different time steps, which in turn leads to a change of the resulting time integration scheme.

3.3 Discretization of Material Equations

The overview: As discussed before and in Appendix C.2, the discretised Maxwell’s equations are the same in FIT and Whitney FEM on the primal/dual cell complex. From computational point of view, the only difference is in the discretization of material laws. Before presenting general FIT or FEM material matrices in Sections 3.3.4 and 3.3.5, we focus first on the interesting special case when the FIT material matrix construction leads to diagonal matrices. As they are beneficial due to computational reasons, in Section 3.3.1 we derive a necessary and sufficient condition (3.44) for FIT material matrices to be diagonal. We would like to mention that FEM material matrices are never diagonal; although they can be diagonalised via so-called mass lumping, this process may decrease the convergence order of the scheme. It should be kept in mind that the explicit formula for material matrices in Section 3.3.1 is valid only when material matrices are diagonal, i.e., when (3.44) holds. The derived condition for diagonal matrices is employed in Section 4 to optimise meshes for FIT simulations. In Section 3.3.2 we discuss the necessity of dealing with non-diagonal material matrices; see also the limitations of mesh optimisation derived in Section 4.2, e.g., (4.23). In Section 3.3.3 we elaborate on n -vector valued Whitney interpolating functions N_i^n , which are later used to derive explicit expressions for material matrices in both methods. We treat our proposed extension of FIT material matrices in Section 3.3.4. However, the convergence proof for this method is missing; therefore, we incorporate FEM with Galerkin Hodge star (or Energetic Approach) [13, 7] in our framework in Section 3.3.5. FEM will be later used to calculate reference solutions in Section 5, because the convergence of FEM has been proved.

In both approaches the discretisation error is introduced via discrete material laws⁵⁹. In the following we assume that the material is allocated in primal grid, i.e., in each 4D cell K_4^i there is a constant material mapping ξ_i .

3.3.1 Diagonal Material Matrices

The Overview. The constitutive material equation ξ (2.212) relates G to F . Thus its discrete equivalent will link \underline{g} to \underline{f} in (3.13). Due to computational efficiency, it is beneficial if the obtained relation links one dual DoF g_j with exactly one primal DoF f_j . In other words the discrete equivalent \underline{M}_ξ of material mapping ξ is a diagonal matrix, and

$$\underline{g} = \underline{M}_\xi \underline{f}. \quad (3.29)$$

If that is the case, then one can take advantages like low memory requirements of storage or ease of inverting diagonal matrices. Our goal here is to investigate when the material matrices obtained by general FIT reasoning happen to be diagonal.

Considering a single primal DoF in (3.13) as a (linear) functional of F , i.e.,

$$f_j[F] = \int_{K_2^j} (d^2x) \cdot F, \quad (3.30)$$

leads naturally to the fields $F_j^0 \in \ker(f_j)$, which are not “visible” to f_j , i.e.,

$$f_j[F_j^0] \equiv 0. \quad (3.31)$$

⁵⁹ Provided one is interested in DoFs, e.g., \underline{f} . If the continuous field $F(x)$ needs to be calculated from DoFs, the interpolation error is present.

This might be seen as follows. After the discretisation (and in numerical simulations as well), we have access only to \underline{f} , and not to F . However, there are many field configurations F that produces the same \underline{f} . Therefore, our knowledge about F from \underline{f} is limited to an equivalence class $[F]$, members of which differ by some gauging. Since we are interested in relating exactly one dual DoF with a primal one, it is important that g_j is well defined by the information about F captured by f_j . By definition we can add any $F_j^0 \in \ker(f_j)$ without changing the value of f_j , i.e.,

$$f_j[F + F_j^0] = f_j[F] + f_j[F_j^0] = f_j[F]. \quad (3.32)$$

This can be expressed as that after the discretisation we work with the quotient space of bivector fields divided by kernels (null-spaces) of all DoFs f_j . Therefore, we cannot refer to the unique field described by \underline{f} , but rather to the whole equivalence class comprising of all elements differing by an element F_j^0 of the kernel.

The dual DoF g_j will be well defined in terms of f_j , if it is independent of the choice of the representative of an equivalence class, i.e.,

$$g_j[F + F_j^0] = g_j[F] \Rightarrow g_j[F_j^0] = 0. \quad (3.33)$$

Being more explicit,

$$g_j[F_j^0] = I^{-1} \int_{\tilde{K}_2^j} (d^2x) \wedge \xi(F_j^0) = \int_{\tilde{K}_2^j} (Id^2x) \cdot \xi(F_j^0) = \int_{\tilde{K}_2^j} \xi^\dagger(Id^2x) \cdot F_j^0 = 0, \quad (3.34)$$

where ξ^\dagger is the conjugate of ξ . The conjugate is defined such that for all bivectors A_1, A_2 it holds

$$\xi^\dagger(A_1) \cdot A_2 = A_1 \cdot \xi(A_2) \quad (3.35)$$

and it coincides with the conjugate in the traditional linear algebra sense. Please note that for all materials considered in this dissertation $\xi^\dagger = \xi$.

Thus the material matrix \underline{M}_ξ is diagonal (without making any additional approximations) if and only if

$$f_j[F_j^0] = 0 \Rightarrow g_j[F_j^0] = 0, \quad (3.36)$$

i.e.,

$$\left[\int_{K_2^j} (d^2x) \cdot F_j^0 = 0 \right] \Rightarrow \left[\int_{\tilde{K}_2^j} \xi^\dagger(Id^2x) \cdot F_j^0 = 0 \right], \forall F_j^0. \quad (3.37)$$

This condition, although derived without any approximations, is not yet convenient for a practical use. Please note that the two domains of integration above are different, i.e., K_2^j and \tilde{K}_2^j , having however, a single intersection point $x_j = K_2^j \cap \tilde{K}_2^j$. Therefore, we approximate both integrals by a one-point quadrature, with x_j being a quadrature point. For example, f_j is approximated by

$$f_j = \int_{K_2^j} (d^2x) \cdot F \approx \left[\int_{K_2^j} (d^2x) \right] \cdot F_j = W_j \cdot F_j, \quad (3.38)$$

where F_j is the field $F(x_j)$, and W_j is the bivector representing the magnitude and the mean orientation of the facet K_2^j

$$W_j := \int_{K_2^j} (d^2x). \quad (3.39)$$

Analogously, we approximate g_j by

$$g_j = \int_{\tilde{K}_2^j} \xi^\dagger(Id^2x) \cdot F \approx \tilde{\xi}_j^\dagger(I\tilde{W}_j) \cdot F_j, \quad (3.40)$$

where

$$\widetilde{W}_j := \int_{\widetilde{K}_2^j} (d^2x), \quad (3.41)$$

and $\overline{\xi}_j$ is averaged over \widetilde{K}_2^j with respect to ξ , i.e., for every constant bivector A

$$\overline{\xi}_j(A) := |\widetilde{W}_j|^{-1} \int_{\widetilde{K}_2^j} |d^2x| \xi(A), \quad \forall A = \text{const}. \quad (3.42)$$

We note that if we represent ξ as a matrix with entries $\xi_{\alpha\beta} = \xi(\gamma_\alpha \wedge \gamma_\beta)$, then $\overline{\xi}_{j,\alpha\beta}$ is an average of $\xi_{\alpha\beta}$, i.e., we can average each entry independently.

Thus after these approximations the condition (3.37) can be written solely in the tangent space at x_j

$$[W_j \cdot F_j^0 = 0] \implies [\overline{\xi}_j^\dagger(I\widetilde{W}_j) \cdot F_j^0 = 0], \quad \forall F_j^0, \quad (3.43)$$

which we show now to be equivalent to

$$\boxed{\alpha_j W_j = \overline{\xi}_j^\dagger(I\widetilde{W}_j)}, \quad (3.44)$$

where $\alpha_j \in \mathbb{R}$ is a scalar proportionality factor.

Proof. Assume that (3.43) holds. First, note that if F_j^0 is not in the kernel of f_j , then $W_j \cdot F_j^0 \neq 0$, and the implication (3.43) is true. Therefore, it is sufficient to consider the case when F_j^0 is in the kernel of f_j , i.e., $W_j \cdot F_j^0 = 0$ holds. Second, by (3.43) and F_j^0 being in the kernel, we obtain

$$[\alpha_j W_j - \overline{\xi}_j^\dagger(I\widetilde{W}_j)] \cdot F_j^0 = 0, \quad \forall F_j^0. \quad (3.45)$$

Finally, using the orthogonality property of non-degenerate inner products, we arrive at (3.43) \implies (3.44). Conversely, let us assume (3.44) and multiply it by any F_j^0 ,

$$\alpha_j [W_j \cdot F_j^0] = [\overline{\xi}_j^\dagger(I\widetilde{W}_j) \cdot F_j^0], \quad \forall F_j^0. \quad (3.46)$$

It immediately implies (3.43), and we have just proven (3.43) \iff (3.44).

Material Matrices. The discrete material mapping enables us to express $\{g_j\}$ in terms of $\{f_j\}$. If we arrange $\{g_j\}$ and $\{f_j\}$ into column vector \underline{g} and \underline{f} , this can be written in the case of linear materials as

$$\underline{g} = \underline{M}_\xi \underline{f}, \quad (3.47)$$

where \underline{M}_ξ is called material matrix. In general, the matrix \underline{M}_ξ is not diagonal, however, if (3.44) holds then it is diagonal with entries

$$[M_\xi]_{jj} = I^{-1} \widetilde{W}_j \wedge \overline{\xi}_j(W_j^{-1}). \quad (3.48)$$

Proof. We approximate primal Dof f_j by

$$f_j \approx W_j \cdot F_j. \quad (3.49)$$

Since g_j is well defined in the quotient space, we can choose any representative, e.g., by adding F_j^0 to F_j . Particularly, we are looking for a gauged $F_j' := F_j + F_j^0$ for which the dot product above can be replaced with the geometric one⁶⁰, because then the equation can be solved easily for F_j' , i.e.,

$$f_j \approx W_j \cdot F_j' = W_j F_j' \implies F_j' \approx f_j W_j^{-1}. \quad (3.50)$$

⁶⁰ In other words this is our gauging condition to specify the representative of an equivalence class $[F_j]$.

Please note that W_j is invertible as it is a non-null 2-blade associated with a 2D facet. In order to exploit (3.50) we need to fulfil ($W_j \cdot F_j^0 = 0$ because F_j^0 is in the kernel of f_j)

$$W_j \cdot F_j' = W_j F_j' \Leftrightarrow W_j \cdot F_j + \overbrace{W_j \cdot F_j^0}^{=0} = W_j F_j + W_j F_j^0, \quad (3.51)$$

which is easily solved (as W_j^{-1} exists) for F_j^0

$$F_j^0 = (W_j \cdot F_j)W_j^{-1} - F_j. \quad (3.52)$$

Starting from the definition (3.13) of g_j , i.e.,

$$I g_j = \int_{\tilde{K}_2^j} (d^2x) \wedge G = \int_{\tilde{K}_2^j} (d^2x) \wedge \xi(F),$$

and using the same numerical quadrature to approximate the integral as in (3.40),

$$I g_j \approx \widetilde{W}_j \wedge \widetilde{\xi}_j(F_j),$$

and choosing F_j' as a representative and using (3.50), we arrive at

$$I g_j \approx \widetilde{W}_j \wedge \widetilde{\xi}_j(W_j^{-1})f_j, \quad (3.53)$$

which leads to a diagonal material matrix with entries (3.48).

Now we will point out why the orthogonal dual mesh does not guarantee diagonal material matrices for anisotropic material. Suppose \tilde{K}_2^j is a purely spatial facet, i.e., $\widetilde{W}_j \cdot \gamma_t = 0$. Then the DoF associated with \tilde{K}_2^j is related to the electric flux \vec{D} only:

$$\widehat{d}_j = \int_{\tilde{K}_2^j} dS \vec{n} \cdot \vec{D} = \int_{\tilde{K}_2^j} dS \vec{n} \cdot \varepsilon(\vec{E}) \approx \Delta S \left(\vec{n} \cdot \bar{\varepsilon}(\vec{p})\vec{e}_j + \vec{n} \cdot \bar{\varepsilon}(\vec{q})\vec{e}_j^0 \right), \quad (3.54)$$

where \vec{p} is a unit vector along primal edge, \vec{n} is a unit vector normal to the dual facet \tilde{K}_2^j , ΔS is the area of \tilde{K}_2^j , and \vec{q} is a unit vector⁶¹ normal to \vec{p} , i.e., $\vec{p} \cdot \vec{q} = 0$. \vec{e}_j^0 is the non-stored component of the field, which has to be interpolated using the DoFs stored at neighboring edges $\vec{e}_j^0 = \theta_j(\{\vec{e}_{k \neq j}\})$, thus leading to non-diagonal entries in M . We see that non-diagonal entries will vanish if $\vec{n} \cdot \bar{\varepsilon}(\vec{q}) = 0$. Noting that in orthogonal grid $\vec{n} = \vec{p}$, we see that for $\vec{p} \cdot \vec{q} = 0$ the second term in (3.54)

$$\vec{p} \cdot \bar{\varepsilon}(\vec{q}) \quad (3.55)$$

is in general not zero, since $\bar{\varepsilon}$ will change the direction of \vec{q} . However, if \vec{q} is the main axis of the $\bar{\varepsilon}$, then its direction will not be changed, and consequently

$$\vec{p} \cdot \bar{\varepsilon}(\vec{q}) = \varepsilon_{qq} \vec{p} \cdot \vec{q} = 0, \quad (3.56)$$

thus M is diagonal in this special case. Please note that in 3D case, we will obtain analogous restrictions coming from the reluctivity ν .

Mesh Optimisation. Naturally (3.44) does not hold in general, i.e., for arbitrary materials and meshes. However, for a given material one may seek for a mesh that satisfies (3.44) in order to gain computational efficiency coming from diagonal material matrices. We will pursue this idea in Section 4.

⁶¹ Please note that \vec{q} is not unique as it can be rotated around \vec{p} .

3.3.2 Non-diagonal Material Matrices

Although diagonal material matrices are tempting, and the condition (3.44) for their existence seems promising, i.e., one may hope that starting from any primal mesh and materials one can just calculate the dual mesh, it is in general not possible to satisfy the condition (3.44). Although it can be successfully applied to optimise 2D meshes (as exemplified in Section 4.1), it has severe limitations in 3D (derived in Section 4.2) coming from the fact that the bivectors associated with 2D facets present in (3.44) are not independent of each other. For example in 3D, it is in general not possible to change the direction of only one edge. Moreover, even if that was the case in some extraordinary situation, changing an edge belonging to a facet will in general change the facet as well. Therefore, one needs to deal with non-diagonal material matrices. First, they should lead to a convergent scheme (preferably with highest order of convergence). Second, they should be as easy to invert as possible as at each time step we are going to solve the system of equations associated with them. In the case of diagonal matrices, the inversion is clearly trivial. Third, the formulae for the entries of material matrices should be easy to implement.

In the following, we present two space-time discretisation methods, namely 4D FIT with Whitney interpolation and Whitney FEM with Galerkin Hodge. In both approaches Whitney elements are used, which are introduced in the next subsection.

3.3.3 Whitney Interpolation

The overview: The concept of Whitney elements is explained in GA notation. We motivate Whitney interpolation by showing that the numerical exterior derivative is uniquely defined for Whitney elements. Then we present them for a particular reference element used in this thesis, namely 4D hexahedrons. First we investigate a 4D cube, and later we perform an affine transformation to the physical domain in order to study generic 4D hexahedron. The special properties of the lowest-order basis functions are discussed in the reference element as well as in the physical ones, that is the images of the reference element with respect to an affine mapping.

General Introduction.

With every n -vector field A_n there is associated its discrete counterpart n -cochain \hat{A}_n

$$\hat{A}_n(s_n) := \int_{s_n} (d^n x) \cdot A_n, \quad (3.57)$$

where s_n is an n -chain, and can be represented in the basis K_n^i , i.e.,

$$s_n = \sum_i s_n^i K_n^i. \quad (3.58)$$

The action of \hat{A}_n on arbitrary n -chain is then given by

$$\hat{A}_n \left(\sum_i s_n^i K_n^i \right) = \sum_i s_n^i \hat{A}_n(K_n^i) = \underline{s}_n \underline{A}_n^T. \quad (3.59)$$

Therefore, it is sufficient to store \underline{A}_n , i.e., a component representation of an n -cochain \hat{A}_n with respect to the canonical basis induced by the K_n^i . \underline{A}_n is a vector in linear algebra sense, whose components are given by

$$A_n^i := \hat{A}_n(K_n^i) = \int_{K_n^i} (d^n x) \cdot A_n. \quad (3.60)$$

As \underline{A}_n are functionals of A_n , we introduce discretisation operators R^n via

$$\underline{A}_n = R^n(A_n). \quad (3.61)$$

In Maxwell's equations (2.209) there is an exterior derivative of a bivector $\nabla \wedge F$ present. Since we solve Maxwell's equations numerically, it makes sense to ask how a derivative, e.g., $\nabla \wedge$, should be discretised. Suppose, we would like to obtain a discrete representation of the derivative of a continuous multivector field A_n . One possibility is to calculate $\nabla \wedge A_n$ and then discretise the result; we denote the obtained numerical derivative as

$$D_{\text{num}} = R^{n+1} \nabla \wedge, \quad (3.62)$$

and the result as

$$\underline{A}_{n+1} := D_{\text{num}} A_n = R^{n+1} \nabla \wedge A_n. \quad (3.63)$$

The other choice is to first discretise A_n obtaining $\underline{A}_n = R^n A_n$, and then calculate the discrete derivative $D^n \underline{A}_n$, using the definition (3.15) of D^n . This alternative numerical derivative is denoted by

$$D'_{\text{num}} := D^n R^n \quad (3.64)$$

and the obtained discrete representation is

$$\underline{A}'_{n+1} := D'_{\text{num}} A_n = D^n R^n A_n, \quad (3.65)$$

where in general $\underline{A}'_{n+1} \neq \underline{A}_{n+1}$. Our considerations can be compactly represented as the following diagram

$$\begin{array}{ccccc} A_n & \xrightarrow{\nabla \wedge} & A_{n+1} & & \\ \downarrow R^n & \searrow D'_{\text{num}} & \searrow D_{\text{num}} & \searrow R^{n+1} & \\ \underline{A}_n & \xrightarrow{D^n} & \underline{A}'_{n+1} & \xrightarrow{R^{n+1}} & \underline{A}_{n+1} \end{array} \quad (3.66)$$

However, the situation is not satisfactory, as that means that the numerical derivative of A_n is not uniquely defined. Therefore, it is reasonable to require that $\underline{A}'_{n+1} = \underline{A}_{n+1}$ for any A_n , i.e., the numerical derivative $D_{\text{num}} = D'_{\text{num}}$ is uniquely defined. Then, we can make this requirement explicit, which leads to a commutative⁶² diagram

$$\begin{array}{ccc} A_n & \xrightarrow{\nabla \wedge} & A_{n+1} \\ \downarrow R^n & \searrow D_{\text{num}} & \downarrow R^{n+1} \\ \underline{A}_n & \xrightarrow{D^n} & \underline{A}_{n+1} \end{array} \quad (3.67)$$

In other words, requiring that this diagram commutes is equivalent to requiring that the exterior differentiation and discretisation commute:

$$R^{n+1} [\nabla \wedge A_n] = D^n R^n [A_n]. \quad (3.68)$$

In the following, we also use the reconstruction operators W^n being right inverses of R^n , i.e., $W^n \underline{A}_n$ gives an n -vector field A_n obtained, e.g., by means of interpolation field values from DoFs, whose discretisation leads to \underline{A}_n again. In other words

$$\underline{A}_n \equiv R^n W^n \underline{A}_n. \quad (3.69)$$

Moreover, if $A'_n = W^n \underline{A}_n$ is the field reconstructed from arbitrary \underline{A}_n , then

$$A'_n \equiv W^n R^n A'_n. \quad (3.70)$$

These considerations leads us to the deRham complex [29, page 259, Point (2), Equation (3.7) and page 263, Corollary 3.3]

$$\begin{array}{ccccccccc} A_0 & \xrightarrow{\nabla \wedge} & A_1 & \xrightarrow{\nabla \wedge} & A_2 & \xrightarrow{\nabla \wedge} & A_3 & \xrightarrow{\nabla \wedge} & A_4 \\ \uparrow W^0 & \left(\begin{array}{c} \uparrow \\ \downarrow \end{array} \right) R^0 & \uparrow W^1 & \left(\begin{array}{c} \uparrow \\ \downarrow \end{array} \right) R^1 & \uparrow W^2 & \left(\begin{array}{c} \uparrow \\ \downarrow \end{array} \right) R^2 & \uparrow W^3 & \left(\begin{array}{c} \uparrow \\ \downarrow \end{array} \right) R^3 & \uparrow W^4 & \left(\begin{array}{c} \uparrow \\ \downarrow \end{array} \right) R^4 \\ \underline{A}_0 & \xrightarrow{D^0} & \underline{A}_1 & \xrightarrow{D^1} & \underline{A}_2 & \xrightarrow{D^2} & \underline{A}_3 & \xrightarrow{D^3} & \underline{A}_4 \end{array} \quad (3.71)$$

will only commute, i.e., numerical exterior derivatives will be uniquely defined, for a proper choice of basis functions, namely, those belonging to the class of Whitney elements. In general there are infinitely many members of this class. However, we restrict our attention to the lowest-order elements, and thus they are uniquely defined up to a sign coming from the orientation of the facets in the reference element. Therefore, in the sequel by Whitney elements, we mean

⁶² A diagram is called commutative, if the result, e.g., \underline{A}_{n+1} , is independent on the chosen path in the diagram to arrive at it.

lowest-order Whitney elements. For lowest-order elements one can define Whitney reconstruction operator (Whitney map), see [17, Equation (4.4)], as

$$W^n \underline{A}_n = \sum_i A_n^i N_i^n(x), \quad (3.72)$$

with $N_i^n(x)$ the n -vector valued basis function associated with n -cell K_n^i .

Our Choice of Whitney Forms on the Reference Element. So far, we have not specified any particular form of basis functions $N_i^n(x)$. Due to the fact that we intend to obtain a computational scheme, the explicit formulas for Whitney functions $N_i^n(x)$ are necessary. Since in this thesis we consider 4D “hexahedral” elements, we shall extend here the 3D reasoning described in [30, Chapter 8.3.] to 4D.

We start by constructing the interpolating functions, that is Whitney elements, for a single tesseract (“4D reference cube”) $\Xi = [-1, +1] \otimes [-1, +1] \otimes [-1, +1] \otimes [-1, +1]$. The vertices of this tesseract are at the points $(t, x, y, z) = (\pm 1, \pm 1, \pm 1, \pm 1)$. Let us suppose we are interested in the basis function associated with the facet $[-1, +1] \otimes [-1, +1] \otimes -1 \otimes -1$. Since this is a tx -facet, we know that the DoF living on such a facet is related to the $(\gamma_t \gamma_x) \cdot F = E^x$ component of the Faraday field $F = \vec{E} + I\vec{B}$. Clearly the function

$$N_1^2 = \frac{1}{16} \gamma^x \gamma^t (1-y)(1-z) \quad (3.73)$$

vanishes at the other tx -facets and is orthogonal to the remaining facets, thus

$$\int_{\Delta_i} (d^2x) \cdot N_1^2 = \delta_1^i, \quad (3.74)$$

where Δ_i , with $i = 1, \dots, 24$ are 2D facets of the reference tesseract.

One may construct basis functions for all 2D facets, such that they fulfil the so-called interpolation property

$$\int_{\Delta_i} (d^2x) \cdot N_j^2 = \delta_j^i, \quad i, j = 1, \dots, 24, \quad (3.75)$$

and give an exact interpolation for constant fields. Moreover, these basis functions guarantee that the tangential component of the interpolated field F is continuous across a 2D facet described by a bivector W , viz.

$$W \cdot F_1 = W \cdot F_2, \quad (3.76)$$

where F_1 and F_2 are the limits of the field F as approached from any two directions. Mathematically speaking

$$F_i = \lim_{\delta \rightarrow 0} F(x + \delta v_i), \quad i = 1, 2, \quad (3.77)$$

where v_i is a unit vector describing the direction.

The space-time split of (3.76) leads to the more familiar 3D continuity relations

$$\vec{B}_1 \cdot \vec{n} = \vec{B}_2 \cdot \vec{n} \quad \vec{E}_1 \cdot \vec{l} = \vec{E}_2 \cdot \vec{l}, \quad (3.78)$$

with \vec{n} and \vec{l} , respectively, a normal and a tangent vector to an arbitrary surface.

If we group the basis functions N_i^2 , $i = 1 \dots 24$ according to a type of facet they correspond to, i.e., we change the enumeration of N_i^2 ,

$$N_{i_{\pm 1, j_{\pm 2}}}^2 := \frac{1}{16} (\gamma_i \wedge \gamma_j) (\gamma^t \wedge \gamma^x \wedge \gamma^y \wedge \gamma^z) (1 \pm_1 x^i) (1 \pm_2 x^j) \quad (3.79)$$

Regarding the physical interpretation of $N_{i_{\pm 1, j_{\pm 2}}}^2$ (see also (C.27) in Appendix C.3) in the case of the map from a reference to physical domain Φ_1 being an identity map, Table 2 provides a complete description.

We observe that the chosen basis functions N_i^2 , besides being Whitney forms (see Appendix C.3), do also comply with the requirements⁶³ of an energetic approach (as introduced in [13]) in our space-time extension [12, equation iii)], that is

$$\int_{\Xi} N_j^2 |d^4x| = I^{-1} \widetilde{W}_j, \quad (3.80)$$

⁶³ Namely, they fulfil interpolation property (3.75), they represent constant fields exactly, and less popular and less obvious (3.80).

(i, j)	(x, t)	(y, t)	(z, t)	(x, y)	(z, x)	(y, z)
Field component	B^x	B^y	B^z	E^z	E^y	E^x

Table 2: The physical interpretation of DoFs associated with the basis functions $N_{i\pm, j\pm}^2$.

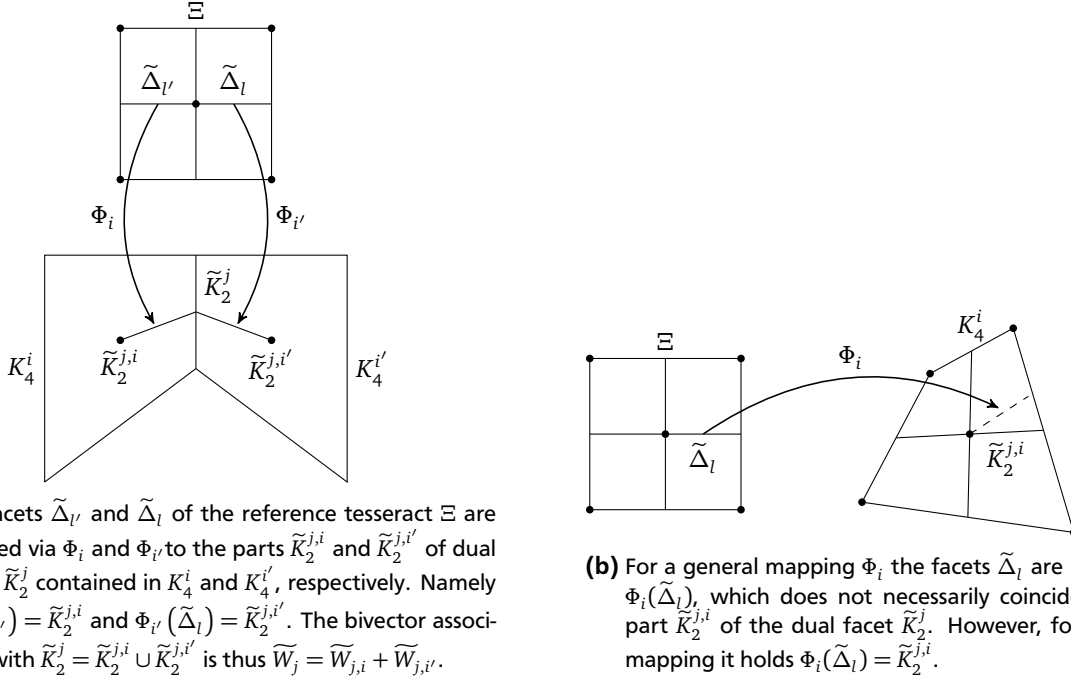


Figure 5

where Ξ is the reference tesseract and \tilde{W}_j is the bivector associated with the facet $\tilde{\Delta}_l$ dual to Δ_l , which is only the part contained in the reference tesseract Ξ .

Remark: Please note that the dual facets \tilde{K}_2^j in the whole mesh complex are unions of the facets $\Phi_i(\tilde{\Delta}_j)$ in neighbouring 4D cells K_4^i , where Φ_i is a map from the reference to physical domain defined in (3.83). Therefore, the bivectors associated with $\tilde{K}_2^{j,i}$, being the part of the dual facet \tilde{K}_2^j contained in the primal cell K_4^i , are later referred as $\tilde{W}_{j,i}$. This explanation is sketched schematically in Fig. 5a.

Please note, if $\tilde{K}_2^j = \tilde{K}_2^{j,i} \cup \tilde{K}_2^{j,i'}$, then by definitions of \tilde{W}_j and property of integration:

$$\tilde{W}_j = \int_{\tilde{K}_2^j} (d^2x) = \int_{\tilde{K}_2^{j,i}} (d^2x) + \int_{\tilde{K}_2^{j,i'}} (d^2x) = \tilde{W}_{j,i} + \tilde{W}_{j,i'}. \quad (3.81)$$

Basis Functions in the Physical Domain. In the following, by \tilde{N}_i^n and N_i^n we denote Whitney basis functions in the reference and physical domain, respectively. Summing up, the basis functions \tilde{N}_i^n satisfy the following set of properties:

1. they satisfy the interpolation property (3.75),
2. they fulfil (C.20)

$$\nabla \wedge \tilde{N}_i^n = \sum_j [D^n]_{ji} \tilde{N}_j^{n+1}, \quad (3.82)$$

i.e., guarantee that (3.71) commutes (see Appendices C.2 and C.3),

3. they are eligible for 4D energetic approach, i.e., meet (3.80).

All these properties hold for the reference tesseract; however, in many applications one is interested in using meshes with non-cubic elements in order to approximate geometries more accurately. Moreover, if one even uses a 3D Cartesian grid, the 4D elements are certainly deformed by the movement, which is encoded in the geometry of the 4D mesh. Therefore, one needs to construct analogous functions for a deformed tesseract. This is conveniently done by first defining a mapping (diffeomorphism) from the reference to the physical tesseract and then by transforming the basis functions accordingly.

We define a set of affine mappings

$$\Phi_p : \Xi \rightarrow K_4^p \quad (3.83)$$

from the reference domain to the physical 4D cells. Since Φ_p is an affine map, the barycenters of any object in the reference domain are mapped to the barycenters of a corresponding object in the physical domain. For details see Appendix C.4.

Property 1. involves the integral of a differential form, see (2.144), which is invariant with respect to the change of the metric properties; therefore, this property will hold for the transformed functions. As explained in [29, text below Equation (2.13)], the transformed (pulled-back) functions will satisfy the Property 2. on a deformed element.

Open research question 5. *Even if the Property 3. would not hold, one could still hope that the energetic approach works, by ensuring that some different dual (not necessary the barycentric one) is implied. Namely, if one could **define** the physical dual as the image of the barycentric dual in the reference mesh. Since in general, one does not need to calculate the dual mesh in FEM, this would bear no additional computational cost. The price to pay would be that one cannot easily relate d and h to \vec{D} and \vec{H} without explicitly calculating the dual. What is the most general class of mappings to physical domain that can be employed within Galerkin Hodge? Can the method itself be generalised to extend this class?*

Property 3. is not guaranteed for general mappings as the dual elements of Ξ might be not mapped to the barycentric dual elements of the deformed tesseract. However, as Φ_p is an affine map, it is the case, i.e., barycenters are mapped to barycenters, and the reference barycentric dual is mapped to the physical barycentric dual; see Fig. 5b. Hence, all required properties are inherited by the deformed tesseract. The Property 3. (3.80) transfers to the physical domain as follows.

Suppose it holds in the reference domain. In this reasoning the quantities in the reference domain are denoted by a bar. First, we note that⁶⁴

$$\int_{K_4^i} N_j |d^4 x| = \lim_{\Delta^4 x \rightarrow 0} \sum_{a, x_a \in K_4^i} N_j(x_a) |\Delta^4 x_a| = \quad (3.84)$$

$$= \lim_{\Delta^4 \bar{x} \rightarrow 0} \sum_{a, \bar{x}_a \in \Xi} \Phi_i(\bar{N}_j(\bar{x}_a)) \Phi_i(|\Delta^4 \bar{x}_a|) = \quad (3.85)$$

$$= \lim_{\Delta^4 \bar{x} \rightarrow 0} \sum_{a, \bar{x}_a \in \Xi} \Phi_i(\bar{N}_j(\bar{x}_a) |\Delta^4 \bar{x}_a|) = \quad (3.86)$$

$$= \Phi_i \left(\lim_{\Delta^4 \bar{x} \rightarrow 0} \sum_{a, \bar{x}_a \in \Xi} \bar{N}_j(\bar{x}_a) |\Delta^4 \bar{x}_a| \right) = \Phi_i \left(\int_{\Xi} \bar{N}_j |d^4 \bar{x}| \right), \quad (3.87)$$

where $|\Delta^4 x|$ is a finite 4D volume element and we assumed that interchanging the order of diffeomorphism and the limit of the sum is justified. Moreover, we have used the fact that both the reference and the physical domain are equipped with the flat Minkowski metric, thus the connection is trivial and is not necessary in the sum.

Second; in order to calculate the equivalent of (3.80) in physical domain

$$\int_{K_4^i} N_j |d^4 x| = \Phi_i \left(\int_{\Xi} \bar{N}_j |d^4 \bar{x}| \right), \quad (3.88)$$

we note that from (3.80) it follows that

$$\Phi_i \left(\int_{\Xi} \bar{N}_j |d^4 \bar{x}| \right) = \Phi_i(\vec{I}^{-1} \vec{W}). \quad (3.89)$$

As Φ_i is a change of coordinates, it does not change the metric g nor the tangent space identified with the underlying linear space L and consequently the geometric product of GA $\mathcal{G}(L, g)$ is not changed by the change of coordinates. In other words geometric product has been defined without introducing the coordinates; therefore, changing them cannot

⁶⁴ By Φ_i applied to a multivector, we mean the multivector obtained if the coordinates induced by Φ_i are used. In the Differential Forms literature this transformations are split into push-forward and pull-back depending on the argument being a differential form or a vector.

change the product, which is independent of their existence⁶⁵. Therefore, from the invariance of the geometric product with respect to Φ_i we obtain

$$\Phi_i(\bar{I}^{-1}\tilde{W}) = \Phi_i(\bar{I}^{-1})\Phi_i(\tilde{W}). \quad (3.90)$$

Since the pseudoscalar I in Section 2.1.1 is also well defined (provided the orientation of L is fixed) without introducing coordinates, it is invariant⁶⁶, i.e., $\bar{I} = \Phi(I) = I$. In turn, it allows us to simplify

$$\Phi_i(\bar{I}^{-1})\Phi_i(\tilde{W}) = I^{-1}\Phi_i(\tilde{W}). \quad (3.91)$$

Thus we have arrived at

$$\int_{\kappa_4^i} N_j |d^4x| = I^{-1}\Phi_i(\tilde{W}), \quad (3.92)$$

and by comparing with (3.80) we conclude that (3.80) will hold in physical domain if

$$\Phi_i(\tilde{W}) = \tilde{W}, \quad (3.93)$$

which holds if Φ_i maps the reference barycentric dual facet to the physical barycentric dual facet. Therefore, since Φ_i is an affine mapping, then (3.93) holds, and subsequently (3.80) in physical domain follows. Equivalently, as the mapping preserves (weighted) barycenters thus (3.80) holds in physical domain.

To summarise, properties 1. and 2. come from differential topology, thus change in the metric, i.e., shape of an element, does not influence them. In contrast, the property 3. depends on metric in a twofold way. First, the barycentric dual depends on metric. That is due to barycenter depending on affine structure compatible with the metric. Second, the integrand in (3.80) is not a scalar; therefore, the Levi-Civita connection is used, which depends on the metric.

Performing Transformation to the Physical Domain. The map (3.83) can be perceived as a change of coordinates. Therefore, it is important to establish how multivectors transform due to this change. Here we will focus only on basis vectors. There is no unique approach in the literature how to define the basis vectors. We opt for the following definitions, see Section 2.1; especially (2.54) or (2.87),

$$\bar{\gamma}_i := \frac{\partial x}{\partial \bar{x}^i}, \quad \bar{\gamma}^i := \nabla \bar{x}^i(x), \quad (3.94)$$

where x is a position vector in physical space and $\bar{x}^i(x)$ are reference coordinates in physical space (and in $\bar{\gamma}_i$ basis) of x . Please note that all quantities with a bar refer to their induced counterparts in physical domain, and not in the reference domain.

Then we easily verify that they “transform” according to, see Section 2.1.4,

$$\bar{\gamma}_i = \frac{\partial}{\partial \bar{x}^i} x = \frac{\partial x^j}{\partial \bar{x}^i} \frac{\partial}{\partial x^j} x = \frac{\partial x^j}{\partial \bar{x}^i} \gamma_j, \quad (3.95)$$

$$\bar{\gamma}^i = \nabla \bar{x}^i = \left(\gamma^j \frac{\partial}{\partial x^j} \right) \bar{x}^i = \frac{\partial \bar{x}^i}{\partial x^j} \gamma^j. \quad (3.96)$$

It means that basis vectors transform like vectors, and the reciprocal basis vectors as one-forms. It is less surprising if one recalls that $\gamma_i \doteq \partial_i$ and $\gamma^i \doteq (dx^i)^\#$, where the quantities on the right hand side are defined in exterior algebra of differential forms (the canonical musical isomorphism is used, as we assume the existence of some metric). The technical details of transforming N_i^2 are gathered in the Appendix C.6.

⁶⁵ If by Φ we denote the change of coordinates from Cartesian to polar, then the 2D example about geometric derivative in both coordinate systems on page 16 may be perceived as an example of the fact that

$$\Phi(\nabla A) = \Phi(\nabla)\Phi(A) = \nabla A,$$

and follows directly from the fact that the geometric derivative ∇A is well defined without introducing any coordinates. The first equality sign comes from the invariance of the geometric product with respect to the change of coordinates, while the second one incorporates the invariance of the factors. See Appendix C.5 for the examples of transformation of different objects due to the change of coordinates.

⁶⁶ Please note that we consider the domains of physical and reference space (thus their tangent spaces as well) isomorphic, i.e., “the same”. Therefore, it makes sense to talk about the invariance of some objects due to transformation Φ_i . In general setting the reference domain might be different than the physical one, and then the quantities in both spaces cannot be compared, thus invariance is not well defined.

3.3.4 Finite Integration Technique with Whitney Interpolation

The overview: Since we work with a non-orthogonal mesh pair, the traditional FIT approach for creating diagonal material matrices is not possible. The construction of FIT material matrices on non-orthogonal grids has been approached by several authors. The two closest approaches to ours are described in [46] and [47]. Although in [46] Whitney interpolation within overall FIT framework has been investigated, the final formula for the material matrix is different (and thus its properties too), compare (3.105) with [46, Equation (13)]. This comes from the fact that we have explicitly used one point quadrature to approximate the integral in (3.98), while in [46, Equations (11)–(14)] the integration is carried out exactly. On the other hand, in [47] the construction of material matrices for (non-orthogonal) 2D quadrilateral meshes in FIT framework was proposed. However, it is not clear how this work can be extended to space-time. Thus, we rather use our general Space-Time Algebra discretization and Whitney interpolation, which are ready to be applied in space-time. We would like to mention that the sparsity pattern of the material matrices are exactly the same as in [47]⁶⁷ and are sparser than in 4D energetic approach. The discretisation error is introduced in (3.98) by assuming that the fields are constant on every dual facet \tilde{K}_2^j . This assumption is needed, to recover the fields by knowing only the DoFs, i.e., integrals over \tilde{K}_2^j . Then ξ can be used to relate the fields, resulting in the relation between DoFs.

We recall cf. (3.13) that the dual DoFs are defined as

$$I g_j = \int_{\tilde{K}_2^j} (d^2 x) \wedge G = \int_{\tilde{K}_2^j} (d^2 x) \wedge \xi(F). \quad (3.97)$$

In order to construct the material matrices, we express F in terms of the primal DoFs f_j and use the formula above.

We follow the general FIT approach for approximating the integral in (3.97); namely, approximate it by taking the value of F at only one point x_j . It may be thus perceived as an extension of a one-point quadrature rule⁶⁸ to the geometric calculus. Thus, we approximate (3.97) by

$$\int_{\tilde{K}_2^j} (d^2 x) \wedge \xi(F) \approx \left[\int_{\tilde{K}_2^j} (d^2 x) \right] \wedge \bar{\xi}(F_j) = \tilde{W}_j \wedge \bar{\xi}(F_j), \quad (3.98)$$

where $F_j := F(x_j)$ is the field at a collocation point x_j , which is often chosen to be the intersection of \tilde{K}_2^j with K_2^j (or the barycenter of \tilde{K}_2^j according to the midpoint rule). $\bar{\xi}$ is ξ averaged over the dual facet \tilde{K}_2^j . However, due to the fact that it is easy to interpolate the field at the barycenter of the primal facet K_2^j we have used that point, see Fig. 3b. Therefore, we are approximating the integral in (3.97) by the value of F at a point which is not necessarily lying on \tilde{K}_2^j .

The affine mapping (C.29)–(C.32)

$$t = \sum_{i=1}^{16} T_i(\bar{t}, \bar{x}, \bar{y}, \bar{z}) t_i \quad (3.99)$$

$$x = \sum_{i=1}^{16} T_i(\bar{t}, \bar{x}, \bar{y}, \bar{z}) x_i \quad (3.100)$$

$$y = \sum_{i=1}^{16} T_i(\bar{t}, \bar{x}, \bar{y}, \bar{z}) y_i \quad (3.101)$$

$$z = \sum_{i=1}^{16} T_i(\bar{t}, \bar{x}, \bar{y}, \bar{z}) z_i, \quad (3.102)$$

is easy to calculate, i.e., having given $(\bar{t}, \bar{x}, \bar{y}, \bar{z})$ it is easy to calculate (t, x, y, z) . However, it is difficult to invert analytically⁶⁹, i.e., having given (t, x, y, z) it is not possible to obtain an analytic expression for $(\bar{t}, \bar{x}, \bar{y}, \bar{z})$; one needs to rather go for numerical techniques to do that. Although it is difficult to invert it is easy to “guess” $(\bar{t}, \bar{x}, \bar{y}, \bar{z})$ of some

⁶⁷ Of course, to compare the 3D method [47] and our 4D one, one needs to either extend the first one to 4D or more straightforwardly reduce our scheme to 3D in the case of no rotation $\Omega = 0$. For the reduction of our scheme to 3D FIT with leap-frog, see (3.123)–(3.126).

⁶⁸ We do not fix the point as we do not address the convergence proof in this paper. The convergence properties may depend on the choice of the quadrature.

⁶⁹ One may invert it numerically, but this would require to solve for $(\bar{t}, \bar{x}, \bar{y}, \bar{z})$ for each 2D facet. Thus if the mesh has N 4D elements, it requires solving it $24N$ times, and N is assumed to be big.

interesting points, e.g., barycenters. Being more precise: barycenters are mapped to barycenters. Therefore, if one is interested in the interpolated fields at the barycenter of K_2^j which corresponds to, e.g., 2D facet Δ_1 in the reference tesseract with vertices $(\pm 1, \pm 1, -1, -1)$, then its barycenter is given by $(\bar{x}, \bar{y}, \bar{z}) = (0, 0, -1, -1)$. The same holds true for barycenters of edges, 2D facets, 3D volumes and the whole tesseract.

Using Whitney interpolation

$$F(x) = \sum_k f_k N_k^2(x), \quad (3.103)$$

we calculate

$$\begin{aligned} I g_j &= \int_{\tilde{K}_2^j} (d^2 x) \wedge \xi(F) = \sum_i \int_{\tilde{K}_2^{j,i}} (d^2 x) \wedge \xi_i(F) \approx \sum_i \tilde{W}_{j,i} \wedge \xi_i(F(x_j)) = \sum_i \tilde{W}_{j,i} \wedge \xi_i \left(\sum_k f_k N_k^2(x_j) \right) = \\ &= \sum_k \left[\sum_i \tilde{W}_{j,i} \wedge \xi_i(N_k^2(x_j)) \right] f_k \end{aligned} \quad (3.104)$$

and thus, we are led to the material matrix M_ξ

$$\boxed{[M_\xi]_{jk} := I^{-1} \sum_i \tilde{W}_{j,i} \wedge \xi_i(N_k^2(x_j))}. \quad (3.105)$$

Above, $\tilde{K}_2^{j,i}$ is the part of \tilde{K}_2^j contained in K_4^i .

In the formula above the averaging over the dual facet $\tilde{K}_2^j = \cup_i \tilde{K}_2^{j,i}$ is done explicitly. Therefore, it might be used to define the averaged $\bar{\xi}_j$ in (3.98) by requiring that it satisfies

$$\tilde{W}_j \wedge \bar{\xi}_j(F_j) = \sum_i \tilde{W}_{j,i} \wedge \xi_i(F_j). \quad (3.106)$$

Remark: Due to the simplicity of predicting reference position of barycenters, we have used $x_j :=$ barycenter of Δ_j . The choice of $x_j \in K_2^j$ does not influence the fact that the obtained material matrix M_ξ is non-symmetric and thus endangers stability in the sense that for general, positive definite, symmetric material matrices stability can be proven [48, Section 3]. However, this issue can be heuristically solved by taking only the symmetric part of M_ξ as the material matrix. The numerical experiments (without rotation) carried out in Section 5.7 show that such operation does not influence the convergence of the scheme, while making it stable. The scheme obtained by taking only the symmetric part of (3.105) is referred to as symmetrised FIT.

3.3.5 Energetic Approach and Galerkin Hodge

The overview: We extend here to the space-time setting the energetic⁷⁰ approach in [12] also known as Galerkin Hodge star [7]. The discretisation error is introduced in (3.113) by assuming that the field G is constant in each 4D element K_4^i .

Maxwell's equations can be obtained by applying variational principle $\delta S = 0$ to the action integral, e.g., [56, Sections 2.4 and 2.5]

$$S = \frac{1}{2} \int_{K_4} F \cdot G |d^4 x|. \quad (3.107)$$

Since we have already discretized the operators, we will use S only to derive discrete material equations.

We define the action integral with explicitly applied material laws

$$S_F = \frac{1}{2} \int_{K_4} F \cdot \xi(F) |d^4 x|. \quad (3.108)$$

The core idea is to spot that

$$G = 2 \frac{\delta S}{\delta F} = \frac{\delta S_F}{\delta F} = \xi(F), \quad (3.109)$$

⁷⁰ The term "energetic" is a bit misleading, as in 3D two separate functionals are employed, both of them proportional, respectively, to electric $1/2 \vec{D} \cdot \vec{E}$ and magnetic $1/2 \vec{H} \cdot \vec{B}$ energy. However, in space-time setting an invariant $\vec{D} \cdot \vec{E} - \vec{H} \cdot \vec{B}$ is employed, which is not proportional to the energy, which is reasonable as energy is observer dependent.

where $\delta/\delta F$ is partial functional derivative with respect to F . Indeed, the variation of S with respect to F is

$$\delta S = \int_{K_4} \frac{G}{2} \cdot \delta F |d^4x|, \quad (3.110)$$

and the variation of S_F

$$\delta S_F = \frac{1}{2} \int_{K_4} \delta F \cdot \xi(F) |d^4x| + \frac{1}{2} \int_{K_4} F \cdot \xi(\delta F) |d^4x| = \int_{K_4} \xi(F) \cdot \delta F |d^4x|, \quad (3.111)$$

where we used the fact that the material mapping is self-conjugate, i.e., $B_1 \cdot \xi(B_2) = \xi(B_1) \cdot B_2$ for all bivectors B_1 and B_2 .

Here we extend the 3D reasoning found in [12, Section III] to our space-time setting. Approximating G by a piecewise constant field, i.e., in each element K_4^i it has the value G_i and assuming the basis functions satisfy (3.80)

$$\int_{K_4^i} N_j^2 |d^4x| = I^{-1} \widetilde{W}_{j,i} \Rightarrow \sum_i G_i \cdot \int_{K_4^i} N_j^2 |d^4x| = g_j, \quad (3.112)$$

we obtain (the approximation sign is due to using $G(x) \approx G_i$ if $x \in K_4^i$)

$$S = \frac{1}{2} \sum_{i,j} \int_{K_4^i} f_j N_j^2 \cdot G |d^4x| \approx \frac{1}{2} \sum_{i,j} f_j G_i \cdot \int_{K_4^i} N_j^2 |d^4x| = \frac{1}{2} \sum_j f_j g_j, \quad (3.113)$$

from which follows

$$g_i \approx 2 \frac{\partial S}{\partial f_i}. \quad (3.114)$$

The action integral reads

$$S_F = \frac{1}{2} \int_{K_4} F \cdot \xi(F) |d^4x| = \frac{1}{2} \sum_{i,j} f_i f_j \int_{K_4} N_i^2 \cdot \xi(N_j^2) |d^4x|. \quad (3.115)$$

Using $S_F = S$ and comparing action integrals in (3.113) and (3.115) one gets

$$g_i \approx \sum_j \left[\int_{K_4} N_i^2 \cdot \xi(N_j^2) |d^4x| \right] f_j =: [M_{\xi} f]_i. \quad (3.116)$$

By this construction, we have translated (3.109) to the discrete setting in an approximate sense

$$g_i \approx 2 \frac{\partial S}{\partial f_i} = \frac{\partial S_F}{\partial f_i} = [M_{\xi} f]_i, \quad (3.117)$$

with resulting material matrix

$$\boxed{[M_{\xi}]_{ij} := \int_{K_4} N_i^2 \cdot \xi(N_j^2) |d^4x|.} \quad (3.118)$$

3.4 Summary: the Discrete Equations

The overview: In this section, we perform linear algebraic manipulations to obtain the numerical scheme. The FIT case, (3.132)–(3.133), may be seen as an extension of leapfrog to the rotating case or material equations, for which d and h depend on e and b as well. We have avoided any extrapolation w.r.t. time as it may be the cause of instabilities as mentioned in [37, Appendix] and confirmed by our numerical examples in Section 5.5.

Both FIT (3.105) and FEM (3.118) material matrices relate f_i 's to g_j 's via $\underline{g} = \underline{M}_\xi \underline{f}$. However, in (3.17) and (3.18) we split \underline{f} into (e, b) and \underline{g} into (d, h) due to computational reasons. Therefore, we need to obtain the relation between (e, b) and (d, h) implied by $\underline{g} = \underline{M}_\xi \underline{f}$. In general the decomposition of $\underline{g} = \underline{M}_\xi \underline{f}$ according to e, b, d, h would read

$$h^n = M_{vb}^-(n)b^{n-1} + M_{ve}^-(n)e^{n-1/2} + M_{vb}(n)b^n + M_{ve}^+(n)e^{n+1/2} + M_{vb}^+(n)b^{n+1} \quad (3.119)$$

$$d^{n+1/2} = M_{eb}^-(n+1/2)b^n + M_{ee}(n+1/2)e^{n+1/2} + M_{eb}^+(n+1/2)b^{n+1}, \quad (3.120)$$

where the material matrices are defined according to

$$\begin{bmatrix} h^0 \\ d^{1/2} \\ h^1 \\ d^{3/2} \\ h^2 \\ \vdots \\ h^{n-1} \\ d^{n-1/2} \\ h^n \end{bmatrix} = \begin{bmatrix} M_{vb}^- & M_{ve}^+ & M_{vb}^+ & 0 & 0 & \dots & 0 & 0 & 0 \\ M_{eb}^- & M_{ee}^- & M_{eb}^+ & 0 & 0 & \dots & 0 & 0 & 0 \\ M_{vb}^- & M_{ve}^- & M_{vb}^- & M_{ve}^+ & M_{vb}^+ & \dots & 0 & 0 & 0 \\ 0 & 0 & M_{eb}^- & M_{ee}^- & M_{eb}^+ & \dots & 0 & 0 & 0 \\ 0 & 0 & M_{vb}^- & M_{ve}^- & M_{vb}^- & \dots & 0 & 0 & 0 \\ \vdots & \vdots & \vdots & \vdots & \vdots & \ddots & \vdots & \vdots & \vdots \\ 0 & 0 & 0 & 0 & 0 & \dots & M_{vb}^- & M_{ve}^+ & M_{vb}^+ \\ 0 & 0 & 0 & 0 & 0 & \dots & M_{eb}^- & M_{ee}^- & M_{eb}^+ \\ 0 & 0 & 0 & 0 & 0 & \dots & M_{vb}^- & M_{ve}^- & M_{vb}^- \end{bmatrix} \begin{bmatrix} b^0 \\ e^{1/2} \\ b^1 \\ e^{3/2} \\ b^2 \\ \vdots \\ b^{n-1} \\ e^{n-1/2} \\ b^n \end{bmatrix}. \quad (3.121)$$

Being more explicit, the block $M_{ve}^+(n)$ is $n_f \times n_e$ matrix with entries

$$[M_{ve}^+(n)]_{i,j} := [M_\xi]_{n(n_f+n_e)+i, n(n_f+n_e)+n_f+j} \quad \text{with } i = 1 \dots n_f, j = 1 \dots n_e \quad (3.122)$$

where n_f and n_e are, respectively, the number of facets and edges in the reference mesh. The other blocks are defined analogously.

In general all material matrices depend on the time step n . However, if the angular velocity Ω is constant and we use a constant time step Δt , then all the matrices are constant in time. This comes from the fact that the 4D mesh has certain symmetry. Namely, the layer of cells below (=before) and above (=after) time n has the same geometry as the layer corresponding to $n+1$. Thus in what follows we skip the dependency on n to simplify the notation.

We can recover 3D FIT with leapfrog time integration in our framework when the angular velocity $\Omega = 0$. The relation between our DoFs and the ones used in [60] is (the signs come from the conventions employed in this treatise)

$$d = -\widehat{\widehat{d}} \quad b = \widehat{\widehat{b}} \quad e = -\Delta t \widehat{e} \quad h = -\Delta t \widehat{h}. \quad (3.123)$$

Then the time step looks as follows

$$\begin{aligned} h^n &= M_{vb} b^n \\ d^{n+1/2} &= d^{n-1/2} + \widetilde{C} h^n \\ e^{n+1/2} &= M_{ee}^{-1} d^{n+1/2} \\ b^{n+1} &= b^n + C e^{n+1/2}, \end{aligned} \quad (3.124)$$

which is usually written in more compact form as

$$e^{n+1/2} = e^{n-1/2} + M_{ee}^{-1} \widetilde{C} M_{vb} b^n \quad (3.125)$$

$$b^{n+1} = b^n + C e^{n+1/2}. \quad (3.126)$$

In the case of Cartesian mesh, the above equations coming from our space-time discretisation have been shown, see [31], to be equivalent with 3D FIT with leapfrog time integration [60], and Cell Method [58].

The Maxwell's grid equations (3.27) do not change with the geometry of the mesh. Only material matrices are affected by this change. Therefore, when $\Omega \neq 0$ then we obtain (the first and the third line are (3.119) and (3.120), respectively)

$$h^n = M_{\nu b}^- b^{n-1} + M_{\nu e}^- e^{n-1/2} + M_{\nu b} b^n + M_{\nu e}^+ e^{n+1/2} + M_{\nu b}^+ b^{n+1} \quad (3.127)$$

$$d^{n+1/2} = d^{n-1/2} + \tilde{C}h^n \quad (3.128)$$

$$e^{n+1/2} = M_{\varepsilon e}^{-1} [d^{n+1/2} - M_{\varepsilon b}^- b^n - M_{\varepsilon b}^+ b^{n+1}] \quad (3.129)$$

$$b^{n+1} = b^n + C e^{n+1/2}. \quad (3.130)$$

For 4D FIT $M_{\nu b}^- = M_{\nu b}^+ = 0$. This comes from the fact that the basis functions associated with b^{n+1} and b^{n-1} vanish at the time step n . Therefore, there is no contribution of b^{n+1} and b^{n-1} to h^n . This is the manifestation of the fact that our extension of FIT has narrower stencil.

For 4D FEM symmetry of M_ξ translates to the following symmetries of M 's

$$M_{\nu b} = M_{\nu b}^T \quad M_{\varepsilon e} = M_{\varepsilon e}^T \quad M_{\varepsilon b}^- = (M_{\nu e}^+)^T \quad M_{\varepsilon b}^+ = (M_{\nu e}^-)^T \quad M_{\nu b}^- = (M_{\nu b}^+)^T. \quad (3.131)$$

To keep the workflow, i.e., keep the time integrator scheme explicit, as in stationary case, one would need to, e.g., extrapolate $e^{n+1/2}$ and b^{n+1} in (3.127) and (3.129). This however, may lead to instabilities as we will demonstrate later.

Therefore, we derive an implicit scheme. This can be achieved by, e.g., plugging (3.130), (3.128) and (3.127) into (3.129). After some algebra one arrives at

$$e^{n+1/2} = M^{-1} [\gamma b^n + \beta e^{n-1/2} + \alpha b^{n-1}] \quad (3.132)$$

$$b^{n+1} = b^n + C e^{n+1/2}, \quad (3.133)$$

where

$$M := M_{\varepsilon e} - \tilde{C}M_{\nu e}^+ - \tilde{C}M_{\nu b}^+ C + M_{\varepsilon b}^+ C \quad (3.134)$$

$$\alpha := M_{\varepsilon b}^- + \tilde{C}M_{\nu b}^- \quad (3.135)$$

$$\beta := M_{\varepsilon e} + \tilde{C}M_{\nu e}^- \quad (3.136)$$

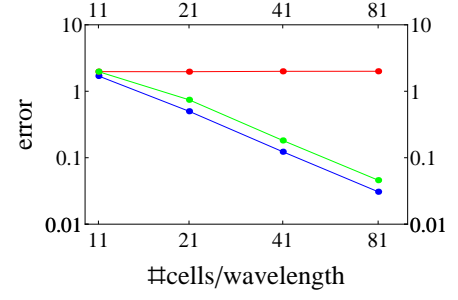
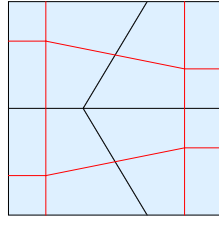
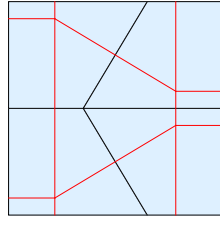
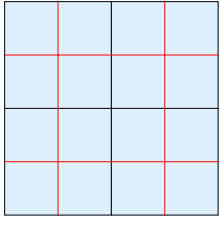
$$\gamma := \tilde{C}M_{\nu b} + \tilde{C}M_{\nu b}^+ - M_{\varepsilon b}^-. \quad (3.137)$$

We would like to stress that we need to solve only one system of equations related to M at each time step, which was also already the case for 3D FIT with $\Omega = 0$ (system related to $M_{\varepsilon e}$) on a non-orthogonal mesh pair.

Remark about Solution Strategies of the Linear System. In Section 5.5 we will see that extrapolating $e^{n+1/2}$ and b^{n+1} (from DoFs at previous time steps) on the right-hand-side of (3.127) and (3.129) leads to instabilities. To avoid instabilities (due to usage of extrapolated values, which are not solutions to the system) one can repeat the whole solution procedure (3.127)–(3.130) with $e^{n+1/2}$ and b^{n+1} on the right-hand-side equal to the just obtained (on the left-hand-side) values of $e^{n+1/2}$ and b^{n+1} . One can iteratively repeat this process until $e^{n+1/2}$ and b^{n+1} are converged, and then proceed to the next time step. This approach however, exhibits slow convergence with respect to number of iterations, which is in accordance with the theory. It can be related to calculating the inverse of a matrix via truncated Neumann series, see Appendix D. Therefore, we rather solve (3.132)–(3.133) by a well-established solver, such as sparse LU decomposition or iterative Krylov subspace methods.

4 Mesh Pair Optimization

Here we will follow [32] and exploit that the condition for diagonal material matrices (3.44) is quantitative. Namely, we use it to derive a goal function, whose minimisation results in Hodge-optimized material matrices being diagonal or diagonal-dominant. Effectively we propose an optimization of the primal/dual mesh pair of a finite difference based discretization scheme taking into account the material properties. In other words, the goal function is a measure how much off-diagonal material matrix is; or equivalently, how serious the numerical crime is committed by taking only diagonal and disregarding non-diagonal entries of the material matrix. We would like to stress that although the mesh optimisation process requires some computational time, it is carried out only once before the time integration consisting potentially of millions of time steps, which in the end results in the lower simulation time. In Section 4.1 we verify that this approach works well in 2D. As a research example a standing wave in 2D cavity filled with an anisotropic material is investigated. Convergence of the scheme for various choices of mesh pairs is discussed. However, in Section 4.2 we derive the limitations of the method in 3D. That is, restriction on allowed material properties (ε , ν) coming from mutual edges' and facets' dependency in a 3D mesh.



(a) Classical orthogonal Cartesian mesh (b) Deformed orthogonal mesh, not optimized (c) Deformed optimal mesh (for $\varepsilon_x/\varepsilon_y = 3$)

(d) Convergence plot

Figure 6: From left to right: plots of (a) classical orthogonal FIT, (b) deformed orthogonal, (c) optimal (for $\varepsilon_x/\varepsilon_y = 3$) mesh pairs. Black and red lines represent primal and dual mesh, respectively. Figure (d) shows the convergence plot for $\varepsilon = \text{Diag}(100, 1)$ and diagonal material matrices: Cartesian mesh (blue), deformed orthogonal (red) and deformed optimal (green). The error is defined as the relative error with respect to the analytic reference solution. It illustrates that in 2D the proposed optimisation method keeps the convergence of original FIT, while enabling more flexibility in meshing.

4.1 Numerical Example in 2D

A standing wave in a square cavity is reduced to 2D by assuming $E^z = B^x = B^y = 0$. The wavelength is equal to the dimension of the cavity. The time interval of the simulation is $T = [0, t_{max}]$, where t_{max} is equal to five periods of the wave. The permittivity tensor is assumed to be diagonal $\varepsilon = \text{Diag}(\varepsilon_x, \varepsilon_y)$. The analytic solutions associated with these standing waves are

$$E^x = \sin(k_y y) \cos(k_y c_y t) \quad E^x = 0 \quad (4.1)$$

$$E^y = 0 \quad E^y = \sin(k_x x) \cos(k_x c_x t) \quad (4.2)$$

$$B^z = -c_y^{-1} \cos(k_y y) \sin(k_y c_y t) \quad B^z = -c_x^{-1} \cos(k_x x) \sin(k_x c_x t), \quad (4.3)$$

where

$$k_x = \frac{\pi m}{l_x} \quad c_x = \frac{1}{\sqrt{\varepsilon_x \mu_x}} \quad (4.4)$$

$$k_y = \frac{\pi m}{l_y} \quad c_y = \frac{1}{\sqrt{\varepsilon_y \mu_y}}, \quad (4.5)$$

m is a natural number and we investigate only the case $m = 1$; c_x and c_y is speed of light in x and y direction, respectively; $2l_x$ and $2l_y$ is dimension of the cavity in x and y direction, respectively; the computational domain is thus given by

$$x \in [-l_x, l_x] \quad y \in [-l_y, l_y] \quad t \in [0, 5 \frac{2\pi}{k_d c_d}] = [0, 5 \frac{2l_d}{c_d}], \quad d = x, y. \quad (4.6)$$

The Cartesian barycentric grid as depicted in Fig. 6a is well-suited for this exemplary problem. However, in traditional FIT the skew edges of a deformed grid, Fig. 6b, lead to non-diagonal entries in the material matrix as explained in Section 3.3.1. Disregarding these entries endangers stability and convergence of the scheme. The red line in Fig. 6d shows that the numerical solution does not converge to the exact one in the case of orthogonal dual, where non-diagonal entries in M have been neglected. In our proposed approach, where the dual mesh is adapted to the material property, the convergence of the scheme is conserved, while keeping the material matrices diagonal, as can be seen from the green line in Fig. 6d. For comparison, the convergence of the traditional 2D FIT is plotted with blue line.

In 2D case the condition (3.44) for diagonal FIT material matrices, reduces to

$$\vec{p}_j = \alpha_j \bar{\varepsilon}_j (\vec{n}_j), \quad (4.7)$$

where \vec{p}_j is a vector representing a primal edge and \vec{n}_j is a vector normal (in Euclidean sense) to the dual edge, $\alpha_j \in \mathbb{R}$ a scalar proportionality factor, and $\bar{\varepsilon}_j$ averaged electric permittivity of the material. An exemplary mesh pair satisfying this condition is found analytically as depicted in Fig. 6c.

Let us define the simulation error as a relative error of the line integrated electric field strength in the discrete ℓ^2 vector norm and ℓ^∞ in time with respect to the analytic reference solution

$$\text{error} := \max_{t \in T} |\widehat{e} - \widehat{e}_a|_2 / \max_{t \in T} |\widehat{e}_a|_2, \quad (4.8)$$

where \widehat{e} , see (3.24) and (3.17), is a vector (in linear algebra sense) composed of electric degrees of freedom at time $t = i\Delta t$, \widehat{e}_a is calculated from the exact solution and $|\cdot|_2$ is the ℓ^2 -norm.

We have considered the example where $\varepsilon = \text{const}$. because in this case the exact solution is known and traditional FIT approach works well. This has made comparison of numerical solutions transparent. However, the idea of mesh optimization is by no means restricted to homogenous materials. For example in Fig. 7a we present a mesh pair obtained by numerical optimization for

$$\varepsilon = \begin{pmatrix} 1 & \varepsilon_{xy}(x, y) \\ \varepsilon_{xy}(x, y) & 1 \end{pmatrix}, \quad (4.9)$$

and

$$\varepsilon_{xy}(x, y) = \begin{cases} \left(\frac{1}{2} - \frac{|y|}{l_y}\right) \sin\left(\frac{\pi}{l_x} \left(x + \frac{l_x}{2}\right)\right) & \text{if } |x| \leq \frac{l_x}{2} \\ 0 & \text{if } |x| > \frac{l_x}{2} \end{cases}, \quad (4.10)$$

where $2l_x$ and $2l_y$ are lengths of the mesh in x and y direction, respectively. The mesh shown in Fig. 7a guarantees that the material matrix constructed is diagonal. It has been obtained as follows. We allow the primal nodes to vary positions without leading to a change of the boundary nor the connectivity of the primal mesh; the dual nodes are free to move within the corresponding primal cell. The primal and dual nodes' positions constitute DoFs of the optimisation procedure. From primal nodes, we obtain vectors \vec{p}_j representing primal edges, and subsequently from (3.44) we can calculate the unique optimal direction of the dual edge, which we represent by a non-normalised vector

$$\vec{d}_j^{\text{opt}} := I^{-1} \varepsilon^{-1} (\vec{p}_j). \quad (4.11)$$

Since we would like the actual vector \vec{d}_j associated with the j -th dual edge to be parallel to the optimal one, we define the error K_j associated with j -th primal/dual edges as

$$K_j := |(\vec{d}_j^{\text{opt}} \wedge \vec{d}_j)| = (\vec{d}_j^{\text{opt}} \times \vec{d}_j)^2, \quad (4.12)$$

and the **goal function** K of the optimisation procedure is the sum of errors associated with individual edges, i.e.,

$$K := \sum_j^{\#\text{edges}} K_j = \sum_j (\vec{d}_j^{\text{opt}} \times \vec{d}_j)^2. \quad (4.13)$$

Clearly K is a non-negative function, and if $K = 0$ the condition (3.44) is satisfied and we obtain diagonal material matrices. Therefore, we look for a local minimum (taking as starting value DoFs associated with the 2D Cartesian grid) using Quasi-Newton method as implemented in `FindMinimum[]` built-in function of Mathematica version 11.0.0. We indeed observe that the obtained minimum is (up to machine precision) zero, and all the dual nodes are within the respective primal cells. If the latter was not the case, one can add a penalty term

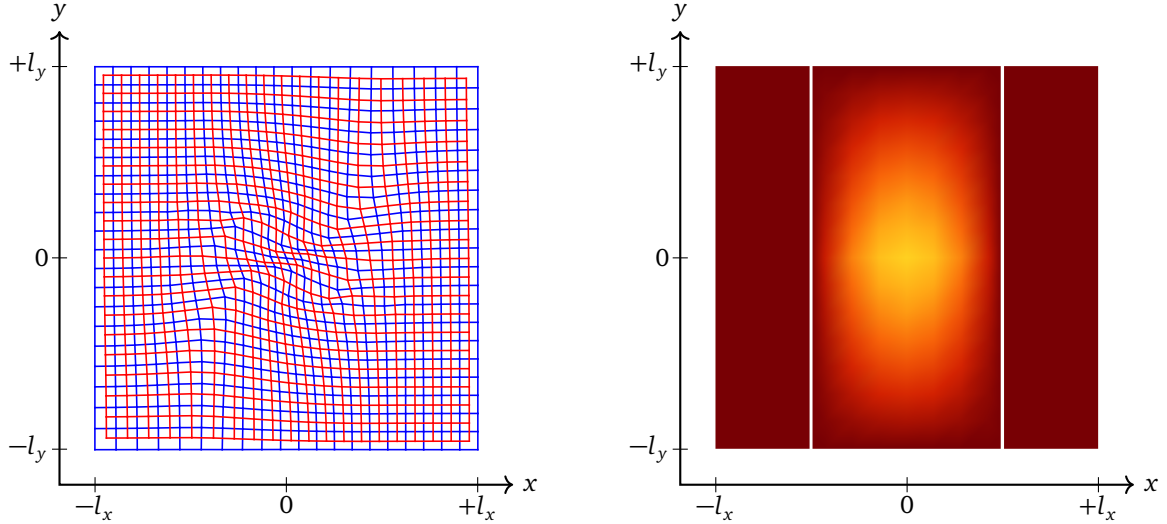
$$P := \sum_k^{\#\text{cells}} (\vec{r}_k^{\text{d}} - \vec{r}_k^{\text{b}})^2, \quad (4.14)$$

which is the sum over all primal cells of squared distances between the dual node \vec{r}_k^{d} and the barycenter \vec{r}_k^{b} of the corresponding k -th primal cell.

4.2 3D Considerations

In Section 3.3.1 we have shown that material matrices are diagonal if and only if (3.44) holds. As we will see in this Section, the set of conditions (3.44) can be fulfilled by a 3D mesh pair⁷¹ only for a certain class of materials. Origins of this restriction can be intuitively explained as follows. Please note that the bivectors, present in (3.44), associated with, e.g., primal, 2D facets are in general dependent on each other as there are geometric constraints coming from

⁷¹ In 2D case this issue has been irrelevant as the analogous requirements are contained in the assumptions necessary for a 3D problem to be reducible to 2D.



(a) The optimized mesh for continuous but not constant $\varepsilon(x, y)$. Blue lines represent the primal mesh and the red ones the dual one. (b) Density plot of anisotropic entry ε_{xy} in material permittivity tensor.

Figure 7: Optimization mesh (a) for the anisotropy ε_{xy} depicted qualitatively in (b).

the fact that they stem from a certain mesh. We will derive here a more detailed condition for 3D (non-rotating) case taking into account interdependency of edges and facets, and write it in a traditional 3D vector algebra form. Although the considerations here are not generally valid in 4D space-time we nevertheless present them, because they clarify limitations of 3D FIT in handling anisotropic materials.

For simplicity we assume that the material properties are constant in space and time, $\xi = \text{const.}$, and therefore no averaging is needed, i.e., $\bar{\xi} = \xi$. We also use the fact that the material mapping ξ is self-conjugate, see (2.216). We assume that all edges and facets are flat. A proportionality relation \sim is defined as

$$a \sim b \Leftrightarrow a = \alpha b, \quad (4.15)$$

where $\alpha \in \mathbb{R}$ is the proportionality factor.

For simplicity, let us assume that the primal mesh consists of two facets and one edge, which is their intersection. The multivectors associated with the facets and the edge are p_1, p_2 and \vec{l} , c.f. Fig. 8, and their duals \vec{l}_1, \vec{l}_2 and \vec{p} , respectively. The reasoning below extends naturally to meshes with more facets and edges. Now we will find a restriction on p_1, p_2 and \vec{l} . For convenience, we introduce normal vectors \vec{n}_1, \vec{n}_2 to the two facets, i.e.,

$$p_i =: I\vec{n}_i, \quad i = 1, 2. \quad (4.16)$$

The fact that the edge is the intersection of the two flat facets means that

$$\vec{l} \sim \vec{n}_1 \times \vec{n}_2. \quad (4.17)$$

Additionally, the dual facet is spanned by the two dual edges, which translates to

$$\vec{p} \sim \vec{l}_1 \wedge \vec{l}_2. \quad (4.18)$$

Assumption that material matrices are diagonal is equivalent to (3.44) and thus for our mesh it means that⁷²

$$\vec{W}_j \sim I\xi^{-1}(W_j) \Leftrightarrow \begin{cases} \vec{p} \sim I\xi^{-1}(\vec{l}) & \text{(Primal edge and its dual facet)} \\ \vec{l}_1 \sim I\xi^{-1}(p_1) & \text{(Primal facet and its dual edge)} \\ \vec{l}_2 \sim I\xi^{-1}(p_2) & \text{(Primal facet and its dual edge)} \end{cases}. \quad (4.19)$$

⁷² Please note that 3D vectors and 3D bivectors are both 4D bivectors and are valid arguments of the material mapping ξ . For example, a 3D vector $\sigma_x = \gamma_x \gamma_t$ and 3D bivector $\sigma_x \sigma_y = -\gamma_x \gamma_y$ are clearly bivectors. As we are interested here in 3D reasoning and intuition, we replace 4D bivector W_j immediately by an equivalent 3D vector or bivector, and notify this by assigning symbols with arrows, e.g., \vec{l} , to 3D vectors, while 3D bivectors, e.g., p_1 , are noted as general 3D multivectors.

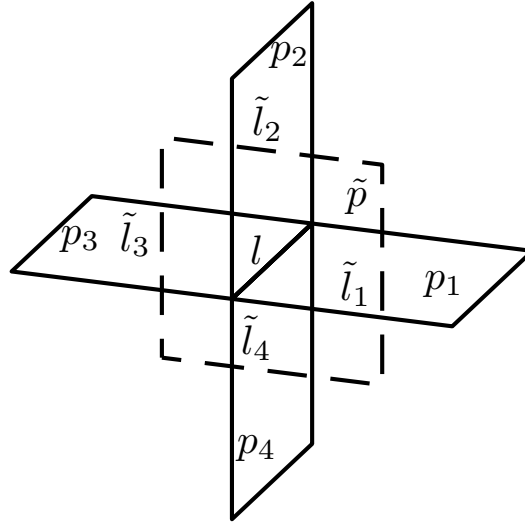


Figure 8: Primal edge l and its dual facet \tilde{p} . Depicted are also neighbouring facets p_i and their dual edges \tilde{l}_i .

See (2.174) and (2.219) for the explanation how the material mapping can be applied to 3D vectors and bivectors. Plugging it into (4.18) leads to

$$I\xi^{-1}(\vec{l}) \sim [I\xi^{-1}(p_1)] \wedge [I\xi^{-1}(p_2)] = [I\xi^{-1}(I\vec{n}_1)] \wedge [I\xi^{-1}(I\vec{n}_2)]. \quad (4.20)$$

Introducing a more 3D compatible notation for material relations, i.e.,

$$\xi^{-1}(\vec{l}) = \varepsilon^{-1}(\vec{l}) \quad \xi^{-1}(I\vec{n}) = I\mu(\vec{n}), \quad (4.21)$$

c.f., (2.219), where $\mu(\vec{n})$ is a vector understood as

$$\mu(\vec{n}) = \begin{bmatrix} \sigma_x & \sigma_y & \sigma_z \end{bmatrix} \begin{bmatrix} \mu_{xx} & \mu_{xy} & \mu_{xz} \\ \mu_{yx} & \mu_{yy} & \mu_{yz} \\ \mu_{zx} & \mu_{zy} & \mu_{zz} \end{bmatrix} \begin{bmatrix} n_x \\ n_y \\ n_z \end{bmatrix}, \quad (4.22)$$

and analogously for $\varepsilon^{-1}(\vec{l})$, which expression come from expanding the vectors \vec{l} and \vec{n} in σ_i basis. Taking that into account and using (4.17) simplifies (4.20) to

$$\boxed{\varepsilon^{-1}(\vec{n}_1 \times \vec{n}_2) \sim \mu(\vec{n}_1) \times \mu(\vec{n}_2)}, \quad (4.23)$$

which holds if and only if material matrices are diagonal.

Please note that (4.23) involves material properties (ε , μ) as well as geometric information about the mesh (\vec{n}_1 , \vec{n}_2). Intuitively speaking, the more distinct pairs of primal normal vectors (\vec{n}_1 , \vec{n}_2) are present in the mesh, the more restrictive on the material (ε , μ) is the condition (4.23). In other words, requiring more flexibility in meshing, leads to narrowing the set of materials that produce diagonal material matrices. We will now exemplify this statement by deriving explicit restrictions on material properties in the case of a Cartesian and an unstructured meshes, and showing that the former is less restrictive than the latter.

Handling Anisotropic Materials with FIT on a Cartesian Grid. For example, for a Cartesian grid \vec{n}_1 and \vec{n}_2 take only values in $\{\sigma_x, \sigma_y, \sigma_z\}$. Let us consider $\vec{n}_1 = \sigma_x$ and $\vec{n}_2 = \sigma_y$, thus $\vec{n}_1 \times \vec{n}_2 = \sigma_z$. Then the condition (4.23) for diagonal material matrices reads

$$\varepsilon^{-1}(\sigma_z) = [\varepsilon^{-1}]_{za} \sigma_a \sim \varepsilon_{abc} \mu_{xb} \mu_{yc} \sigma_a = \mu(\sigma_x) \times \mu(\sigma_y), \quad (4.24)$$

where ε_{abc} is a permutation symbol: $\varepsilon_{abc} = +1$ if (a, b, c) is an even permutation of $(1, 2, 3)$ and $\varepsilon_{abc} = -1$ if (a, b, c) is an odd permutation of $(1, 2, 3)$. Taking into account that $\varepsilon_{abc} \mu_{xb} \mu_{yc} = [\mu^{-1}]_{za}$, is equivalent to requiring that

$$\varepsilon_{za} = \alpha_z \mu_{za}. \quad (4.25)$$

Repeating the just performed calculations for other directions in Cartesian grid, i.e., $(\vec{n}_1, \vec{n}_2) = (\sigma_y, \sigma_z)$ and $(\vec{n}_1, \vec{n}_2) = (\sigma_x, \sigma_z)$, leads to

$$\varepsilon_{ab} = \alpha_a \mu_{ab} \quad (\text{no summation over } a). \quad (4.26)$$

If the axes of Cartesian grid are the same as principal axes of ε and μ , thus assuming they have the same principal axes, then both matrix representations of ε and μ are diagonal, i.e., $\varepsilon_{ab} = 0$ if $a \neq b$, and same for μ . In that case, the condition for diagonal material matrices (3.44) implies (4.26), which is fulfilled by any pair of diagonal matrices ε_{ab} , μ_{ab} . In other words, the only restriction on materials is that permittivity and permeability tensors have the same main axes, and we choose Cartesian axes as exactly these axes. In particular, both ε_{ab} and μ_{ab} may have arbitrary positive entries on the diagonal.

Anisotropic Materials on General Meshes. As yet another example, let us consider the most general set of normal vectors \vec{n}_1 and \vec{n}_2 , i.e., require that (4.23) holds for all \vec{n}_1 and \vec{n}_2 . This assumption is reasonable in the case of an unstructured mesh, where 2D facets might be oriented in principle arbitrarily and randomly. Rewriting (4.23) in Cartesian components, i.e.,

$$[\varepsilon^{-1}]_{ab} \varepsilon_{bde} n_{1d} n_{2e} \sim \varepsilon_{abc} \mu_{bd} \mu_{ce} n_{1d} n_{2e}, \quad (4.27)$$

and taking into account that the components n_{1d} and n_{2e} of \vec{n}_1 and \vec{n}_2 , respectively, are arbitrary, results in

$$[\varepsilon^{-1}]_{ab} \varepsilon_{bde} = \alpha' \varepsilon_{abc} \mu_{bd} \mu_{ce}. \quad (4.28)$$

Multiplying and contracting both sides of the above equation with $\varepsilon_{fde}/2$ reads

$$[\varepsilon^{-1}]_{ab} \overbrace{\varepsilon_{bde} \varepsilon_{fde} / 2}^{\delta_{bf}} = \frac{\alpha'}{2} \overbrace{\varepsilon_{fde} \varepsilon_{abc} \mu_{bd} \mu_{ce}}^{\text{Det}(\mu) [\mu^{-1}]_{af}}, \quad (4.29)$$

i.e.,

$$[\varepsilon^{-1}]_{af} = \alpha^{-1} [\mu^{-1}]_{af}, \quad (4.30)$$

and is equivalent to

$$\varepsilon = \alpha \mu, \quad (4.31)$$

which is more restrictive than (4.26). Namely, (4.31) states that not only ε and μ must have the same main axes as in (4.26), but also the same ratio of eigenvalues associated with the main axes. This condition is not necessary, as it relaxes in the case of Cartesian grid considered just before.

4.3 Conclusion

The classical orthogonal FIT mesh pair is a proper choice for scalar and diagonal material tensors. However, in the case of deformed primal grids, the orthogonal dual results in diagonal material matrices only for scalar material coefficients. When ε is a tensor and non-diagonal entries in material matrix are disregarded, the convergence is in general lost. However, adapting the dual mesh according to our criterion fixes the problem and allows to treat arbitrary material tensor consistently. In 3D setting we have shown that the permittivity tensor being proportional to the permeability tensor implies existence of the mesh pair guaranteeing diagonal material matrices. However, proportionality of material tensors is very restrictive for physical applications.

5 Sagnac Effect in a Rotating Ring Resonator

Chapter Overview. In this chapter we apply the theory developed in Section 3 to a particular problem in order to verify the scheme as well as to study properties of the scheme in more details. In Section 5.1 the structure studied in [55, Section IV] is described and linked to our framework. Section 5.2 adapts the results stated in [55] such that they can be compared with the ones coming from our numerical simulation. The comparison of our results with the non-relativistic ones [55], as well as analysis and interpretation of this comparison is carried out in Section 5.3. In Section 5.4 the update matrix, which steers the evolution of DoFs solution vector, is derived. The stability of schemes follows from spectral properties of this matrix. We also illustrate the stability by initialising solvers with random initial data and observe the accordance with stability test coming from the update matrix. We devote Section 5.5 to show that temporal extrapolation of DoFs to make a scheme explicit leads to instabilities. This idea has been already criticised in [37, Appendix], and the analogous criticism can be established using the method proposed in Section 5.4. In Sections 5.6 and 5.7 we numerically analyse convergence of 3D FEM and symmetrised 3D FIT. The purpose there is to check the convergence of symmetrised FIT on non-orthogonal mesh pairs. We perform this study in a non-rotating 3D setting, as the asymmetry of the material matrix is the property of the method independent of considered dimension, while in 3D the comparison of methods is more transparent. The same numerical experiment is carried out in both Sections with the difference that in Section 5.6 the mesh pair is orthogonal, while in Section 5.7 not. Therefore, the convergence of both methods in Section 5.6 is in accordance with the convergence proof [8]. The proof could be applied to FIT as

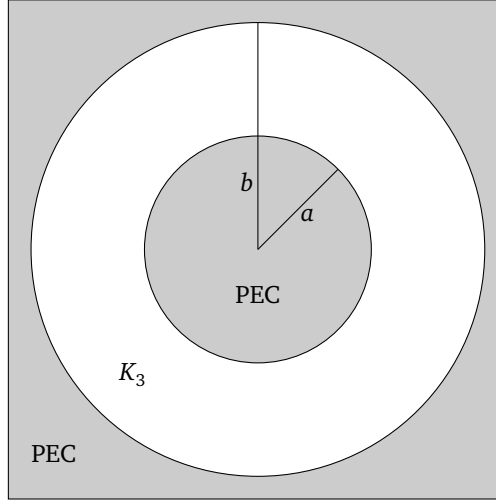


Figure 9: Geometry of the resonator. $a = 5\text{mm}$, $b = 10\text{mm}$. The height in z dimension is 2mm . K_3 is the 3D domain under study.

the material matrix is diagonal on orthogonal mesh pairs, and thus symmetric which is one of the requirements of the proof [8]. However, in the case of non-orthogonal mesh pairs in Section 5.7 the material matrices are non-diagonal and non-symmetric, and the symmetrisation step is non-trivial. As a consequence, the proof cannot be applied to FIT here. Nevertheless, we observe that FIT converges to the same solution as FEM for which the proof [8] applies independently on orthogonality of a mesh pair. We conclude this Chapter with an alternative and simpler treatment of Sagnac's effect in the structure considered in Section 5.8. However, this simple treatment cannot be applied to general structures, e.g., the Photonic Crystal considered in Chapter 6.

5.1 Description of the Numerical Experiment

We investigate the Sagnac effect in the rotating ring resonator depicted in Fig. 9. We assume that it is filled with vacuum, and the boundary is modelled by PEC. First, we calculate the eigenmodes $\hat{e}_{\text{eig},m}$ of the non-rotating structure using 3D FIT in frequency domain [60]. The first $m = 0, \dots, 5$ modes are collected in Fig. 10. Afterwards they are used as initial values for the time-domain simulation of the rotating structure.

Being more explicit; we solve the eigenvalue problem [59, 60] in the 3D domain K_3

$$\text{Continuous} \quad \nabla \times (\nu \nabla \times \vec{E}) = \omega^2 \epsilon \vec{E} \quad \vec{n} \times \vec{E}|_{\partial K_3} = 0 \quad (5.1)$$

$$\text{Discretized} \quad \tilde{C} M_\nu C \hat{e} = \omega^2 M_\epsilon \hat{e} \quad \hat{e}|_{\text{Idx}(\partial K_3)} = 0, \quad (5.2)$$

with M_ν and M_ϵ the 3D material matrices, \hat{e} the DoFs associated with \vec{E} , and $\text{Idx}(\partial K_3)$ gives the indices of edges lying on the boundary ∂K_3 . We take the mode $\hat{e}_{\text{eig},m}$ to calculate $\hat{d}_{\text{eig},m}$ (discrete equivalent of \vec{D}) and set $\vec{B}(t=0) = 0$ and pass to the time domain solver for rotating structures, i.e., the initial values are

$$d^{1/2} = -\hat{d}_{\text{eig},m} = -M_\epsilon \hat{e}_{\text{eig},m} \quad b^0 = [0, 0, \dots, 0]^T. \quad (5.3)$$

Next, the time marching procedure is started, i.e., the system (3.127)–(3.130) is solved repeatedly for $n = 1, \dots, n_{\text{max}}$.

According to the discussion in Section 3.2 the d and b values correspond to the stationary observer. Therefore, they can be passed directly (without any processing) from the eigenvalue solver for non-rotating structures to the time integrator for rotating observers. This is interpreted as exciting the mode field pattern in a stationary frame, while the PEC boundary is rotating. One may perceive it that the stationary mode pattern $\vec{E}_s(x)$ and $\vec{B}_s(x)$ is transformed to the rotating reference frame via local Lorentz transformations, yielding $\vec{E}_r(x) \neq \vec{E}_s(x)$ and $\vec{B}_r(x) \neq \vec{B}_s(x)$. See Section 2.5 for the definitions of the fields in a stationary, $\vec{E}_s(x)$ and $\vec{B}_s(x)$, and a rotating, $\vec{E}_r(x)$ and $\vec{B}_r(x)$, reference frame.

Remark: The other choice would be to insist that the mode pattern should be excited in rotating reference frame, i.e., should not be transformed, i.e., $\vec{E}_r(x) = \vec{E}_s(x)$ and $\vec{B}_r(x) = \vec{B}_s(x)$. This can be achieved by taking

$$e_i^{1/2} := \int_0^{\Delta\tau} d\tau \hat{e}_i(\tau) \approx \Delta\tau \hat{e}_i(0) = \sqrt{1 - v_i^2} \Delta t \hat{e}_i = \frac{\Delta t}{\cosh(r_i \Omega)} \hat{e}_i \quad (5.4)$$

$$h_i^0 := \int_0^{\Delta\tau} d\tau \hat{h}_i(\tau) \approx \Delta\tau \hat{h}_i(0) = \sqrt{1 - v_i^2} \Delta t \hat{h}_i = \frac{\Delta t}{\cosh(r_i \Omega)} \hat{h}_i, \quad (5.5)$$

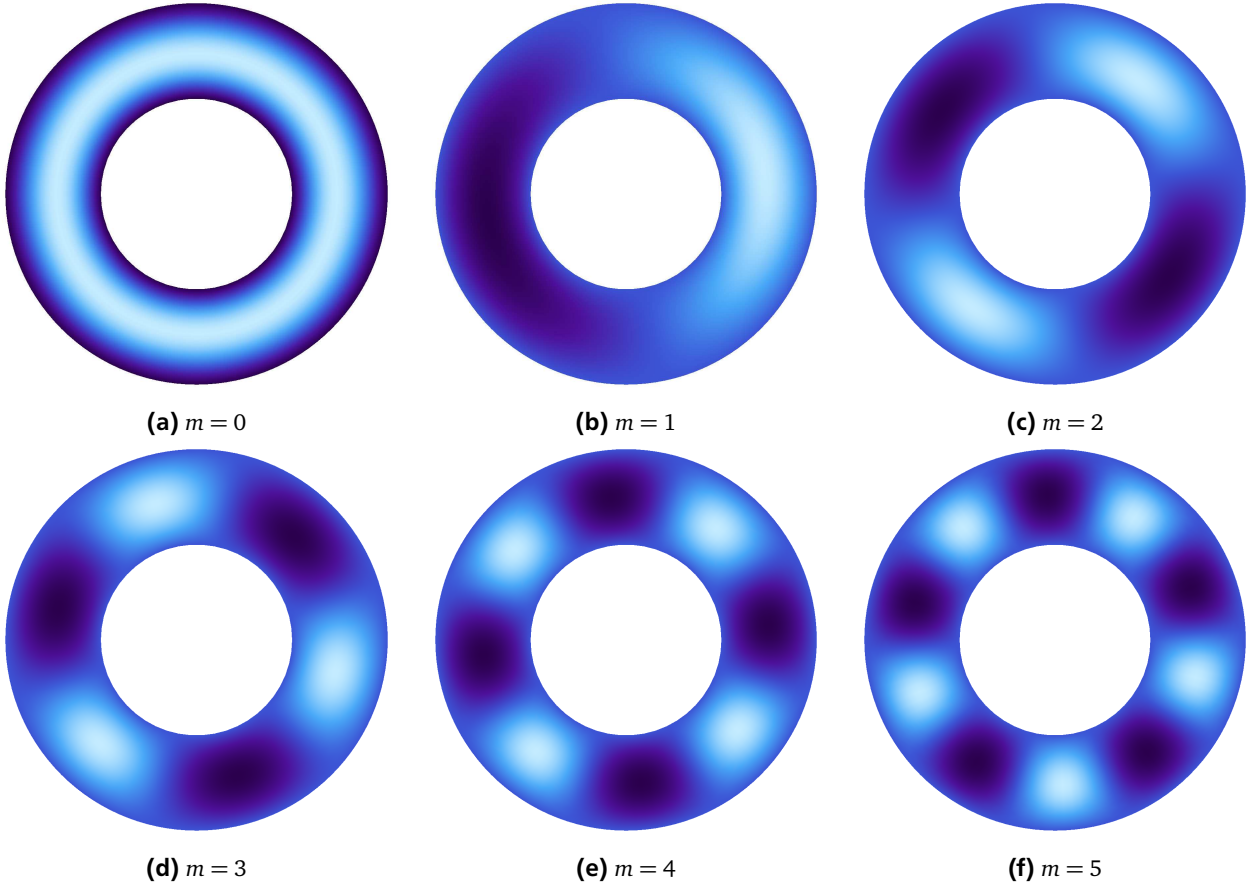


Figure 10: Considered eigenmodes.

where v_i and thus r_i are values of 3D velocity and radial coordinate at, e.g., the middle of, the edge corresponding to \hat{e}_i or \hat{h}_i . Depending on the setting of a particular physical situation one may freely chose whether the fields should be excited in the rotating or stationary reference frame by transferring d and b or e and h as initial conditions.

5.2 Analytic Predictions

The eigenmodes have harmonic azimuthal and time dependency

$$E_{\text{stat}}^z = E^z(r, \theta, z, t) = E^z(r, z) \cos(k_\theta \theta) \cos(\omega t). \quad (5.6)$$

They may be perceived as two clockwise and counterclockwise modes

$$E^z(r, z) \cos(k_\theta \theta) \cos(\omega t) = E^z(r, z) \frac{1}{2} [\cos(k_\theta \theta + \omega t) + \cos(k_\theta \theta - \omega t)] = E_{\text{stat}}^+ + E_{\text{stat}}^-, \quad (5.7)$$

where

$$E_{\text{stat}}^+ := \frac{1}{2} E^z(r, z) \cos(k_\theta \theta + \omega t) \quad (5.8)$$

$$E_{\text{stat}}^- := \frac{1}{2} E^z(r, z) \cos(k_\theta \theta - \omega t). \quad (5.9)$$

According to [55], where the authors neglect relativistic effects, these two modes should decouple if the structure is rotating

$$E_{\text{rot}}^+ := \frac{1}{2} E^z(r, z) \cos(k_\theta \theta + \omega_+ t) = \frac{1}{2} E^z(r, z) \cos(k_\theta \theta + \omega t + \delta \omega t) \quad (5.10)$$

$$E_{\text{rot}}^- := \frac{1}{2} E^z(r, z) \cos(k_\theta \theta - \omega_- t) = \frac{1}{2} E^z(r, z) \cos(k_\theta \theta - \omega t + \delta \omega t). \quad (5.11)$$

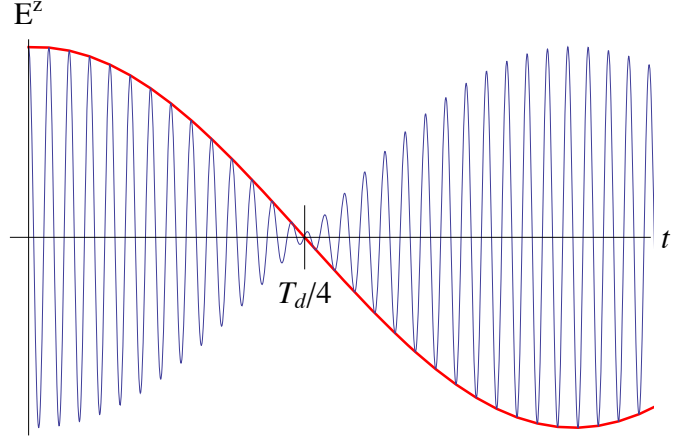
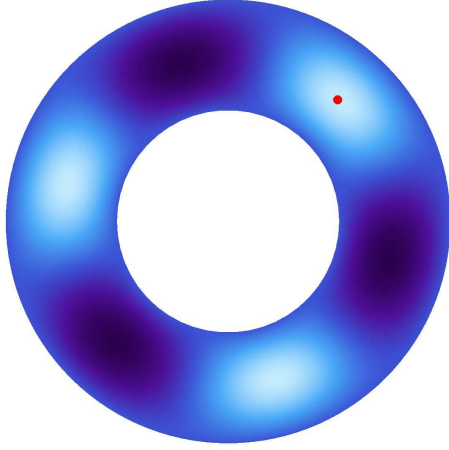


Figure 11: Behavior of the electric field $\vec{E} = [0, 0, E^z][\sigma_x, \sigma_y, \sigma_z]^T$ at the sample point. T_d is the beating period. The amplitude vanishes at $t = T_0 = T_d/4$.

Thus imposing initial value $E^z(r, \theta, z, 0)$ is equivalent to exciting these modes with the same amplitude. The solution therefore is

$$\begin{aligned} E_{\text{rot}}^z(r, \theta, z, t) &= E_{\text{rot}}^+ + E_{\text{rot}}^- = \frac{1}{2} E^z(r, z) [\cos(k_\theta \theta + \omega t + \delta \omega t) + \cos(k_\theta \theta - \omega t + \delta \omega t)] = \\ &= E^z(r, z) \cos(k_\theta \theta + \delta \omega t) \cos(\omega t). \end{aligned} \quad (5.12)$$

If we chose a reference point $(r, \theta, z) = (r_0, 0, z_0)$ and $E^z(r_0, z_0) \neq 0$, the observed time signal, i.e.,

$$\frac{E_{\text{rot}}^z(r_0, 0, z_0, t)}{E^z(r_0, z_0)} = \cos(\delta \omega t) \cos(\omega t), \quad (5.13)$$

should be beating with base frequency ω and beating period $T_d = 2\pi/\delta\omega$. According to [55, Equation (4.5)] the rotation induced frequency shift⁷³ should be

$$\delta \omega \approx m\Omega, \quad (5.14)$$

where m is the number of wavelengths in azimuthal direction.

5.3 Comparison with Analytic Formula

We study the temporal L^2 difference between the analytic solution at a sample point (5.13) and third order interpolation of the numerical solution. Namely, the L^2 norm is given by

$$\|f\|_2 := \sqrt{\int_{\Delta t/2}^{T-\Delta t/2} dt [f(t)]^2}, \quad (5.15)$$

where the integration limits are chosen such that the extrapolation is not necessary. This comes from the fact that we will interpolate the solution from $e^{n+1/2}$ DoFs, which are located at times $\Delta t/2, (1+1/2)\Delta t, \dots, (n_{\text{max}}-1/2)\Delta t$, thus the interpolated solution is defined on the interval $t \in [\Delta t/2, T - \Delta t/2]$. The signal interpolated from DoFs is denoted by $E_{\text{int}}^z(t)$ and is compared with $E_{\text{anal}}^z := E_{\text{rot}}^z(r_0, 0, z_0, t)$, i.e., the relative difference is defined as

$$\Delta E := \frac{\|E_{\text{int}}^z - E_{\text{anal}}^z\|_2}{\|E_{\text{anal}}^z\|_2}. \quad (5.16)$$

First, we study the mode $\widehat{e}_{\text{eig},0}$ with $m = 0$, i.e., the mode for which the frequency shift $\delta\omega$ is expected to be zero. In other words, this particular mode should not be affected by relativistic effects due to rotation. Thus the difference ΔE for relativistic velocities $v_{\text{max}}/c \geq 3.14\%$ is smaller than 1%. For the case of $v_{\text{max}}/c = 0.31\%$ and $v_{\text{max}}/c = 0.03\%$

⁷³ For slow rotation rates, i.e., $r\Omega/c \ll 1$ and $\Omega/\omega_0 \ll 1$.

the relative difference ΔE is equal to 6% and 58.3%, respectively. This can be explained as follows, as there is lack of relativistic effects for $m = 0$, even for relativistic velocities both approaches agree. However, due to the fact that for low velocities the necessary (to extract frequencies with desired accuracy) simulation time t_{\max} and the required number of time steps is high (order of millions), the numerical dispersion is a major factor leading to solutions, which are different in terms of the L^2 norm. Second, all other modes with $m \neq 0$ exhibit similar behaviour. For example, mode $m = 3$ for ultra-relativistic cases gives $\Delta E = 142\%$. This can be explained by recalling that the analytic solution was derived using non-relativistic assumptions and, in general, is expected to fail in relativistic scenarios. For intermediate velocities, we observe a small relative difference ΔE , e.g., for $v_{\max}/c = 3.14\%$ it is 2.19%. In the sequel we are interested in the frequencies of the obtained signal. Two solutions with the same frequency $\sin(\omega t)$ and $\sin(\omega t + \varphi)$ may have a large L^2 error, although they both correspond to the same quantity of interest $\delta\omega$. In other words; in low velocity regime the accuracy is hampered by the large simulation time that is required to extract low frequency components from the numerical simulation accurately enough. For high velocities, the analytical solution becomes inaccurate, since it is based on non-relativistic assumptions, except for $m = 0$, in which case relativistic effects are absent.

According to (5.13) the field should look like in Fig. 11. At time $T_0 = T_d/4$ the amplitude is approximately zero and this point correspond to the quarter of beating period T_d . Therefore, the frequency shift is

$$\delta\omega = \frac{2\pi}{T_d} = \frac{\pi}{2T_0}. \quad (5.17)$$

The runtime statistics are collected in Table 3. The frequencies of the discrete time-domain signal are extracted using Soft-Thresholding with Exact Line search Algorithm (STELA) described in [61].

Computer	
CPU	Intel(R) Core(TM) i7-3820, 4x 3.60 GHz
RAM	16 GB
Operating system	openSUSE 13.2
Programming environment	Mathematica 11.0.0
Mesh/linear system size	
# edges	133 200
# facets	122 640
# edge DoFs	91 920
# facet DoFs	102 000
3D Eigensolver (FEM)	
Method	Shifted Arnoldi
Peak memory	0.71 GB
CPU time	26 s
Material matrix assembly (vacuum)	
Peak memory	3.65 GB
CPU time	2.48 mins
Time integration	
Linear solver	Direct sparse LU decomposition
Time steps	31 200
Peak memory	1.85 GB
CPU time	41.4 mins

Table 3: Runtime statistics of a particular simulation.

The obtained relative difference with the analytic formula (5.14)

$$\eta := \frac{|\delta\omega^{\text{simulation}} - m\Omega|}{m\Omega} \quad (5.18)$$

for various m and Ω is presented in Tables 4 and 5. As we can see the numerical results are in close agreement with the analytic formula (5.14) for velocities $< 30\%$ speed of light. This can also be seen from Fig. 12. This is expected as this formula was derived assuming that the rotation rate Ω is low, i.e., $r\Omega/c \ll 1$. We want to stress that the closed-form and numerical solution suffer from two different types of error. The closed-form solution suffers from the modelling error, namely, absence of relativistic effects. The numerical solution was obtained without any non-relativistic assumptions. Therefore, it suffers only from the error coming from discretization discussed in Sections 5.6 and 5.7. This relative error of $\delta\omega$ is expected to be of the order of 1% based on the comparison of $\delta\omega$ for coarse $n_r = 20$ and fine $n_r = 40$ grid,

		v_{\max}/c					
		< 100%	99.63%	30.42%	3.14%	0.31%	0.03%
m	0	Null	Null	Null	Null	Null	Null
	1	95.7%	58.1%	*1.5%	0.0%	0.2%	3.2%
	2	95.8%	58.5%	*1.7%	*1.1%	0.9%	1.0%
	3	95.8%	*58.2%	*1.8%	*2.8%	3.9%	3.4%
	4	96.0%	*58.5%	4.6%	1.3%	1.3%	2.4%
	5	96.2%	*58.8%	*2.3%	*1.5%	8.2%	2.6%

Table 4: FIT case: the relative difference η (5.18) vs. mode number and rotation rate/velocity of the outer rim of the ring. The results obtained using STELA algorithm are denoted by a star, while the remaining ones have been obtained using a computationally less expensive ad-hoc procedure.

		v_{\max}/c					
		< 100%	99.63%	30.42%	3.14%	0.31%	0.03%
m	0	Null	Null	Null	Null	Null	Null
	1	95.6%	*57.8%	3.5%	0.4%	6.7%	5.4%
	2	95.7%	57.8%	*2.2%	*0.9%	3.5%	3.9%
	3	95.7%	58.0%	*0.6%	*2.0%	4.9%	5.0%
	4	95.8%	*58.4%	0.7%	1.1%	3.4%	7.9%
	5	*95.8%	58.7%	*1.8%	*1.5%	*0.5%	2.4%

Table 5: FEM case: the relative difference η (5.18) vs. mode number and rotation rate/velocity of the outer rim of the ring. The results obtained using STELA algorithm are denoted by a star, while the remaining ones have been obtained using a computationally less expensive ad-hoc procedure.

where n_r is the number of nodes in radial direction; mesh is refined in azimuthal dimension accordingly. For example, for the mode $m = 3$ the relative difference of the frequency shift obtained using the meshes with 40 and 80 nodes per wavelength is 0.78%. In other words, the mesh used in a simulation is assumed to be fine enough for the numerical solution to be accurate.

5.4 Numerical Investigation of Stability of the Implicit Schemes

Starting from (3.132)–(3.133) one can derive the recursive formula

$$\begin{bmatrix} b^{n+1} \\ e^{n+1/2} \\ b^n \end{bmatrix} = \begin{bmatrix} 1 + CM^{-1}\gamma & CM^{-1}\beta & CM^{-1}\alpha \\ M^{-1}\gamma & M^{-1}\beta & M^{-1}\alpha \\ 1 & 0 & 0 \end{bmatrix} \begin{bmatrix} b^n \\ e^{n-1/2} \\ b^{n-1} \end{bmatrix}, \quad (5.19)$$

where 0 and 1 above are zero and identity matrices of proper dimensions. The matrix

$$U := \begin{bmatrix} 1 + CM^{-1}\gamma & CM^{-1}\beta & CM^{-1}\alpha \\ M^{-1}\gamma & M^{-1}\beta & M^{-1}\alpha \\ 1 & 0 & 0 \end{bmatrix} \quad (5.20)$$

is called the update matrix and since

$$\begin{bmatrix} b^{n+1} \\ e^{n+1/2} \\ b^n \end{bmatrix} = U^n \begin{bmatrix} b^1 \\ e^{1/2} \\ b^0 \end{bmatrix}, \quad (5.21)$$

the solution vector will stay bounded if the modulus of all eigenvalues λ of U is less or equal than unity, $|\lambda| \leq 1$.

We have calculated the eigenvalue λ_{\max} with the greatest absolute value on exemplary meshes used in simulations. For FEM material matrices we have obtained $|\lambda_{\max}^{\text{FEM}}| = 1$ up to the numerical precision of the eigensolver. Thus we anticipate 4D FEM to be stable. For our extension of FIT we obtain $|\lambda_{\max}^{\text{FIT}}| > 1$, thus anticipating FIT to be unstable⁷⁴ for $\Omega \neq 0$.

⁷⁴ However, our heuristic solution to symmetrise the material matrix M_{ξ} leads to the update matrix U with the biggest eigenvalue $|\lambda_{\max}| = 1$, which indicates that might be a solution to stabilise our extension of FIT. See Section 5.7.

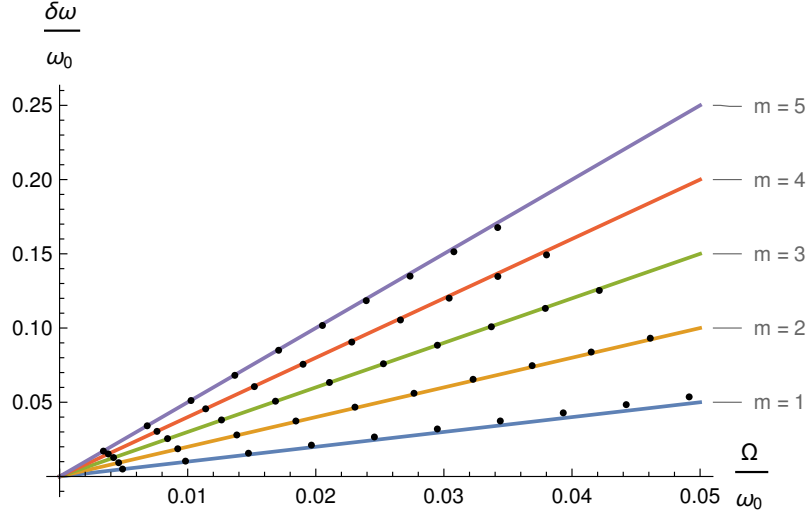


Figure 12: Comparison of analytical (5.14) (solid lines) and numerical (points) frequency shifts in case of non-relativistic velocities.

We illustrate stability considerations performed above, by time integration with random initial values. At each time step we monitor the discrete ℓ^2 norm of e and b , respectively,

$$\|e\|_2 := \sqrt{ee^T}, \quad \|b\|_2 := \sqrt{bb^T}. \quad (5.22)$$

The results are plotted in Fig. 13. In accordance with the just outlined theory based on the eigenvalues of the update matrix U the FEM solution remains stable, while FIT does not.

We have only studied the implicit FIT/FEM schemes in this subsection. However, if temporal extrapolation is used, one can start from (3.127)–(3.130), replace extrapolated DoFs by explicit extrapolation formula used, and calculate the greatest eigenvalue of the resulting update matrix U in order to check stability.

5.5 Numerical Investigation of Instabilities due to Extrapolation

Let us recall the system (3.127)–(3.130)

$$\begin{aligned} h^n &= M_{yb}^- b^{n-1} + M_{ye}^- e^{n-1/2} + M_{yb} b^n + M_{ye}^+ e^{n+1/2} + M_{yb}^+ b^{n+1} \\ d^{n+1/2} &= d^{n-1/2} + \tilde{C}h^n \\ e^{n+1/2} &= M_{ee}^{-1} [d^{n+1/2} - M_{eb}^- b^n - M_{eb}^+ b^{n+1}] \\ b^{n+1} &= b^n + C e^{n+1/2}. \end{aligned}$$

It has to be solved consistently at each time step once. However, one may try to extrapolate $e^{n+1/2}$ in the first and b^{n+1} in the first and the third row from the values at previous time steps. This has been proposed in [39] and criticised in [37, Appendix] by showing that the first order extrapolation leads to an unstable scheme. However, one may wonder whether more accurate extrapolation would improve stability; we will address this question numerically now.

Temporal Extrapolation of DoFs. Namely, by j -th order extrapolation we mean the following; the values of $e^{n+1/2}$ and b^n on the right-hand-side of (3.127) and (3.129) above are extrapolated using⁷⁵

$$f^{k+1} = \sum_{i=0}^j a_i f^{k-i}, \quad (5.23)$$

where $f = \{e, b\}$, $k = \frac{1}{2}, 1, 1\frac{1}{2}, 2, 2\frac{1}{2}, \dots, n_{\max}$,

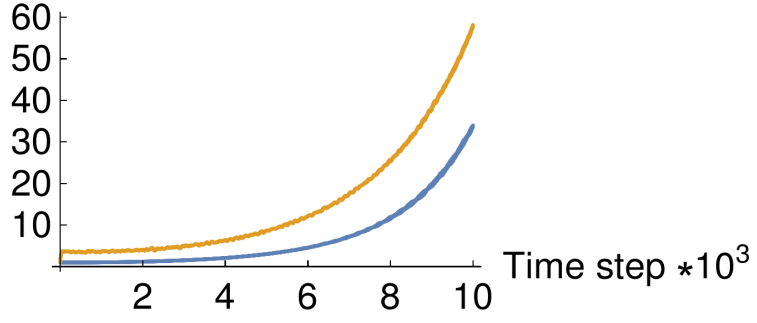
$$f^k := f(k\Delta t), \quad (5.24)$$

and $f(t)$ is assumed to be a j -th order polynomial

$$f(t) = \sum_{i=0}^j \beta_i t^i \quad (5.25)$$

⁷⁵ Please note that by doing so, the extrapolated f^{k+1} does not necessary fulfil Maxwell's Equations.

Normalised discrete electric/magnetic energy



Normalised discrete electric/magnetic energy

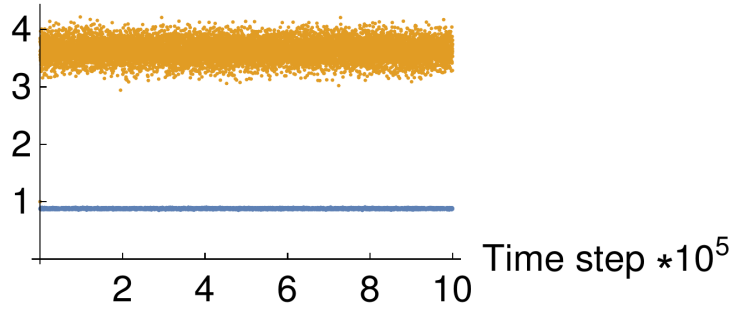


Figure 13: The discrete ℓ^2 norm of the FIT and FEM solutions for random initial data. The norm $\|e\|_2$ associated with the electric field is depicted in blue, while the norm $\|b\|_2$ associated with the magnetic field is depicted in orange. In FIT case (above) the norm grows exponentially, exhibiting thus its instability. The FEM case (below) remains stable for 1 million of time steps, after which the simulation is stopped.

fitting exactly the last $j + 1$ known points f^{k-i} , $i = 0, 1, \dots, j$,

$$f^{k-i} = f((k-i)\Delta t). \quad (5.26)$$

Due to constant time step sizes the coefficients a_i can be precomputed as follows. We use (5.25) in (5.26) and solve for β_i in terms of f^{k-i} , $i = 0, 1, \dots, j$. Subsequently, the obtained polynomial is used in (5.23) to calculate f^{k+1} . The resulting extrapolated values for $j = 0, 1, 2$, respectively, are

$$f^{k+1} = f^k \quad (5.27)$$

$$f^{k+1} = 2f^k - f^{k-1} \quad (5.28)$$

$$f^{k+1} = 3f^k - 3f^{k-1} + f^{k-2}. \quad (5.29)$$

Discrete Energetic Norm. The electric energy is proportional to

$$\int \vec{E} \cdot \vec{E} dV = \int \vec{E}^2 dV. \quad (5.30)$$

Taking into account that

$$\vec{E}^2 \approx \left(\frac{e_i}{l_i \Delta T} \right)^2 \quad (5.31)$$

it is natural to define the norm

$$\|e\|_E := \frac{1}{n_{\text{edges}}} \sum_{i=1}^{n_{\text{edges}}} \left(\frac{e_i}{l_i \Delta T} \right)^2, \quad (5.32)$$

with n_{edges} number of edges, ΔT the time step, l_i the length of i -th edge. Conservation of this energy is shown in Fig. 15.

We consider the mode $\hat{e}_{\text{eig},3}$ with $m = 3$. The results for zeroth, first and second order extrapolation in our 4D extension of FIT are depicted in Fig. 14. We can see that although first order extrapolation is more stable than zeroth one, increasing

the extrapolation order to two gives less stable result. Therefore, suggestion in [39] to apply more accurate extrapolation is not an option as it leads to even less stable scheme. However, even applying an implicit time-integration⁷⁶ with FIT non-symmetric matrices as defined in (3.105) leads to an unstable scheme.⁷⁷ However, it remains stable for a few millions of time steps as presented in Fig. 15. Therefore, extrapolation increases the overall instability of the scheme.

Analogous results for FEM are shown in Fig. 14. We see that the zeroth order extrapolation becomes immediately unstable. First order extrapolation starts tending to infinity after 9000 time steps. Second order extrapolation, although stable, leads to undesired dissipation. However, there is no general guarantee that for other geometries or initial values this extrapolation will lead to a stable scheme. The implicit FEM scheme remains stable up to 50 millions of time steps as shown in Fig. 15.

5.6 Numerical Convergence Analysis (non-rotating case)

We run the simulations for the mode $m = 3$ on the sequence of refined (not necessarily nested) grids to check the convergence of FIT and FEM predicted by the theory. The simulation is carried out up to the time equal to the one period of the wave (coming from the eigenmode solver). The (temporally interpolated) magnitudes of electric field obtained using FIT and FEM at sample point for the s -th mesh in the sequence are denoted by $E^{\text{FIT}}(s)$ and $E^{\text{FEM}}(s)$, respectively. The results are gathered in Fig. 16.

In the Fig. 16 n_r is the number of nodes per wavelength and the differences for the s -th mesh of the sequence are⁷⁸

$$\Delta E_{\text{FIT-FEM}}(s) := \frac{\|E^{\text{FIT}}(s) - E^{\text{FEM}}(s)\|_2}{\|E^{\text{FEM}}(s)\|_2} \quad (5.33)$$

$$\Delta E_{\text{FIT}}(s) := \frac{\|E^{\text{FIT}}(s) - E^{\text{FIT}}(s-1)\|_2}{\|E^{\text{FIT}}(s)\|_2} \quad (5.34)$$

$$\Delta E_{\text{FEM}}(s) := \frac{\|E^{\text{FEM}}(s) - E^{\text{FEM}}(s-1)\|_2}{\|E^{\text{FEM}}(s)\|_2}, \quad (5.35)$$

where we have used the L^2 norm (5.15).

Therefore, we see that both methods exhibit second order convergence for meshes with $n_r > 50$. However, it does not guarantee that they converge to the true solution. This guarantee is given by the theory, e.g., [8]. Please note that the convergence of FIT here is not in a contradiction with the non-stable behaviour explained in Section 5.5, because instability comes from non-orthogonality of the mesh pair, while they are orthogonal in the case of no rotation, $\Omega = 0$, i.e., an orthogonal 3D mesh is extruded orthogonally in the temporal dimension resulting in an orthogonal 4D mesh (pair). Nevertheless, the instability on non-orthogonal grids is an important issue⁷⁹ and we are going to study it now.

5.7 Symmetrised FIT Material Matrices (non-rotating case)

The material matrix developed in Section 3.3.4 is asymmetric in general. The problem of the asymmetry is already apparent in 3D, therefore we will investigate it in case of no rotation $\Omega = 0$, i.e., when our approach reduces to a standard 3D approach. The convergence proof in the case of symmetric positive-definite material matrices was carried out in [8]. Therefore, one may ask a question whether the scheme with the symmetrized material matrices

$$M_{\xi}^{\text{sym}} := \frac{1}{2} (M_{\xi} + M_{\xi}^T) \quad (5.36)$$

is convergent. Unfortunately, it is difficult to repeat the convergence proof for symmetrized matrices as the consistency criterion [8, Equation (18)] does not hold. The attempt to fix this issue is described in the Appendix C.7. Nevertheless, we can explore numerically the convergence of the scheme for a particular problem.

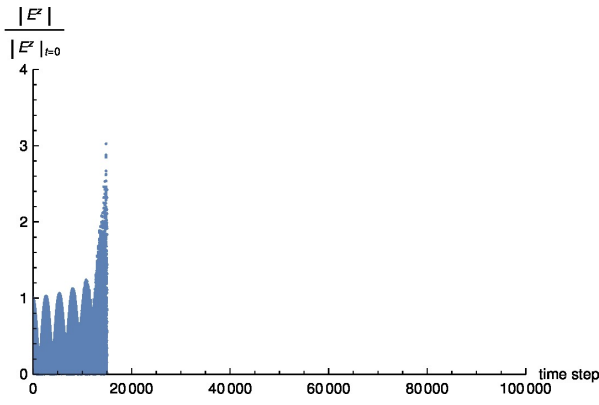
In the previous subsection the FIT material matrices were diagonal, thus symmetric, and we could apply the standard convergence theory. However, now the situation is different; the non-symmetrized matrices lead to an unstable scheme, but for the symmetrized ones we cannot prove the convergence. Therefore, we compare numerically symmetrized FIT with FEM, for which the convergence is proven.

⁷⁶ By “implicit” it is meant that the system (3.127)–(3.130) is solved, e.g., by sparse LU decomposition in (3.132)–(3.133).

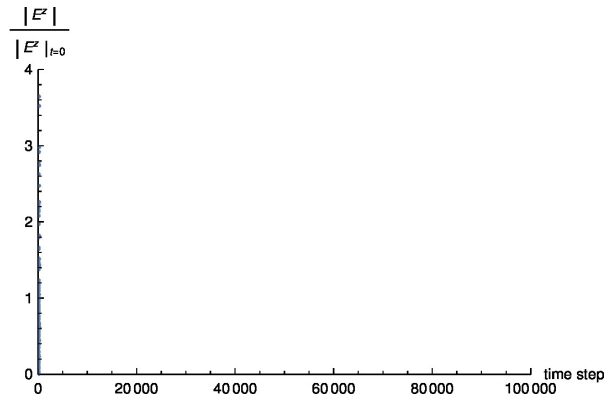
⁷⁷ This has been proven for Cartesian grid and first order extrapolation in [37, Appendix]. For other (unstructured) meshes one can calculate the eigenvalues of the update matrix and verify that some of them have absolute value greater than 1. This is caused by the antisymmetric part of the material matrix, and can be circumvented heuristically by taking only the symmetric part of the material matrix. This attempt to stabilise time integration within FIT is described in Section 5.7.

⁷⁸ Namely, for $s = 1, 2, 3, \dots$, we have chosen $n_r(s) = 5, 10, 15, \dots, 35, 40, 50, 60, \dots, 200$.

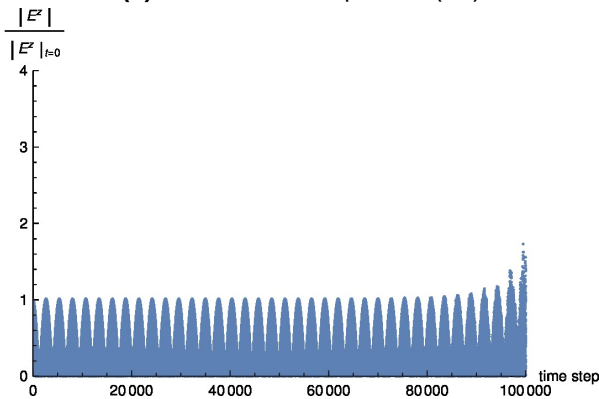
⁷⁹ Due to potential limitation of the method to the orthogonal grids.



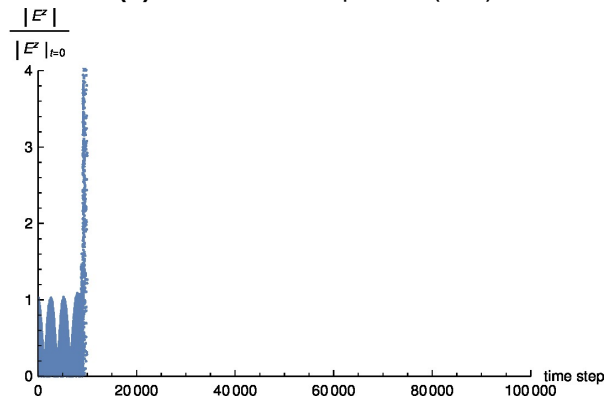
(a) Zeroth order extrapolation (FIT)



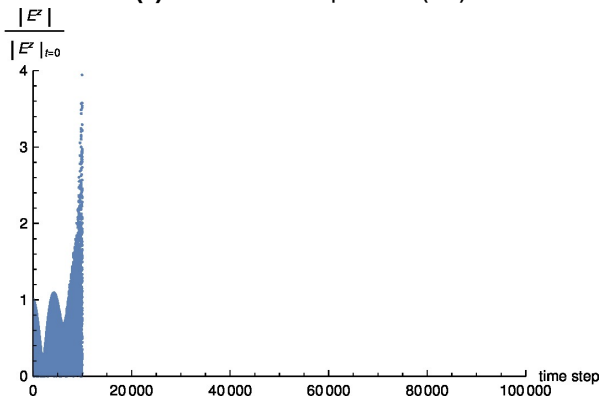
(b) Zeroth order extrapolation (FEM)



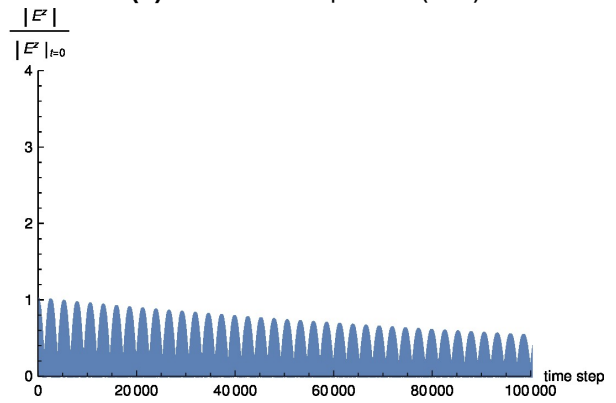
(c) First order extrapolation (FIT)



(d) First order extrapolation (FEM)

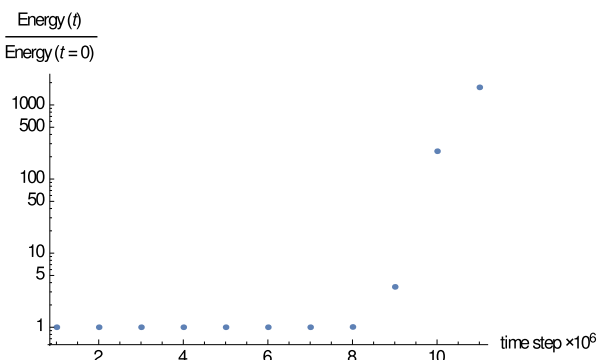


(e) Second order extrapolation (FIT)

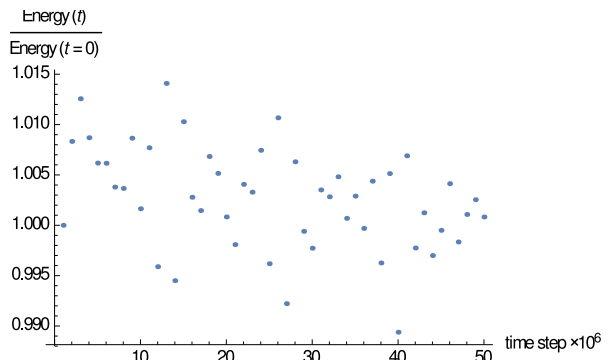


(f) Second order extrapolation (FEM)

Figure 14: Amplitude of the field for various extrapolations (FIT).



(a) FIT



(b) FEM

Figure 15: Energy (5.32) conservation for implicit schemes.

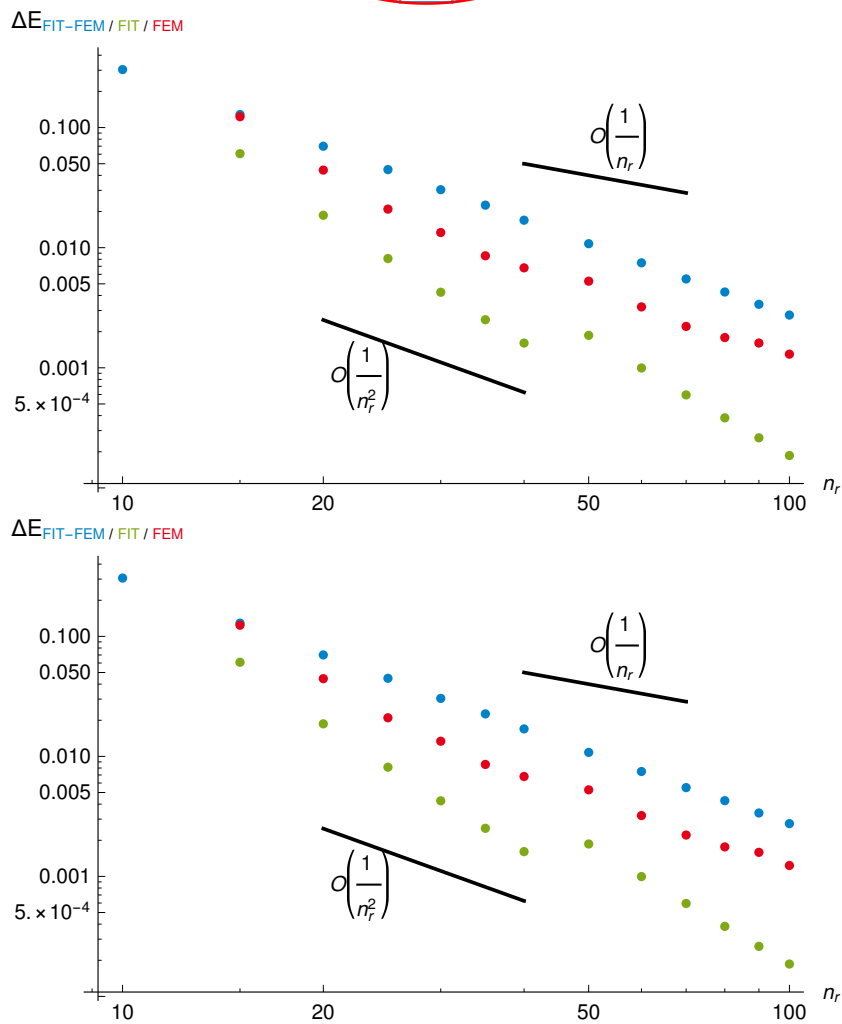
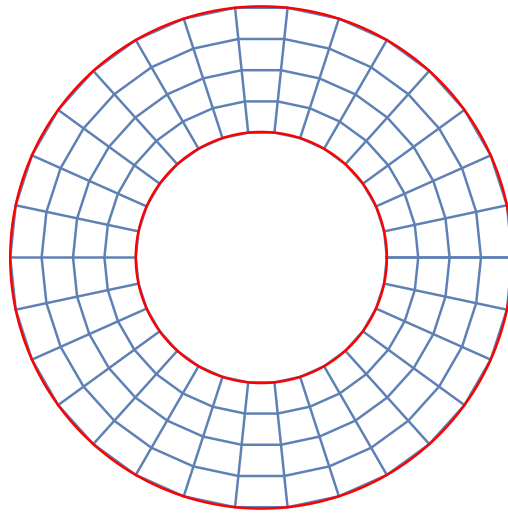


Figure 16: Legend: $\bullet \Delta E_{\text{FIT-FEM}}$, $\bullet \Delta E_{\text{FIT}}$, $\bullet \Delta E_{\text{FEM}}$. Top: the coarsest mesh with $n_r = 5$ nodes in radial direction. Only the 2D section at $z = 0$ is depicted. The barycentric dual is **orthogonal** in this case. For each mesh in the sequence we plot the difference between FIT and FEM solutions as well as the difference between current and previous FIT/FEM solution. Below: convergence plots associated with the initial values coming from FIT (middle) and FEM (bottom) eigenmode solver. The lines correspond to the first $\mathcal{O}(n_r^{-1})$ and second $\mathcal{O}(n_r^{-2})$ order convergence. Convergence of successive FIT/FEM differences, and FIT-FEM difference is in accordance with the proof [8]. C.f. Figure 17.

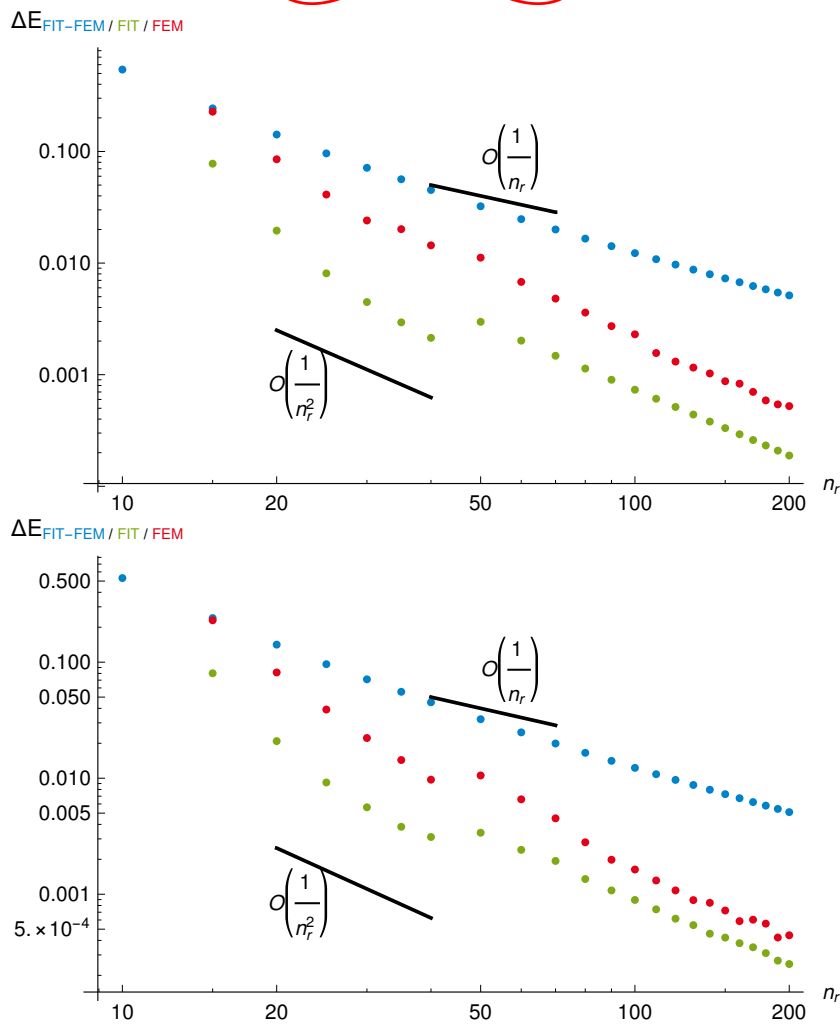
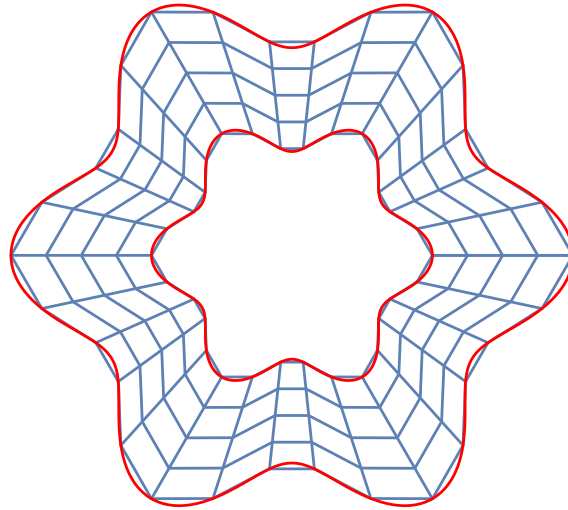


Figure 17: Legend: $\bullet \Delta E_{\text{FIT-FEM}}$, $\bullet \Delta E_{\text{FIT}}$, $\bullet \Delta E_{\text{FEM}}$. Top: the coarsest mesh with $n_r = 5$ nodes in radial direction. Only the 2D section at $z = 0$ is depicted. The barycentric dual is **non-orthogonal** in this case. For each mesh in the sequence we plot the difference between FIT and FEM solutions as well as the difference between current and previous FIT/FEM solution. Below: convergence plots associated with the initial values coming from FIT (middle) and FEM (bottom) eigenmode solver. The lines correspond to the first $\mathcal{O}(n_r^{-1})$ and second $\mathcal{O}(n_r^{-2})$ order convergence. Convergence of successive FEM differences is in accordance with the proof [8]. The convergence of FIT cannot be established using the method in [8]. However, we see that FIT solutions converge to some limit, and moreover, this limit is the same as for FEM, for which the proof [8] applies. Thus, we conclude that FIT converges to the true solution although the proof [8] does not apply here. C.f. Figure 16.

Method	Stability		Consistency	
	Numerical tests	General proof	Numerical tests	General proof
4D FEM	Stable	Stable	Consistent	Consistent
4D FIT	Unstable	Not known	Consistent	Consistent
Symmetrised	Stable	Not known	Consistent	Not known
4D FEM/FIT with temporal extrapolation	Unstable	Not known	Consistent	Not known

Table 6: Summary of features of the discussed schemes. Consistency is meant in the sense of [8]. By stability of time-stepping it is understood that the modulus of all the eigenvalues λ of the update matrix (5.20) is at most one, i.e., $|\lambda| \leq 1$.

In order to obtain non-diagonal entries in FIT material matrices, we deform the ring resonator as shown in Fig. 17, such that the barycentric dual with straight edges does not lead to an orthogonal mesh pair. The boundary of the resonator is given by

$$r_{\min}(1 + a \cos(b\varphi)) \quad \text{and} \quad r_{\max}(1 + a \cos(b\varphi)), \quad (5.37)$$

with $r_{\min} = 5$, $r_{\max} = 10$, $a = 0.15$ and $b = 6$. We construct the first mesh of the sequence with $n_r = 5$ and then we refine that mesh without forcing new nodes to lay on the boundary of the resonator.⁸⁰ In such a way, we eliminate the error associated with the approximation of the curved geometry; the convergence analysis is associated with discretization of the fields only. As can be seen from Fig. 17 both methods converge to the same solution with similar convergence order. Thus, we can conclude that for this particular case the symmetrized FIT converges to the true solution, as FEM is known to converge [8].

Open research question 6. *Motivated by Appendix. C.7 and the just explained particular example, we are eager to ask: Can we prove that the symmetrized FIT converges to the true solution? Does it exhibit the same order convergence as standard FIT and FEM?*

Open research question 7. *Can we redefine the centres of lower dimensional elements like in Appendix C.7, such that a requirement of the convergence proof [8], that is (C.61), holds in n dimensions? Is the material matrix obtained using the dual mesh guaranteeing the convergence related (in terms of explicit formula) to the one obtained using the barycentric dual?*

We conclude this Section with the following Table 6 summarising the properties of the discussed schemes.

5.8 Geometric Optics Approximation

The structure considered in this subsection is simple enough that one can study it using geometric optics approximation. Let us consider a rotating wave-guide bent into circular shape, Fig. 18. Suppose at time zero we send two signals from some point (red line) of the wave-guide; one to the left and one to the right, and we wait until they come back to the point. Due to rotation, the point will move to another position (dashed red line) during the time both signals travel around. Consequently, the (counter)clockwise signal travels less (more) distance than the circumference, and thus they will arrive back to the point at different times. Please note that if we had considered the situation in the reference frame co-rotating with the wave-guide Fig. 18(Right) and disregarding relativistic effects associated with the fact that the frame is non-inertial, we would not have obtained any difference in time of arrival, and thus any frequency shift. Therefore, the right treatment of relativistic effects is crucial in building the computational scheme to simulate Sagnac effect.

According to [41, Equation (6)] the difference in time of arrival is

$$\Delta t = \frac{4\pi R^2 \Omega}{c^2 - R^2 \Omega^2} \approx \frac{4\pi R^2 \Omega}{c^2}, \quad (5.38)$$

where R is the average radius of the ring, i.e., $R = (a+b)/2$, and Ω is the rotation rate. Consequently the phase difference is

$$\Delta \phi = \frac{2\pi c}{\lambda} \Delta t, \quad (5.39)$$

with λ wavelength. This may be perceived that the two waves propagate with slightly different frequencies

$$\omega_{\pm} = \omega_0 \pm \delta \omega. \quad (5.40)$$

⁸⁰ I.e., we regard the boundary geometry of the coarsest mesh as the reference geometry.

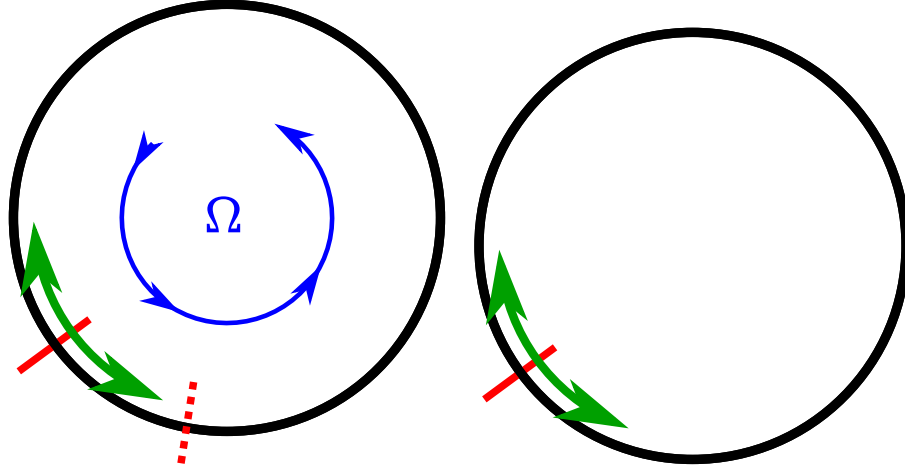


Figure 18: Left: (Right:) Sagnac loop as seen by stationary (co-rotating) observer.

The frequency shift $\delta\omega$ can be easily calculated. Upon introducing the period $T = 2\pi R/c$ and the mode number $m = 2\pi R/\lambda$ we obtain

$$\delta\omega \approx \frac{\Delta\phi}{2T} = \frac{2\pi R}{\lambda} \Omega = m\Omega, \quad (5.41)$$

which coincides with the analytic approximation (5.14) obtained in [55, Equation (4.5)]⁸¹ using field-theoretical framework.

Although investigating Sagnac's effect with the geometric optics approximation is probably much simpler than field-theoretical study, it cannot be applied to generic structures. One of such examples is a Photonic Crystal to whose study we now turn.

6 Rotating Photonic Crystal

In the previous section, we have seen that the effect of rotation is splitting the equal eigenfrequencies of degenerate eigenmodes into non-equal ones. Therefore, by measuring the rotation induced frequency shift one can detect rotation; in other words one can build an optical gyroscope. The possibilities of electromagnetic rotation sensing has been already discussed in [41]. However, in order to apply such approach one needs to know the light path, i.e., be in a geometric optics regime. This is not always the case as for example in the case of photonic crystals. Then the calculation of properties of such structures should be based on solving Maxwell's equations. This has been done for 2D problems and low-velocities in [38, 53, 55] and citations therein. For example, in [38, Section 3] the authors investigate the influence of imperfections (unavoidable in fabrication process) on the behaviour of the system under rotation. However, the generic defects break the symmetry in z -direction⁸² and thus one needs a 3D code to study the effect of such defects on the whole device.

According to [54, Equations (3.18)–(3.20)] the properties of the entire gyroscope depend on the behaviour of a single isolated resonator under rotation. Therefore, as another application, we will study the photonic crystal depicted in Fig. 19, cf. [53, Fig. 2]. Motivated by the eigenmodes of the complete structure, see Fig. 20 and [53, Fig. 1], we introduce an artificial PEC boundary as PEC boundary conditions are easily implemented, while the fields outside our artificial boundary are close to zero, therefore the artificial boundary should not disturb the system significantly. We will refer to the structure surrounded by the artificial PEC boundary as a simplified Photonic Crystal (PhC).

Here we calculate the rotation induced frequency shift according to [53, Section 2]. First, from (5.2) we calculate the eigenmodes $\widehat{e}_{\text{eig},m}$ of the non-rotating simplified PhC. We focus our attention on the two degenerate eigenmodes $m = 1, 2$, whose electric field magnitude $|\vec{E}_{\text{eig},m}|$ is depicted in Fig. 20. Subsequently, we calculate the discrete magnetic fluxes in frequency domain⁸³

$$\widehat{b}_{\text{eig},m} := \frac{1}{i\omega_0} C \widehat{e}_{\text{eig},m}, \quad (6.1)$$

⁸¹ See also the discussion around [55, Equation (4.6)] for relation to classical Sagnac effect.

⁸² Such as non-parallel cylinders or non-uniform cross-section in z -dimension.

⁸³ We assume that at time $t = 0$ the electric field is maximal, while the magnetic one is zero. Thus the resulting $\widehat{e}_{\text{eig},m}$ is real, and $\widehat{b}_{\text{eig},m}$ purely imaginary.

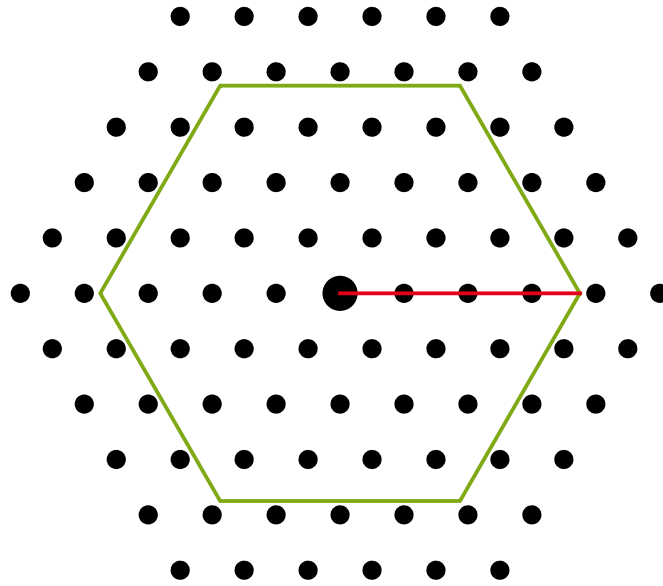


Figure 19: The photonic crystal under study, see [53, Section 4]. The black cylinders are made of a dielectric with $\epsilon_r = 8.41$, while the background material is vacuum. Smaller cylinders have radius $0.6\mu m$ and are organised in a hexagonal lattice with distance $4\mu m$. The radius of the central cylinder is $1.1\mu m$. The green contour depicts the artificial PEC boundary introduced by us to simplify the simulation. The distance (red line) from the center to PEC is $15\mu m$.

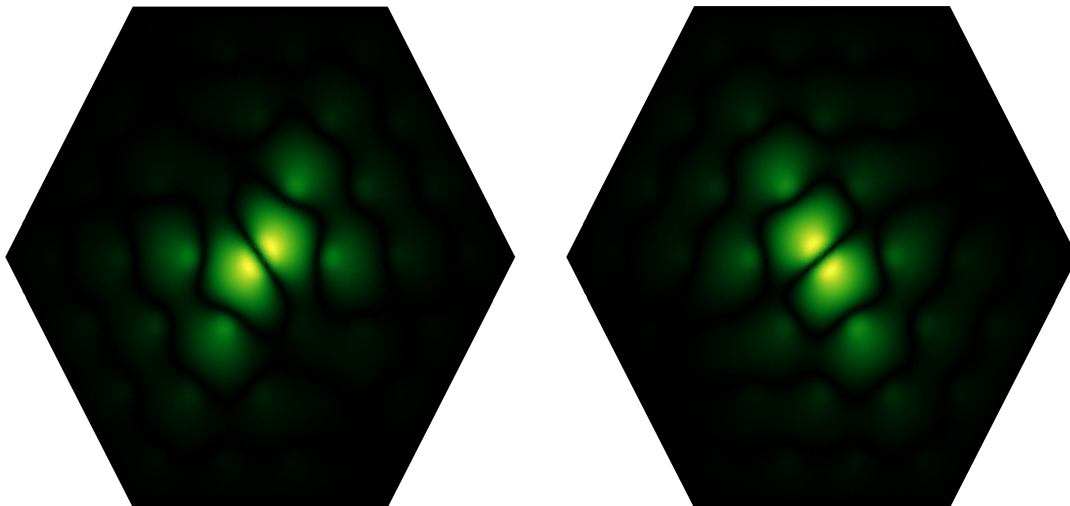


Figure 20: The electric field magnitude $|\vec{E}_{\text{eig},m}|$ of the two eigenmodes of the simplified PhC structure being considered here. First, we note the close similarity to [53, Fig. 1]; second, the fields are close to zero at the artificial boundary.

which is a discrete equivalent of calculating them from $\vec{B} = 1/(i\omega_0)\vec{\nabla} \times \vec{E}$. From the knowledge of $\widehat{e}_{\text{eig},m}$ and $\widehat{b}_{\text{eig},m}$ the value of electric $\vec{E}_{\text{eig},m}$ and magnetic $\vec{B}_{\text{eig},m}$ field at any point in K_3 is calculated by means of interpolation on the 3D primal mesh. The values of $\vec{D}_{\text{eig},m}$ and $\vec{H}_{\text{eig},m}$ are calculated by using the material equations.

According to [53, Equation (2.17)] the rotation induced frequency shifts are

$$\delta\omega_{\pm} = \omega_0\Omega\Lambda_{\pm}, \quad (6.2)$$

where Λ_{\pm} are all two (as we consider only two degenerate eigenmodes) eigenvalues of [53, Equation (2.16)]

$$C = \frac{1}{2}A^{-1}B, \quad (6.3)$$

with A having entries [53, Equation (2.12a)]

$$A_{mn} = \langle \vec{H}_{\text{eig},m} | \vec{H}_{\text{eig},n} \rangle, \quad (6.4)$$

and B [53, Equation (2.13a)]

$$B_{mn} = \varepsilon_0 \langle \vec{e}_z \times \vec{r} | \vec{H}_{\text{eig},n}^* \times \vec{E}_{\text{eig},m} + \vec{H}_{\text{eig},m} \times \vec{E}_{\text{eig},n}^* \rangle, \quad (6.5)$$

where a superscript star, e.g., in $\vec{E}_{\text{eig},n}^*$, denotes complex conjugation and

$$\langle \vec{a} | \vec{b} \rangle := \int_{K_3} \vec{a} \cdot \vec{b}^* d^3\vec{r}, \quad (6.6)$$

c.f., [53, Equation (2.8)]. We evaluate the integral over the whole domain K_3 , by subdividing it into integrals over single 3D primal cells, and approximating the integral over each cell by the one-point quadrature, choosing the barycenter as the quadrature point. In other words,

$$\int_{K_3} \vec{a} \cdot \vec{b}^* d^3\vec{r} = \sum_j \int_{K_3^j} \vec{a} \cdot \vec{b}^* d^3\vec{r} \approx \sum_j \vec{a}(\vec{r}_j^{\text{b}}) \cdot \vec{b}^*(\vec{r}_j^{\text{b}}) \Delta V_j, \quad (6.7)$$

where \vec{r}_j^{b} is the barycenter, and

$$\Delta V_j = \int_{K_3^j} d^3\vec{r} \quad (6.8)$$

the volume of j -th 3D cell K_3^j . Therefore, we see that the only missing part to calculate $\delta\omega$ from (6.2) is the explicit formula for the $\vec{E}(\vec{r}_j^{\text{b}})$ and $\vec{H}(\vec{r}_j^{\text{b}})$ in terms of DoFs. Whitney interpolation is employed to solve this issue; the rather technical details are collected in the Appendix C.8.

First, we note that the dimensionless proportionality factor in (6.2) for the simplified PhC structure is $\omega_0\Lambda_{\pm} = \pm 0.2296$, which is very close to the one $\omega_0\Lambda_{\pm} = \pm 0.229$ obtained in [53, Section 4] for the full PhC structure. Therefore, our assumption that the artificial boundary does not influence the physics (rotation induced frequency shifts) significantly is justified. Second; calculating the rotation induced frequency shifts as in the previous section⁸⁴, but this time for the simplified PhC structure leads to the conclusion that again they are in close agreement with analytic predictions, see Fig. 21. The runtime statistics are collected in Table 7.

7 Conclusion and Outlook

Let us state three main results of this dissertation;

- **Space-Time Algebra is compatible with (and in certain sense convenient for) relativistic and coordinate-free treatment of classical electromagnetism.** Space Time-Algebra, i.e., Clifford's Geometric Algebra associated with flat, four-dimensional, Minkowski metric, introduced in Section 2.1 has been successfully used throughout the thesis to express in simple formulae the first principles, which are consistent with Special Relativity Theory (thus holding in relativistic as well as non-relativistic scenarios) and remain valid in any coordinate system, i.e., arbitrary coordinates might be employed while working with these formulae. Examples of such are Maxwell's, Equations (2.209) or (2.210), and material, Equation (2.212), equations in their space-time form. By the "classical" electromagnetism we mean "not quantum and not coupled to gravity".

⁸⁴ Namely solving (5.2) and then (3.127)–(3.130) to obtain the time signal at a sample point from which frequencies are extracted.

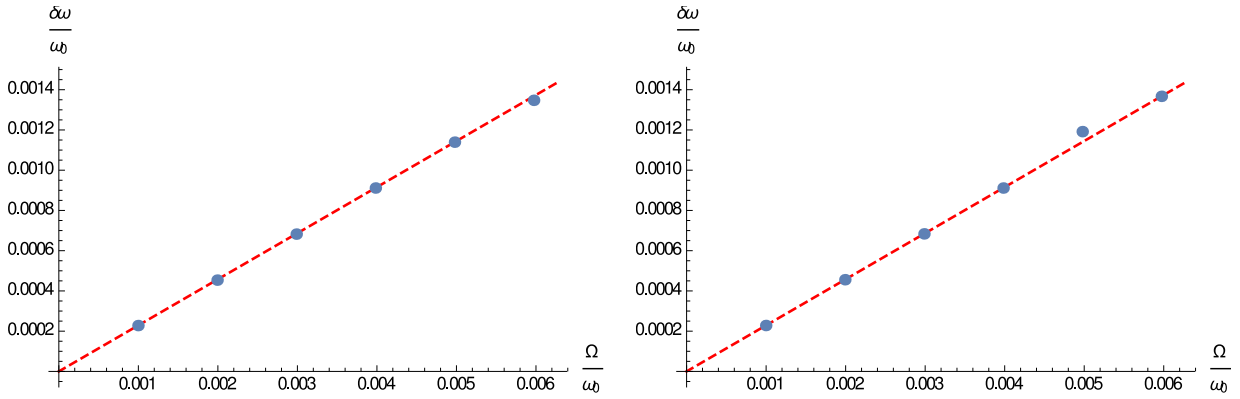


Figure 21: Obtained frequency shifts $\delta\omega$ for the modes in Fig. 20 versus rotation rate Ω . The left (right) plot correspond to the left (right) mode in Fig. 20. The red dashed line correspond to the analytical result (6.2), and blue dots are obtained by numerical simulation. We normalise $\delta\omega$ and Ω by dividing by the frequency ω_0 of the corresponding stationary mode.

Computer	
CPU	Intel(R) Core(TM) i7-3820, 4x 3.60 GHz
RAM	16 GB
Operating system	openSUSE 13.2
Programing environment	Mathematica 11.0.0
Mesh/linear system size	
# edges	221 042
# facets	200 107
# edge DoFs	138 310
# facet DoFs	158 741
3D Eigensolver (FEM)	
Method	Shifted Arnoldi
Peak memory	1.68 GB
CPU time	185.5 s
Material matrix assembly	
Peak memory	5.96 GB
Sequential CPU time	3.77 mins
Parallel CPU time (8 threads)	14.43 mins (each)
Time integration	
Linear solver	Direct sparse LU decomposition
Time steps	5 020 000
Peak memory	3.76 GB
CPU time	132.36 hrs \approx 5.5 days

Table 7: Runtime statistics of a simulation.

- **Requiring Finite Integration Technique’s (FIT) material matrices to be diagonal imposes restrictions on materials that can be simulated.** Although non-diagonal material matrices may be employed in FIT’s framework as in Sections 5 and 6, it is interesting when they are actually diagonal, because of a significant boost in performance of the numerical scheme in that case. Thus in Section 4.2 we have derived the necessary and sufficient condition (4.23) for obtaining diagonal material matrices on a 3D mesh. We have restricted our attention to the material matrices obtained without making any further approximations, which might lead to decreasing the order of convergence of the scheme.
- **The numerical method proposed here can be applied to the simulation of electromagnetic devices in a rotating reference frame.** The FIT-like numerical scheme (3.127)–(3.130) derived in Section 3.4 has been successfully applied to simulate a rotating ring resonator in Section 5. Moreover, the stability and convergence of the scheme has been numerically verified in that section. In Section 6 we have recovered with good accuracy the quantity of interest, namely, rotation induced frequency shift of eigenmodes, which is important in the design of optical gyroscopes as indicated by [53].

Possible extensions of this work, besides the ones suggested by Open Research Questions on pages 13, 25, 49 and 72, include the following;

- The scheme in Section 3.4 has been derived assuming that the medium is local, linear and possibly anisotropic. However, we expect that the scheme can be applied to simulate electromagnetic behaviour of systems composed of more general class of materials, e.g., non-linear or lossy, i.e., include Ohm's law.
- Conduct a mathematically strict proof (or falsification) of convergence of the symmetrised FIT. By "symmetrised" we mean that we take only the symmetric part of FIT's material matrix with Whitney interpolation (3.105). In Section 5.7 we have investigated the convergence numerically.
- Apply the method to a system moving in a more general way than rotation. Derive the condition for time synchronisation guaranteeing that 3D material matrices are the same at each time step. For example, we expect that in case of constant acceleration, one can use the coordinates of a constantly accelerated observer to obtain constant material matrices. Moreover, we expect that whenever there exists a timelike Killing vector field, it can be leveraged to construct a 4D mesh which guarantees constant in time material matrices. However, the general condition in terms of (space-time) symmetries of the system is not known, while would be helpful, because calculating material matrices at each time-step is computationally very expensive.
- Apply the method to study the system undergoing angular acceleration, i.e., the rotation rate Ω is not constant. For example, calculate material matrices for some sample Ω 's and obtain the material matrix $M_{\xi}(\Omega)$ depending on the rotation rate, e.g., via interpolation⁸⁵. Besides letting rotation rate Ω , i.e., the magnitude of the angular velocity $\vec{\Omega}$, the direction of the angular velocity, i.e., let the vector $\vec{\Omega}$ vary. As in this case we do not expect any Killing vectors present, we also anticipate that it is not possible to keep material matrices constant in time for such problems.
- Include more boundary conditions without abandoning the relativistic framework. We have only translated Perfect Electric Conductor boundary conditions to relativistic setting. However, another interesting case is Absorbing Boundary Conditions corresponding to simulating a device surrounded by an infinite layer of vacuum.
- Verify the scheme in a relativistic scenario, e.g., by simulating synchrotron radiation.

⁸⁵ As the structure of non-zero entries in M_{ξ} is independent of the angular velocity, all non-zero entries may be interpolated independently.

Grade	Name	Basis	Linear dimension
0	scalar	{1}	1
1	vector	$\{\gamma_t, \gamma_x, \gamma_y, \gamma_z\}$	4
2	bivector	$\{\gamma_t \wedge \gamma_x, \gamma_t \wedge \gamma_y, \gamma_t \wedge \gamma_z, \gamma_x \wedge \gamma_y, \gamma_x \wedge \gamma_z, \gamma_y \wedge \gamma_z\}$	6
3	pseudovector	$\{\gamma_t \wedge \gamma_x \wedge \gamma_y, \gamma_t \wedge \gamma_x \wedge \gamma_z, \gamma_t \wedge \gamma_y \wedge \gamma_z, \gamma_x \wedge \gamma_y \wedge \gamma_z\}$	4
4	pseudoscalar	{I}	1

Table 8: Basis of STA, i.e., GA build on 4-dimensional Minkowski vector space.

A GA Elaborations

A.1 Basis of GA

The notion that every multivector can be expressed as a sum of blades (2.17) becomes a starting point of computer implementations of GA, see [28, 16]. As every element of GA is a sum of blades, we just need to construct bases for p -blades, $p = 1, \dots, n$, and add them up, see [25, Section 4]. Suppose we have chosen some basis in the underlying vector space L . The basis of p -blades stems from the chosen basis of L

$$\gamma_{i_1} \wedge \gamma_{i_2} \wedge \dots \wedge \gamma_{i_p}, \quad i_1 < i_2 < \dots < i_p, \quad (\text{A.1})$$

where the strictly growing order of indices guarantees lack of redundant elements in the basis. There are $\binom{n}{p}$ linearly independent p -vectors constituting the basis, and thus the basis of GA has [25, Equation (4.7)]

$$\sum_{p=0}^n \binom{n}{p} = 2^n \quad (\text{A.2})$$

elements. The basis of STA is given explicitly in the Table 8. Having the basis in mind (2.17) can be written more explicitly as

$$A = \sum_{p=0}^n \sum_{i_1 < i_2 < \dots < i_p} A^{i_1 \dots i_p} \gamma_{i_1} \wedge \gamma_{i_2} \wedge \dots \wedge \gamma_{i_p} \quad (\text{A.3})$$

and thus the multivector can be stored as a 2^n -dimensional vector in traditional linear algebra sense. One can embed all the products introduced in GA to act in such linear space as done in [28] in order to perform GA computations using programming languages that can handle linear algebra.

A.2 Levi-Civita Connection is Natural to Geometric Calculus.

First, we introduce a directional derivative ∇_u as a projection of ∇ onto a vector u , see [14, Equations (6.1) and (6.197)],

$$\nabla_u A := (u \cdot \nabla)A = \lim_{h \rightarrow 0} \frac{A(x + hu) - A(x)}{h}. \quad (\text{A.4})$$

Above, we have assumed that the manifold is flat, thus transport of $A(x + hu)$ to x (in order to subtract $A(x)$ from it) is canonically well defined; c.f., (2.47)–(2.48). Then, we may formally try to compute the derivative of a scalar product

$$\nabla_u g(a, b) = (\nabla_u g)(a, b) + g(\nabla_u a, b) + g(a, \nabla_u b) = (\nabla_u g)(a, b) + (\nabla_u a) \cdot b + a \cdot (\nabla_u b), \quad (\text{A.5})$$

which is purely formal, because $\nabla_u g$ is not defined. However, we may use this equation to **define** it, and finding that this is exactly the non-metricity Q introduced in [24, Equation (C.2.111)]

$$Q(u, a, b) = (\nabla_u g)(a, b) := g(\nabla_u a, b) + g(a, \nabla_u b) - \nabla_u (g(a, b)). \quad (\text{A.6})$$

The directional derivative ∇_u inherits the Leibnitz property from the assumption that the geometric derivative ∇ satisfies it. Thus

$$\nabla_u g(a, b) = \nabla_u (a \cdot b) = \frac{1}{2} \nabla_u (ab + ba) = \frac{1}{2} [(\nabla_u a)b + a(\nabla_u b) + (\nabla_u b)a + b(\nabla_u a)] = (\nabla_u a) \cdot b + a \cdot (\nabla_u b). \quad (\text{A.7})$$

By comparison of (A.5) and (A.7), we see that the non-metricity (A.6) is $Q \equiv 0$. In other words, by assuming that the geometric derivative satisfies the Leibnitz rule with respect to the geometric product⁸⁶ we implicitly assume that the connection is metric compatible, i.e., $\nabla g = 0$.

Now we investigate the other property of connection, namely the torsion. Let x^i be some coordinate system. Then the coordinate coframe $\vartheta^i = dx^i$ satisfies [24, Equation (A.2.33)]

$$d\vartheta^i = dd x^i = 0, \quad (\text{A.8})$$

as $dd = 0$ by definition. Let us try to mimic this calculation in GA in the case of non-vanishing torsion. First, we see that for holonomic⁸⁷ (as our coordinate one) bases it follows from [24, Equation (C.1.42)] that

$$T_{lk}^i = \Gamma_{lk}^i - \Gamma_{kl}^i \Rightarrow \Gamma_{lk}^i = \frac{1}{2} [\Gamma_{lk}^i + \Gamma_{lk}^i] = \frac{1}{2} [\Gamma_{lk}^i + \Gamma_{kl}^i + T_{lk}^i]. \quad (\text{A.9})$$

The GA equivalent of $d\vartheta^i$ is, see (2.127) and (2.141),

$$(d\vartheta^i)^\sharp \doteq \nabla \wedge \gamma^i = \gamma^k \wedge (\nabla_{\gamma_k} \gamma^i) = -\Gamma_{lk}^i \gamma^k \wedge \gamma^l = -\frac{1}{2} (\Gamma_{lk}^i + \Gamma_{kl}^i + T_{lk}^i) \gamma^k \wedge \gamma^l = -\frac{1}{2} T_{lk}^i \gamma^k \wedge \gamma^l, \quad (\text{A.10})$$

where $(\Gamma_{lk}^i + \Gamma_{kl}^i) \gamma^k \wedge \gamma^l = 0$, because $(\Gamma_{lk}^i + \Gamma_{kl}^i)$ is symmetric in summation indices k and l , while $\gamma^k \wedge \gamma^l$ is antisymmetric. Thus we see that $(d\vartheta^i)^\sharp \doteq \nabla \wedge \gamma^i$ if and only if the torsion vanishes, $T = 0$. This argumentation can be extended to arbitrary elements of algebras, yielding that

$$d \doteq \nabla \wedge \iff T = 0. \quad (\text{A.11})$$

To conclude, if one accepts the Leibnitz property of the geometric derivative ∇ , then the connection is necessarily metric compatible, i.e., $\nabla g = 0$. Moreover, if one would like to have the exterior derivative incorporated gently in GA, then the connection has to be torsion-free, i.e., $T = 0$. The connection satisfying both these requirements is unique and referred in the literature as Levi-Civita connection.

A.3 Inverse of a Pseudoscalar

Let us try to find the inverse element of the pseudoscalar I ; first, we note that in an orthonormal basis

$$II^\dagger = \gamma_1 \dots \gamma_n \gamma_n \dots \gamma_1 = (-1)^s, \quad (\text{A.12})$$

where s is the number of basis vectors squaring to -1 . As I is a geometric object, the mentioned property does not depend on the particular basis. Thus we can state the general result

$$I^{-1} = (-1)^s I^\dagger = (-1)^{s+n(n-1)/2} I. \quad (\text{A.13})$$

B Technical Relativistic Derivations

B.1 Lorentz Boost as a Rotation

In order to calculate

$$p' = e^{-\vec{\beta}/2} p e^{\vec{\beta}/2}, \quad (\text{B.1})$$

with $\vec{\beta} = \beta \gamma_x \gamma_t$, we start with noting that

$$(\gamma_x \gamma_t)^2 = \gamma_x \gamma_t \gamma_x \gamma_t = -\gamma_x \gamma_x \gamma_t \gamma_t = +1 \Rightarrow (\gamma_x \gamma_t)^{2k} = 1 \quad (\text{B.2})$$

and

$$e^{\beta/2 \gamma_x \gamma_t} = \sum_{k=0}^{\infty} \frac{(\beta/2)^k (\gamma_x \gamma_t)^k}{k!} = \sum_{k=0}^{\infty} \left[\frac{(\beta/2)^{2k} (\gamma_x \gamma_t)^{2k}}{(2k)!} \right] + (\gamma_x \gamma_t) \sum_{k=0}^{\infty} \left[\frac{(\beta/2)^{2k+1} (\gamma_x \gamma_t)^{2k}}{(2k+1)!} \right] = \cosh \beta/2 + \gamma_x \gamma_t \sinh \beta/2. \quad (\text{B.3})$$

⁸⁶ Which is always the case, introduced as an axiom or following from any definition of the geometric derivative.

⁸⁷ Thus the object of anholonomy [24, Equation (A.2.35)] is $C = 0$.

Then we expand

$$p' = (\cosh \beta/2 - \gamma_x \gamma_t \sinh \beta/2)(t\gamma_t + x\gamma_x + y\gamma_y + z\gamma_z)(\cosh \beta/2 + \gamma_x \gamma_t \sinh \beta/2) \quad (\text{B.4})$$

and calculate term by term, e.g.,

$$(\cosh \beta/2 - \gamma_x \gamma_t \sinh \beta/2)\gamma_t(\cosh \beta/2 + \gamma_x \gamma_t \sinh \beta/2) = (\cosh^2 \beta/2 + \sinh^2 \beta/2)\gamma_t - 2 \sinh \beta/2 \cosh \beta/2 \gamma_x = \quad (\text{B.5})$$

$$= \gamma_t \cosh \beta - \gamma_x \sinh \beta, \quad (\text{B.6})$$

to find

$$p' = [\gamma_t, \gamma_x, \gamma_y, \gamma_z] \begin{bmatrix} \cosh(\beta) & -\sinh(\beta) & 0 & 0 \\ -\sinh(\beta) & \cosh(\beta) & 0 & 0 \\ 0 & 0 & 1 & 0 \\ 0 & 0 & 0 & 1 \end{bmatrix} \begin{bmatrix} t \\ x \\ y \\ z \end{bmatrix}. \quad (\text{B.7})$$

Recalling that

$$v = \tanh \beta, \quad \sinh \beta = \frac{\tanh \beta}{\sqrt{1 - \tanh^2 \beta}} = \frac{v}{\sqrt{1 - v^2}}, \quad \cosh \beta = \frac{1}{\sqrt{1 - \tanh^2 \beta}} = \frac{1}{\sqrt{1 - v^2}}, \quad (\text{B.8})$$

we find that the rotation in (x, t) -plane corresponds to the Lorentz boost in x -direction that can be found in all basic textbooks

$$t' = \frac{t - vx}{\sqrt{1 - v^2}}, \quad (\text{B.9})$$

$$x' = \frac{x - vt}{\sqrt{1 - v^2}}, \quad (\text{B.10})$$

$$y' = y, \quad (\text{B.11})$$

$$z' = z. \quad (\text{B.12})$$

B.2 Velocity Field of a Rotating Observer

For simplicity we set $c = 1$, obtaining

$$\frac{dp}{dt} = [1, -\sin(\theta) \tanh(r\Omega), \cos(\theta) \tanh(r\Omega), 0][\gamma_t, \gamma_x, \gamma_y, \gamma_z]^T \quad (\text{B.13})$$

$$\left| \frac{dp}{dt} \right| = \frac{1}{\cosh(r\Omega)} \quad (\text{B.14})$$

$$u = \frac{dp}{dt} \left/ \left| \frac{dp}{dt} \right| \right. = [\cosh(r\Omega), -\sinh(r\Omega) \sin(\theta), \sinh(r\Omega) \cos(\theta), 0][\gamma_t, \gamma_x, \gamma_y, \gamma_z]^T \quad (\text{B.15})$$

$$v_x = \frac{dx}{dt} = \frac{u_x}{u_t} = -\tanh(r\Omega) \sin(\theta) \quad (\text{B.16})$$

$$v_y = \frac{dy}{dt} = \frac{u_y}{u_t} = \tanh(r\Omega) \cos(\theta) \quad (\text{B.17})$$

$$v = \sqrt{v_x^2 + v_y^2} = \tanh(r\Omega) \quad (\text{B.18})$$

B.3 Technical Details of Derivation of the Gauss Law in Rotating Reference Frame

To facilitate rather technical calculations of connection coefficients we use a simple trick

$$\nabla_{\hat{\gamma}_\alpha} \hat{\gamma}_\beta = \hat{\gamma}_\alpha \cdot \nabla \hat{\gamma}_\beta = (\hat{\gamma}_\alpha \cdot \gamma^\gamma) \partial_\gamma \hat{\gamma}_\beta, \quad (\text{B.19})$$

where we expanded the geometric derivative in arbitrary coordinate frame. Our particular choice is to use non-rotating cylindrical coordinates t, r, θ, z in this expansion. Therefore, we need to calculate dot products of our orthonormal frame with reciprocal basis vectors of coordinate frame:

$$\gamma^t = \gamma_t \quad (\text{B.20})$$

$$\gamma^r = -\gamma_r \quad (\text{B.21})$$

$$\gamma^\theta = -\frac{1}{r} \hat{e}_\theta \quad (\text{B.22})$$

$$\gamma^z = -\gamma_z, \quad (\text{B.23})$$

which is an easy part. Moreover, we need to calculate derivatives $\partial_\gamma \hat{\gamma}_\beta$, which is more tedious part to which we now turn.

The derivatives $\partial_\alpha \hat{\gamma}_0$ are

$$\partial_t \hat{\gamma}_0 = 0 \quad (\text{B.24})$$

$$\partial_r \hat{\gamma}_0 = \frac{\Omega \hat{e}_\varphi}{\sqrt{1-\Omega^2 r^2}} + \frac{\Omega^2 r (\gamma_t + \Omega r \hat{e}_\varphi)}{\sqrt{1-\Omega^2 r^2}^3} = \frac{\Omega}{1-\Omega^2 r^2} \frac{\hat{e}_\varphi + \Omega r \gamma_t}{\sqrt{1-\Omega^2 r^2}} = \frac{\Omega}{1-\Omega^2 r^2} \hat{\gamma}_\varphi \quad (\text{B.25})$$

$$\begin{aligned} \partial_\theta \hat{\gamma}_0 &= \frac{\Omega r}{\sqrt{1-\Omega^2 r^2}} \partial_\theta \hat{e}_\varphi = \frac{\Omega r}{\sqrt{1-\Omega^2 r^2}} \partial_\theta (-\sin \theta \gamma_x + \cos \theta \gamma_y) = \\ &= \frac{\Omega r}{\sqrt{1-\Omega^2 r^2}} (-\cos \theta \gamma_x - \sin \theta \gamma_y) = \frac{-\Omega r}{\sqrt{1-\Omega^2 r^2}} \hat{\gamma}_r \end{aligned} \quad (\text{B.26})$$

$$\partial_z \hat{\gamma}_0 = 0, \quad (\text{B.27})$$

which enable us to calculate $\nabla_{\hat{\gamma}_\alpha} \hat{\gamma}_0$

$$\nabla_{\hat{\gamma}_0} \hat{\gamma}_0 = (\hat{\gamma}_0 \cdot \gamma^\theta) \partial_\theta \hat{\gamma}_0 = \frac{\Omega}{\sqrt{1-\Omega^2 r^2}} \frac{-\Omega r}{\sqrt{1-\Omega^2 r^2}} \hat{\gamma}_r = \frac{-\Omega^2 r}{1-\Omega^2 r^2} \hat{\gamma}_r \quad (\text{B.28})$$

$$\nabla_{\hat{\gamma}_r} \hat{\gamma}_0 = (\hat{\gamma}_r \cdot \gamma^r) \partial_r \hat{\gamma}_0 = \frac{\Omega}{1-\Omega^2 r^2} \hat{\gamma}_\varphi \quad (\text{B.29})$$

$$\nabla_{\hat{\gamma}_\varphi} \hat{\gamma}_0 = (\hat{\gamma}_\varphi \cdot \gamma^\theta) \partial_\theta \hat{\gamma}_0 = \frac{1}{r \sqrt{1-\Omega^2 r^2}} \frac{-\Omega r}{\sqrt{1-\Omega^2 r^2}} \hat{\gamma}_r = \frac{-\Omega}{1-\Omega^2 r^2} \hat{\gamma}_r \quad (\text{B.30})$$

$$\nabla_{\hat{\gamma}_z} \hat{\gamma}_0 = 0. \quad (\text{B.31})$$

The derivatives $\partial_\alpha \hat{\gamma}_r$ are

$$\partial_t \hat{\gamma}_r = 0 \quad (\text{B.32})$$

$$\partial_r \hat{\gamma}_r = 0 \quad (\text{B.33})$$

$$\partial_\theta \hat{\gamma}_r = \partial_\theta (\cos \theta \gamma_x + \sin \theta \gamma_y) = -\sin \theta \gamma_x + \cos \theta \gamma_y = \hat{e}_\varphi \quad (\text{B.34})$$

$$\partial_z \hat{\gamma}_r = 0, \quad (\text{B.35})$$

which enable us to calculate $\nabla_{\hat{\gamma}_\alpha} \hat{\gamma}_r$

$$\nabla_{\hat{\gamma}_0} \hat{\gamma}_r = (\hat{\gamma}_0 \cdot \gamma^\theta) \partial_\theta \hat{\gamma}_r = \frac{\Omega}{\sqrt{1-\Omega^2 r^2}} \hat{e}_\varphi = \Omega \frac{\hat{\gamma}_\varphi - \Omega r \hat{\gamma}_0}{1-\Omega^2 r^2} \quad (\text{B.36})$$

$$\nabla_{\hat{\gamma}_r} \hat{\gamma}_r = 0 \quad (\text{B.37})$$

$$\nabla_{\hat{\gamma}_\varphi} \hat{\gamma}_r = (\hat{\gamma}_\varphi \cdot \gamma^\theta) \partial_\theta \hat{\gamma}_r = \frac{1}{r \sqrt{1-\Omega^2 r^2}} \hat{e}_\varphi = \frac{1}{r} \frac{\hat{\gamma}_\varphi - \Omega r \hat{\gamma}_0}{1-\Omega^2 r^2} \quad (\text{B.38})$$

$$\nabla_{\hat{\gamma}_z} \hat{\gamma}_r = 0, \quad (\text{B.39})$$

where we have used

$$\hat{e}_\varphi = \frac{\hat{\gamma}_\varphi - \Omega r \hat{\gamma}_0}{\sqrt{1-\Omega^2 r^2}}. \quad (\text{B.40})$$

The derivatives $\partial_\alpha \hat{\gamma}_\varphi$ are

$$\partial_t \hat{\gamma}_\varphi = 0 \quad (\text{B.41})$$

$$\partial_r \hat{\gamma}_\varphi = \frac{\Omega}{1-\Omega^2 r^2} \hat{\gamma}_0 \quad (\text{B.42})$$

$$\partial_\theta \hat{\gamma}_\varphi = \frac{-1}{\sqrt{1-\Omega^2 r^2}} \hat{\gamma}_r \quad (\text{B.43})$$

$$\partial_z \hat{\gamma}_\varphi = 0, \quad (\text{B.44})$$

which enable us to calculate $\nabla_{\hat{\gamma}_\alpha} \hat{\gamma}_\varphi$

$$\nabla_{\hat{\gamma}_0} \hat{\gamma}_\varphi = (\hat{\gamma}_0 \cdot \gamma^\theta) \partial_\theta \hat{\gamma}_\varphi = \frac{\Omega}{\sqrt{1-\Omega^2 r^2}} \frac{-1}{\sqrt{1-\Omega^2 r^2}} \hat{\gamma}_r = \frac{-\Omega}{1-\Omega^2 r^2} \hat{\gamma}_r \quad (\text{B.45})$$

$$\nabla_{\hat{\gamma}_r} \hat{\gamma}_\varphi = (\hat{\gamma}_r \cdot \gamma^r) \partial_r \hat{\gamma}_\varphi = \frac{\Omega}{1-\Omega^2 r^2} \hat{\gamma}_0 \quad (\text{B.46})$$

$$\nabla_{\hat{\gamma}_\varphi} \hat{\gamma}_\varphi = (\hat{\gamma}_\varphi \cdot \gamma^\theta) \partial_\theta \hat{\gamma}_\varphi = \frac{1}{r\sqrt{1-\Omega^2 r^2}} \frac{-1}{\sqrt{1-\Omega^2 r^2}} \hat{\gamma}_r = \frac{-1}{r(1-\Omega^2 r^2)} \hat{\gamma}_r \quad (\text{B.47})$$

$$\nabla_{\hat{\gamma}_z} \hat{\gamma}_\varphi = 0. \quad (\text{B.48})$$

Since all partial derivatives $\partial_\alpha \hat{\gamma}_z = 0$ vanish, so do all covariant derivatives

$$\nabla_{\hat{\gamma}_\alpha} \hat{\gamma}_z = 0. \quad (\text{B.49})$$

Now when all connection coefficients are calculated we can turn back to (2.233). We will investigate each term separately. The first term contains

$$\begin{aligned} \hat{\gamma}^k \wedge \hat{\gamma}_i \wedge (\nabla_{\hat{\gamma}_k} \hat{\gamma}_0) \wedge \hat{\gamma}_0 &= -\hat{\gamma}_k \wedge \hat{\gamma}_i \wedge (\nabla_{\hat{\gamma}_k} \hat{\gamma}_0) \wedge \hat{\gamma}_0 = \\ &= -\hat{\gamma}_r \wedge \hat{\gamma}_i \wedge \left(\frac{\Omega}{1-\Omega^2 r^2} \hat{\gamma}_\varphi \right) \wedge \hat{\gamma}_0 - \hat{\gamma}_\varphi \wedge \hat{\gamma}_i \wedge \left(\frac{-\Omega}{1-\Omega^2 r^2} \hat{\gamma}_r \right) \wedge \hat{\gamma}_0 = \\ &= \frac{-\Omega}{1-\Omega^2 r^2} \delta_i^z (\hat{\gamma}_r \wedge \hat{\gamma}_z \wedge \hat{\gamma}_\varphi \wedge \hat{\gamma}_0 - \hat{\gamma}_\varphi \wedge \hat{\gamma}_z \wedge \hat{\gamma}_r \wedge \hat{\gamma}_0) = \frac{-\Omega}{1-\Omega^2 r^2} \delta_i^z (2I). \end{aligned} \quad (\text{B.50})$$

Therefore, the first term of (2.233) is equal to

$$\hat{E}^i \hat{\gamma}^k \wedge \hat{\gamma}_i \wedge (\nabla_{\hat{\gamma}_k} \hat{\gamma}_0) \wedge \hat{\gamma}_0 = \frac{-2\Omega \hat{E}^z}{1-\Omega^2 r^2} I. \quad (\text{B.51})$$

The second term contains

$$\begin{aligned} \hat{\gamma}^k \wedge (I \hat{\gamma}_i \hat{\gamma}_0) \wedge \hat{\gamma}_0 &= \hat{\gamma}^k \wedge \frac{1}{2} (I \hat{\gamma}_i \hat{\gamma}_0 \hat{\gamma}_0 + \hat{\gamma}_0 I \hat{\gamma}_i \hat{\gamma}_0) = \hat{\gamma}^k \wedge \frac{1}{2} (I \hat{\gamma}_i + I \hat{\gamma}_i) = \\ &= \hat{\gamma}^k \wedge (I \hat{\gamma}_i) = \frac{1}{2} (\hat{\gamma}^k I \hat{\gamma}_i - I \hat{\gamma}_i \hat{\gamma}^k) = \frac{1}{2} (I \hat{\gamma}^k \hat{\gamma}_i + I \hat{\gamma}_i \hat{\gamma}^k) = -I \hat{\gamma}^k \cdot \hat{\gamma}_i = -\delta_i^k I. \end{aligned} \quad (\text{B.52})$$

Therefore, the second term of (2.233) is equal to

$$\nabla_{\hat{\gamma}_k} \hat{B}^i \hat{\gamma}^k \wedge (I \hat{\gamma}_i \hat{\gamma}_0) \wedge \hat{\gamma}_0 = -\nabla_{\hat{\gamma}_k} \hat{B}^k I. \quad (\text{B.53})$$

The third term contains

$$\begin{aligned} \hat{\gamma}^k \wedge (I (\nabla_{\hat{\gamma}_k} \hat{\gamma}_i) \wedge \hat{\gamma}_0) \wedge \hat{\gamma}_0 &= \hat{\gamma}^r \wedge (I (\nabla_{\hat{\gamma}_r} \hat{\gamma}_i) \wedge \hat{\gamma}_0) \wedge \hat{\gamma}_0 + \hat{\gamma}^\varphi \wedge (I (\nabla_{\hat{\gamma}_\varphi} \hat{\gamma}_i) \wedge \hat{\gamma}_0) \wedge \hat{\gamma}_0 = \\ &= \hat{\gamma}^r \wedge \left(I \left(\delta_i^\varphi \frac{\Omega}{1-\Omega^2 r^2} \hat{\gamma}_0 \right) \wedge \hat{\gamma}_0 \right) \wedge \hat{\gamma}_0 + \hat{\gamma}^\varphi \wedge \left(I \left(\delta_i^r \frac{1}{r} \frac{\hat{\gamma}_\varphi - \Omega r \hat{\gamma}_0}{1-\Omega^2 r^2} \right) \wedge \hat{\gamma}_0 \right) \wedge \hat{\gamma}_0 + \\ &+ \hat{\gamma}^\varphi \wedge \left(I \left(\delta_i^\varphi \frac{-1}{r(1-\Omega^2 r^2)} \hat{\gamma}_r \right) \wedge \hat{\gamma}_0 \right) \wedge \hat{\gamma}_0 = \frac{\delta_i^r}{r(1-\Omega^2 r^2)} \hat{\gamma}^\varphi \wedge (I \hat{\gamma}_\varphi \wedge \hat{\gamma}_0) \wedge \hat{\gamma}_0 = \\ &= \frac{-\delta_i^r}{r(1-\Omega^2 r^2)} I. \end{aligned} \quad (\text{B.54})$$

Therefore, the third term of (2.233) is equal to

$$\hat{B}^i \hat{\gamma}^k \wedge (I (\nabla_{\hat{\gamma}_k} \hat{\gamma}_i) \wedge \hat{\gamma}_0) \wedge \hat{\gamma}_0 = \frac{-\hat{B}^r}{r(1-\Omega^2 r^2)} I. \quad (\text{B.55})$$

The fourth term of (2.233) is equal to zero

$$\hat{B}^i \hat{\gamma}^k \wedge (I \hat{\gamma}_i \wedge (\nabla_{\hat{\gamma}_k} \hat{\gamma}_0)) \wedge \hat{\gamma}_0 = 0, \quad (\text{B.56})$$

because $\nabla_{\hat{\gamma}_k} \hat{\gamma}_0$ does not contain $\hat{\gamma}_0$, therefore

$$I \hat{\gamma}_i \wedge (\nabla_{\hat{\gamma}_k} \hat{\gamma}_0) = a \wedge \hat{\gamma}_0, \quad (\text{B.57})$$

where a is some vector. This obviously vanish when wedged with $\hat{\gamma}_0$.

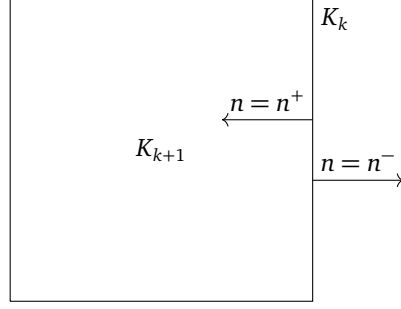


Figure 22: We check whether primal cells K_{k+1} and K_k have matching orientations, by calculating multivectors W^{k+1} and W^k associated with them, and construct a vector n satisfying $W^{k+1} = W^k \wedge n$. If n placed on K_k points inside then they have matching orientations, and when outside the orientations are opposite. Equivalently, we calculate the sign of $n^{-1} \cdot n^+$, and conclude that the orientations match if it is positive, and not if negative.

C Elaborations Associated with Whitney Elements

C.1 Dual Exterior Derivative

By $\underline{\partial}^k$ we denote the boundary operator taking k -chain and giving its boundary as a $(k-1)$ -chain. Boundary operator on the dual mesh is denoted by $\tilde{\underline{\partial}}^k$. K_k^j denotes j -th k -cell in the mesh. Dual k -cells are denoted by \tilde{K}_k^j .

Our goal is to derive the relation between $\tilde{\underline{\partial}}^{k+1}$ and ∂^{d-k} , where d is the dimension of the ambient space. Often in the literature, e.g., [58, Fig. 13 and Equation (6) on page 27] or [9, Section 5, pages 125 (bottom) – 126 (top)], the dual mesh bears outer orientation as opposed to the inner orientation of the primal mesh, which leads to the analogous expressions for dual discrete exterior derivatives, i.e., they are transposes of the primal ones, however without any additional sign change as compared to our result (C.15). This comes from the fact that we have inner oriented the primal as well as the dual mesh. First we note that:

$$[[\tilde{\underline{\partial}}^{k+1}]_{ij} = \pm 1] \Leftrightarrow [\tilde{K}_{k+1}^i \supset \tilde{K}_k^j] \Leftrightarrow [K_{d-k-1}^i \subset K_{d-k}^j] \Leftrightarrow [[\partial^{d-k}]_{ji} = \pm 1]. \quad (\text{C.1})$$

Therefore, the dual boundary operator has the same structure (of non-zero entries) as the transposed primal one, i.e.,

$$|[\tilde{\underline{\partial}}^{k+1}]_{ij}| = |[\partial^{d-k}]_{ji}|. \quad (\text{C.2})$$

Now, we need to check the orientations in order to get proper sign of the nonzero entries. We skip the indices denoting the number of the facet in this reasoning. The multivector describing the magnitude and the orientation of K_k is denoted by W^k .

We use the general observation that “the inner orientation of the primal mesh induces the outer orientation of the dual one”. This is equivalent to the statement

$$\widetilde{W}^{d-l} \wedge W^l = +I, \quad (\text{C.3})$$

where I encodes the orientation of the ambient space - something like the volume form. Moreover, we note that if the orientation of K_k matches the orientation of K_{k+1} then

$$W^{k+1} = W^k \wedge n, \quad (\text{C.4})$$

and n (living at K_k) is pointing inside K_{k+1} , see Fig. 22. If the orientation does not match, then n is pointing outside. The same statement is true for the dual mesh, i.e.,

$$\widetilde{W}^{k+1} = \widetilde{W}^k \wedge \tilde{n}, \quad (\text{C.5})$$

where \tilde{n} points inside (outside) \tilde{K}_{k+1} if the orientations are (not) matching.

For simplicity, we will assume that all multivectors used below are orthogonal. This assumption does not affect the signs in resulting equations, and we are interested only in the correct sign in the relation between primal and dual discrete exterior derivatives or boundary operators. Now suppose, we choose n and \tilde{n} such that they are orthogonal to

W^k and \widetilde{W}^k , respectively. Moreover, we assume that the multivector \widetilde{W}^{d-l} describing the dual orientation in (C.3) is orthogonal to the primal one. Then we can rewrite our equations of interest as

$$\widetilde{W}^{d-l}W^l = I \quad (\text{C.6})$$

$$W^{l+1} = W^l n \quad (\text{C.7})$$

$$\widetilde{W}^{l+1} = \widetilde{W}^l \tilde{n}. \quad (\text{C.8})$$

From the first equation we get

$$\widetilde{W}^{d-l} = I(W^l)^{-1}. \quad (\text{C.9})$$

From the second one we get (when $l \rightarrow d-l-1$)

$$W^{d-l} = W^{d-l-1}n = (-1)^{d-l-1}nW^{d-l-1} \Leftrightarrow W^{d-l}(W^{d-l-1})^{-1} = (-1)^{d-l-1}n. \quad (\text{C.10})$$

From the third one we get (using the results obtained above)

$$\tilde{n} = (\widetilde{W}^l)^{-1}\widetilde{W}^{l+1} = [I(W^{d-l})^{-1}]^{-1}I(W^{d-l-1})^{-1} = \quad (\text{C.11})$$

$$= W^{d-l}I^{-1}I(W^{d-l-1})^{-1} = W^{d-l}(W^{d-l-1})^{-1} = (-1)^{d-l-1}n. \quad (\text{C.12})$$

To conclude, if we orient the dual mesh according to (C.3) we get the relation between vectors indicating the matching of orientations:

$$\tilde{n} = (-1)^{d-l-1}n. \quad (\text{C.13})$$

Let us denote the vectors indicating matching orientations on primal and dual grids by n_0 and \tilde{n}_0 , respectively. Then the entry in primal boundary operator corresponds to n being parallel or antiparallel to n_0 , compare with Fig. 22. In other words, the entry is $\text{Sign}[n \cdot n_0^{-1}]$. The entry in the dual boundary operator is $\text{Sign}[\tilde{n} \cdot \tilde{n}_0^{-1}]$. First, we note that if n_0 points inside K_{d-l} then $\tilde{n}_0 = -n_0$ points inside \tilde{K}_{l+1} , see Fig. 23. One can easily check that after noting that n_0 and \tilde{n}_0 lie in the line segment $K_{d-l} \cap \tilde{K}_{l+1}$ and are oriented in opposite directions, such that they point inside the corresponding cell. Thus we know how \tilde{n}_0 is related to n_0 and \tilde{n} to n . Therefore, the entry in the dual boundary operator is easily expressed in terms of vectors associated with the primal mesh as follows

$$\text{Sign}[\tilde{n} \cdot \tilde{n}_0^{-1}] = \text{Sign}[(-1)^{d-l-1}n \cdot (-n_0^{-1})] = (-1)^{d-l}\text{Sign}[n \cdot n_0^{-1}]. \quad (\text{C.14})$$

Therefore, we finally get the relation

$$\boxed{\tilde{\partial}^{k+1} = (-1)^{d-k}(\partial^{d-k})^T}, \quad (\text{C.15})$$

which immediately translates to the relation between discrete exterior derivatives, which are just transposed discrete boundary operators, i.e.,

$$\underline{D}^k = [\underline{\partial}^{k+1}]^T, \quad \underline{\tilde{D}}^k = [\underline{\tilde{\partial}}^{k+1}]^T. \quad (\text{C.16})$$

C.2 Whitney Interpolation

We can derive a condition for basis functions N_i^n following from (3.71) and (3.72). Namely, plugging (3.72) into (3.71) leads to

$$\nabla \wedge (W^n \underline{A}_n) = W^{n+1} (D^n \underline{A}_n), \quad (\text{C.17})$$

$$\sum_i \nabla \wedge (A_n^i N_i^n(x)) = \sum_{i,j} ([D^n]_{ji} A_n^i) N_j^{n+1}(x), \quad (\text{C.18})$$

$$\sum_i A_n^i \nabla \wedge N_i^n(x) = \sum_{i,j} A_n^i [D^n]_{ji} N_j^{n+1}(x), \quad (\text{C.19})$$

$$\nabla \wedge N_i^n(x) = \sum_j [D^n]_{ji} N_j^{n+1}(x). \quad (\text{C.20})$$

In Appendix C.3 we give explicit definitions of functions N_i^n satisfying (C.20). One can indeed verify that Whitney interpolation is compatible with the approximation-free discretization introduced in (3.14); namely, they lead to the same

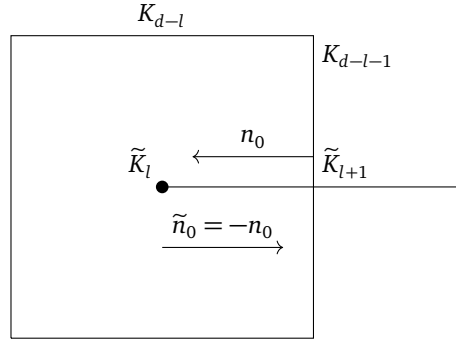


Figure 23: A primal cell (denoted as the vertical edge on the right) K_{d-l-1} lying on the boundary of a primal cell (depicted as a square) K_{d-l} , and the dual (to K_{d-l-1}) cell \tilde{K}_{l+1} (horizontal edge). The part \tilde{K}_l of the boundary of \tilde{K}_{l+1} lying inside K_{d-l} is depicted as a fat dot, i.e., $\tilde{K}_l = K_{d-l} \cap \partial\tilde{K}_{l+1}$. The intersection of two dual to each other cells K_{d-l-1} and \tilde{K}_{l+1} is a single point, i.e., $K_{d-l-1} \cap \tilde{K}_{l+1}$ is zero-dimensional. The intersection of the primal cell K_{d-l} with \tilde{K}_{l+1} is a line segment, i.e., $K_{d-l} \cap \tilde{K}_{l+1}$ is one-dimensional, and constitute a line parallel to n_0 and \tilde{n}_0 . The vector n_0 (placed on K_{d-l-1}) points inside K_{d-l} as K_{d-l} and K_{d-l-1} have matching orientations, while \tilde{n}_0 (placed on \tilde{K}_l) points inside \tilde{K}_{l+1} as \tilde{K}_{l+1} and \tilde{K}_l have matching orientations. The vectors n_0 and \tilde{n}_0 indicating matching orientations of primal and dual cells, respectively, although lying in the one line segment, are antiparallel, i.e., $\tilde{n}_0 = -n_0$.

system of equations as we prove next. In order to obtain the discrete system of equations, we plug the reconstructed field $F = W^2 \underline{f}$ in $\nabla \wedge F = 0$

$$\nabla \wedge F = \sum_i f_i \nabla \wedge N_i^2(x) = \sum_{i,j} f_i [D^2]_{ji} N_j^3(x) = \sum_j \left(\sum_i [D^2]_{ji} f_i \right) N_j^3(x) = 0, \quad (\text{C.21})$$

and since the basis functions $N_j^3(x)$ are linearly independent, it is equivalent to

$$\sum_i [D^2]_{ji} f_i = 0 \iff \underline{D^2 f} = 0, \quad (\text{C.22})$$

which is exactly (3.14)-left, and which, we would like to stress, follows directly from (C.20).

C.3 Explicit Formulae for Whitney Elements

Let us now elaborate on the explicit construction of the basis functions. Since we consider one 4D element, there is only one basis function associated with a 4-vector, that is

$$N_1^4 := I^{(4)}, \quad (\text{C.23})$$

where

$$I^{(4)} := \gamma^t \wedge \gamma^x \wedge \gamma^y \wedge \gamma^z. \quad (\text{C.24})$$

Similarly, there are eight 3D facets and thus eight basis functions associated with 3-vectors, viz.

$$N_{i\pm}^3 := \pm \gamma_i I^{(4)} (1 \pm x^i), \quad i = t, x, y, z. \quad (\text{C.25})$$

We can check that (C.20) with $n = 3$ holds and the rightmost part of the deRham complex (3.71) commutes, namely

$$\nabla \wedge N_{i\pm}^3 = \sum_k (\gamma^k \partial_k) \wedge (\pm \gamma_i I^{(4)} (1 \pm x^i)) = \sum_k \gamma^k \wedge (\gamma_i I^{(4)}) \delta_k^i = I^{(4)} = N_1^4. \quad (\text{C.26})$$

There are 24 2D facets and thus 24 basis functions associated with 2-vectors, viz.

$$N_{i\pm 1, j\pm 2}^2 := \frac{1}{16} \gamma_i \wedge \gamma_j I^{(4)} (1 \pm_1 x^i) (1 \pm_2 x^j). \quad (\text{C.27})$$

We can verify with (C.20) and $n = 2$ that (C.27) are indeed Whitney forms

$$\begin{aligned}\nabla \wedge N_{i\pm 1, j\pm 2}^2 &= \sum_k \frac{1}{16} \gamma^k \wedge (\gamma_i \wedge \gamma_j I^{(4)}) [\pm_1 \delta_k^i (1 \pm_2 x^j) \pm_2 \delta_k^j (1 \pm_1 x^i)] = \\ &= \frac{1}{16} \left[\pm_1 \gamma_j I^{(4)} (1 \pm_2 x^j) \mp_2 \gamma_i I^{(4)} (1 \pm_1 x^i) \right] = \pm_1 \pm_2 N_{j\pm 2}^3 \mp_2 \pm_1 N_{i\pm 1}^3.\end{aligned}\quad (\text{C.28})$$

In a similar fashion, we can define N^0 and N^1 . Nevertheless, since we never refer to them, we do not state them explicitly.

C.4 Derivation of Affine Mapping to Physical Space

The reference tesseract $\Xi = [-1, +1] \otimes [-1, +1] \otimes [-1, +1] \otimes [-1, +1]$ has to be mapped to a deformed tesseract in the physical domain. This is accomplished with the transformation

$$t = \sum_{i=1}^{16} T_i(\bar{t}, \bar{x}, \bar{y}, \bar{z}) t_i \quad (\text{C.29})$$

$$x = \sum_{i=1}^{16} T_i(\bar{t}, \bar{x}, \bar{y}, \bar{z}) x_i \quad (\text{C.30})$$

$$y = \sum_{i=1}^{16} T_i(\bar{t}, \bar{x}, \bar{y}, \bar{z}) y_i \quad (\text{C.31})$$

$$z = \sum_{i=1}^{16} T_i(\bar{t}, \bar{x}, \bar{y}, \bar{z}) z_i, \quad (\text{C.32})$$

where $(\bar{t}, \bar{x}, \bar{y}, \bar{z})$ are the coordinates in the reference tesseract, and (t, x, y, z) those in the physical one, and (t_i, x_i, y_i, z_i) are the physical coordinates of the i -th vertex. The functions T_i are given by

$$T_i(\bar{t}, \bar{x}, \bar{y}, \bar{z}) = \frac{1}{16} (1 + \bar{t}_i \bar{t}) (1 + \bar{x}_i \bar{x}) (1 + \bar{y}_i \bar{y}) (1 + \bar{z}_i \bar{z}), \quad (\text{C.33})$$

where $(\bar{t}_i, \bar{x}_i, \bar{y}_i, \bar{z}_i) = (\pm 1, \pm 1, \pm 1, \pm 1)$ are the reference coordinates of the i -th vertex.

This transformation comes from the following reasoning, compare [30, Section 8.1.3]. We postulate the map between physical coordinates \bar{x}^i and the reference ones x^i

$$\bar{x}^m = A^m + \sum_i A_i^m x^i + \sum_{i<j} A_{ij}^m x^i x^j + \sum_{i<j<k} A_{ijk}^m x^i x^j x^k + \sum_{i<j<k<l} A_{ijkl}^m x^i x^j x^k x^l. \quad (\text{C.34})$$

There are in total $4 \times (1 + 4 + 6 + 4 + 1) = 64$ parameters associated with $A^m, A_i^m, A_{ij}^m, A_{ijk}^m, A_{ijkl}^m$. Then we impose that this mapping should map the nodes of the reference tesseract to the physical ones. This accounts for 64 linear equations as there are 16 nodes with 4 coordinates each. This linear system is composed of 64 equations with 64 unknowns, and can be solved for A 's in terms of positions \bar{x}_j^i of the nodes in the physical tesseract. By substituting the solution for A 's in (C.34), we obtain the transformations stated in (C.29)–(C.32).

For illustration purposes we discuss here the properties of the linear interpolation in 1D. Coordinate transformation is specified by the function $x(\bar{x})$

$$x = \sum_{i=1}^2 T_i(\bar{x}) x_i, \quad (\text{C.35})$$

with

$$T_i = \frac{1}{2} (1 + \bar{x}_i \bar{x}), \quad (\text{C.36})$$

where $\bar{x}_i = \pm 1$. Being more explicit, we write

$$x = x_1 \frac{1}{2} (1 - \bar{x}) + x_2 \frac{1}{2} (1 + \bar{x}) = \frac{1}{2} (x_1 + x_2) + \frac{\bar{x}}{2} (x_2 - x_1). \quad (\text{C.37})$$

The mapping (C.35) maps the reference domain $\bar{x} \in [-1, +1]$ to the physical domain $x \in [x_1, x_2]$. Moreover, the boundary of the reference domain, e.g., the point $\bar{x} = -1$, is mapped to the boundary of the physical domain, e.g., $x = x_1$. Also the reference barycenter $\bar{x} = 0$ is mapped to the physical barycenter $x = \frac{1}{2} (x_1 + x_2)$.

The linear interpolation is extended to 4D by interpolating four coordinate functions $x^j(\bar{t}, \bar{x}, \bar{y}, \bar{z})$ defined on a tensor product of the 1D reference interval, that is $\Xi = [-1, +1] \otimes [-1, +1] \otimes [-1, +1] \otimes [-1, +1]$. We note that not only the barycenter of the reference tesseract $0 \otimes 0 \otimes 0 \otimes 0$ is mapped to the barycenter of the physical 4D cell, but also the barycenters of the lower dimensional reference elements, e.g., the barycenter $1 \otimes 1 \otimes 0 \otimes 0$ of the 2D facet $1 \otimes 1 \otimes [-1, +1] \otimes [-1, +1]$, are mapped to the barycenters of the corresponding physical elements K_n^i .

C.5 Transformations in Tangent Space Induced due to a Change of Coordinates

In case of a flat manifold M there exists a position vector x associated with each point of M . Coordinates are scalar functions used to parametrise points. Suppose we have introduced two coordinate systems, $x^a : M \rightarrow \mathbb{R}$, $a = 1, \dots, n$ and $\bar{x}^a : M \rightarrow \mathbb{R}$, $a = 1, \dots, n$, with $n = \dim M$ the dimension of the manifold, to parametrise the position

$$x = x(x^1, x^2, \dots, x^n) = x(x^a) = x(\bar{x}^a). \quad (\text{C.38})$$

We assume that the system can be solved for x^a in terms of \bar{x}^a and vice versa, i.e., the functions

$$x^a = x^a(\bar{x}^a) \quad \bar{x}^a = \bar{x}^a(x^a), \quad (\text{C.39})$$

are uniquely defined. By $\Phi : \mathcal{G}(L, g) \rightarrow \mathcal{G}(L, g)$ we denote the mapping of arbitrary multivector (including the position vector x and scalar, i.e., 0-vector, coordinate functions x^a) to its equivalent obtained by employing the other, \bar{x}^a , coordinate system. Thus we can rewrite what we have already established

$$\Phi(x) = x, \quad \Phi(x^a) = \bar{x}^a, \quad \Phi^{-1}(\bar{x}^a) = x^a, \quad (\text{C.40})$$

where the first equality comes from the fact that the change of coordinates does not influence the position vector x as this can be defined without introducing any coordinates.

Geometric Product. Since we have not changed the linear space nor the metric, the geometric product of $\mathcal{G}(L, g)$ does not change due to the change of coordinates. Therefore, we arrive at the property

$$\phi(AB) = \phi(A)\phi(B), \quad (\text{C.41})$$

where $A, B \in \mathcal{G}(L, g)$ are generic multivectors.

While the geometric algebra is not affected by the change of coordinates, the calculus, though, might be affected by the change of coordinates (C.39) in the sense that quantities defined using calculus and coordinates might be different. As it turns out, the induced transformations in the tangent space correspond to the so-called (family of) Piola transformations. Let us exemplify this statement for a few simple cases. We would like to note that in Differential Forms literature one usually studies more general maps (diffeomorphisms between two different manifolds) than the change of coordinates, and studies its influence on objects defined in tangent and co-tangent spaces separately. Then one treats the change of coordinates as a special, simplified case of these general mappings. However, since we restrict our attention to the change of coordinates, we refrain ourselves from following this more general (and more complicated) derivations.

Vector. As every vector a can be expressed in coordinate basis, $a = a^i \gamma_i$, let us derive the action of ϕ on a basis vector γ_i , which by definition is the basis vector $\bar{\gamma}_i$ associated with \bar{x}^i coordinates, i.e.,

$$\bar{\gamma}_a := \Phi(\gamma_a) = \Phi\left(\frac{\partial x}{\partial x^a}\right). \quad (\text{C.42})$$

Since $\Phi(x) = x$ and $\Phi(x^a) = \bar{x}^a$, we obtain the well-known formula for transformation of vectors,

$$\bar{\gamma}_a = \frac{\partial \Phi(x)}{\partial \Phi(x^a)} = \frac{\partial x}{\partial \bar{x}^a} = \frac{\partial x^b}{\partial \bar{x}^a} \frac{\partial x}{\partial x^b} = \frac{\partial x^b}{\partial \bar{x}^a} \gamma_b. \quad (\text{C.43})$$

Reciprocal Basis. First we note that the geometric derivative ∇ , see Section 2.1.2, is a coordinate-free object; thus $\Phi(\nabla) = \nabla$. Next we calculate the transformed reciprocal basis vector $\bar{\gamma}^i$ (used to express, e.g., one-forms),

$$\bar{\gamma}^a := \Phi(\gamma^a) = \Phi(\nabla x^a) = \Phi(\nabla)\Phi(x^a) = \nabla \bar{x}^a = (\gamma^b \partial_b) \bar{x}^a = \frac{\partial \bar{x}^a}{\partial x^b} \gamma^b. \quad (\text{C.44})$$

Components g_{ab} of Metric Tensor g . As an example of the induced tensor components transformation, we study the metric tensor g . Since metric tensor g is independent of coordinates, it is not affected by changing the coordinates, i.e., $\Phi(g) = g$. This allows us to calculate the transformation rule for its components $g_{ab} := g(\gamma_a, \gamma_b)$. Namely,

$$\begin{aligned} \bar{g}_{ab} &:= \Phi(g_{ab}) = \Phi(g(\gamma_a, \gamma_b)) = \Phi(g)(\Phi(\gamma_a), \Phi(\gamma_b)) = \\ &= g(\bar{\gamma}_a, \bar{\gamma}_b) = g\left(\frac{\partial x^c}{\partial \bar{x}^a} \gamma_c, \frac{\partial x^d}{\partial \bar{x}^b} \gamma_d\right) = \frac{\partial x^c}{\partial \bar{x}^a} \frac{\partial x^d}{\partial \bar{x}^b} g(\gamma_c, \gamma_d) = \frac{\partial x^c}{\partial \bar{x}^a} \frac{\partial x^d}{\partial \bar{x}^b} g_{cd}. \end{aligned} \quad (\text{C.45})$$

Volume of Geometric Differential. In order to derive the transformation rule for the volume form $|d^n x|$ we first note that from its definition follows

$$|\overline{d^n x}| := \Phi(|d^n x|) = \Phi\left(\left|\frac{\partial x}{\partial x^{i_1}} \wedge \cdots \wedge \frac{\partial x}{\partial x^{i_n}}\right| dx^{i_1} \dots dx^{i_n}\right) = \left|\frac{\partial x}{\partial \bar{x}^{i_1}} \wedge \cdots \wedge \frac{\partial x}{\partial \bar{x}^{i_n}}\right| d\bar{x}^{i_1} \dots d\bar{x}^{i_n} = |d^n \bar{x}|. \quad (\text{C.46})$$

Since $\Phi(x) = x$, we conclude that the volume form $|d^n x|$ is invariant with respect to the change of coordinates, i.e.,

$$\Phi(|d^n x|) = |d^n \Phi(x)| = |d^n x|. \quad (\text{C.47})$$

By exploiting the chain rule for partial derivatives, which reads

$$\frac{\partial x}{\partial \bar{x}^{i_m}} = \frac{\partial x^{j_m}}{\partial \bar{x}^{i_m}} \frac{\partial x}{\partial x^{j_m}}, \quad (\text{C.48})$$

it is easy to verify that indeed $|d^n \bar{x}| = |d^n x|$,

$$\begin{aligned} |d^n \bar{x}| &= \left|\frac{\partial x}{\partial \bar{x}^{i_1}} \wedge \cdots \wedge \frac{\partial x}{\partial \bar{x}^{i_n}}\right| d\bar{x}^{i_1} \dots d\bar{x}^{i_n} = \left|\frac{\partial x}{\partial x^{j_1}} \wedge \cdots \wedge \frac{\partial x}{\partial x^{j_n}}\right| \frac{\partial x^{j_1}}{\partial \bar{x}^{i_1}} \dots \frac{\partial x^{j_n}}{\partial \bar{x}^{i_n}} d\bar{x}^{i_1} \dots d\bar{x}^{i_n} = \\ &= \left|\frac{\partial x}{\partial x^{j_1}} \wedge \cdots \wedge \frac{\partial x}{\partial x^{j_n}}\right| dx^{j_1} \dots dx^{j_n} = |d^n x|. \end{aligned} \quad (\text{C.49})$$

On the one hand, it should not be surprising that $\phi(|d^n \bar{x}|) = |d^n x|$ as this is a scalar and should not change due to the change of coordinates. On the other hand, it might be surprising as in multivariable calculus the coordinate change induces a change (multiplication by Jacobian) of differentials. Let us investigate it briefly in 2D.

Suppose the geometric differential $d^2 \bar{x}$ takes a simple form

$$|d^2 \bar{x}| = \overbrace{\left|\frac{\partial \bar{x}}{\partial x^1} \wedge \frac{\partial \bar{x}}{\partial x^2}\right|}^{=1} d\bar{x}^1 d\bar{x}^2 = d\bar{x}^1 d\bar{x}^2, \quad (\text{C.50})$$

which means the coordinate system is such that the basis vectors span a parallelogram with unit area in each point. Since $|d^2 \bar{x}|$ is an invariant, i.e., $|d^2 \bar{x}| = |d^2 x|$, it is also equal to

$$|d^2 \bar{x}| = |d^2 x| = \left|\frac{\partial x}{\partial x^1} \wedge \frac{\partial x}{\partial x^2}\right| dx^1 dx^2 = \left|\left(\frac{\partial x}{\partial \bar{x}^1} \frac{\partial \bar{x}^1}{\partial x^1} + \frac{\partial x}{\partial \bar{x}^2} \frac{\partial \bar{x}^2}{\partial x^1}\right) \wedge \left(\frac{\partial x}{\partial \bar{x}^1} \frac{\partial \bar{x}^1}{\partial x^2} + \frac{\partial x}{\partial \bar{x}^2} \frac{\partial \bar{x}^2}{\partial x^2}\right)\right| dx^1 dx^2 = \quad (\text{C.51})$$

$$= \left[0 + \left|\frac{\partial x}{\partial \bar{x}^1} \wedge \frac{\partial x}{\partial \bar{x}^2}\right| \frac{\partial \bar{x}^1}{\partial x^1} \frac{\partial \bar{x}^2}{\partial x^2} + \left|\frac{\partial x}{\partial \bar{x}^2} \wedge \frac{\partial x}{\partial \bar{x}^1}\right| \frac{\partial \bar{x}^2}{\partial x^1} \frac{\partial \bar{x}^1}{\partial x^2} + 0\right] dx^1 dx^2 = \quad (\text{C.52})$$

$$= \overbrace{\left|\frac{\partial x}{\partial \bar{x}^1} \wedge \frac{\partial x}{\partial \bar{x}^2}\right|}^{=1} \left(\frac{\partial \bar{x}^1}{\partial x^1} \frac{\partial \bar{x}^2}{\partial x^2} - \frac{\partial \bar{x}^2}{\partial x^1} \frac{\partial \bar{x}^1}{\partial x^2}\right) dx^1 dx^2 = \Lambda dx^1 dx^2, \quad (\text{C.53})$$

where Λ is the determinant of Jacobi matrix associated with the transformation (C.39),

$$\Lambda := \text{Det} \begin{bmatrix} \frac{\partial \bar{x}^1}{\partial x^1} & \frac{\partial \bar{x}^1}{\partial x^2} \\ \frac{\partial \bar{x}^2}{\partial x^1} & \frac{\partial \bar{x}^2}{\partial x^2} \end{bmatrix}. \quad (\text{C.54})$$

Therefore, we see that $|d^2 \bar{x}| = |d^2 x|$ implies in our example the more familiar transformation rule for products of scalar differentials from multivariable calculus, i.e.,

$$|d^2 \bar{x}| = |d^2 x| \implies d\bar{x}^1 d\bar{x}^2 = \Lambda dx^1 dx^2. \quad (\text{C.55})$$

C.6 The Transformation to the Physical Domain

Having introduced a map Φ from reference to physical domain, we also need to perform induced transformation of objects living in the tangent space of the manifold, e.g., basis functions N_i^2 . Manipulations below correspond to calculating the pullback of a differential form with respect to a diffeomorphism. The N_i^2 should transform as a 2-form. For example in our implementation, for the function

$$N_{x+,y+}^2 = \frac{1}{16} \bar{\gamma}_x \wedge \bar{\gamma}_y I(1+x)(1+y) \quad (\text{C.56})$$

we have used

$$\bar{\gamma}_x \wedge \bar{\gamma}_y I = \bar{\gamma}_x \cdot (\bar{\gamma}_y \cdot I) = \bar{\gamma}_x \cdot (\bar{\gamma}^t \wedge \bar{\gamma}^x \wedge \bar{\gamma}^z) = -\bar{\gamma}^t \wedge \bar{\gamma}^z = (\nabla \bar{z}) \wedge (\nabla \bar{t}). \quad (\text{C.57})$$

We need to express $\nabla \bar{x}^\alpha$ in terms of basis vectors γ^α of physical space

$$\nabla \bar{x}^\alpha = \bar{\gamma}^\alpha = \frac{\partial \bar{x}^\alpha}{\partial x^\beta} \gamma^\beta. \quad (\text{C.58})$$

However, since we do not have an analytic expression for the inverse mapping (C.39) $\bar{x}^\alpha(x^\beta)$ of (C.29)–(C.32), we need to use

$$\frac{\partial \bar{x}^\alpha}{\partial x^\beta} = \left[\text{inv} \left(\frac{\partial x}{\partial \bar{x}} \right) \right]_\beta^\alpha, \quad (\text{C.59})$$

where $\text{inv} \left(\frac{\partial x}{\partial \bar{x}} \right)$ is the inverse of the Jacobi matrix with the entries $\left[\frac{\partial x}{\partial \bar{x}} \right]_\beta^\alpha = \frac{\partial x^\alpha}{\partial \bar{x}^\beta}$. After making this substitutions we obtain N_i^2 expressed in terms of the basis vectors associated with Minkowski space-time and its metric, but the reference coordinates are used, i.e.,

$$N_{x+,y+}^2 = \frac{\partial \bar{z}}{\partial x^a} (\bar{t}, \bar{x}, \bar{y}, \bar{z}) \frac{\partial \bar{t}}{\partial x^b} (\bar{t}, \bar{x}, \bar{y}, \bar{z}) \gamma^a \wedge \gamma^b, \quad (\text{C.60})$$

where by $\frac{\partial \bar{z}}{\partial x^a} (\bar{t}, \bar{x}, \bar{y}, \bar{z})$ we mean that the result (the partial derivatives) is expressed as a function of reference coordinates, while γ^a are basis vectors associated with Minkowski metric.

C.7 Changing the Dual in Order to Prove Convergence

Here we try to apply the proof presented in [8] to our extension of FIT. As explained in [8, the text between Equations (18) and (19)] the material matrix should be exact for locally constant fields. This is equivalent to requiring that

$$I g_i = \widetilde{W}_i \wedge \xi(F_0) = I [M_\xi]_{ik} f_k, \quad (\text{C.61})$$

where $f_k = W_k \cdot F_0$ and F_0 is constant in each primary cell.

According to (3.105) we can decompose the material matrix M_ξ into the parts M_ξ^i originating from a single 4D cell K_4^i

$$g_j = \left[\sum_i M_\xi^i \right]_{jk} f_k = \sum_i [M_\xi^i]_{jk} f_k. \quad (\text{C.62})$$

Thus it is sufficient to show that (C.61) holds for each cell separately.

In the proof it is assumed that the material matrix is symmetric; therefore, it cannot be applied to (3.105). However, we can try to repeat the proof for the symmetric part of (3.105). For simplicity, we assume that the material mapping is an identity, i.e., $G = \xi(F) = F$. This comes from the fact that any homogeneous and isotropic material can be reduced to the vacuum (ξ being an identity) case. Since the considerations below concern only one primal cell and we have assumed that in each cell material properties, thus ξ as well, are constant, i.e., homogeneous, our only additional assumption here is that the material is isotropic. Thus the considerations in this Appendix are valid for isotropic materials homogeneous in each primal cell, while material properties may vary from cell to cell.

We rewrite the condition (C.61) for the symmetrised local material matrix

$$\widetilde{W}_j \wedge F_0 = \frac{I}{2} \left([M_\xi^1]_{jk} + [M_\xi^1]_{kj} \right) f_k. \quad (\text{C.63})$$

We note that only due to the fact that Whitney interpolation is exact for constant fields, i.e.⁸⁸, $F_0 = N_k f_k$, it holds⁸⁹

$$I [M_\xi^1]_{jk} f_k = [\widetilde{W}_j \wedge N_k] f_k = \widetilde{W}_j \wedge (N_k f_k) = \widetilde{W}_j \wedge F_0. \quad (\text{C.64})$$

⁸⁸ We use the notation N_k instead of N_k^n as we do not want to specify the dimension of the ambient space nor of the elements corresponding to basis functions N_k .

⁸⁹ As compared to (3.105) there is no summation over the neighbouring cells, because we consider only one element here.

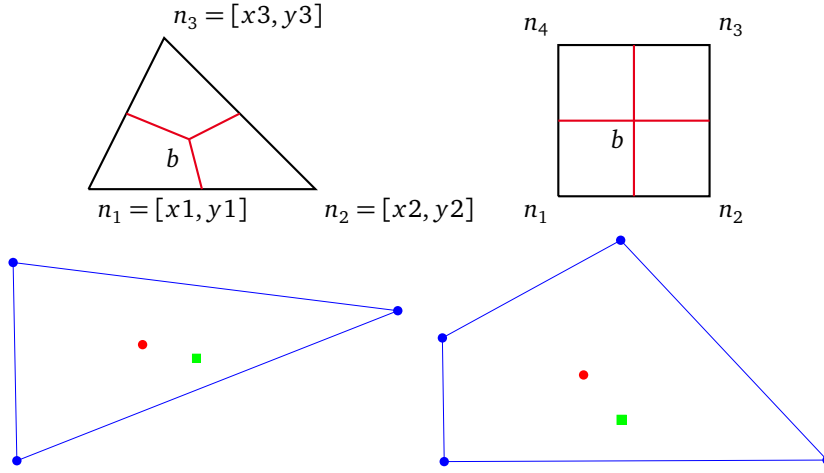


Figure 24: We redefine the center b of a triangle and a quadrilateral in order to comply with [8, Equation (18)]. For any practical implementation it is important to have a symmetric (with respect to input arguments being nodes) definition, i.e., $b(n_1, n_2, n_3) = b(n_2, n_1, n_3) = \dots$ and so on for all other permutations of (n_1, n_2, n_3) . The coordinates of the node n_i are $[x_i, y_i]$, e.g., n_3 has coordinates $[x_3, y_3]$. In a similar manner the coordinates of b are $[b_x, b_y]$. Bottom: the barycenter (red dot) and the redefined center (green square) for an exemplary triangle and quadrilateral. In particular, for an equilateral triangle and a rectangle, the barycenter and the proposed center coincide.

I.e., (C.64) means that (C.61) is fulfilled for non-symmetrised material matrices (3.105), which is equal to the first term in (C.63). Thus the requirement (C.61) reduces to

$$\widetilde{W}_j \wedge F_0 = I \left[M_{\xi}^1 \right]_{k,j} f_k = \widetilde{W}_k \wedge N_j(x_k) f_k = \widetilde{W}_k \wedge N_j(x_k) W_k \cdot F_0, \quad (\text{C.65})$$

where we have explicitly stated the evaluation point x_k of N_j , to keep in mind that it is evaluated at the point associated with \widetilde{W}_k (or equivalently with W_k) rather than W_j associated with N_j .

Let us first consider a 2D case of a triangle and a quadrilateral. In order to improve readability of general formulae in 2D situation, we change the notation according to

$$\widetilde{W}_j \rightarrow \vec{d}_j \quad F_0 \rightarrow \vec{E}_0 \quad N_j \rightarrow \vec{N}_j \quad W_k \rightarrow \vec{p}_k. \quad (\text{C.66})$$

Thus the requirement (C.61) now reads

$$\forall \vec{E}_0 = \text{const.} \quad \vec{d}_j \wedge \vec{E}_0 = \vec{d}_k \wedge \vec{N}_j(x_k) \vec{p}_k \cdot \vec{E}_0, \quad (\text{C.67})$$

with \vec{d}_j vector associated with the j -th dual edge, \vec{p}_k with k -th primal edge, \vec{E}_0 constant vector field, \vec{N}_j Whitney basis function of j -th edge and $x_k \in k$ -th edge.

Unfortunately, the equation (C.67) does not hold for the barycentric dual.

As a consequence the consistency condition [8, Equation (18)] does not hold, and the proof presented there cannot be applied.

However, as so far we have not used the flexibility of the dual mesh (previous result does not depend on the definition of the dual mesh) we can try to redefine the center b , see Fig. 24. We express (C.67) in terms of positions of primal nodes and the dual node treated as unknown. For a triangle (C.67) are 3 equations, each containing two components of

$\vec{E}_0 = [E^x, E^y]$, thus equalising coefficients of E^x and E^y of each equation to zero leads to 6 equations for two unknown coordinates $[bx, by]$ of the center b . However, it turns out that the solution to this system exists, and is given by⁹⁰

$$bx = \frac{x3^2(y1 - y2) + (x1^2 + (y1 - y2)(y1 - y3))(y2 - y3) + x2^2(-y1 + y3)}{2(x3(y1 - y2) + x1(y2 - y3) + x2(-y1 + y3))} \quad (C.68)$$

$$by = \frac{-x2^2x3 + x1^2(-x2 + x3) + x3(y1 - y2)(y1 + y2) + x1(x2^2 - x3^2 + y2^2 - y3^2) + x2(x3^2 - y1^2 + y3^2)}{2(x3(y1 - y2) + x1(y2 - y3) + x2(-y1 + y3))}, \quad (C.69)$$

with the coordinates of primal points $n_i = [xi, yi]$. Thus $b = [bx, by]$ satisfies all 6 equations, i.e., the requirement (C.61) of convergence proof is fulfilled.

By the same reasoning we can find the definition of a center of a quadrilateral, which guarantees a convergent scheme. We would like to stress that the obtained centers b treated as functions of nodes' positions are symmetric (both for triangle and quadrilateral) with respect to permutation of input arguments, i.e., $b(n_1, n_2, n_3) = b(n_2, n_1, n_3) = \dots$

To conclude, we have shown that in 2D case we can construct a dual, which results in stable and convergent FIT-like scheme.

Attempt to redefine the center of a 3D tetrahedron leads to a system of $6 \times 3 = 18$ equations, which cannot be fulfilled by any $b = [bx, by, bz]$. Namely, the solution $[bx, by, bz]$ to 3 of 18 equations is not the solution to the remaining $18 - 3 = 15$ equations. However, we have not used the flexibility of redefining the centres of 2D facets in 3D element.

C.8 3D Whitney Interpolation at the Barycenter of a Hexahedron

Our goal here is to present an explicit expression (in terms of DoFs) for Whitney interpolated $\vec{E}(\vec{r}^b)$ and $\vec{H}(\vec{r}^b)$, where \vec{r}^b is the barycenter of a 3D cell. First, we note that we can interpolate \vec{B} and then use material equations to obtain $\vec{H} = \nu\vec{B}$. Thus it is sufficient to interpolate \vec{E} and \vec{B} solely on the primal mesh from e and b , respectively.

Hexahedron has 12 oriented edges, and with each there is associated a vector \vec{l}_i pointing from the beginning to the end of the edge. It is convenient to group these 12 edges into 3 groups depending on the direction of the associated edge in the reference domain; in other words

$$[\vec{l}_1, \dots, \vec{l}_{12}] = [\vec{l}_{x1}, \dots, \vec{l}_{x4}, \vec{l}_{y1}, \dots, \vec{l}_{y4}, \vec{l}_{z1}, \dots, \vec{l}_{z4}]. \quad (C.70)$$

Next, we construct 3 basis vectors at $\vec{r}^{\text{barycenter}}$

$$\sigma^i := \frac{1}{4} \sum_{k:\text{direction}(k)=i} \vec{l}_k \equiv \frac{1}{4} \sum_{j=1}^4 \vec{l}_{ij}, \quad (C.71)$$

where we introduce an auxiliary function

$$\text{direction}(k) := \begin{cases} x, & k = 1 \dots 4 \\ y, & k = 5 \dots 8 \\ z, & k = 9 \dots 12 \end{cases}. \quad (C.72)$$

We introduce the normalised basis as

$$\hat{\sigma}^i := \frac{\sigma^i}{|\sigma^i|}, \quad (C.73)$$

and its reciprocal dual as

$$\hat{\sigma}_i := \epsilon_{ijk} \frac{\hat{\sigma}^j \times \hat{\sigma}^k}{\hat{\sigma}^i \cdot (\hat{\sigma}^j \times \hat{\sigma}^k)} \quad (\text{no summation over } j \text{ nor } k). \quad (C.74)$$

For convenience we introduce local e DoFs as

$$\hat{e}_{\text{local},k} := \pm \frac{\hat{e}_i}{|\vec{l}_k|}, \quad (C.75)$$

⁹⁰ This solution has been obtained using Computer Algebra System. We express (C.67) in terms of coordinates of primal nodes, dual points, and field components $[E^x, E^y]$. Then, we set a center of an edge to be its midpoint (barycenter). This leads us to 3 equations with the structure $eqn_x E^x + eqn_y E^y = 0$, which should hold for all $\vec{E} = [E^x, E^y]$, thus each such equation is equivalent to two equations $eqn_x = 0 = eqn_y$. Subsequently, we solve any 2 from 6 equations $eqn_i(\text{primal positions}, b)$ for two unknowns $[bx, by]$, and substitute obtained solution to the remaining $6 - 2 = 4$ equations to check whether it is a solution to the complete system, which turns out to be the case. In the end, we verify that the obtained center function is symmetric, in the sense it is independent of the order of input nodes, e.g., $b(n_1, n_2, n_3) = b(\text{any permutation of } \{n_1, n_2, n_3\})$. Analogous reasoning and results are valid for a quadrilateral case.

where the minus sign is chosen when local and global orientation of the edge are different, and i is the global edge index corresponding to the local edge number k . Finally, the Whitney interpolated electric field at the barycenter is given by

$$\vec{E}_{\text{local}} := \frac{1}{4} \sum_{k=1}^{12} \hat{e}_{\text{local},k} \hat{\sigma}^{\text{direction}(k)}, \quad (\text{C.76})$$

which is convenient for computer implementation. Both (C.76) and (C.77) can be easily derived via direct calculation.

Analogously, Whitney interpolated \vec{B} (\vec{r}^b) reads

$$\vec{B}_{\text{local}} := \frac{1}{2} \sum_{k=1}^6 \hat{b}_{\text{local},k} \hat{\sigma}^{\text{direction}(k)}, \quad (\text{C.77})$$

where local DoFs are

$$\hat{b}_{\text{local},k} := \pm \frac{\hat{b}_i}{S_k}, \quad (\text{C.78})$$

with S_k the k -th facet's area; i is the global facet index corresponding to local facet number k , and the auxiliary function for facets is

$$\text{direction}(k) := \begin{cases} x, & k = 1, 2 \\ y, & k = 3, 4 \\ z, & k = 5, 6 \end{cases} \quad (\text{C.79})$$

which corresponds to a certain grouping of the facets, similar to (C.72).

D Neumann Series as a Predictor-Corrector Scheme

Here we will relate the iterative application of (3.127)–(3.130) with some initial guess to inverting a matrix via truncated Neumann series. By iterative application of (3.127)–(3.130) we mean calculating the i -th iterative solution $\tilde{e}_i^{n+1/2}$ from

$$\tilde{h}_{i+1}^n = M_{yb}^- b^{n-1} + M_{ve}^- e^{n-1/2} + M_{yb} b^n + M_{ve}^+ \tilde{e}_i^{n+1/2} + M_{yb}^+ \tilde{b}_i^{n+1} \quad (\text{D.1})$$

$$\tilde{d}_{i+1}^{n+1/2} = d^{n-1/2} + \tilde{C} \tilde{h}_{i+1}^n \quad (\text{D.2})$$

$$\tilde{e}_{i+1}^{n+1/2} = M_{ee}^{-1} [\tilde{d}_{i+1}^{n+1/2} - M_{eb}^- b^n - M_{eb}^+ \tilde{b}_i^{n+1}] \quad (\text{D.3})$$

$$\tilde{b}_{i+1}^{n+1} = b^n + C \tilde{e}_{i+1}^{n+1/2}, \quad (\text{D.4})$$

where by a tilde over a DoF we denote that it is changing during the iterative process, while the DoFs without a tilde are assumed to be already calculated in the time marching procedure. The above system is equivalent to calculating $\tilde{e}_i^{n+1/2}$ from

$$\tilde{e}_{i+1}^{n+1/2} = A \tilde{e}_i^{n+1/2} + a, \quad (\text{D.5})$$

where

$$A := M_{ee}^{-1} \tilde{C} M_{ve}^+ + M_{ee}^{-1} \tilde{C} M_{yb}^+ C - M_{ee}^{-1} M_{eb}^+ C \quad (\text{D.6})$$

$$a := M_{ee}^{-1} [d^{n-1/2} + \tilde{C} M_{yb}^- b^{n-1} + \tilde{C} M_{ve}^- e^{n-1/2} + \tilde{C} M_{yb} b^n + \tilde{C} M_{yb}^+ b^n - M_{eb}^- b^n - M_{eb}^+ b^n]. \quad (\text{D.7})$$

By k -times repeated application of (D.5) we obtain

$$\tilde{e}_{i+1}^{n+1/2} = A^{k+1} \tilde{e}_{i-k}^{n+1/2} + \sum_{l=0}^k A^l a, \quad (\text{D.8})$$

which results in (by taking $k = i$)

$$\tilde{e}_{i+1}^{n+1/2} = A^{i+1} \tilde{e}_0^{n+1/2} + \sum_{l=0}^i A^l a, \quad (\text{D.9})$$

where $\tilde{e}_0^{n+1/2}$ is an initial guess for $e^{n+1/2}$, which has to be specified before starting the iterative process. By choosing

$$\tilde{e}_0^{n+1/2} = a, \quad (\text{D.10})$$

we obtain

$$\tilde{e}_{i+1}^{n+1/2} = \sum_{l=0}^{i+1} A^l a, \quad (\text{D.11})$$

which is equivalent to using a truncated Neumann series for the inverse of $1 - A$, i.e.,

$$(1 - A)^{-1} = \sum_{l=0}^{\infty} A^l \approx \sum_{l=0}^{i+1} A^l. \quad (\text{D.12})$$

References

- [1] R. A. Adams. *Sobolev spaces*. Pure and applied mathematics. Academic Press, New York, 1978.
- [2] B. Auchmann and S. Kurz. Observers and splitting structures in relativistic electrodynamics. *Journal of Physics A: Mathematical and Theoretical*, 47(43):435202, 2014.
- [3] R. A. Bernatz. *Fourier Series and Numerical Methods for Partial Differential Equations*. John Wiley & Sons, Inc., 2010.
- [4] D. Bini, C. Germani, and R. T. Jantzen. Gravitoelectromagnetism and the Integral Formulation of Maxwell's Equations. *International Journal of Modern Physics D*, 10(05):633–647, 2001.
- [5] A. Bossavit. Whitney forms: a class of finite elements for three-dimensional computations in electromagnetism. *IEE Proceedings A - Physical Science, Measurement and Instrumentation, Management and Education - Reviews*, 135(8):493–500, Nov 1988.
- [6] A. Bossavit. *Computational Electromagnetism*. Academic Press, San Diego, 1998.
- [7] A. Bossavit. Computational electromagnetism and geometry. (5): The "Galerkin Hodge". *The Japan Society of Applied Electromagnetics and Mechanics*, 8(2):203–209, 2000.
- [8] A. Bossavit. "Generalized Finite Differences" in Computational Electromagnetics. *PIER*, 32:45–64, 2001.
- [9] A. Bossavit and L. Kettunen. Yee-like schemes on a tetrahedral mesh, with diagonal lumping. *International Journal of Numerical Modelling: Electronic Networks, Devices and Fields*, 12(1-2):129–142, 1999.
- [10] F. Brackx, R. Delanghe, and F. Sommen. Differential forms and/or multi-vector functions. *CUBO - A MATHEMATICAL JOURNAL*, 7(2):139–169, 2005.
- [11] W. K. Clifford. *Mathematical Papers*. Macmillan, London, 1882.
- [12] L. Codecasa, R. Specogna, and F. Trevisan. Symmetric Positive-Definite Constitutive Matrices for Discrete Eddy-Current Problems. *IEEE Transactions on Magnetics*, 43(2):510–515, Feb 2007.
- [13] L. Codecasa and F. Trevisan. Piecewise uniform bases and energetic approach for discrete constitutive matrices in electromagnetic problems. *International Journal for Numerical Methods in Engineering*, 65(4):548–565, 2006.
- [14] C. Doran and A. Lasenby. *Geometric Algebra for Physicists*. Cambridge University Press, Cambridge, second edition, 2003.
- [15] L. Dorst. The inner products of geometric algebra. In L. Dorst, C.J.L. Doran, and J. Lasenby, editors, *Applications of Geometric Algebra in Computer Science and Engineering*, pages 37–48. Birkhäuser, 2002.
- [16] L. Dorst, D. Fontijne, and S. Mann. *Geometric Algebra for Computer Science: An Object-Oriented Approach to Geometry (The Morgan Kaufmann Series in Computer Graphics)*. Morgan Kaufmann Publishers Inc., San Francisco, CA, USA, 2007.
- [17] T. Euler. *Consistent Discretization of Maxwell's Equations on Polyhedral Grids*. PhD thesis, Technische Universität, Darmstadt, November 2007.
- [18] M. Fecko. On 3+1 decompositions with respect to an observer field via differential forms. *Journal of Mathematical Physics*, 38(9):4542–4560, 1997.
- [19] M. Fecko. *Differential Geometry and Lie Groups for Physicists*. Cambridge books online. Cambridge University Press, 2006.
- [20] M. R. Francis and A. Kosowsky. Geometric algebra techniques for general relativity. *Annals of Physics*, 311:459–502, June 2004.
- [21] C. Garola. A Formulation of the Ohm's Law Consistent with Maxwell's Equations and Relativity. *Rendiconti del Seminario Matematico dell'Università e del Politecnico di Torino*, 37:93–106, 1979.
- [22] D. F. Griffiths. *Introduction to Electrodynamics*. Prentice-Hall, New Jersey, September 1999.

- [23] F. W. Hehl. Maxwell's equations in Minkowski's world: their premetric generalization and the electromagnetic energy-momentum tensor. *Annalen der Physik*, 17(9-10):691–704, 2008.
- [24] F. W. Hehl and Y. N. Obukhov. *Foundations of Classical Electrodynamics: Charge, Flux, and Metric*. Progress in Mathematical Physics. Birkhäuser Boston, 2012.
- [25] D. Hestenes. *Space-time algebra*. Documents on modern physics. Gordon and Breach, 1966.
- [26] D. Hestenes. Differential Forms in Geometric Calculus. In F. Brackx, R. Delanghe, and H. Serras, editors, *Clifford Algebras and their Applications in Mathematical Physics*, pages 269–285. Springer, 1993.
- [27] D. Hestenes. The Shape of Differential Geometry in Geometric Calculus. In Leo Dorst and Joan Lasenby, editors, *Guide to Geometric Algebra in Practice*, pages 393–410. Springer, 2011.
- [28] D. Hildenbrand. *Foundations of Geometric Algebra Computing*, volume 8 of *Geometry and computing*. Springer, Berlin, 2013.
- [29] R. Hiptmair. Finite elements in computational electromagnetism. *Acta Numerica*, 11:237–339, 1 2002.
- [30] J.-M. Jin. *The finite element method in electromagnetics*. Wiley, New York, 2002.
- [31] M. Klimek, U. Römer, S. Schöps, and T. Weiland. Space-time discretization of Maxwell's equations in the setting of Geometric Algebra. In *2013 International Symposium on Electromagnetic Theory*, pages 1101–1104, May 2013.
- [32] M. Klimek, S. Schöps, and T. Weiland. Mesh optimization for Maxwell's equations with respect to anisotropic materials using geometric algebra. *Progress In Electromagnetics Research M*, 46:153–163, 2016.
- [33] C. Mattiussi. The Geometry of Time-Stepping. *Progress In Electromagnetics Research*, 32:123–149, 2001.
- [34] C. W. Misner, K. S. Thorne, and J. A. Wheeler. *Gravitation*. W.H. Freeman and Company, 1973.
- [35] T. C. Mo. Theory of Electrodynamics in Media in Noninertial Frames and Applications. *Journal of Mathematical Physics*, 11(8):2589–2610, 1970.
- [36] J. Nash. C^1 -isometric imbeddings. *Annals of Mathematics*, 60(3):383–396, 1954.
- [37] R. Novitski, J. Scheuer, and B. Z. Steinberg. Unconditionally stable finite-difference time-domain methods for modeling the Sagnac effect. *Phys. Rev. E*, 87:023303, Feb 2013.
- [38] R. Novitski, B. Z. Steinberg, and J. Scheuer. Finite-difference time-domain study of modulated and disordered coupled resonator optical waveguide rotation sensors. *Opt. Express*, 22(19):23153–23163, Sep 2014.
- [39] C. Peng, R. Hui, X. Luo, Z. Li, and A. Xu. Finite-difference time-domain algorithm for modeling Sagnac effect in rotating optical elements. *Opt. Express*, 16(8):5227–5240, Apr 2008.
- [40] E. Poisson. *A Relativist's Toolkit: The Mathematics of Black-Hole Mechanics*. Cambridge University Press, Cambridge, UK: Cambridge University Press, 2004.
- [41] E. J. Post. Sagnac Effect. *Rev. Mod. Phys.*, 39:475–493, Apr 1967.
- [42] A. Quarteroni, R. Sacco, and F. Saleri. *Numerical Mathematics*, volume 37 of *Texts in Applied Mathematics*. Springer, New York, 2000.
- [43] G. Rizzi and M. L. Ruggiero. Space Geometry of Rotating Platforms: An Operational Approach. *Foundations of Physics*, 32(10):1525–1556, 2002.
- [44] J. Salamon, J. Moody, and M. Leok. Geometric Representations of Whitney Forms and their Generalization to Minkowski Spacetime. *arXiv:1402.7109v1*, Feb. 2014.
- [45] S. Sauter and C. Schwab. *Boundary Element Methods*. Springer Series in Computational Mathematics. Springer Berlin Heidelberg, 2010.
- [46] R. Schuhmann, P. Schmidt, and T. Weiland. A new Whitney-based material operator for the finite-integration technique on triangular grids. *IEEE Transactions on Magnetics*, 38(2):409–412, Mar 2002.

-
- [47] R. Schuhmann and T. Weiland. A Stable Interpolation Technique for FDTD on Nonorthogonal Grids. *International Journal of Numerical Modelling: Electronic Networks, Devices and Fields*, 11(6):299–306, 1998.
- [48] R. Schuhmann and T. Weiland. Conservation of Discrete Energy and Related Laws in the Finite Integration Technique. *Progress in Electromagnetic Research (PIER) Monograph Series: Special Issue on Geometric Methods for Computational Electromagnetics*, 32:301–316, 2001. TEMF-Pub-DB TEMF000326.
- [49] J. Snugg. *A New Approach to Differential Geometry using Clifford's Geometric Algebra*. SpringerLink : Bücher. Birkhäuser Boston, 2011.
- [50] G. Sobczyk. Simplicial Calculus with Geometric Algebra. In *Clifford Algebras and Their Applications in Mathematical Physics*, pages 279–292. Springer, 2011.
- [51] R. Starke and G. A. H. Schober. Relativistic covariance of Ohm's law. *International Journal of Modern Physics D*, 25(11):1640010, 2016.
- [52] O. Steinbach. *Numerical Approximation Methods for Elliptic Boundary Value Problems: Finite and Boundary Elements*. Texts in applied mathematics. Springer New York, 2007.
- [53] B. Z. Steinberg and A. Boag. Splitting of microcavity degenerate modes in rotating photonic crystals—the miniature optical gyroscopes. *J. Opt. Soc. Am. B*, 24(1):142–151, Jan 2007.
- [54] B. Z. Steinberg, J. Scheuer, and A. Boag. Rotation-induced superstructure in slow-light waveguides with mode-degeneracy: optical gyroscopes with exponential sensitivity. *J. Opt. Soc. Am. B*, 24(5):1216–1224, May 2007.
- [55] B. Z. Steinberg, A. Shamir, and A. Boag. Two-dimensional Green's function theory for the electrodynamics of a rotating medium. *Phys. Rev. E*, 74:016608, Jul 2006.
- [56] A. Stern, Y. Tong, M. Desbrun, and J. E. Marsden. Geometric computational electrodynamics with variational integrators and discrete differential forms. arXiv:0707.4470v2, 2009.
- [57] J. L. Synge. *Relativity: The Special Theory*. Series in Physics. Amsterdam: North-Holland Publishing Company; New York: Interscience Publishers, 1956.
- [58] E. Tonti. Finite Formulation of the Electromagnetic Field. *PIER*, 32:1–44, 2001.
- [59] T. Weiland. On the unique numerical solution of Maxwellian eigenvalue problems in three dimensions. *Particle Accelerators*, 17(227–242), 1985.
- [60] T. Weiland. Time Domain Electromagnetic Field Computation with Finite Difference Methods. *International Journal of Numerical Modelling*, 9:295–319, Jul. 1996.
- [61] Y. Yang and M. Pesavento. A Unified Successive Pseudoconvex Approximation Framework. *IEEE Transactions on Signal Processing*, 65(13):3313–3328, July 2017.

Mariusz Maksymilian Klimek
Curriculum Vitae

Personal details

Date of birth: 12 October 1987
Place of birth: Lublin, Poland
e-mail: klimek@gsc.tu-darmstadt.de

Education

PhD, Computational Engineering 01.12.2012 - 19.01.2018

Research Stay, 01.09.2012 - 30.11.2012

Technische Universität Darmstadt
Graduate School of Computational Engineering
Supervisors: Sebastian Schöps, Stefan Kurz, Thomas Weiland
Thesis: Space-Time Discretization of Maxwell's Equations in the Setting of Geometric Algebra
Final grade: "very good"

PhD, Physics October 2011 - unfinished

University of Maria Curie-Skłodowska in Lublin
Faculty of Mathematics Physics and Informatics
Physics: Theoretical Section: Mathematical Physics
Thesis Advisor: Andrzej Gózdź
Title: Quantum Theory of Time

M. Sc., Physics 2009 - 2011

B. Sc., Physics 2006 - 2009

University of Maria Curie-Skłodowska in Lublin
Faculty of Mathematics Physics and Informatics
Physics: Theoretical Section
Thesis Advisor: Jerzy Matyjasek
Master's Thesis: Renormalized Stress-Energy Tensor in Black Hole Spacetimes
Bachelor's Thesis: Visualising Exact Solutions of Einstein's Equations. Embedding Diagrams
Average grade: 5.0 (best possible)

High school 2003-2006

IX Liceum Ogólnokształcące im. Mikołaja Kopernika in Lublin

Practice internship 1-28.09.2010

Institute of Agrophysics of the Polish Academy of Sciences
Supervisor: Artur Zdunek
Topic: Preparation and Testing of Computational Procedures for Analysis of Biospeckle Activity

Acknowledgements

I would like to thank all colleagues from the university who I met during my stay in Darmstadt for a pleasant and inspiring atmosphere of conducting research. I am grateful to my supervisors for the guidance and sharing their knowledge. I would like to acknowledge the 'Excellence Initiative' of the German Federal and State Governments and the Graduate School of Computational Engineering at Technische Universität Darmstadt as well as "Ingenium - Young Researchers at TU Darmstadt" for funding opportunities. This thesis would have not been accomplished without the excellent support from the administrative team at the graduate school. Finally, I would like to appreciate the (not necessarily research related) support of my friends, family and strangers, who (consciously or not) have helped me to pursue the path of a scientist.